ISBN: 978-979-8510-59-5

KATALOG

JURNAL MAHASISWA PASCASARJANA UNIVERSITAS LAMPUNG

VOLUME 2 NOMOR 2 TAHUN 2022

BUKU 5
FMIPA

PASCASARJANA
UNIVERSITAS LAMPUNG
NOVEMBER 2022

TIM PENELAAH

PENANGGUNG JAWAB
Prof. Dr. Ahmad Saudi Samosir, ST., MT

TIM PENELAAH
Prof. Dr. Abdurrahman, M.Si
Dr. Maulana Mukhlis, S.Sos, M.IP
Prof. Rudy Situmeang, M.Sc
Hari Kaskoyo, S.Hut., M.P., Ph.D
Ahyani, S.I.Kom
Haidawati, S.T.P., M.Si
Hernadi Susanto, S.H
Hasan Azhari Nawi, S.Kom
Hardian Sanjaya, S.Pd

Desain Cover dan Tata Letak
Tim Aura Publishing

ISBN
978-979-8510-59-5

Penerbit
Pascasarjana Universitas Lampung

Alamat Redaksi
GEDUNG PASCASARJANA
UNIVERSITAS LAMPUNG

Jalan Prof. Dr. Soemantri Brojonegoro, No. 1 Gedong Meneng
Bandar Lampung, 35145
Telp (0721) 783682
e-mail: pasca@kpa.unila.ac.id

SAMBUTAN DIREKTUR PASCASARJANA

Assalamu'alaikum Warahmatullahi Wabaraakatuh

Alhamdulilahirobbil 'aalamiin. Puji dan syukur kita panjatkan kehadirat Allah SWT, Tuhan Yang Maha Kuasa atas keberhasilan Pascasarjana Universitas Lampung menerbitkan Katalog Jurnal Mahasiswa Pascasarjana Universitas Lampung Volume II Nomor 2 Tahun 2022. Sejak awal penerbitan, kami berharap media ini dapat menjadi informasi dan membuka jalan interaksi yang lebih intens antara Pascasarjana Universitas Lampung dengan *stakeholders* di luar kampus. Katalog Jurnal Mahasiswa Pascasarjana ini dimaksudkan sebagai upaya penyebarluasan hasil penelitian mahasiswa Magister (S2) sehingga pemanfaatan hasil-hasil penelitian mahasiswa yang dibimbing oleh para dosen dapat dioptimalkan dalam meningkatkan kontribusi Universitas Lampung terhadap pembangunan daerah, bangsa, dan negara.

Saat ini, Pascasarjana sedang bertransformasi baik pada aspek kelembagaan, penjaminan mutu maupun aspek tridarma perguruan tinggi dalam mendorong peningkatan pencapaian Indikator Kinerje Utama (IKU). Pada aspek kelembagaan, Pascasarjana sedang berupaya untuk meningkatkan status menjadi sekolah yang secara teknis berimplikasi terhadap skenario pembukaan program studi baru baik pada jenjang magister maupun jenjang doktor. Pada aspek penjaminan mutu, Pascasarjana sedang mendesain sistem penjaminan mutu internal yang lebih relevan dan aplikatif sehingga target peningkatan jumlah program studi magister dan doktor yang terakreditasi unggul dapat dicapai. Adapun pada aspek tri darma, sistem pembelajaran yang relavan dengan dunia kerja terus dikembangkan termasuk di dalamnya penelitian, pengabdian, dan publikasi ilmiah oleh dosen maupun mahasiswa.

Atas nama pimpinan Pascasarjana Universitas Lampung, saya menyampaikan terima kasih kepada Tim Penelaah, para mahasiswa Pascasarjana di lingkungan Universitas Lampung, dan seluruh pihak yang telah berkontribusi pada terbitnya Katalog Jurnal Mahasiswa Pascasarjana Universitas Lampung Volume 2 Nomor 2 Tahun 2022 ini. Semoga Allah SWT senantiasa memberikan petunjuk dan barokah-Nya untuk kita semua.

Wassalamu'alaikum warahmatullahi wabarakatuh

Bandar Lampung, 10 November 2022

Direktur.

Prof. Dr. Ahmad Saudi Samosir, ST, MT
NIP. 197104151998031005

DAFTAR ISI

SYNTHESIS, CHARACTERIZATION, AND COMPARISON OF DISINFECTANT BIOACTIVITY TEST OF TWO TRIPHENYLTIN(IV) COMPOUNDS

Aisyah L. Susangka, Sutopo Hadi*, Noviany Noviany, Agung A. Kiswandono, Nurhasanah, Kamisah D. Pandiangan

Department of Chemistry, Universitas Lampung, Bandar Lampung, Indonesia 35145
*Corresponding author: sutopo.hadi@fmipa.unila.ac.id

Abstract

This paper aims to report the synthesis of two new organotin(IV) carboxylate derivatives, triphenyltin(IV) 4-aminobenzoate (**2**) and triphenyltin(IV) 4-nitrobenzoate (**3**) and to examine their antibacterial activity as a disinfectant. These compounds were prepared by reacting triphenyltin(IV) hydroxide (**1**) with 4-aminobenzoic acid and 4-nitrobenzoic acid, respectively. Compound (**2**) was obtained as a yellow solid with a yield of 84.09% and compound (**3**) in the form of a white solid with a yield of 80.70%. These compounds were well characterized using UV-Vis spectrometry, FT-IR spectrometry and NMR spectroscopy. The bioactivity test as a disinfectant was tested against *Salmonella typhosa* and *Staphylococcus aureus*. The activity test was carried out by measuring the optical density (OD) of the tested compounds with concentration variations of $5x10^{-3}$, $1x10^{-3}$, and $5x10^{-4}$ M in methanol and 5% dimethyl sulfoxide (DMSO), commercial Wipol (2.5% pine oil) was used as a positive control with observations monitored at contact times of 0, 5, 10, and 15 minutes. The results showed that of both compounds were active against the two bacteria compared to the positive control with compound **3** found to be more active than compound **2**.

Keywords: antibacterial, disinfectant, S. *typhosa*, S. *aureus*, triphenyltin(IV) compounds

INTRODUCTION

Health is a very important aspect of life. Health enables every human being to live socially and economically productive with conditions of physical, spiritual and social well-being. In the current state of health, the level of health faces very serious challenges (1). Some developing countries still have relatively low levels of health. This is caused by several factors, especially the lack of awareness to maintain good personal and environmental hygiene. Due to the lack of public awareness in maintaining cleanliness, they are susceptible to various kinds of infectious diseases such as diarrhoea, typhoid or typhoid fever, MRSA (methicillin-resistant *Staphylococcus aureus*), respiratory tract infections and other infectious diseases due to microbial contamination (2, 3). Thus, infection is still one of the main health problems causing death in many countries (4).

Bacteria generally have the ability to live freely in the environment, so they are very easy to move from one place to another. This movement can cause bacteria to stick on any object in public places, thus causing other living things to be easily contaminated (5). Therefore, in order to minimize the spread of these bacteria, a substance is needed

to kill or reduce the spread of microbes or bacteria found in the environment or inanimate objects. Disinfectants are chemicals used to kill microbes (bacteria, viruses, fungi, etc.), especially on inanimate objects and object surfaces. Disinfectants are widely used for sanitation in public places, homes, laboratories and hospitals. However, the chemicals used in disinfectants tend to be harmful to humans, animals and nearby plants (6).

Another alternative is to obtain compounds that are effective as disinfectants that can kill microorganisms in the shortest time and without damaging the affected material by developing new compounds and testing their activities (7-12). The derivative of organotin(IV) compounds have been reported to have very interesting biological activities such as anticancer and antitumor (13-16), antimalarial (17-20), corrosion inhibitors (21-23), and antifungal (24), are also known to have excellent activity in inhibiting the bacterial growth (7-11) and as antiviral agents (25-27).

The strength of the activity of organotin(IV) compounds against bacteria is not only influenced by the number of organic groups attached to the central atom of tin (Sn), but the type of organic groups also plays a role as a determinant in their activity (25, 28). The organic group of phenyl that is bound to the central atom of Sn is known to have a stronger antibacterial activity than the butyl group (27) and the higher the number of phenyl groups, the higher the antibacterial activity observed (29). In addition, the type of anion ligands bound to Sn atom also has an important role as a secondary determinant of reactivity. Therefore, in this paper, we reported the synthesis of two triphenyltin(IV) compounds with ligands of 4-aminobenzoic acid and 4-nitrobenzoic acid and performed activity tests as disinfectant agent against Gram-positive *S. aureus* and Gram-negative *S. typhosa* bacteria.

EXPERIMENTAL SECTION

Materials

The reagents used were triphenyltin(IV) hydroxide ([$(C_6H_5)_3SnOH$]), 4-aminobenzoic acid ([$(C_6H_4(4\text{-}NH_2)COOH$]), 4-HABz, 4-nitrobenzoic acid ([$(C_6H_4(4\text{-}NO_2)COOH$]), 4-HNBz, methanol, dimethylsulfoxide ($(CH_3)_2SO$, DMSO), nutrient broth, and nutrient agar. They were obtained from Sigma-Aldrich (Burlington, MA, USA) with Pro Analysis (PA) quality and were used as received. The culture of Gram-positive bacteria *S. aureus* and Gram- negative bacteria *S. typhosa* were obtained from Laboratory of Veterinary Centre, Directorate General of Livestock and Animal Health, Ministry of Agriculture, Lampung, Indonesia. A commercial product Wipol (containing 2.5% pine oil) was used as a positive control.

Instrumentantion

Elemental analysis was carried out on an EA Fission 1108 series elemental analyzer, the UV spectra were recorded in the UV region and measured using a UV-Shimadzu UV-245 Spectrophotometer. Measurements were carried in 1 mL quartz cells. The solution was prepared using methanol solvent with a concentration of 1.0×10^{-5} M. The IR spectra were recorded on a Bruker VERTEX 70 FT-IR spectrophotometer with a KBr disc in the range of 4000-400 cm^{-1}. ^{1}H and ^{13}C NMR spectra were recorded on a Bruker AV 600 MHz NMR (600 MHz for ^{1}H and 150 MHz for ^{13}C). All experiments were run in DMSO-d_6 at 298 K.

Preparation of Triphenyltin(IV) Compounds

Two target compounds of triphenyltin(IV) 4-aminobenzoate (**2**) and organotin(IV) 4-nitrobenzoate (**3**) were prepared by the reaction between the starting compound triphenyltin(IV) hydroxide (**1**) with 4-HABz and 4-HNBz using the published method (8-12, 14, 17, 29). The following procedure was performed:

The synthesis of $[(C_6H_5)_3Sn(4\text{-}OCOC_6H_4NH_2)]$ (2)

A total of 1.1010 g compound **1** in 20 mL of methanol was reacted with 0.4114 g 4-aminobenzoate acid $[(C_6H_4(COOH)NH_2]$ in 10 mL of methanol (mole ratio was 1:1) and they were refluxed for 4 hours at 60-61 °C. The water formed in the synthesis process was separated by a Dean and Stark apparatus. The remaining methanol solvent was evaporated by putting the synthesized solution into a vial and covered with aluminium foil that had been perforated and stored in a desiccator until it was obtained. The same procedure was applied in the preparation of compound **3**. The compounds synthesized obtained were as follows:

$[Ph_3Sn(4\text{-}HABz)]$ (**2**): white solid; UV $\lambda_{max.}$ (MeOH) nm (log ε): 234 and 293; IR $\nu_{max.}$ (KBr) cm^{-1}: 3437.3 (OH), 1624.7 (C=O), 1632.9 (CO_2 asym), 1551.8; 730.8 (phen), 1290.1 (Sn-O-C), 726.4 (Sn-O); ^{1}H-NMR (in DMSO-D_6, 600 MHz) δ (ppm): H_2= H_6 7.59 (d, 6H); H_3 & H_5 7.46 (t, 6H); H_4: 7.33 (t, 3H), H in benzoate: H_9= 7.83 (s); H_{11}=7.60 (d); H_{12}= 7.60 (d); H_{13} = 7.60 (d); ^{13}C-NMR (in DMSO-D_6, 150 MHz): δ (ppm): C(phen) C_2 & C_6= 131.7, C_3 & C_5= 129.2 , C_4= 126.9; C_7= 165.3; C_8= 137.2; C_9 = 132.9; C_{10} = 129.5; C_{11}= 128.4; C_{12}=128.2; C_{13}= 130.0; microelemental analysis: found (calculated): C 60.79 (61.60), H 4.02 (4.11).

$Ph_3Sn(4\text{-}HNBz)]$ (**3**): white solid; UV $\lambda_{max.}$ (MeOH) nm (log ε): 234 and 293; IR $\nu_{max.}$ (KBr) cm^{-1}: 3437.3 (OH), 1624.7 (C=O), 1632.9 (CO_2 asym), 1551.8; 730.8 (phen), 1290.1 (Sn-O-C), 726.4 (Sn-O); ^{1}H-NMR (in DMSO-D_6, 600 MHz) δ (ppm): H_2= H_6 7.59 (d, 6H); H_3 & H_5 7.46 (t, 6H); H_4: 7.33 (t, 3H), H in benzoate: H_9= 7.83 (s); H_{11}=7.60 (d); H_{12}= 7.60 (d); H_{13} = 7.60 (d); ^{13}C-NMR (in DMSO-D_6, 150 MHz): δ (ppm): C(phen) C_2 & C_6= 131.7, C_3 & C_5= 129.2 , C_4= 126.9; C_7= 165.3; C_8= 137.2; C_9 = 132.9; C_{10} = 129.5; C_{11}= 128.4; C_{12}=128.2; C_{13}= 130.0; microelemental analysis: found (calculated): C 60.79 (61.60), H 4.02 (4.11).

Disinfectant Bioactivity Test

The disinfectant bioactivity test was carried using procedure similar to the previous work (11) and as follows: Bacterial inoculum was made by taking one ose of rejuvenated S. *aureus* and S. *typhosa*, each bacteria was placed into 2 different Erlenmeyer flasks containing 100 mL of sterile Nutrient Broth media, and then they were shaker at room temperature for 24 hours. The optical density was measured at a wavelength of 600 nm using a UV-Visible Spectrophotometer. The tested solutions were prepared with varying concentrations of $5x10^{-3}$, $1x10^{-3}$, and $5x10^{-4}$ M and 5 mL of each compounds tested were placed into three different test tubes. Each tube was added with 500 µL of S. *aureus* and S. *typhosa* inoculums and then vortexed. At contact times of 0, 5, 10, and 15 minutes, the optical density of this mixture was measured using a UV-Visible Spectrophotometer instrument. Then, the same treatment was also carried out with a solution of methanol added with 5% dimethyl sulfoxide as a negative control, and a positive control solution of Wipol (2.5% pine oil).

RESULTS AND DISCUSSION

The synthesis of organotin(IV) compound

Two organotin(IV) compounds, triphenyltin(IV) 4-aminobenzoate (**2**) and triphenyltin(IV) 4-nitrobenzoate (**3**) compound were obtained as yellow and white solid, respectively have been successfully synthesized from the reaction of compound **1** with 4-HABz and 4-HNBz based on the procedures described in the literature [8-12, 14, 17, 29]. The schematic reaction for the synthesis of compounds **2** and **3** are shown in Figure 1, the products of the synthesis for compounds **2** and **3** were 84.09% and 80.70%, respectively.

(a)

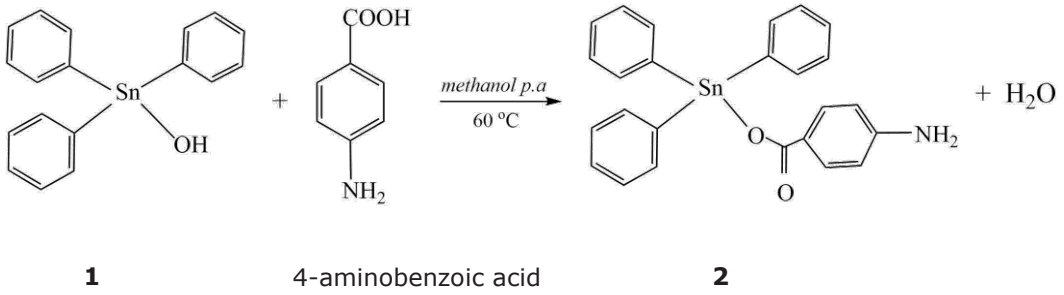

1 4-aminobenzoic acid **2**

(b)

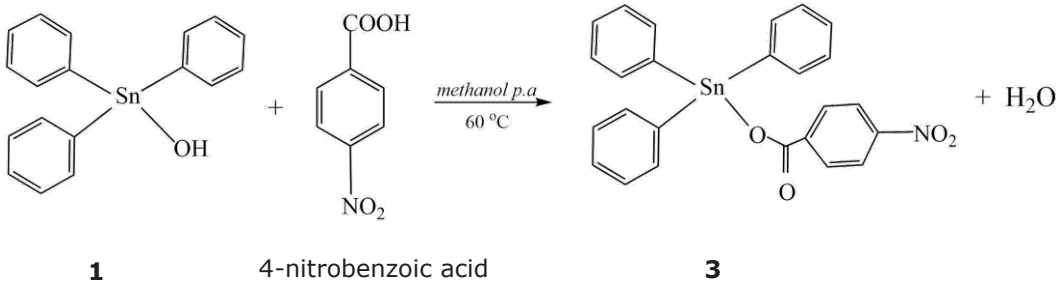

1 4-nitrobenzoic acid **3**

Figure 1: *The prepration of (a) compound* **2**; *(b) compound* **3**.

Characterization of Organotin(IV) Compounds

The success of the synthesis the targeted compounds was analyzed using some spectroscopy techniques. The result of IR characterization was proven by the appearance and disappearance of certain characteristic peaks (Table 1). The appearance of the characteristic absorption in the two target compounds **2** and **3** is the presence of peak in the regions of 782.07 cm^{-1} and 723.53 cm^{-1} which are characteristics for the vibration of the Sn-O bond, and it is supported with the peaks from Sn-O-C bond in 1177.08 cm^{-1} and 1170. 04 cm^{-1} which indicated that the central atom of tin (Sn) has been bonded to the ligands of 4-HABz and 4-HNBz via oxygen (O) atom (19, 24).

Table 1. Absorption characteristics of important groups in the synthesized compound

Compound	Analysis (cm^{-1})		References (cm^{-1})
	(2)	(3)	(19, 24)
Sn-O	782.07	723.53	800-400
Sn–O–C	1177.08	1170.04	1250-1000
CO_2 asymmetry	1528.02	1520.08	1600-1400
C-O	1602.08	1600.23	1760-1600
C-H aromatic	3049.00	3047.20	3100-3000
N-H	3473.09	-	3500-3300
N–O	-	1334.40	1400-1300

The UV spectroscopic analysis produced the maximum wavelength (λ_{max}) of the compound measured and the results in this work are presented in Table 2. From these data, there are several important shifts for each compound. The two compounds give two main characteristic bands of π→π* and n→π* transitions. For example, in compound **1**, there is π→π* transition at 234 nm, after conversion **1** to **2** there are changes in λ_{max} for the n→π* transition to 234 and 278 nm. The presence of a bathochromic shift is an indication that the substitution of ligand has occurred at the central atom because the 4-HABz ligand is a chromophore molecule, with the presence of a –C=O group and a -C=C- bond which causes a shift in wavelength towards a longer one and the effect of auxochrome with the presence of the $-NH_2$ group. Compound **3** also undergoes a change in max for the n→π* transition to 234 and 290 nm originating from the free electrons of O atoms such as $-NO_2$ and –COOH groups from 4-HNBz ligand.

Table 2. The changes in the maximum wavelength (λ_{max}) of organotin compounds.

Compound	λ_{maks} (nm)	
	π→π*	n→π*
$[(C_6H_5)_3SnOH]$ (**1**)	234	-
$[(C_6H_5)_3(C_6H_4(4\text{-}NH_2)COO]$ (**2**)	234	278
$[(C_6H_5)_3(C_6H_4(4\text{-}NO_2)COO]$ (**3**)	234	290

Table 3 presents the NMR spectra of the compounds synthesized were closely analyzed to ascertain the successful in the synthesis of compounds **2** and **3**. The typical chemical shifts for compounds **2** and **3** prepared were characterized carefully and compared to the data available in the literature (8-12, 14, 17, 19, 30). Based on the data of ^{1}H NMR spectrum for compound **2**, the chemical shifts of phenyl protons attached to tin metal appeared as expected in the range of 7.40 for H_2 and H_6 to 7.46 ppm for H_3 and H_5, while the protons in benzoate ring appeared at 7.79-7.81 ppm. The ^{13}C NMR values of the compounds synthesized were close to the values reported by others (8-12, 14, 17, 19, 30). The analyses are as follows the carbon in the carboxyl group as expected appeared in the region of 164 ppm. The δ of carbons in the phenyl ligand in compounds **2** and **3** are at 126.9-131.8 ppm and the carbons in the benzoate are in δ range of 129.1-132.9 ppm (8-12, 14, 17, 19, 30).

Table 3. ^{1}H (600 MHz, DMSO-d6) and ^{13}C (150 MHz, DMSO-d6) spectra of the triphenyltin(IV) compounds synthesized

Compound	H in phenyl (ppm)	H in benzoate (ppm)	C in phenyl and benzoate (ppm)
2	H2 & H6 7.41 (6H, d, Ar-H); H3 &H5 7.46 (6H, d, Ar-H)	7.79-7.81 (4H, m, Ar-H)	131.6 (C2 & C6 Ar-C), 129.1(C3 & C5 Ar-C), C4= 126.9; 163.8 (C7 C=O); 135.9 (C8 Ar-C Benzoate); 130.2 (C9 & C13 Ar-C Benzoate); 129.1 (C10 & C12 Ar-C Benzoate); 129.5 (C11 Ar-C Benzoate)
3	H2&H6 7.47 (6H, d, Ar-H); H3&H5 7.49 (6H, d, Ar-H)	7.84-7.86 (4H, m, Ar-H)	131.8 (C2 & C6 Ar-C); 129.5 (C3 & C5 Ar-C), 127.3 (C4 Ar-C); 164.5 (C7 C=O); 136.9 (C8 Ar-C Benzoate); 130.5 (C9 & C13 Ar-C Benzoate); 129.3 (C10 & C12 Ar-C Benzoate); 129.8 (C11 Ar-C Benzoate)

The disinfectant bioactivity tests for compounds **2** and **3** at variation concentrations of $5x10^{-3}$, $1x10^{-3}$, and $5x10^{-4}$ M, solvent as negative control, and positive control with contact times of 0, 5, 10 and 15 minutes were carried. This is performed to find out the optical density of the disinfectant solutions that show the ability to inhibit the bacterial growth (Tables 4-6). The result clearly showed that compounds **2** and **3** have strong antibacterial activity against Gram-positive *S. aureus* and Gram-negative *S. typhosa* bacteria.

Table 4. The OD values of compounds **2** against *S. aureus* and *S. typhosa*

Type of bacteria	**Results**											
	5 x 10^{-3} M				**1 x 10^{-3} M**				**5 x 10^{-4} M**			
	0′	5′	10′	15′	0′	5′	10′	15′	0′	5′	10′	15′
S. aureus **($A_{initial}$ = 0.655)**	0.585	0.480	0.420	0.375	0.301	0.210	0.218	0.122	0.256	0.226	0.185	0.110
S.typhosa **($A_{initial}$ = 0.661)**	1.112	0.452	0.330	0.133	0.300	0.252	0.260	0.110	0.235	0.193	0.195	0.102

Table 5. The OD values of compound **3** against *S. aureus* and *S. typhosa*

Type of bacteria	**Results**											
	5 x 10^{-3} M				**1 x 10^{-3} M**				**5 x 10^{-4} M**			
	0′	5′	10′	15′	0′	5′	10′	15′	0′	5′	10′	15′
S. aureus **($A_{initial}$ = 0.655)**	0.200	0.160	0.113	0.075	0.135	0.127	0.085	0.070	0.127	0.082	0.065	0.025
S.typhosa **($A_{initial}$ = 0.661)**	0.172	0.157	0.110	0.080	0.113	0.089	0.077	0.045	0.089	0.073	0.055	0.032

The compounds **2** and **3** have strong activity as a disinfectant, which characterized by the decrease in the absorbance value with variations from the maximum concentration to the minimum concentration where the longer the contact time to the disinfectant agent, the more disinfectant agent was absorbed by bacteria, and because of this process causing the destruction of bacteria and inhibits the growth of these bacteria, so that the absorbance value will decrease (11).

Compounds **2** and **3** were more capable in inhibiting *S. aureus* than *S. typhosa*, this was indicated by a greater decrease in the absorbance value when these compounds were tested against *S. aureus* bacteria. The difference in the decrease of absorbance values is because the two bacteria have different sensitivities and it was fount that *S. aureus* has a higher sensitivity than *S. typhosa*. This is due to fact that the differences in the structure of the cell walls of the two bacteria, causing differences in the decrease of optical density to the compounds tested in the intracellular bacteria. Gram positive bacteria *S. aureus* has a greater sensitivity level than Gram negative bacteria *S. typhosa* because the cell wall of Gram negative bacteria *S. typhosa* is composed of an outer membrane, an inner membrane and peptidoglycan with a more complex structure than that of Gram-positive bacteria (31-33).

Based on the test results, compound **3** has activity as a better disinfectant because it is characterized by a greater decrease in absorbance value than compound **2**, this is because compound **3** has the effect of electron withdrawing anion (NO_2) which causes the central atom of Sn to become more positive, so it is easier to penetrate the peptidoglycan layer on the bacterial cell wall which is electronegative, causing inhibition of bacterial cell growth.

Table 6. The OD values of solvent and positive control against S. *aureus* and S. *typhosa*

Compound	Results							
	S. *aureus* ($A_{initial}$ = 0.655)				S. *typhosa* ($A_{initial}$ = 0.661)			
	0′	5′	10′	15′	0′	5′	10′	15′
P	0.522	0.494	0.492	0.490	0.598	0.486	0.480	0.484
KP	0.651	0.596	0.572	0.570	0.638	0.624	0.599	0.594

Note:
P = solvent as negative control
KP = positive control

The results of the bioactivity test of organotin disinfectant with a comparison of solvent as negative control and positive control against S. *aureus* and S.*typhosa* bacteria showed that both organotin compounds **2** and **3** had activity as effective disinfectants, compared to solvents and positive control characterized by a greater decrease in absorbance. large compared to the decrease in absorbance of the solvent and positive control. The MIC value (Minimum Inhibitory Concentration) of the two organotin compounds tested against S. *aureus* and S. *typhosa* was $5x10^{-4}$ M. This MIC value is stronger than fractions obtained from the stem roots extracts of *Archidendron jiringa* (34) or other synthetic products reported by others (35). The most effective contact time to inhibit the growth of the test bacteria was 15 minutes. This proves that the length of contact time has an effect on the magnitude of the inhibition of growth and reproduction of bacteria.

CONCLUSIONS

The synthesis of two organotin(IV) compounds, triphenyltin(IV) 4-aminobenzoate (**2**) and triphenyltin(IV) 4-nitrobenzoate (**3**) has been successfully carried out. The synthesized compounds, the ligands and the starting compounds **1** have been tested for their antibacterial activity. Based on optical density data, compound **3** showed the best antibacterial activity at a minimum inhibitory concentration value of $5x10^{-4}$ M and the most effective contact time to inhibit the growth of the test bacteria was 15 minutes. Organotin compounds **2** and **3** have activity as effective disinfectants, compared to the ligands, starting compound and positive control characterized by a greater decrease in absorbance compared to other substances during the test.

ACKNOWLEDGMENTS

The authors would like to thank to the Institute of Research and Community Services, Universitas Lampung as well as Directorate of Research and Community Services, The Ministry of Education, Cultural, Research and Technology, Indonesia for the funding through Penelitian Dasar (Basic Research Grant Scheme) 2022 with contract numbers of 027/E5/PG.02.00/PT/2022, dated March 16, 2022 and 2143/UN26.21/PN/2022 dated April 29, 2022.

CONFLICTS OF INTEREST

The authors declare no conflicts of interest

REFERENCES

1. Tenglan PA. The goals of health work: Quality of life, health and welfare. *Med. Health Care Philos.* 2013; 9: 155-67.
2. Rai SK. Changing Trend of Infectious Diseases in Nepal. In: Adhikari R., Thapa S. (eds) Infectious Diseases and Nanomedicine III. Singapore: *Adv. Expe. Med. Biol., Springer*. 2018; 1052: 19-38.
3. Shears P. Resistance as a worldwide problem. In Bacterial Resistance to Antimicrobials, Eds: Wax, R.G., Lewis K, Salyers AA, Taber H. Boca Raton: *CRC Press*. 2008; pp. 364-73.
4. Peggy T. Bacteria and Viruses. London: *The Lucent Library of Sciences*. 2004; 112 pages.
5. Amala S, Ejikema I. Bacteria Associated with the Mobile Phones of Medical Personel. *Am. J. Biomed. Sci.* 2015; 7: 26-32.
6. Koh D. Occupational risks for COVID-19 infection. *Occup. Med.* 2020; 70(1): 3–5.
7. Mantravadi PK, Kalesh KA, Dobson RCJ, Hudson AO, Parthasarathy A. The Quest for Novel Antimicrobial Compounds: Emerging Trends in Research, Development, and Technologies. *Antibiot*. 2019; 8(8): 1–34.
8. Hadi S, Lestari S, Suhartati T, Qudus HI, Rilyanti M, Herasari D, Yandri Y. Synthesis and Comparative Study on the Antibacterial Activity Organotin (IV) 3-hydroxybenzoate Compounds. *Pure Appl. Chem*. 2021; 93(5): 623–8.
9. Samsuar S, Simanjuntak W, Qudus HI, Yandri Y, Herasari H, Hadi S. In Vitro Antimicrobial Activity Study of Some Organotin (IV) Chlorobenzoates against Staphylococcus aureus and Escherichia coli. *J. Adv. Pharm. Edu. Res.* 2021; 11(2): 17–22.
10. Hadi S, Samsuar S, Qudus HI, Simanjuntak W. In Vitro Antibacterial Activity of Some of Dibutyltin (IV) Chlorobenzoate Derivatives against *Staphylococcus aureus* and *Escherichia coli*. ARPN *J. Eng. Appl. Sci.* 2021; 16(15): 1623-9.
11. Hadi S, Suhartati T, Noviany N, Pandiangan K, Yandri Y, Simanjuntak W. Disinfecting activity of some diphenyltin (IV) benzoate derivative compounds. *Pure Appl. Chem.* 2022; 94 (in press).
12. Hadi S, Irianti NT, Noviany N. Sintesis, Karakterisasi, dan Uji Aktivitas Antibakteri Senyawa Organotimah(IV) 4-Nitrobenzoat. *Alchemy*. 2022; 18(1): 19-29. (in Indonesian)
13. Rehman W, Badshah A, Khan S, & Tuyet LTA. Synthesis, Characterization, Antimicrobial and Antitumor Screening of Some Diorganotin(IV) Complexes of 2-[(9H-Purin-6-ylimino)]-phenol. *Eur. J. Med. Chem*. 2009; 44 (10): 3981–5.
14. Hadi S, Rilyanti M, Suharso. In Vitro Activity and Comparative Studies of Some Organotin(IV) Benzoate Derivatives Against Leukemia Cancer Cell: L-1210. *Indo. J. Chem*. 2012; 12(2): 172–7.
15. Sirajuddin M, Ali S, Tahir MN. Organotin(IV) Derivatives Based on 2-((2-methoxyphenyl) carbamoyl) Benzoic Acid: Synthesis, Spectroscopic Characterization, Assessment of Antibacterial, DNA Interaction, Anticancer and Antileishmanial Potentials. *J. Mol. Struct*. 2021; 1229: 129600.
16. Uddin N, Rashid F, Haider A, Tirmizi SA, Raheel A, Imran M, Zaib S, Diaconescu PL, Iqbal J, Ali S. Triorganotin(IV) Carboxylates as Potential Anticancer Agents: Their Synthesis, Physiochemical Characterization, and Cytotoxic Activity against HeLa and MCF-7 Cancer Cells. *Appl. Organomet. Chem*. 2021; 35(4): e6165.
17. Hadi S, Noviany, Qudus HI, Wattana-Amorn P. The Potency Study of Organotin(IV) 3-Nitrobenzoate Compounds as Antimalarial Agents. *J. Phys.: Conf. Series*. 2019; 1338: 012012

18. Hansch C, Verma RP. Larvicidal Activities of Some Organotin Compounds on Mosquito Larvae: A QSAR Study. *Eur. J. Med. Chem.* 2009; 44 (1): 260–73.
19. Hadi S, Noviany, Rilyanti M. In Vitro Antimalarial Activity of Some Organotin(IV) 2-Nitrobenzoate Compounds Against Plasmodium falciparum. *Maced. J. Chem. Chem. Eng.* 2018; 37(2): 185–91.
20. Hadi S, Fenska MD, Noviany N, Satria H, Simanjuntak W, Naseer MM. Synthesis and Antimalarial Activity of Some Triphenyltin(IV) Aminobenzoate Compounds against *Plasmodium falciparum*. *Main Metal Group Chem.* 2021; 44(1): 256260.
21. Singh R, Chaudary P, Khausik NK. A Review: Organotin Compounds in Corrosion Inhibition. *Rev. Inorg. Chem.* 2010; 30 (40: 275–94.
22. Hadi S, Afriyani H, Qudus HI, Noviany. The anticorrosion activity of dibutyltin(IV) and diphenyltin(IV) dihydroxybenzoate compounds towards HRP mild steel in NaCl. *J. Chem. Pharm. Res.* 2016; 8 (8): 975-80.
23. Hazani NN, Mohd Y, Ghazali SAISM, Farina Y, Dzulkifli NN. Electrochemical Studies on Corrosion Inhibition Behaviour of Synthesised 2-acetylpyridine 4-ethyl-3-thiosemicarbazone and Its Tin(IV) Complex for Mild Steel in 1 M HCl Solution. *J. Electrochem. Sci. Technol.* 2019; 10 (1): 29-36.
24. Rocha CS, de Morais BP, Rodrigues BL, Donnici CL, de Lima GM, Ardisson JD, Takahashi JA, Bitzer RS. Spectroscopic and X-ray Structural Characterization of New Organotin Carboxylates and Their In Vitro Antifungal Activities. *Polyhedron.* 2016; 117: 35–47.
25. Baul TSB. Antimicrobial Activity of Organotin(IV) Compounds: A Review. *Appl. Organomet. Chem.* 2008; 22 (4): 195–204.
26. Hadi S, Hermawati E, Noviany, Suhartati T, Yandri Y. Antibacterial Activity Test of Diphenyltin(IV) Dibenzoate and Triphenyltin(IV) Benzoate Compounds against Bacillus substilis and Pseudomonas aeruginosa. *Asian J. Microbiol. Biotechnol. Env. Sci.* 2018; 20 (1): 113–9.
27. Ahmed S, Ali S, Ahmed, Bhatti, MH, Badshah A, Mazhar M, Khan KM. Synthesis, Spectroscopic Characterization, and Biological Applications of Organotin(IV) Derivatives of 2-(N-Maleoyl)-3-Phenylpropanoic Acid. *Synth. React. Inorg. Met.-Org. Chem.* 2002; 32 (8): 1521–36.
28. Pellerito L, Nagy L. Organotin(IV)$^{n+}$ Complexes Formed with Biologically Active Ligands: Equilibrium and Structural Studies, and Some Biological Aspects. *Coord. Chem. Rev.* 2002; 224 (1-2): 111–50.
29. Szorcsik A, Nagy L, Gadja-Schrantz K, Pellerito L, Nagy E, Edelmann ET. Structural Studies on Organotin(IV) Complexes Formed with Ligands Containing {S, N, O} Donor Atoms. *J. Radioanal. Nucl. Chem.* 2002; 252 (3): 523-30.
30. Hadi S, Appleton TG. Reactions of the First Cisplatin Hydrolytes cis-[Pt($^{15}NH_3$)$_2$(H_2O)Cl]$^+$ with L-Cysteine. *Pol. J. Chem.* 2009; 83 (3): 437–43.
31. Pelczar MJ, Chan ECS. Elements of microbiology. Auckland: *McGraw-Hill.* 1981; 698 pages.
32. Lorian V. Antibiotics in Laboratory Medicine, pp. Baltimore. London: *William and Wilkins Co.* 1980; 1–22, 170–178, 511–512.
33. Amsterdam D. Antibiotics in Laboratory Medicine; 6th ed. Philadelphia: *LWW Publisher.* 2014; 807.
34. Noviany, Sialdian D, Setiawan A, Irawan B, Azmi MN, Hadi S. Bioassay-Guided Separation Approach for Characterization of New Antibacterial Fractions from the Stem Roots Extracts of *Archidendron jiringa*. *J. Turk. Chem. Soc. Sect. A: Chem.* 2021; 8 (2): 393-404.
35. Sulaiman M, Hassan Y, Taşkın-Tok T, Noundou XS. Synthesis, Antibacterial Activity and Docking Studies of Benzyl Alcohol Derivatives. *J. Turk. Chem. Soc. Sect. A: Chem.* 2020;7 (2):481–8.

THE RELATIONSHIP OF MULTISET, STIRLING NUMBER AND CATALAN NUMBER

Attiya Yuliana[1,2], Wamiliana[1,*], Fitriani[1]

[1]Dept. of Mathematics, FMIPA, Universitas Lampung, Indonesia.
[2]Senior High School 1, Gedung Tataan, Pesawaran, Indonesia.
Email: wamilianakhan@gmail.com

Abstract

Catalan numbers is not as famous as Fibonacci numbers, however this number has own its beauty and arts. Catalan numbers was discovered by Ming Antu in 1730, however, this numbers is credited to Eugene Catalan when he was studying parentheses in 1838. Catalan numbers mostly occurs in counting or enumeration problems. The Catalan numbers can be defined in more than one forms, and the most famous form is $C_n = \frac{1}{n+1}\binom{2n}{n}$. In this study we will discuss the multiset construction and the relationship of the results of Multiset with Stirling and Catalan numbers.

Keywords: *Counting*, *Enumeration*, *Multiset*, *Catalan numbers*, *Stirling numbers.*

1. INTRODUCTION

In mathematics, there are many types of sequence of numbers. Each sequence has its own definition, uniqueness and benefits. For example, a very famous number sequence, namely the Fibonacci number sequence, which has a uniqueness, namely the Golden Ratio and its benefits have also been widely applied in life. Catalan numbers are not as popular as the Fibonacci numbers, but this sequence of numbers also has many benefits. Catalan numbers were introduced by Eugene Charles Catalan in 1838 when he observed the sequences of parentheses (Koshy, 2009). In addition to brackets, other forms related to Catalan numbers are the triangular forms of the convex polygon (Cayley, 1891). Other geometric shapes that turn out to form Catalan numbers include the combination of the Laticce Path based on Catalan numbers (Saracevis et al, 2018). Catalan numbers are also used to solve the pill problem (Bayer and Brandt, 2015). So, actually there are a lot of benefits from the Catalan numbers themselves. In addition, Catalan numbers have also been widely applied in various fields, such as engineering, in computational geometry, geographic information systems, cryptographic geodesy, and medicine (Selimi, 2019).

Catalan numbers are named after the Belgian scientist Eugene C. Catalan based on his work while studying parentheses sequences in 1838. The parentheses in question are sequences that are well formed form parentheses (Pak, 2014). Actually in 1730 Ming Antu had discovered the Catalan Numbers based on the geometrical models constructed, however because the results were in China and not known in the Western world, Catalan was bettern known, and the numbers are called as Catalan Numbers. This number is unique in that it can be defined in several forms and the most famous form is

$C_n = \frac{1}{n+1}\binom{2n}{n}$. The specialty of Catalan numbers is that they often appear in different problems with different solutions, but have the same final solution, namely Catalan numbers. One of the problems whose solution is Catalan numbers is the problem of Catalan numbers in Algebra, namely the Parker permutation problem. This problem was published by Parker in 1993. In the book Catalan numbers and their applications written by T. Koshy it was informed that this problem had been answered by Ira M. Gessel of Brandies University, Waltham, Massachusetts in 1993, by providing a solution in determining the number of multisets with n-elements $\{a_1, a_2, a_3, \ldots, a_n\}$ are members of $a_i \in Z_n$ such that $a_1 + a_2 + a_3 + \ldots + a_n$ = is the identity of the sum Z_n (Koshy, 2009).

In this study we will discuss the multisets of Group Additive $\mathbb{Z}_n$ with $1 \leq n \leq 10$, and shows the ralations of those multisets with Bell Numbers, Stirling Numbers, and Catalan Numbers.

2. THE METHOD

Multiset

A multiset, as opposed to a regular set, is a set with repeated elements, for example a multiset of integers {1,3,3,3,4,5} which has duplicate elements.

Let S be a non-empty set. A multiset M from a set S is an ordered pair:
$M = \{(s_i, n_i) | s_i \in S, n_i \in \mathbb{Z}^+, s_i \neq s_j \text{ for } i \neq j\}$, where $\mathbb{Z}^+ = \{1,2,\ldots\}$, n_i is called as the multiplicity of elemen s_i in M. If the underlying set is finite, the multiset is called finite. The size of a finite multiset M is defined as the sum of the multiplicities of all of its elements (Roman, 2008). For example, M = {(*p*,3), (*q*,1), (*r*,2)} is a multiset of underlying set S = {*p*, *q*, *r*} in which element *p* has multiplicity 3, *q* has multiplicity 1 and *r* has multiplicity 2. Another way to write this multiset is by writting out all elements according the multiplicities, for above example write M as M= {*p*, *p*, *p*, *q*, *r*, *r*}.

The following table shows the example of possible multiset with n elements of additive group $\mathbb{Z}_{n+1}$, $1 \leq n \leq 4$ (Koshy,2009)

Table 1. The number of multisets with n elements of group $\mathbb{Z}_{n+1}$, $1 \leq n \leq 4$

n	$\mathbb{Z}_{n+1}$	*Multiset* with n-elements	The number of multisets
1	$\{\bar{0}, \bar{1}\}$	$\{\bar{0}\}$	1
2	$\{\bar{0}, \bar{1}, \bar{2}\}$	$\{\bar{0}, \bar{0}\}$ $\{\bar{1}, \bar{2}\}$	2
3	$\{\bar{0}, \bar{1}, \bar{2}, \bar{3}\}$	$\{\bar{0}, \bar{0}, \bar{0}\}$ $\{\bar{0}, \bar{1}, \bar{3}\}$ $\{\bar{0}, \bar{2}, \bar{2}\}$ $\{\bar{1}, \bar{1}, \bar{2}\}$ $\{\bar{2}, \bar{3}, \bar{3}\}$	5
4	$\{\bar{0}, \bar{1}, \bar{2}, \bar{3}, \bar{4}\}$	$\{\bar{0}, \bar{0}, \bar{1}, \bar{4}\}$ $\{\bar{0}, \bar{0}, \bar{2}, \bar{3}\}$ $\{\bar{0}, \bar{1}, \bar{1}, \bar{3}\}$ $\{\bar{0}, \bar{1}, \bar{2}, \bar{2}\}$ $\{\bar{0}, \bar{2}, \bar{4}, \bar{4}\}$ $\{\bar{0}, \bar{3}, \bar{3}, \bar{4}\}$ $\{\bar{1}, \bar{1}, \bar{1}, \bar{2}\}$ $\{\bar{1}, \bar{1}, \bar{4}, \bar{4}\}$ $\{\bar{1}, \bar{2}, \bar{3}, \bar{4}\}$ $\{\bar{1}, \bar{3}, \bar{3}, \bar{3}\}$ $\{\bar{2}, \bar{2}, \bar{2}, \bar{4}\}$ $\{\bar{2}, \bar{2}, \bar{3}, \bar{3}\}$ $\{\bar{3}, \bar{4}, \bar{4}, \bar{4}\}$	14

Catalan numbers

There are some definitions regarding Catalan numbers. However, the most famous way of defining Catalan numbers is (Koshy, 2009):

$$C_n = \frac{1}{n+1}\binom{2n}{n} \text{ where } n \geq 0, n \in \mathbb{Z}^+ \quad (1)$$

The next three equations are other forms of Catalan numbers:

$$C_n = \frac{(2n)!}{(n+1)!n!}. \quad (2)$$

$$C_n = \binom{2n}{n} - \binom{2n}{n-1} \quad (3)$$

$$C_n = \frac{4n-2}{n+1} C_{n-1} \ , C_0 = 1, \ n \geq 1 \quad (4)$$

Bell Numbers

A partition of a set S is a collection of non-empty subsets $A_i \subseteq S, 1 \leq i \leq k$, such that $\bigcup_{i=1}^{k} A_i = S$ and for every $i \neq j$ $A_i \cap A_j = \emptyset$. Bell number B_n is the number of partitions of an n-element set and is defined as: $B_n = \sum_{k=0}^{n} S(n,k)$. Since $B_n = 1$, then $B_{n+1} = \sum_{k=0}^{n} \binom{n}{k} B_k$. For example, B_2 = 2 because the 2-element set {a, b} can be partitioned in 2 distinct ways: {a, b}, and {{a}, {b}}, and B_3 = 5, because there are 5 different partitions of 3-element set {a,b,c} which are: {{a}, {b}, {c}}, {{a,b}, {c}}, {{a,c},{b}}, {{b, c}, {c]}, and {a, b, c}.

Striling Numbers

Stirling numbers appear in a variety of combinatorial situations. Stirling numbers are classified into two kinds: Stirling numbers of the first kind and Stirling numbers of the second kind.

The Stirling number of the first kind $c(n,k)$ is the number of permutations of an n -elemen set with exactly k cycles. Second-kind stirring number $S(n, k)$ counts the number of ways that n distinct objects can be partitioned into k indistinguishable subsets, with each subset containing at least one object. According to Riordan (2002), Stirling numbers of the first kind is $s(n, k)$, where $s(n, k)$ satisfies the recursion relation $s(n,k)=(n-1)\ \ s(n-1, k)+\ \ s(n-1, k-1)$, where k and n are integers, $1 \leq n \leq k-1$ with initial conditions $s(n, 0)=0$, for n≥1 and $s(n, n)=1$, for $n \geq 0$.

3. RESULTS AND DISCUSSION

Before discussing the relationship of multisets, Stirling numbers, Bell numbers and Catalan numbers, we give the following definition about partitions of numbers. Let N, M, n integers, the partition p(N,M,n) denote the number partitions of n into at most M parts and each partition ≤ N.

Based on the analysis of the enumeration results in Table 1, the multiset of the additive group $\mathbb{Z}_{n+1}$ formed can be grouped into several blocks, where the number of multiset elements in the block is a multiplication of n+1. The following will give a multiset table of the additive group $\mathbb{Z}_{n+1}$ with $1 \leq n \leq 7$, divided by block. For $n > 7$ can be obtained by using algorithms and computer programs using Python.

Table 2. Multiset of additive group $\mathbb{Z}_{n+1}$ with $1 \leq n \leq 7$ with n − 1 block

n	$\mathbb{Z}_{n+1}$	k	Multiset	The number of Multiset	Total
1	$\{\bar{0}, \bar{1}\}$	0	$\{\bar{0}\}$	1	1
2	$\{\bar{0}, \bar{1}, \bar{2}\}$	0	$\{\bar{0}, \bar{0}\}$	1	2
		1	$\{\bar{1}, \bar{2}\}$	1	
3	$\{\bar{0}, \bar{1}, \bar{2}, \bar{3}\}$	0	$\{\bar{0}, \bar{0}, \bar{0}\}$	1	5
		1	$\{\bar{0}, \bar{1}, \bar{3}\}$ $\{\bar{0}, \bar{2}, \bar{2}\}$ $\{\bar{1}, \bar{1}, \bar{2}\}$	3	
		2	$\{\bar{2}, \bar{3}, \bar{3}\}$	1	
4	$\{\bar{0}, \bar{1}, \bar{2}, \bar{3}, \bar{4}\}$	0	$\{\bar{0}, \bar{0}, \bar{0}, \bar{0}\}$	1	14
		1	$\{\bar{0}, \bar{0}, \bar{1}, \bar{4}\}$ $\{\bar{0}, \bar{0}, \bar{2}, \bar{3}\}$ $\{\bar{0}, \bar{1}, \bar{1}, \bar{3}\}$ $\{\bar{0}, \bar{1}, \bar{2}, \bar{2}\}$ $\{\bar{1}, \bar{1}, \bar{1}, \bar{2}\}$	5	
		2	$\{\bar{0}, \bar{2}, \bar{4}, \bar{4}\}$ $\{\bar{0}, \bar{3}, \bar{3}, \bar{4}\}$ $\{\bar{1}, \bar{1}, \bar{4}, \bar{4}\}$ $\{\bar{1}, \bar{2}, \bar{3}, \bar{4}\}$ $\{\bar{1}, \bar{3}, \bar{3}, \bar{3}\}$ $\{\bar{2}, \bar{2}, \bar{2}, \bar{4}\}$ $\{\bar{2}, \bar{2}, \bar{3}, \bar{3}\}$	7	
		3	$\{\bar{3}, \bar{4}, \bar{4}, \bar{4}\}$	1	

n	$\mathbb{Z}_{n+1}$	k	Multiset	The number of Multiset	Total
5	$\{\bar{0},\bar{1},\bar{2},\bar{3},\bar{4},\bar{5}\}$	0	$\{\bar{0},\bar{0},\bar{0},\bar{0},\bar{0}\}$	1	42
		1	$\{\bar{0},\bar{0},\bar{0},\bar{1},\bar{5}\}$ $\{\bar{0},\bar{0},\bar{0},\bar{2},\bar{4}\}$ $\{\bar{0},\bar{0},\bar{0},\bar{3},\bar{3}\}$ $\{\bar{0},\bar{0},\bar{1},\bar{1},\bar{4}\}$ $\{\bar{0},\bar{0},\bar{1},\bar{2},\bar{3}\}$ $\{\bar{0},\bar{0},\bar{2},\bar{2},\bar{2}\}$ $\{\bar{0},\bar{1},\bar{1},\bar{1},\bar{3}\}$ $\{\bar{0},\bar{1},\bar{1},\bar{2},\bar{2}\}$ $\{\bar{1},\bar{1},\bar{1},\bar{1},\bar{2}\}$	9	
		2	$\{\bar{0},\bar{0},\bar{2},\bar{5},\bar{5}\}$ $\{\bar{0},\bar{0},\bar{3},\bar{4},\bar{5}\}$ $\{\bar{0},\bar{0},\bar{4},\bar{4},\bar{4}\}$ $\{\bar{0},\bar{1},\bar{1},\bar{5},\bar{5}\}$ $\{\bar{0},\bar{1},\bar{2},\bar{4},\bar{5}\}$ $\{\bar{0},\bar{1},\bar{3},\bar{3},\bar{5}\}$ $\{\bar{0},\bar{1},\bar{3},\bar{4},\bar{4}\}$ $\{\bar{0},\bar{2},\bar{2},\bar{4},\bar{4}\}$ $\{\bar{0},\bar{2},\bar{2},\bar{3},\bar{5}\}$ $\{\bar{0},\bar{2},\bar{3},\bar{3},\bar{4}\}$ $\{\bar{0},\bar{3},\bar{3},\bar{3},\bar{3}\}$ $\{\bar{1},\bar{1},\bar{1},\bar{4},\bar{5}\}$ $\{\bar{1},\bar{1},\bar{2},\bar{3},\bar{5}\}$ $\{\bar{1},\bar{1},\bar{2},\bar{4},\bar{4}\}$ $\{\bar{1},\bar{1},\bar{3},\bar{3},\bar{4}\}$ $\{\bar{1},\bar{2},\bar{2},\bar{2},\bar{5}\}$ $\{\bar{1},\bar{2},\bar{2},\bar{3},\bar{4}\}$ $\{\bar{1},\bar{2},\bar{3},\bar{3},\bar{3}\}$ $\{\bar{2},\bar{2},\bar{2},\bar{2},\bar{4}\}$ $\{\bar{2},\bar{2},\bar{2},\bar{3},\bar{3}\}$	20	
		3	$\{\bar{0},\bar{3},\bar{5},\bar{5},\bar{5}\}$ $\{\bar{0},\bar{4},\bar{4},\bar{5},\bar{5}\}$ $\{\bar{1},\bar{2},\bar{5},\bar{5},\bar{5}\}$ $\{\bar{1},\bar{3},\bar{4},\bar{5},\bar{5}\}$ $\{\bar{1},\bar{4},\bar{4},\bar{4},\bar{5}\}$ $\{\bar{2},\bar{2},\bar{4},\bar{5},\bar{5}\}$ $\{\bar{2},\bar{3},\bar{3},\bar{5},\bar{5}\}$ $\{\bar{2},\bar{3},\bar{4},\bar{4},\bar{5}\}$ $\{\bar{2},\bar{4},\bar{4},\bar{4},\bar{4}\}$ $\{\bar{3},\bar{3},\bar{3},\bar{4},\bar{5}\}$ $\{\bar{3},\bar{3},\bar{4},\bar{4},\bar{4}\}$	11	
		4	$\{\bar{4},\bar{5},\bar{5},\bar{5},\bar{5}\}$	1	
		4	$\{\bar{0},\bar{0},\bar{4},\bar{7},\bar{7},\bar{7},\bar{7}\}$ $\{\bar{0},\bar{0},\bar{5},\bar{6},\bar{7},\bar{7},\bar{7}\}$ $\{\bar{0},\bar{0},\bar{6},\bar{6},\bar{6},\bar{7},\bar{7}\}$ $\{\bar{0},\bar{1},\bar{3},\bar{7},\bar{7},\bar{7},\bar{7}\}$ $\{\bar{0},\bar{1},\bar{4},\bar{6},\bar{7},\bar{7},\bar{7}\}$ $\{\bar{0},\bar{1},\bar{5},\bar{5},\bar{7},\bar{7},\bar{7}\}$ $\{\bar{0},\bar{1},\bar{5},\bar{6},\bar{6},\bar{7},\bar{7}\}$ $\{\bar{0},\bar{1},\bar{6},\bar{6},\bar{6},\bar{6},\bar{7}\}$ $\{\bar{0},\bar{2},\bar{2},\bar{7},\bar{7},\bar{7},\bar{7}\}$ $\{\bar{0},\bar{2},\bar{3},\bar{6},\bar{7},\bar{7},\bar{7}\}$ $\{\bar{0},\bar{2},\bar{4},\bar{5},\bar{7},\bar{7},\bar{7}\}$ $\{\bar{0},\bar{2},\bar{4},\bar{6},\bar{6},\bar{7},\bar{7}\}$ $\{\bar{0},\bar{2},\bar{5},\bar{5},\bar{6},\bar{7},\bar{7}\}$ $\{\bar{0},\bar{2},\bar{5},\bar{6},\bar{6},\bar{6},\bar{7}\}$ $\{\bar{0},\bar{2},\bar{6},\bar{6},\bar{6},\bar{6},\bar{6}\}$ $\{\bar{0},\bar{3},\bar{3},\bar{5},\bar{7},\bar{7},\bar{7}\}$ $\{\bar{0},\bar{3},\bar{3},\bar{6},\bar{7},\bar{7},\bar{7}\}$ $\{\bar{0},\bar{3},\bar{4},\bar{4},\bar{7},\bar{7},\bar{7}\}$ $\{\bar{0},\bar{3},\bar{4},\bar{5},\bar{6},\bar{7},\bar{7}\}$ $\{\bar{0},\bar{3},\bar{4},\bar{6},\bar{6},\bar{6},\bar{7}\}$ $\{\bar{0},\bar{3},\bar{5},\bar{5},\bar{5},\bar{7},\bar{7}\}$ $\{\bar{0},\bar{3},\bar{5},\bar{5},\bar{6},\bar{6},\bar{7}\}$ $\{\bar{0},\bar{3},\bar{5},\bar{6},\bar{6},\bar{6},\bar{6}\}$ $\{\bar{0},\bar{4},\bar{4},\bar{4},\bar{6},\bar{7},\bar{7}\}$ $\{\bar{0},\bar{4},\bar{4},\bar{5},\bar{5},\bar{7},\bar{7}\}$ $\{\bar{0},\bar{4},\bar{4},\bar{5},\bar{6},\bar{6},\bar{7}\}$ $\{\bar{0},\bar{4},\bar{4},\bar{6},\bar{6},\bar{6},\bar{6}\}$ $\{\bar{0},\bar{4},\bar{5},\bar{5},\bar{5},\bar{6},\bar{7}\}$ $\{\bar{0},\bar{4},\bar{5},\bar{5},\bar{6},\bar{6},\bar{6}\}$ $\{\bar{0},\bar{5},\bar{5},\bar{5},\bar{5},\bar{5},\bar{7}\}$ $\{\bar{0},\bar{5},\bar{5},\bar{5},\bar{5},\bar{6},\bar{7}\}$ $\{\bar{0},\bar{5},\bar{5},\bar{5},\bar{6},\bar{6},\bar{6}\}$ $\{\bar{1},\bar{1},\bar{2},\bar{7},\bar{7},\bar{7},\bar{7}\}$ $\{\bar{1},\bar{1},\bar{3},\bar{6},\bar{7},\bar{7},\bar{7}\}$ $\{\bar{1},\bar{1},\bar{4},\bar{5},\bar{7},\bar{7},\bar{7}\}$ $\{\bar{1},\bar{1},\bar{4},\bar{6},\bar{6},\bar{7},\bar{7}\}$ $\{\bar{1},\bar{1},\bar{5},\bar{5},\bar{6},\bar{7},\bar{7}\}$ $\{\bar{1},\bar{1},\bar{5},\bar{6},\bar{6},\bar{6},\bar{7}\}$ $\{\bar{1},\bar{1},\bar{6},\bar{6},\bar{6},\bar{6},\bar{7}\}$ $\{\bar{1},\bar{2},\bar{2},\bar{6},\bar{7},\bar{7},\bar{7}\}$ $\{\bar{1},\bar{2},\bar{3},\bar{5},\bar{7},\bar{7},\bar{7}\}$ $\{\bar{1},\bar{2},\bar{3},\bar{6},\bar{6},\bar{7},\bar{7}\}$ $\{\bar{1},\bar{2},\bar{4},\bar{4},\bar{7},\bar{7},\bar{7}\}$ $\{\bar{1},\bar{2},\bar{4},\bar{5},\bar{6},\bar{7},\bar{7}\}$ $\{\bar{1},\bar{2},\bar{4},\bar{6},\bar{6},\bar{6},\bar{7}\}$ $\{\bar{1},\bar{2},\bar{5},\bar{5},\bar{5},\bar{7},\bar{7}\}$ $\{\bar{1},\bar{2},\bar{5},\bar{5},\bar{6},\bar{6},\bar{7}\}$ $\{\bar{1},\bar{2},\bar{5},\bar{6},\bar{6},\bar{6},\bar{6}\}$ $\{\bar{1},\bar{3},\bar{3},\bar{4},\bar{7},\bar{7},\bar{7}\}$ $\{\bar{1},\bar{3},\bar{3},\bar{5},\bar{6},\bar{7},\bar{7}\}$ $\{\bar{1},\bar{3},\bar{3},\bar{6},\bar{6},\bar{6},\bar{7}\}$ $\{\bar{1},\bar{3},\bar{4},\bar{4},\bar{6},\bar{7},\bar{7}\}$ $\{\bar{1},\bar{3},\bar{4},\bar{5},\bar{5},\bar{7},\bar{7}\}$ $\{\bar{1},\bar{3},\bar{4},\bar{5},\bar{6},\bar{6},\bar{7}\}$ $\{\bar{1},\bar{3},\bar{4},\bar{6},\bar{6},\bar{6},\bar{6}\}$ $\{\bar{1},\bar{3},\bar{5},\bar{5},\bar{5},\bar{6},\bar{7}\}$ $\{\bar{1},\bar{3},\bar{5},\bar{5},\bar{6},\bar{6},\bar{6}\}$ $\{\bar{1},\bar{4},\bar{4},\bar{4},\bar{5},\bar{7},\bar{7}\}$ $\{\bar{1},\bar{4},\bar{4},\bar{4},\bar{6},\bar{6},\bar{7}\}$ $\{\bar{1},\bar{4},\bar{4},\bar{5},\bar{5},\bar{6},\bar{7}\}$ $\{\bar{1},\bar{4},\bar{4},\bar{5},\bar{6},\bar{6},\bar{6}\}$ $\{\bar{1},\bar{4},\bar{5},\bar{5},\bar{5},\bar{5},\bar{7}\}$ $\{\bar{1},\bar{4},\bar{5},\bar{5},\bar{5},\bar{6},\bar{6}\}$ $\{\bar{1},\bar{5},\bar{5},\bar{5},\bar{5},\bar{5},\bar{6}\}$	112	

n	$\mathbb{Z}_{n+1}$	k	Multiset			The number of Multiset	Total
			$\{\bar{2},\bar{2},\bar{2},\bar{5},\bar{7},\bar{7},\bar{7}\}$	$\{\bar{2},\bar{2},\bar{2},\bar{6},\bar{6},\bar{7},\bar{7}\}$	$\{\bar{2},\bar{2},\bar{3},\bar{4},\bar{7},\bar{7},\bar{7}\}$		
			$\{\bar{2},\bar{2},\bar{3},\bar{5},\bar{6},\bar{7},\bar{7}\}$				
			$\{\bar{2},\bar{2},\bar{3},\bar{6},\bar{6},\bar{6},\bar{7}\}$	$\{\bar{2},\bar{2},\bar{4},\bar{4},\bar{6},\bar{7},\bar{7}\}$	$\{\bar{2},\bar{2},\bar{4},\bar{5},\bar{5},\bar{7},\bar{7}\}$		
			$\{\bar{2},\bar{2},\bar{4},\bar{5},\bar{6},\bar{6},\bar{7}\}$				
			$\{\bar{2},\bar{2},\bar{4},\bar{6},\bar{6},\bar{6},\bar{6}\}$	$\{\bar{2},\bar{2},\bar{5},\bar{5},\bar{5},\bar{6},\bar{7}\}$	$\{\bar{2},\bar{2},\bar{5},\bar{5},\bar{6},\bar{6},\bar{6}\}$		
			$\{\bar{2},\bar{3},\bar{3},\bar{3},\bar{7},\bar{7},\bar{7}\}$				
			$\{\bar{2},\bar{3},\bar{3},\bar{4},\bar{6},\bar{7},\bar{7}\}$	$\{\bar{2},\bar{3},\bar{3},\bar{5},\bar{5},\bar{7},\bar{7}\}$	$\{\bar{2},\bar{3},\bar{3},\bar{5},\bar{6},\bar{6},\bar{7}\}$		
			$\{\bar{2},\bar{3},\bar{3},\bar{6},\bar{6},\bar{6},\bar{6}\}$				
			$\{\bar{2},\bar{3},\bar{4},\bar{4},\bar{5},\bar{7},\bar{7}\}$	$\{\bar{2},\bar{3},\bar{4},\bar{4},\bar{6},\bar{6},\bar{7}\}$	$\{\bar{2},\bar{3},\bar{4},\bar{5},\bar{5},\bar{6},\bar{7}\}$		
			$\{\bar{2},\bar{3},\bar{4},\bar{5},\bar{6},\bar{6},\bar{6}\}$				
			$\{\bar{2},\bar{3},\bar{5},\bar{5},\bar{5},\bar{5},\bar{7}\}$	$\{\bar{2},\bar{4},\bar{4},\bar{4},\bar{4},\bar{7},\bar{7}\}$	$\{\bar{2},\bar{4},\bar{4},\bar{4},\bar{5},\bar{6},\bar{7}\}$		
			$\{\bar{2},\bar{4},\bar{4},\bar{4},\bar{6},\bar{6},\bar{6}\}$				
			$\{\bar{2},\bar{4},\bar{4},\bar{5},\bar{5},\bar{5},\bar{7}\}$	$\{\bar{2},\bar{4},\bar{4},\bar{5},\bar{5},\bar{6},\bar{6}\}$	$\{\bar{2},\bar{4},\bar{5},\bar{5},\bar{5},\bar{5},\bar{6}\}$		
			$\{\bar{2},\bar{5},\bar{5},\bar{5},\bar{5},\bar{5},\bar{5}\}$				
			$\{\bar{3},\bar{3},\bar{3},\bar{3},\bar{6},\bar{7},\bar{7}\}$	$\{\bar{3},\bar{3},\bar{3},\bar{4},\bar{5},\bar{7},\bar{7}\}$	$\{\bar{3},\bar{3},\bar{3},\bar{4},\bar{6},\bar{6},\bar{7}\}$		
			$\{\bar{3},\bar{3},\bar{3},\bar{5},\bar{5},\bar{6},\bar{7}\}$				
			$\{\bar{3},\bar{3},\bar{3},\bar{5},\bar{6},\bar{6},\bar{6}\}$	$\{\bar{3},\bar{3},\bar{4},\bar{4},\bar{4},\bar{7},\bar{7}\}$	$\{\bar{3},\bar{3},\bar{4},\bar{4},\bar{5},\bar{6},\bar{7}\}$		
			$\{\bar{3},\bar{3},\bar{4},\bar{4},\bar{6},\bar{6},\bar{6}\}$				
			$\{\bar{3},\bar{3},\bar{4},\bar{5},\bar{5},\bar{5},\bar{7}\}$	$\{\bar{3},\bar{3},\bar{4},\bar{5},\bar{5},\bar{6},\bar{6}\}$	$\{\bar{3},\bar{3},\bar{5},\bar{5},\bar{5},\bar{5},\bar{6}\}$		
			$\{\bar{3},\bar{4},\bar{4},\bar{4},\bar{4},\bar{6},\bar{7}\}$				
			$\{\bar{3},\bar{4},\bar{4},\bar{4},\bar{5},\bar{5},\bar{7}\}$	$\{\bar{3},\bar{4},\bar{4},\bar{4},\bar{5},\bar{6},\bar{6}\}$	$\{\bar{3},\bar{4},\bar{4},\bar{5},\bar{5},\bar{5},\bar{6}\}$		
			$\{\bar{3},\bar{4},\bar{5},\bar{5},\bar{5},\bar{5},\bar{5}\}$				
			$\{\bar{4},\bar{4},\bar{4},\bar{4},\bar{4},\bar{5},\bar{7}\}$	$\{\bar{4},\bar{4},\bar{4},\bar{4},\bar{4},\bar{6},\bar{6}\}$	$\{\bar{4},\bar{4},\bar{4},\bar{4},\bar{5},\bar{5},\bar{6}\}$		
			$\{\bar{4},\bar{4},\bar{4},\bar{5},\bar{5},\bar{5},\bar{5}\}$				
		5	$\{\bar{0},\bar{5},\bar{7},\bar{7},\bar{7},\bar{7},\bar{7}\}$	$\{\bar{0},\bar{6},\bar{6},\bar{7},\bar{7},\bar{7},\bar{7}\}$	$\{\bar{1},\bar{4},\bar{7},\bar{7},\bar{7},\bar{7},\bar{7}\}$		
			$\{\bar{1},\bar{5},\bar{6},\bar{7},\bar{7},\bar{7},\bar{7}\}$				
			$\{\bar{1},\bar{6},\bar{6},\bar{6},\bar{7},\bar{7},\bar{7}\}$	$\{\bar{2},\bar{3},\bar{7},\bar{7},\bar{7},\bar{7},\bar{7}\}$	$\{\bar{2},\bar{4},\bar{6},\bar{7},\bar{7},\bar{7},\bar{7}\}$		
			$\{\bar{2},\bar{5},\bar{5},\bar{7},\bar{7},\bar{7},\bar{7}\}$				
			$\{\bar{2},\bar{5},\bar{6},\bar{6},\bar{7},\bar{7},\bar{7}\}$	$\{\bar{2},\bar{6},\bar{6},\bar{6},\bar{6},\bar{6},\bar{7}\}$	$\{\bar{3},\bar{3},\bar{6},\bar{7},\bar{7},\bar{7},\bar{7}\}$		
			$\{\bar{3},\bar{4},\bar{5},\bar{7},\bar{7},\bar{7},\bar{7}\}$				
			$\{\bar{3},\bar{4},\bar{6},\bar{6},\bar{7},\bar{7},\bar{7}\}$	$\{\bar{3},\bar{5},\bar{5},\bar{6},\bar{7},\bar{7},\bar{7}\}$	$\{\bar{3},\bar{5},\bar{6},\bar{6},\bar{6},\bar{7},\bar{7}\}$	26	
			$\{\bar{3},\bar{6},\bar{6},\bar{6},\bar{6},\bar{6},\bar{7}\}$				
			$\{\bar{4},\bar{4},\bar{4},\bar{7},\bar{7},\bar{7},\bar{7}\}$	$\{\bar{4},\bar{4},\bar{5},\bar{6},\bar{7},\bar{7},\bar{7}\}$	$\{\bar{4},\bar{4},\bar{6},\bar{6},\bar{6},\bar{7},\bar{7}\}$		
			$\{\bar{4},\bar{5},\bar{5},\bar{5},\bar{7},\bar{7},\bar{7}\}$				
			$\{\bar{4},\bar{5},\bar{5},\bar{6},\bar{6},\bar{7},\bar{7}\}$	$\{\bar{4},\bar{5},\bar{6},\bar{6},\bar{6},\bar{6},\bar{7}\}$	$\{\bar{4},\bar{6},\bar{6},\bar{6},\bar{6},\bar{6},\bar{6}\}$		
			$\{\bar{5},\bar{5},\bar{5},\bar{5},\bar{6},\bar{7},\bar{7}\}$				
			$\{\bar{5},\bar{5},\bar{5},\bar{6},\bar{6},\bar{6},\bar{7}\}$	$\{\bar{5},\bar{5},\bar{6},\bar{6},\bar{6},\bar{6},\bar{6}\}$			
		6	$\{\bar{6},\bar{7},\bar{7},\bar{7},\bar{7},\bar{7},\bar{7}\}$			1	

We need a computer program to determine a multiset. The following is an algorithm and a computer program for determining all multisets of the additive group $\mathbb{Z}_{n+1}$ using Python.

#Multiset Grup Aditif $\mathbb{Z}_{n+1}$
inisiasi
Input : n, k, n, k integer
Output : Multiset, jumlah multiset, multiset untuk setiap bagian k dan jumlah multiset untuk tiap k.

Implementasi

Begin
Read (n, k)
Set $\mathbb{Z}_{n+1} \leftarrow$ Set $\{0,1,2,\cdots,n\}$
Max $k \leftarrow (0,1,2,\cdots,n-1)$

Target(n, k)
repeat $(n+1) * k$ until Max k

candidates←set(Combination with raplecement ($\mathbb{Z}_{n+1}$, Max k));

targets←[Target $(n, k) for\ k\ in$ max k];

multiset (candidates, targets):
for candidate *in* candidates
if (sum(candidate) in targets)
then add multiset in candidate
repeat multisets until Target (n, k)
multiset← multiset (candidates, targets);

Stirling(multisets, targets)
for multiset in multisets
if (sum(multiset)in targets)
then add stirling in multiset
repeat stirling until Target
$k_2 \leftarrow$ target(n, k) for $k = k$ input;

stirling ← Stirling (multiset, k_2);

print("$\mathbb{Z}_{n+1}$: ", Set$\mathbb{Z}_{n+1}$)
print("k : ", Max k)
print("multisets : ", multisets)
print("Bilangan Stirling k=",k,":", stirling)
print("Jumlah Bilangan Stirling k=",k," : ", len(stirling))
print("Total Bilangan Catalan : ", len(multisets))

End

The following is an example of the output of the above program.

```
PROBLEMS    OUTPUT    DEBUG CONSOLE    TERMINAL

Masukkan Jumlah n:4
Masukkan Jumlah k:2
Zn+1 :  [0, 1, 2, 3, 4]
kList :  [0, 1, 2, 3]
multisets :  [(0, 0, 0, 0), (0, 0, 1, 4), (0, 0, 2, 3), (0, 1, 1, 3), (0, 1, 2, 2), (0, 2, 4, 4
), (0, 3, 3, 4), (1, 1, 1, 2), (1, 1, 4, 4), (1, 2, 3, 4), (1, 3, 3, 3), (2, 2, 2, 4), (2, 2, 3
, 3), (3, 4, 4, 4)]
Bilangan Stirling k= 2 : [(0, 2, 4, 4), (0, 3, 3, 4), (1, 1, 4, 4), (1, 2, 3, 4), (1, 3, 3, 3),
 (2, 2, 2, 4), (2, 2, 3, 3)]
Jumlah Bilangan Stirling k= 2  :  7
Total Bilangan Catalan :  14
```

Table 3. The sequence of the multiset of the additive group $\mathbb{Z}_{10}$.

Based on the computational results and the calculation of the coefficient $q^{(k(n+1))}$, where $0 \leq k \leq n-1$, a sequence of numbers is obtained, which is contained in the following table:

Table 3. Number sequences of the possible multiset sums of the additive group $\mathbb{Z}_{10}$.

n \ k	0	1	2	3	4	5	6	7	8	Catalan number
1	1									1
2	1	1								2
3	1	3	1							5
4	1	5	7	1						14
5	1	9	20	11	1					42
6	1	13	48	51	18	1				132
7	1	20	100	169	112	26	1			429
8	1	28	194	461	486	221	38	1		1430
9	1	40	352	1128	1667	1210	411	52	1	4862

Based on Table 3, many possible multisets are formed from the additive group $\mathbb{Z}_{10}$ forming a Catalan number for each n. In addition, if the multiset additive group $\mathbb{Z}_{10}$ is divided into several parts where each part depends on the value of $k(n+1)$ with $0 \leq k \leq n-1$, then the number of multisets formed will form a second type of the new Stirling number.

The Stirling number change that is just visible from the left-hand side (in Table 3, the yellow row) will be smaller, and the rightmost portion (in the red Table 3 row) will be larger than the Stirling number of the second type that is known. As a result, the number of Stirling numbers of the second kind, originally a Bell number, was replaced by a Catalan number.

4. CONCLUSIONS

We can conclude that the multiset formed from the additive group $\mathbb{Z}_{10}$ is a Catalan number based on the results. In addition, if the multiset additive group $\mathbb{Z}_{10}$ is divided into several parts where each part depends on the value of $k(n+1)$ with $0 \leq k \leq n-1$, then the multiset forms a Stirling number of the second kind. However, the second kind of Stirling number formed based on the multiset additive group $\mathbb{Z}_{10}$ has a different initial value, namely $S(n,0) = 1$ and the value $S(n,n) = 0$. For $S(n,1)$ to $S(n,n-2)$ the value is smaller, while for $S(n,n-1)$ it has a larger value. The sum of Stirling's numbers is Bell's numbers, but for Stirling's numbers based on a multiset additive group, $\mathbb{Z}_{10}$ is Catalan numbers. Therefore, the Stirling number of the second kind based on the formation of a multiset additive group $\mathbb{Z}_{10}$ changes the arrangement of the previously known Stirling number of the second kind.

ACKNOWLEDGMENT

The Research Center Universitas Lampung funded this studyunder Postgraduate research grant project No. 815/UN26.21/PN/2022, and the authors gratefully acknowledge the funding.

REFERENCES

Bayer, M and Brandt, K,. *The Pill Problem, Lattice Paths and Catalan Numbers*, Mathematics Magazine, Vol 87, 2015

Brualdi, RA,. *Introductory Combinatorics*, Elsevier Science Publishing Co, Inc, 1983

Cayley, A,. *On Partitions of a Polygon*,.Proceedings of the London Mathematical Society 22, 237 – 262, 1891.

Fraleigh, J.B, Katz J,. *A First Course in Abstract Algebra*, Addison-Wesley, 2003

Jarvis, F,. *Catalan Numbers*, University of Sheffield, 2004

Saracevic, M, Adamovic, S, Bisevac, E,. *Application of Catalan Numbers and the Lattice Path Combinatorial Problem in Cryptography*, Acta Polytechnica Hungarica, Vol 15, No. 7, 2018

Selimi A, Saracevic M,. *Catalan Numbers And Applications*, Vision International Scientific Journal, Vol 4, pp 99-114, 2019

Stojadinovic,. T, *On Catalan Numbers*, The Teaching of Mathematics, Vol. 18, pp 16-24, 2015.

T. Koshy,. *Catalan Numbers With Application*, Oxford University Press, 2009

Wagner C.G. Partition Statistics and q-Bell Numbers (q = -1). Journal of Integer Sequences, Vol. 7 (2004), pp. 1-12

COMPARATIVE BIOACTIVITY STUDY OF SOME ORGANOTIN(IV) 2-CHLOROBENZOATE COMPOUNDS AS DISINFECTANT AGENT

Cindy Moyna Clara[1], Sutopo Hadi[1,*], Yandri Yandri[1], Asep Sukohar[2], Tati Suhartati[1]

[1]Department of Chemistry, Universitas Lampung, Bandar Lampung, 35415, Indonesia
[2]Faculty of Medicine, Universitas Lampung, Bandar Lampung, 35415, Indonesia

*Corresponding Author:
Department of Chemistry
Universitas Lampung
Bandar Lampung, 35415, Indonesia
E-mail address: sutopo.hadi@fmipa.unila.ac.id
Tel: +6281369059733

ABSTRACT:

This research was carried out to study the bioactivity test as disinfectant of two derivatives of organotin(IV) carboxylate compounds; diphenyltin(IV) di-2-chlorobenzoate (DPT2-CBz) (**2**) and triphenyltin(IV) 2-chlorobenzoate (TPT2-CBz) (**4**), against two pathogenic bacteria. Compounds **2** and **3** were successfully prepared by reacting diphenyltin(IV) oxide (DPTO) (**1**) and triphenyltin(IV) hydroxide (TPTOH) (**3**) with 2-chlorobenzoic acid (2-HCBz) with yields of 87.71% and 88.73%, respectively. The characterization of the synthesized compounds was performed with several spectroscopy techniques such as UV, IR, ^{1}H NMR, ^{13}C NMR, and microelemental analyzer. The optical density (OD) test for both compounds measured using UV-Vis at 600 nm showed a good bioactivity against two bacteria, Gram-negative *Salmonella sp.* and Gram-positive *Staphylococcus aureus*. The data revealed that compound **4** has bigger bioactivity than compound **2** and the positive control of commercial disinfectant (2.5 % pine oil). The bioactivity of compound **4** was optimum at concentration of $5x10^{-4}$ M and contact time of 15 minutes. These data corresponding to the decrease of absorbance from 0.6640 to 0.0955 for *Salmonella sp.*, and 0.6565 to 0.1295 for S. *aureus*, whereas although compound **2** reached the optimum activity at the same concentration and contact time with compound **4**, but the decrease of absorbance was less namely 0.6640 to 0.1305 for *Salmonella sp.*, and 0.6565 to 0.196 for S. *aureus*. The decrease of absorbance in the measurement of OD implies that both compounds are potential to be used as disinfectant agent.

KEYWORDS: disinfectant, organotin(IV) carboxylate, optical density, *Salmonella sp.*, S. *aureus*

INTRODUCTION:

Infection is the entry of pathogenic microorganisms, such as bacteria, into the human body and causes disease[1]. Pathogenic bacteria *Salmonella sp.* become a worldwide major health problem, with amount of infection reaching 1.9 billion people per year, and 715.000 of them died[2]. *Salmonella sp.* causes typhoid fever, diarrhea, sepsis (a complication that makes blood pressure drop dramatically thus causes death)[3]. S. *aureus* is also the major pathogenic bacteria for human, since it infects at least 30% of human population[4-7]. S. *aureus* bacteria causes skin infections, poisoning, endocartisis (heart infection) which is very lethal[6, 8] . Chemical disinfectant used with the aim to inhibit microorganism growth, or kill microorganism until certain amount of their safety limit[9-14].

Disinfectant might be sprayed on the object surface, liquids, or surrounding area which is suspected being contamined by bacteria or viruses, to reduce the risk of its exposure through human skin or mucous membrane[11, 12, 15]. Methanol, ethanol, and isopropanol are types of alcohol that widely contained in commercial disinfectant. It has been prove effective against bacteria, viruses, and fungi but excessive use in the long term might causes irritation and poisoning[16].

Based on previous bioactivity studies, other compounds that have great potential to be an active agent for disinfectant are derivative of organotin(IV) carboxylate compounds[17]. These compounds, are non toxic or slightly toxic to mammals, and have a good activity as antibacterial[18-21], anticancer and antitumor[22-26], antiviral[27, 28], antimalaria[29-32] and antifungal agents[33, 34]. The longer alkyl chain of organotin(IV) compund and the presence of halogen groups can increase its biological activity[35]. Based on the fact the derivatives of organotin(IV) compounds have shown many interesting biological activities, in this work we reported the synthesis and disinfectant bioactivity study of two organotin(IV) compounds.

MATERIALS AND METHODS:

Materials:

All reagents used were of Analytical Reagent grade. Diphenyltin(IV) oxide (DPTO) (**1**), triphenyltin(IV) hydroxide (TPTOH) (**3**), and 2-chlorobenzoic acid (2-HCBz) were obtained from Sigm-Aldrich (MA, USA). Methanol and dimethylsulfoxide (DMSO) were obtained from Merck Millipore (MA, USA). All of these reageants were used as received and without any further purification. Nutrient agar and nutrient broth were obtained from Himedia Laboratories Private Limited (Mumbai, India). A commercial disinfectant was used as a positive control containing active agent of 2.5% pine oil. Gram-negative bacteria *Salmonella sp.* and Gram-positive bacteria S. *aureus* were obtained from Laboratory of Vetereiner Center. Directorate General of Livestock and Animal Health, Ministry of Agriculture, Lampung, Indonesia.

Instrumentations:

UV spectra were recorded in the UV region and measured using Shidmadzu UV-245 Spectrophotometer (Japan). Measurements were performed in 1 mL quartz-cells. Solutions were prepared using methanol-DMSO 5% as solvent with concentration $1x10^{-5}$ M. IR Spectra were recorded on Bruker VERTEX 70 FT-IR Spectrophotometer (Germany) with using KBr discs at range of 4000-400 cm^{-1}. ^{1}H dan ^{13}C NMR spectra were recorded on Bruker AV 600 MHz NMR (Germany) (600 MHz for ^{1}H and 150 MHz for ^{13}C), all measurements runs using DMSO-D6 at 298K. Number of runs used in ^{1}H were 32 with reference of TMS signal at 0 ppm, while ^{13}C were 1000-4000 with DMSO reference signal at 39.5 ppm. Elemental analysis (CHNS) were conducted using Fision EA 1108 Elemental Analyzer (Italy)

Synthesis of Organotin(IV) 2-chlorobenzoate:

Synthesis of organotin(IV) 2-chlorobenzoate compounds were carried out in this study following previously reported procedures[17-21, 26, 29, 31, 32].

The following procedure was applied in the synthesis of DPT2-CBz (**2**), and as follows: 0.8667 g (0.003 mol) of DPTO (**1**) was added with 2 moles equivalent of 2-HCBz (0.9394 g), in 30 mL of methanol. These mixtures were refluxed for 4 hours at 60-61°C under stirring condition. The water produced was removed by Dean-Stark apparatus. DPT2-CBz (**2**) compound was then separated from the solvent using vacuum desiccator until constant and ready to be analyzed and tested for its bioactivity. The yield obtained was 87.71%. The same procedure also adapted in the synthesis of TPT2-CBz (**4**), using TPTOH (**3**) with the addition of only one mole equivalent of 2-HCBz.

Bioactivity Test of Disinfectant:

Disinfectant bioactivity test was carried out using the modification of the optical density (OD) method based on the work of others[10-14, 17, 36, 37]. In this study, 5 mL solution containing compounds **2** and **4** with concentration variations of $5x10^{-3}$, $1x10^{-3}$, and $5x10^{-4}$ M were used as the disinfectant. Each of these disinfectants was observed for their bioactivity against 0.5 µL pathogenic bacteria *Salmonella sp.* and *S. aureus* with contact times of 0, 5, 10, and 15 minutes and was monitored with Spectrophotometer UV-Visible at 600 nm[38].

RESULT AND DISCUSIONS:

The synthesis of two derivatives of organotin(IV) carboxylates compound **2** and **4** has successfully been carried out by reacting DPTO (**1**) and TPTOH (**3**) with 2-HCBz using the procedures available in the literature[17-21, 26, 29, 31, 32]. As an example, in the reaction scheme in the preparation of compound **2** is shown in Figure 1.

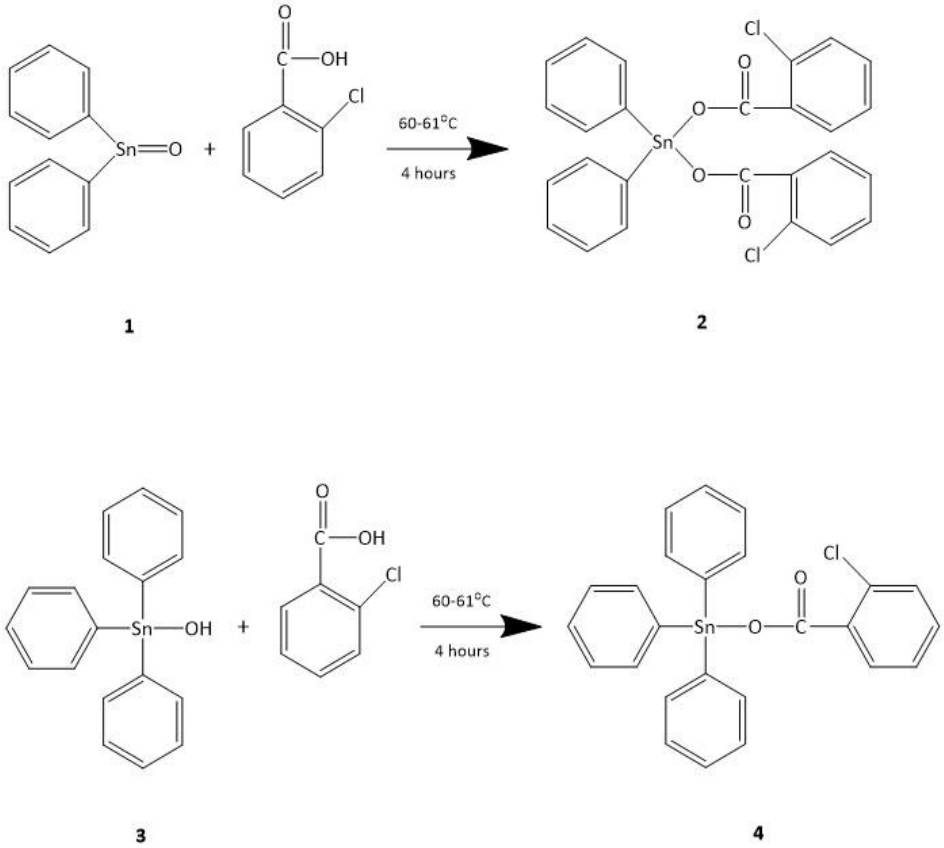

Fig. 1: The reaction scheme in the preparation of (a) compound **2**; (b) compound **4**

Compound **2** was successfully synthesized forming soft pink solid with a total yield of 87.71%, while compound **4** forming pink solid with a total yield 88.73%. The results of characterization from several spectroscopies such as UV, IR, ^{1}H-NMR, ^{13}C-NMR providing good spectra and the elemental analysis data values are very good as close to the theoretical values which are evidence of the success in the synthesis of the compounds studied.

The UV spectroscopy analysis of compounds **2** and **4**, produced characteristic absorption values with λ_{max} as shown in Table 1. The synthesized compounds **2** and **4** had two characteristic peaks with transitions $\pi \rightarrow \pi^*$ and $n \rightarrow \pi^*$, while in the starting materials **1** and **3**, they had only one characteristic peak with the transition $\pi \rightarrow \pi^*$. For example, in compound **1** the transition of $\pi \rightarrow \pi^*$ occurred at 203 nm which is due to the delocalization of phenyl electron. Upon reaction of **1** with 2-chlorobenzoic acid ligand to produce compound **2**, bathochromic shifting occurs due to the influence chromophore group from carbonyl group and addition of benzene rings. In compound **2** there was also $n \rightarrow \pi^*$ transition at 282 nm due to the presence of a lone pair electron from chlorine group. Similar shifts change was also observed in the formation of compound **4** from **2**.

Table 1: UV Data of Organotin(IV) Compounds

Compounds	λ_{max} (nm)	
	$\pi \rightarrow \pi^*$	$n \rightarrow \pi^*$
1	203	-
2	235	282
3	203	-
4	234	289

FT-IR absorption data in Table 2, shows finger print area of each functional group present in the compounds **2** and **4** prepared. Both compounds gave a characteristic absorption of C-H group at wave number 2922,2 cm^{-1}. Stronger absorption of C=O group appeared at 1684.8 cm^{-1} and 1699.7 cm^{-1} in the compounds **2** and **4** was obtained from the ligand 2-HCBz, while C=C group at 1580.4 cm^{-1} from the sp^2 hybridized phenyl in the benzene rings. The ligand 2-HCBz successfully bound in compounds **2** and **4** was proven by the presence of Sn-O-C group at 1155.5 cm^{-1}, Sn-Ph group at 1051.1 cm^{-1}, and Sn-O group at 693.3 cm^{-1}.

Table 2.:FT-IR Data of Organotin(IV) Compounds

Functional Group	Compounds		Reference (cm^{-1})
	2	**4**	
C-H	2922.2	2922.2	3300-2900
C=O	1684.8	1699.7	1760-1600
C=C	1580.4	1580.4	1650-1566
Sn-O-C	1155.5	1155.5	1250-1000
Sn-Ph	1051.1	1051.1	1100-1000
Sn-O	693.3	693.3	800-600

Table 3: Microelemental Analysis Data of Organotin(IV) Compounds

Compound	Analysis Found (Calculated)	
	C	H
2	53.21 (53.43)	3.02 (3.09)
4	59.22 (59.39)	3.71 (3.79)

Table 4: ^{1}H NMR and ^{13}C NMR Data of Organotin(IV) Compounds

Compound	H in Phenyl (ppm)	H in Benzoate (ppm)	C in Phenyl and Benzoate (ppm)
2	H2 & H6 7.44 (d,4H); H3 &H5 7.46 (t, 4H); H4 7.47 (t,2H)	7.79-7.81 (m)	C1-6 (phenyl): 126.9; C7 167.68; C8 131.2; C9 132.15; C10, C11 130.4; C12-C13 130.5
4	H2&H6 7.48 (d,6H); H3&H5 7.50 (t 6); H4 7.51	7.88-7.89 (d)	C1-6 (phenyl): 128.4 – 129.21; C7: 166.64; C8: 136.76; C9-C10: 137.4; C11, C13: 136.8; C12: 131.45

The characterization results based on ^{1}H and ^{13}C NMR data of the compounds synthesized are shown in Table 4. By careful analysis, the data for compounds prepared have been compared with the previous available[17-21, 26, 29, 31, 32]. In ^{1}H NMR, the chemical shift (δ) of phenyl proton bound to Sn atom as expected appeared in the range of 7.44-7.47 ppm, while the chemical shift of proton benzote were at 7.79-7.81 ppm. The ^{13}C NMR of the phenyl bound to Sn atom gave δ at 126.9-130.5 ppm and the carbon benzoate at 137. The chemical shift (δ) of carbon carbonyl as exptected appeared ad 166-167 ppm[17-21, 26, 29, 31, 32].

Table 5 shows bioactivity tests results of compounds **2** and **4** against pathogenic bacteria *Salmonella sp.* and S. *aureus* measured using optical density method. This method was used to determine the density of bacteria before and after the addition of disinfectant and based on the absorbance value measured with UV-Visible at 600 nm. The decrease of absorbance value on the optical density method, is equivalent with the decrease of bacteria amount[36].

Tabel 5: Optical Density Data of Disinfectant against Bacteria

Compound	Optical Density at MIC 5x10^{-4} M (15 minutes)	
	Salmonella sp. (0.6640)	*S. aureus* (0.6570)
2	0.1305	0.1960
4	0.0955	0.1295
Positive Control (2.5% pine oil)	0.4025	0.4600

The absorbance data of McFarland's standard solution in Table 6, can be used to calculate bacteria density in units (CFU/mL), through linear regression equation[4]. The average initial absorbance of *Salmonella sp.* was 0.6640 and its equivalent to 10.6942 x 10^{8} CFU/mL, while S. *aureus* was 0.657 its equivalent to 10.5804 x 10^{8} CFU/mL. Bioactivity of compounds **2**, **4** and commercial disinfectant as positive control (2.5% pine oil), optimum at 5x10^{-4} M and contact time with bacteria 15 minutes. Bacteria absorbance of compound **4**, decreased from 0.6640 to 0.0955 for *Salmonella sp.*, and 0.6570 to 0.1295 for S. *aureus*. Bacteria absorbance of compound **2**, decreased from 0.6640 to 0.1305 for *Salmonella sp.*, and 0.6570 to 0.196 for S. *aureus*. Positive control showed a decrease in the absorbance of bacteria from 0.6640 to 0.4025 for *Salmonella sp.*, and 0.6570 to 0.4600 for S. *aureus*.

Table 6: McFarland Nephelometer Standards[38]

McFarland standard No.	0.5	1	2	3	4
CFU/mL (x10^8)	1.5	3	6	9	12
Absorbance	0.132	0.257	0.451	0.582	0.669

These absorbance values, indicate the ability of compound **4** against pathogenic bacteria better than compound **2**, corresponded with the reference state that the longer alkyl chain of organotin(IV) compound can increase its biological activity[35]. In this study, all disinfectants showed a better against against *Salmonella sp.* bacteria (Gram-negative) compared to S. *aureus* (Gram-positive), caused by the cell wall of Gram-negative bacteria has little peptidoglycan layer, and causes bacterial cells easily break and damage the immune system[8, 39, 40].

Other possible mechanism actions of disinfectants were the presence of electronegative chlorine substituents causes peptide bonds in bacteria cells oxidized, so that the proteins constituent denatured[20]. It proves that organotin(IV) 2-chlorobenzoate compounds are able to act as disinfectants against pathogenic bacteria.

CONCLUSIONS:

Synthesis of some organotin(IV) compounds with 2-chlorobenzoic acid ligand has been successfully carried out, as proved by the analysis results of UV, IR, 1H-NMR, 13C-NMR Spectrophotometer instruments, and elemental analysis data. Bioactivity of compounds **2** and **4**, using optical density method also shows satisfying results while against pathogenic bacteria *Salmonella sp.* and S. *aureus*. Compound **4** is more effective to kill bacteria than compound **2** and commercial disinfectant as positive control (2.5% pine oil). The large number of phenyl or benzene rings, and presence of chlorine substituents in compounds **2** and **4** also increase their bioactivity. Organotin(IV) 2-chlorobenzoate compounds very potential as recent disinfectant caused by their effectivity against pathogenic bacteria. Further studies and development of bioactivity testing methods for derivative of organotin(IV) compounds required to increase its bioactivity.

ACKNOWLEDGEMENTS:

The authors are grateful to the Institute of Research and Community Services, Universitas Lampung and Directorate of Research and Community Services, The Ministry of Education, Culture, Research, and Technology, Indonesia for the funding given to this research through National Competitive Basic Research Grant Scheme (Penelitian Dasar Kompetitive Nasional) with contract numbers of 027/E5/PG.02.00/PT/2022, dated March 16, 2022 and 2143/UN26.21/PN/2022 dated April 29, 2022.

CONFLIC OF INTEREST:

The authors declare no conflict of interest.

REFERENCES:

1. Brooks GF, Carrol KC, Butel JS, Morse SA, Mietzner TA, Jawetz, Melnick & Adelberg's Medical Microbiology 26th ed. McGraw-Hill, New York, 2013, p. 149.
2. Besser JM, Salmonella epidemiology: A whirlwind of change. Food Microbiology. 2018 May; 71: 55-9. doi: 10.1016/j.fm.2017.08.018
3. Brands D. Salmonella Deadly Deseases and Epidemics. Chelsea House Publisher New York USA, 2006, 1-103.
4. Tong SYC, Davis JS, Eichenberger E, Holland TL, Fowler VG. *Staphylococcus aureus* Infections: Epidemiology, Pathophysiology, Clinical Manifestations, and Management. Clinical Microbiology Reviews. 2015 Jul; 28(3): 603-61. doi: 10.1128/CMR.00134-14
5. Raheem HQ, Hussein EF, Rasheed AH, Imran NK, Antibacterial action of Silver Nanoparticles against Staphylococcus aureus Isolated from wound infection. Research Journal of Pharmacy and Technology. 2022 Jun; 15(6):2413-6. doi: 10.52711/0974-360X.2022.00401
6. Atala ML. Bacteriological and Molecular study on S. aureus bacteria. Research Journal of Pharmacy and Technology. 2021 Mar; 14(3):1380-4. doi: 10.5958/0974-360X.2021.00246.8
7. Umamageswari SSM, George P, Kalyani M. A Study on Coexistence of Panton Valentine Leukocidin Gene from Hospital Acquired Methicillin Resistance Staphylococcus aureus. Research Journal of Pharmacy and Technology. 2019; 12(2):508-12. doi: 10.5958/0974-360X.2019.00089.1
8. Bierowiec K, Ploneczka-Janeczko K, Rypula K. Is the Colonisation of S. aureus in Pets Associated with Their Close Contact with Owners. PLOS One. 2016 May 26; 11(5): e0156052. doi: 10.1371/journal.pone.0156052
9. Maris P. Modes of Action of Disinfectants. Revue Scientifique et Technique (International Office of Epizootics). 1995 Mar; 14(1): 47-55. doi: 10.20506/rst.14.1.829
10. Henry AJ, Sopia Abigail R, Ramamurthy, D. Evaluation of Disinfectant action on Biofilm Bacteria. Research Journal of Pharmacy and Technology 2018 Mar; 11(3): 910-2. doi: 10.5958/0974-360X.2018.00168.3
11. Bhuvaneshwari G, Shameembanu AS, Kalyani M. Disinfectant Susceptibility Testing of Non-Fermenting Gram Negative Bacilli. Research Journal of Pharmacy and Technology. 2018 Apr; 11(4): 1313-5. doi: 10.5958/0974-360X.2018.00244.5
12. Muslem WH, Muslim SN, Muhammde Ali AN, Fayyad RJ. Detection of Disinfectant property of purified Amylopullulanase from Citrobacter freundii SW. Journal: Research Journal of Pharmacy and Technology. 2022; 15(2):847-52 doi: 10.52711/0974-360X.2022.00141
13. Alwarid RJ, Mohammed E, Wehab W. Study the Effects of Two Types of Microbial Disinfectants on Contamination of Dental Unit Water Lines. Research Journal of Pharmacy and Technology. 2018 Feb; 11(2):604-7. doi: 10.5958/0974-360X.2018.00111.7
14. Sujitra RG, Chotaliya UJ. Saltwater as a Disinfectant and Cleaning agent for Environmental Surfaces in the context of SARS-COV-II. Asian Journal of Research in Pharmaceutical Sciences. 2021; 11(2): 165-74. doi 10.52711/2231-5659.2021-11-2-13
15. McDonnel GE. Antisepsis Disinfection and Sterilization Types, Action, and Resistance 2nd Edition. ASM Press, Washington DC USA, 2017, 1- 433.
16. Moorer WR. Antiviral Activity of Alcohol for Surface Disinfection. International Journal of Dental Hygiene. 2003 Aug; 1(3): 138-42. doi: 10.1034/j.1601-5037.2003.00032.x
17. Hadi S, Suhartati T, Noviany N, Pandiangan KD, Yandri Y, Simanjuntak W. Disinfecting activity of some diphenyltin(IV) benzoate derivative compounds. Pure and Applied Chemistry. 2022 Mar 17; 94 (in press). doi: 10.1515/pac-2021-1106

18. Annissa, Suhartati T, Yandri, Hadi S. Antibacterial Activity of Diphenyltin(IV) and Triphenyltin(IV) 3-Chlorobenzoate Against *Pseudomonas aeruginosa* and *Bacillus subtilis*. Oriental Journal of Chemistry. 2017 May-Jun; 33(3): 1133-9. doi: 10.13005/ojc/330310
19. Hadi S, Hermawati E, Noviany, Suhartati T, Yandri. Antibacterial Activity Test of Diphenyltin(IV) Benzoate Compound against *Bacillus subtilis* and *Pseudomonas aeruginosa*. Asian Journal of Microbiology, Biotechnology and Environmental Sciences. 2018 Jan-Mar; 20(1): 113-9.
20. Hadi S, Samsuar, Qudus HI, Simanjuntak W. In Vitro Antibacterial Activity of Some of Dibutyltin(IV) Chlorobenzoate Derivatives against *Staphylococcus aureus* and *Escherichia coli*. ARPN Journal of Engineering and Applied Science. 2021 Aug; 16(15) 1624-9.
21. Samsuar S, Simanjuntak W, Qudus HI, Yandri T, Herasari D, Hadi S. In Vitro Antimicrobial Activity Study of Some Organotin (IV) Chlorobenzoates against *Staphylococcus aureus* and *Escherichia coli*. Journal of Advanced Pharmacy and Education Research. 2021 Apr-Jun; 11(2): 17–22. doi: 10.51847/kaijZKAFCO
22. Sirajuddin M, Ali S, Tahir MN. Organotin(IV) Derivatives Based on 2-((2-methoxyphenyl) carbamoyl) Benzoic Acid: Synthesis, Spectroscopic Characterization, Assessment of Antibacterial, DNA Interaction, Anticancer and Antileishmanial Potentials. Journal of Molecular Structure. 2021 Apr 5; 1229: 129600. doi: 10.1016/j.molstruc.2020.129600
23. Hadi S, Rilyanti M. Synthesis and In Vitro Anticancer Activity of Some Organotin(IV) Benzoate Compounds. Oriental Journal of Chemistry. 2010 Sep; 26(3): 775-9.
24. Uddin N, Rashid F, Haider A, Tirmizi SA, Raheel A, Imran M, Zaib S. Diaconescu PL, Iqbal J, Ali S. Triorganotin(IV) Carboxylates as Potential Anticancer Agents: Their Synthesis, Physiochemical Characterization, and Cytotoxic Activity against HeLa and MCF-7 Cancer Cells. Applied Organometallic Chemistry. 2021; 35(4): e6165. doi: 10.1002/aoc.6165
25. Rehman W, Badshah A, Khan S, Tuyet LTA. Synthesis, Characterization, Antimicrobial and Antitumor Screening of Some Diorganotin(IV) Complexes of 2-[(9H-Purin-6-ylimino)]-phenol. European Journal of Medicinal Chemistry. 2009 Oct; 44(10): 3981–5. doi: 10.1016/j.ejmech.2009.04.027
26. Hadi S, Rilyanti M, Suharso. In Vitro Activity and Comparative Studies of Some Organotin(IV) Benzoate Derivatives Against Leukemia Cancer Cell: L-1210. Indonesian Journal of Chemistry. 2012 Jul; 12(2): 172-7. doi: 10.22146/ijc.21359
27. Roner MR, Carraher Jr CE, Shahi K, Barot K. Antiviral Activity of Metal-Containing Polymers-Organotin and Cisplatin-Like Polymers Materials. Materials (Basel) 2011 Jun; 4(6): 91-112. doi: 10.3390/ma4060991
28. Carraher Jr CE, Roner MR. Organotin polymers as anticancer and antiviral agents. Journal of Organometallic Chemistry. 2014 Feb 1 ; 751: 67-82. doi: 10.1016/j.jorganchem.2013.05.033
29. Hadi S, Noviany, Qudus HI, Wattana-Amorn P, The Potency Study of Organotin(IV) 3-Nitrobenzoate Compounds as Antimalarial Agents. Journal of Physics: Conference Series. 2019; 1338: 012012. doi: 10.1088/1742-6596/1338/1/012012
30. Hansch C, Verma RP. Larvicidal Activities of Some Organotin Compounds on Mosquito Larvae: A QSAR Study. European Journal of Medicinal Chemistry. 2009 Jan; 44(1): 260-73. doi: 10.1016/j.ejmech.2008.02.040
31. Hadi S, Noviany N, Rilyanti M. In Vitro Antimalarial Activity of Some Organotin(IV) 2-Nitrobenzoate Compounds Against *Plasmodium falciparum*. Macedonian Journal of Chemistry and Chemical Engineering. 2018 Nov 7; 37(2): 185-91. doi: 10.20450/mjcce.2018.1414

32. Hadi S, Fenska MD, Noviany N, Satria H, Simanjuntak W, Naseer MM. Synthesis and Antimalarial Activity of Some Triphenyltin(IV) Aminobenzoate Compounds against *Plasmodium falciparum*. Main Metal Group Chemistry. 2021 Sep 30; 44(1): 256-60. doi: 10.1515/mgmc-2021-0028
33. Rocha CS, de Morais BP, Rodrigues BL, Donnici CL, de Lima GM, Ardisson JD, Takahashi JA, Bitzer RS. Spectroscopic and X-ray Structural Characterization of New Organotin Carboxylates and Their In Vitro Antifungal Activities. Polyhedron, 2016 Oct 15; 117: 35-47. doi: 10.1016/j.poly.2016.05.031
34. Hadi S, Rilyanti M, Nurhasanah. Comparative Study on the Antifungal Activity of Some Di-and Tributyltin (IV) Carboxylate Compounds. Modern Appl. Sci. 2009 Jan; 3(2): 12-7. doi: 10.5539/mas.v3n1p12
35. Hadi AG, Jawad K, Ahmed DS, Yousif E. Synthesis and Biological Activities of Organotin(IV) Carboxylates A Review. Systematic Reviews in Pharmacy. 2019; 10(1): 26-31. doi: 10.5530/srp.2019.1.5
36. Matlock BC. Differences in Bacterial Optical Density Measurements between UV-Visible Spectrofotometer. Thermoscientific Technical Note. 2019; 52236: 1-4.
37. Hall BG, Acar H, Nandipati A, Barlow M. Growth Rate Made Easy. Molecular Biology and Evolution. 2014 Jan; 31(1): 232-8. doi: 10.1093/molbev/mst187
38. McFarland J. Nephelometer: An Instrument for Estimating The Number of Bacteria in Suspensions Used for Calculating The Opsonic Index and For Vaccines. Journal of the American Medical Association. 1907 Oct 5; 4: 1176-8. doi: 10.1001/jama.1907.25320140022001f
39. Pahari S, Srikrishnan S, Suneetha V. Evaluating the Potential of Natural extracts as a Fruit Wash. Research Journal of Pharmacy and Technology. 2018; 11(12): 5243-6. doi: 10.5958/0974-360X.2018.00956.3
40. Sadiq SM, Kareem A, Rasheed N, Mohammad AS. Pharmaceutical Importance of Anti-Microbials. Asian Journal of Pharmacy and Technology. 2017; 7(1): 7-10. doi: 10.5958/2231-5713.2017.00002.2

ANALYSIS OF PHENOL, REDUCING SUGAR, AND CHLOROPHYLL OF *DENDROBIUM* SP. PLANTLET AFTER INDUCTION OF FUSARIC ACID *IN VITRO*

Endang Nurcahyani [1, *], Elsi Diana [2], Yuliana Permata Sari [2], Sumardi [2], Hardoko Insan Qudus [3] and Mahfut [4]

[1] *Applied Biology Study Program, Faculty of Mathematics and Natural of Sciences, University of Lampung, Bandar Lampung, Lampung, Indonesia.*

[2] *Biology Masters Study Program, Faculty of Mathematics and Natural of Sciences, University of Lampung, Bandar Lampung, Lampung, Indonesia.*

[3] *Chemistry Study Program, Faculty of Mathematics and Natural of Sciences, University of Lampung , Bandar Lampung, Lampung, Indonesia.*

[4] *Biology Study Program, Faculty of Mathematics and Natural of Sciences, University of Lampung, Bandar Lampung, Lampung, Indonesia.*

GSC Biological and Pharmaceutical Sciences, 2022, 19(03), 133–138

Publication history: Received on 25 April 2022; revised on 04 June 2022; accepted on 06 June 2022

Article DOI: https://doi.org/10.30574/gscbps.2022.19.3.0207

Abstract

Orchids are ornamental plants with varied and beautiful flower colors and are much favored by the public. Orchid plants have a higher economic value when compared to other ornamental plants, both as cut flowers and potted flowers. In the process of growth, orchid plants are disturbed, namely Fusarium wilt disease caused by Genus *Fusarium* which can produce a toxin compound, namely fusaric acid which is widely used in *in vitro* selection of plants. Plant resistance can be formed through the induction of fusaric acid compounds. Induced resistance is an alternative way to obtain disease- resistant plants because plants are able to create natural resistance mechanisms. The purpose o f this study was to determine the concentration of tolerant fusaric acid to select Dendrobium orchid plantlets with optimal growth and specific expression characters of Dendrobium orchid plantlets based on phenol content, reducing sugar content, and total chlorophyll content, chlorophyll a and chlorophyll b. The results of this study indicated that there was an increase in total phenol content, reducing sugar content, and total chlorophyll content, chlorophyll a and chlorophyll b along with the addition of fusaric acid concentration.

Keywords: Chlorophyll; *Dendrobium* sp.; Fusaric Acid; *In vitro*; Phenol; Reducing Sugar

1. Introduction

Orchid plants are included in the Orchidaceae family which based on the nature of their life are divided into 3 namely epiphytic orchids, semi-epiphytic orchids and land or terrestrial orchids. Epiphyte is a type of plant that lives by attaching to other plants that are not harmful to the host plant, its roots are attached and have aerial roots that are used to find food [1]. One type of orchid that is in great demand by the public is *Dendrobium* sp. because it has the characteristics of having varied flower shapes and flower colors, long-lasting flower freshness, and flexible flower stalks so that they are easy to assemble [2].

In the process of growth, *Dendrobium* sp. can be attacked by the disease. One of the compounds that can be used for plant resistance is fusaric acid produced by several species of fungi of the genus *Fusarium*. Fusaric acid (FA) will be more effective at low doses, namely at non-toxic FA concentrations so that plants will respond to resistance by

✉ Corresponding author: Endang Nurcahyani

Applied Biology Study Program, Faculty of Mathematics and Natural of Sciences, University of Lampung, Bandar Lampung, Lampung, Indonesia.

producing phytoalexins to inhibit pathogen activity [3]. The plantlet *Dendrobium* sp. which has been given the addition of fusaric acid can be analyzed based on the content of phenol, reducing sugar and chlorophyll.

Phenol is a compound whose hydroxyl group (-OH) is directly connected to an aromatic ring group. Plants containing phenolic compounds are classified into simple phenols, lignins, phenolic acids, acetophenones, xanthones, flavonoids, coumarin bioflavonoids, stilbenes, hydroxycinnamic acid, tannins, tyrosine derivatives, and benzoquinone [4]. Sugars consist of reducing and non-reducing sugars which have important roles in central metabolic pathways and assist in the production of secondary metabolites that can enhance the medicinal properties of plants [5].

Chlorophyll is a green pigment that plays an important role in photosynthesis, chlorophyll can absorb sunlight and use its energy to synthesize carbohydrates [6].The purpose of this study was to determine the concentration of tolerant fusaric acid for the selection of Dendrobium plantlets with optimum growth and specific expression characters of Dendrobium plantlets based on total phenol content, reducing sugar content, and total chlorophyll content, chlorophyll a and chlorophyll b. The plantlet Dendrobium sp. which has been given the addition of fusaric acid with various concentrations: (A) 0 ppm, (B) 10 ppm, (C) 20 ppm, (D) 30 ppm, and (E) 40 ppm are presented in **Figure 1.**

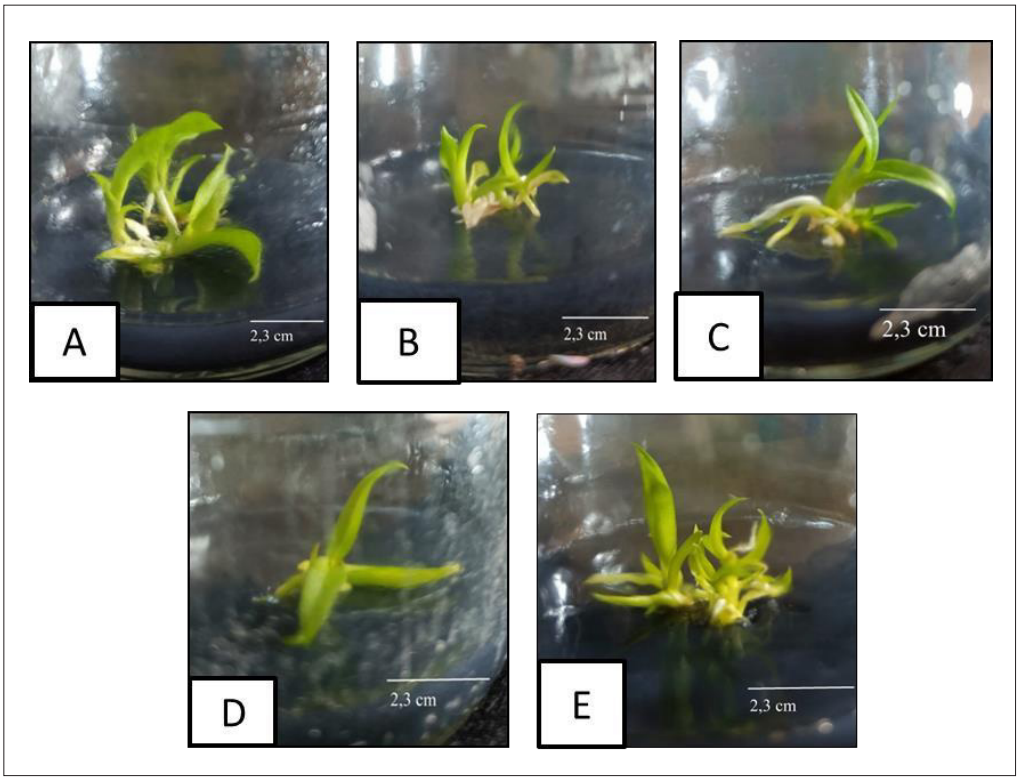

Figure 1 Control *Dendrobium* sp. plantlets (A) and *Dendrobium* sp. plantlets treated with various concentrations of fusaric acid: B.10 ppm; C.20 ppm; D. 30 ppm; and E. 40 ppm

2. Methods

This research was conducted from September 2021 to February 2022 at the *In Vitro* Culture Laboratory, Biology Department, Faculty of Mathematics and Natural Sciences, University of Lampung **.** The character of the *Dendrobium* orchid plantlets that have been given the addition of fusaric acid can be reviewed, includi ng the total phenol content, reducing sugar content, and total chlorophyll content.

The Folin-Ciocalteu method can be used to analyze the content of total phenolic compounds [7] by making a fresh extract of Dendrobium orchid leaves in methanol, 0.2 mL of each extract solution is pipetted and then 15.8 mL of distilled water and 1 mL of Folin-Ciocalteu reagent are added. The solution was shaken until it became homogeneously clear yellowish then allowed to stand for 8 minutes, added 3 mL of 20% Na2CO3 solution and then shaken until homogeneous. The solution was allowed to stand for 30 minutes at room temperature until the solution turned blue. The absorption of the solution was measured with a Vis spectrophotometer at a wavelength of 749 nm. The phenol content obtained is mg gallic acid equivalent/gram sample. Calculation of the total phenol content using the formula:

$$\text{Total Phenol Content (mg/100g)} = \frac{X \,.\, V.\, FP}{BS}$$

Where, X = Concentration (ppm)
V = Volume of sample solution (extract) (mL) FP = Sample solution dilution factor
BS = Sample weight (g)

Analysis of reducing sugar content in this study used Dendrobium plantlets that had been treated with fusaric acid and without treatment (control). The Nelson – Somogyi method can be used to analyze the reducing sugar content by making a sample solution in the form of 1 ml of Dendrobium orchid leaf extract taken from each concentration and then put into each test tube and then added 1 ml of Nelson's reagent in each test tube. The solution was heated on a boiling water bath for 20 minutes. Then the sample was cooled to room temperature. After cooling, added 1 ml of Arsenomolybdate reagent and 7 ml of distilled water, shaken until homogeneous. The solution mixture was put in a cuvette and the absorption of visible light was measured with a wavelength of 695 nm. The absorbance value obtained is reduced by the absorbance value of the blank so that the absorbance value of the sample is obtained. Then based on the standard solution regression equation, the absorbance value of the sample was converted to reducing sugar content (mg/ml).

Calculation of reducing sugar content [8] can use the formula:

$$\text{Reducing Sugar Content (\%)} = \frac{\text{X. FP}}{\text{BS}} \; x \; 100$$

Where, X = Concentration (ppm)
FP = Sample solution dilution factor
BS = Sample weight (g)

Analysis of chlorophyll content using plantlet leaves of *Dendrobium* sp. which has been induced by fusaric acid, using the Harborne method with a spectrophotometer [9]. The way it works is the plantlet leaves of *Dendrobium* sp. 0.1 g of uniform leaf was removed, then crushed with a mortar (pestle) then added 10 mL of 80% acetone. After that the solution was filtered with Whatmann paper No. 1, and put in a flakon and tightly closed. The sample solution and standard solution (80% acetone) were taken as much as 1 mL, then put in a cuvette. After that, the absorption readings were carried out with a UV spectrophotometer at wavelengths (λ) 646 nm and 663 nm. Chlorophyll content is calculated using the following formula:

Chlorophyll a = 12, 21 λ663 – 2, 81 λ646 mg/l Chlorophyll b = 20, 13 λ646 – 5, 03 λ663 mg/l Total Chlorophyll = 17, 3 λ646 + 7,18 λ663 mg/l

Where, λ646 = absorbance at a wavelength of 646 nm λ663 = absorbance at a wavelength of 663 nm

3. Results and discussion

The effect of Fusaric Acid (FA) on *Dendrobium* sp. can be determined by the total phenol content. The content that can be observed in the leaves of the plantlet *Dendrobium* sp. who have been treated with FA and control are presented in Table 1.

Based on Table 1, the total phenol content at a concentration of 0 ppm (control) was 10.66 mg/100g. The results of the total phenol content of *Dendrobium* sp. treated with fusaric acid (FA) showed that the higher the concentration of FA, the higher the total phenol content. The total phenol content at 10 ppm was 10.00 mg/100g, increased to 10.18 mg/100g at a concentration of 20 ppm, followed by 13.19 mg/100g at a concentration of 30 ppm, and 15.25 mg/100g at a concentration of 40 ppm. The results of this study are in line with research [10] on vanilla plantlets, the higher the concentration of FA, the higher the total phenol content.

Phenol compounds are one indicator of disease resistance. The results of the study [11] showed that the higher the phenol content, the more resistant the plant to pathogen attack. One of the results of plant metabolism that can function as a plant chemical resistance system that can prevent the growth and development of pathogens is phenol compounds [10].

Table 1 Results of Total Phenol Content of Planlet *Dendrobium* sp. that has been induced by FA

Treatment (ppm)	**Total Phenol Content *Dendrobium* sp. (mg/100g)**
0 (control)	10.66 ± 0.44[a]
10	10.00 ± 0.40[a]
20	10.18 ± 0.31[a]
30	13.19 ± 2.07[a]
40	15.25 ± 3.16[a]

Note: Numbers followed by the same letter, not significantly different at 95% confidence level

Effect of Fusaric Acid (FA) on *Dendrobium* sp. can also be determined by the content of reducing sugars. The content that can be observed in the leaves of the plantlet *Dendrobium* sp. that have been treated with FA and control are presented in Table 2.

Table 2 Results of Reducing Sugar Content of Plantlet *Dendrobium* sp. that has been induced by FA

Treatment (ppm)	**Reducing Sugar Content of Planlet *Dendrobium* sp. (%)**
0 (control)	11.76 ± 2.20[a]
10	7.71 ± 2.49[a]
20	11.90 ± 1.34[a]
30	15.21 ± 3.16[a]
40	15.26 ± 1.81[a]

Note: Numbers followed by the same letter, not significantly different at 95% confidence level

Based on Table 2, the results of reducing sugar content at a concentration of 0 ppm (control) were 11.76%. The results of the reducing sugar content of *Dendrobium* sp. treated with fusaric acid (FA) showed that the higher the concentration of FA, the more reducing sugar content increased. The reducing sugar content at 10 ppm was 7.71%, increasing to 11.90% at a concentration of 20 ppm, followed by 15.21% at a concentration of 30 ppm, and 15.26% at a concentration of 40 ppm.

Table 3 The Chlorophyll Content of Plantlet *Dendrobium* sp. induced FA

Treatment (ppm)	The Chlorophyll Content of Planlet *Dendrobium* sp. (mg/g tissue)		
	Chlorophyll a content	Chlorophyll b content	Chlorophyll total content
0 (control)	0.39 ▫ 0.015[a]	3.24 ▫ 0.257[a]	3.63 ▫ 0.268[a]
10	0.37 ▫ 0.020[a]	3.96 ▫ 0.316[a]	4.49 ▫ 0.342[a]
20	0.45 ▫ 0.057[a]	4.47 ▫ 0.170[a]	4.84 ▫ 0.184[a]
30	0.53 ▫ 0.066[a]	5.18 ▫ 0.623[b]	5.63 ▫ 0.588[a]
40	1.11 ▫ 0.522[a]	5.30 ▫ 0.668[c]	6.41 ▫ 0.979[b]

Note: Numbers followed by the same letter, not significantly different at 95% confidence level

Based on research [12] suggests that the Somogyi-Nelson method has higher sensitivity and accuracy than other methods, it is recommended to test the reducing sugar content using the Somogyi-Nelson method. In the Somogyi- Nelson method, there is a reaction between specific alkaline Cu (Cu^{2+}) reagent with reducing sugar to Cu^{+} which forms a brick red precipitate, then when arsenomolybdate solution is added, the reaction will turn blue-green.

The effect of Fusaric Acid (FA) on *Dendrobium* sp. can be identified by the chlorophyll content. Chlorophyll content can be observed in the leaves of the plantlet *Dendrobium* sp. who had been treated with FA and control. The method used to analyze the chlorophyll content is the Harboune method.

The results of the chlorophyll content of *Dendrobium* sp. induced FA is presented in Table 3.

Based on Table 3, it shows that the higher the concentration of FA, the higher the chlorophyll content in the *Dendrobium* sp. The highest chlorophyll content at 40 ppm FA concentration was at chlorophyll a 1.11 mg/g, chlorophyll b 5.30 mg/g and total chlorophyll 6.41 mg/g. The results of this study are in line with the results of studies [13] and [14] which showed an increase in chlorophyll a, chlorophyll b and total chlorophyll in soil orchids (*Spathoglottis plicata*) and moon orchids (*Phalaenopsis amabilis*) along with an increase in FA.

Chlorophyll is an important part in plants, is located in chloroplasts in large numbers and can be easily extracted into lipid solvents such as acetone and ether [9]. Chlorophyll in plants has a role in the process of photosynthesis which can produce carbohydrates with the help of solar energy. Plants can have high chlorophyll content because environmental factors are in the right conditions [14].

4. Conclusion

Based on the results of the research that has been carried out, it can be concluded that the induced fusaric acid with 5 concentrations, namely 10 ppm, 20 ppm, 30 ppm and 40 ppm can affect the *Dendrobium* sp plantlets, which can increase the total phenol content, reducing sugar content and chlorophyll content of plantlets compared to control (0 ppm).

Compliance with ethical standards

Acknowledgments

The researcher would like to thank the Botanical Laboratory, especially the *In Vitro* Culture Room, Department of Biology, Faculty of Mathematics and Natural

Sciences, University of Lampung, Bandar Lampung, Lampung, Indonesia, which has provided a place to conduct and process research data.

Disclosure of conflict of interest
All authors have no conflicts of interest

References

[1] Surtinah S, dan Mutryarny E. Frequency of Giving Grow Quick Lb to the Growth of Dendrobium Orchid Seeds at the Pot Community Stadia. *Jurnal Ilmiah Pertanian*. 2013; 10(2): 31-40.
[2] Widiastoety, D. Potential of *Dendrobium* orchids in increasing variety and quality of cut flower orchids. *Journal of Research and Development*. 2010; 29 (3): 101-106.
[3] Bouizgarne B, El-Maarouf BH, Frankart C, Reboutier D, Madiona K, Pennarun AM, Monestiez M, Trouverie J, Amiar Z, Briand J, Brault M, Rona JP, Ouhdouch Y, El Hadrami I. Early physiological responses of Arabidopsis thaliana cells to fusaric acid: Toxic and signallling effects. *New Phytopathologist*. 2006; 169: 209 – 218.
[4] Dhianawaty D, and Ruslin. Polyphenols and Antioxidant Activity of Imperata cylindrica (L.) Beauv. Root Methanol Extract. *Bandung Medical Magazine*. 2015; 47(1): 60–64.
[5] Arsenault PR, Vail DR, Wobbe KK, Weathers PJ. Effect of sugars on artemisinin production in Artemisia annua L.: transcription and metabolite measurements. *Molecules*. 2010; 15(4): 2302–2318.
[6] Khaleghi, E., Arzani, K., Moallemi, N., & Barzegar, M. Evaluation of chlorophyll content and chlorophyll fluorescence parameters and relationships between chlorophyll a, b and chlorophyll content index under water stress in Olea europaea cv. Dezful. *World Acad. Sci. Eng. Technol*. 2012; 68: 1154-1157.
[7] Hardiana R, dan Rudiyansyah, Titin Anita Zaharah. Antioxidant Activity of Phenol Group Compounds from Several Plant Types of the Malvaceae Family. *Clinical Medicine Journal*. 2012; 1: 8-13.
[8] Pujiati P, Primiani CN. Analysis of Reducing Sugar Levels in Fermentation of Gude Beans (Cajanus cajan) by Aspergillus niger. *Biology Seminar Proceedings*. 2016; 13(1): 832-835.
[9] Harbourne JB. *Phytochemical Method*. Translation: Padmawinata K & Sudiro I. ITB Bandung Publisher. 1987; 259-261.
[10] Nurcahyani E, Sumardi I, Hadisutrisno B, dan Suharyanto E. Suppression of development of vanilla foot rot disease (*Fusarium oxysporum* f.sp. *vanillae*) through *in vitro* fusaric acid selection. *Journal of Tropical Plant Pests and Diseases*. 2012; 12(1): 12-22.
[11] Vagiri M, E Johansson, K Rumpunen. Phenolic Compounds In Black Currant Leaves – An Interaction Between The Plant And Foliar Diseases. *Plant Interaction*. 2017; 1(12): 193-199.
[12] Al-kayyis HK, Susanti H. Comparison of the somogyi-nelson and anthrone-sulfate methods for determining reducing sugar content in cilembu (*Ipomea batatas* L.) tubers. *J. Pharmacy Science and Community*. 2016; 13(2): 81-89.
[13] Andari G, Nurcahyani E. Analysis of Chlorophyll Content Result of In Vitro Influenced Resistance of Fusarium oxysporum Against *Spathoglottis plicata*. *Musamus Journal of Animal Livestock Science*. 2018; 1(1): 21-23.
[14] Nurcahyani E, Sumardi, Hardoko IQ, Asma P, Sholekhah. Analysis of Chlorophyll *Phalaenopsis amabilis* (L.) Bl. Results of the Resistance to *Fusarium oxysporum* and Drought Stress. *Journal of Agriculture and Veterinary Science*. 2019; 12(11) I: 41-46.

ROUGH U-EXACT SEQUENCE OF ROUGH GROUPS

Fitri Ayuni, Fitriani*, Ahmad Faisol

Universitas Lampung, Indonesia

Article Info

Submitted : *dd:mm:yyyyy*
Revised : *dd:mm:yyyyy*
Accepted : *dd:mm:yyyyy*
Published : *dd:mm:yyyyy*

*Correspondence:
fitriani.1984@fmipa.unila.ac.id

Abstract

The notion of a U-exact sequence is a generalization of the exact sequence. In this paper, we introduce a rough U-exact sequence in a rough group in an approximation space. Furthermore, we provide the properties of the rough U-exact sequence in a rough group.

Key Words: exact sequence, rough U-exact sequence, rough group.

http://ejournal.radenintan.ac.id/index.php/al-jabar/index

Introduction

In 1982, Zdzislaw Pawlak developed one of the mathematical techniques known as rough set theory (Pawlak, 1982). The fundamental concept of the rough set theory is an equivalence relation. The equivalence class is a partition used to determine the lower and upper bounds of universe subsets.

Assume U is a non-empty set, which we refer to as the universe set, and R is an equivalence relation on U. The pair (U, R) represents an approximation space (Miao et al., 2005). If $X \subseteq U$, the lower approximation of X, denoted by $\underline{X}$, is a union of the equivalence class contained in X. The upper approximation of X, denoted by $\bar{X}$, is a union of the equivalence class intersecting with X. If $\bar{X} - \underline{X} \neq \emptyset$, then the set X is a rough set.

In 1997, Kuroki gave the idea of the ideal rough in semigroups (Kuroki, 1997). Furthermore, Miao et al. introduce the rough groups, rough subgroups, and their properties (Miao et al., 2005). Moreover, Davvaz and Mahdavipour investigate the rough module (Davvaz & Mahdavipour, 2006). Isaac and Neelima introduce the concept of rough ideals and their properties (Isaac & Neelima, 2013). Sinha and Prakash study the exact sequence of rough modules (Sinha, 2016). Furthermore, Jesmalar gives the homomorphism and the rough group isomorphism (Jesmalar, 2017). Besides that, Davvaz and Parnian-Garamaleky give a concept of the U-exact sequence of the R-module (Davvaz & Parnian-Garamaleky, 1999). Then, Fitriani et al. introduce the notion of sub-exact sequence of R-modules (Fitriani et al., 2016). Elfiyanti et al. also give an Abelian property of the category of U-complexes, which is motivated by the U-exact sequence (Elfiyanti et al., 2016). Aminizadeh et al. (Aminizadeh et al., 2017) introduce an exact sequence of S-acts. Fitriani et al. also establish the notion of an X-sub-linearly independent module (Fitriani et al., 2017). They introduce a U_V-generated module (Fitriani et al., 2018b). Furthermore, using the concept of a sub-exact sequence of

modules, they established U-basis and U-free modules (Fitriani et al., 2018a). Moreover, they define the rank of the U_V-generated module (Fitriani et al., 2021). Then, they apply the sub-exact sequences to determine the Noetherian property of the submodule of the generalized power series module (Faisol et al., 2021). In addition, Setyaningsih et al. introduce the sub-exact sequence in the rough groups (Setyaningsih et al., 2021). In this research, we introduce the U-exact sequence of the rough group and its properties.

The Research Methods

This study was based on literature searches, specifically those on rough sets, upper and lower approximation space, rough groups, exact sequence, and U-exact sequence. First, we define the rough U-exact sequence in an approximation space. Then we examine properties of the rough group. In the following step, we use a finite set to construct an example of a U-exact sequence in a rough group. Finally, we examine the properties of the U-exact sequence in the rough group.

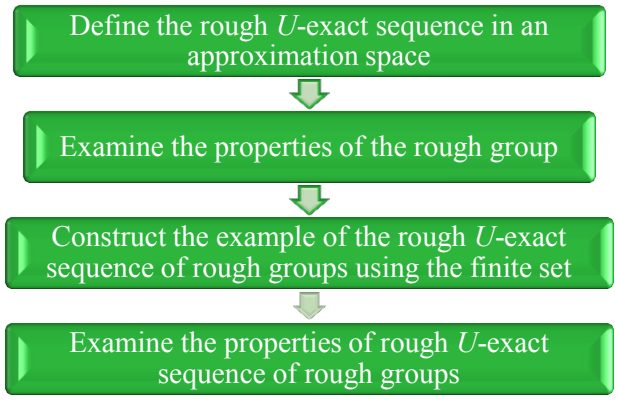

Figure 1. Research stage diagram

The Results of the Research and the Discussion

Motivated by the definitions of the U-exact sequence of the R-module, we construct the definition of the rough U-exact sequence as follows.

Definition 1. Let (S,θ) be an approximation space, and let K, L, M the rough groups in (S,θ), and U is the rough subgroup of M. A sequence

$$\overline{K} \xrightarrow{f} \overline{L} \xrightarrow{g} \overline{M}$$

is called rough U-exact in M, if im $(f) = g^{-1}(\overline{U})$.

Before investigating the properties of the rough U-exact sequence, we give the construction of a rough subgroup in an approximation space.

Example 1. Let $\mathbb{Z}_9 = \{\overline{0}, \overline{1}, \overline{2}, \overline{3}, \overline{4}, \overline{5}, \overline{6}, \overline{7}, \overline{8}\}$ is a set of integers modulo 9 and $+_9$ modulo 9 summation operations. We define $\mathbb{Z}_9$ as the relation on R is aRb where $a, b \in \mathbb{Z}_9$ if and only if $a - b = 4k$, for some $k \in \mathbb{Z}$. From this equivalence relation, we have 4 equivalence classes as follows:

$E_1 = \{\overline{1}, \overline{5}\}$,
$E_2 = \{\overline{2}, \overline{6}\}$,
$E_3 = \{\overline{3}, \overline{7}\}$,
$E_4 = \{\overline{0}, \overline{4}, \overline{8}\}$.

Next, we will construct three rough groups to form a rough U-exact sequence of rough groups. Let $X_1 = \{\overline{0}, \overline{4}, \overline{5}\}$. We obtain $\overline{X_1} = E_1 \cup E_4 = \{\overline{0}, \overline{1}, \overline{4}, \overline{5}, \overline{8}\}$.

Table 1. Table Cayley on X_1

$+_9$	$\bar{0}$	$\bar{4}$	$\bar{5}$
$\bar{0}$	$\bar{0}$	$\bar{4}$	$\bar{5}$
$\bar{4}$	$\bar{4}$	$\bar{8}$	$\bar{0}$
$\bar{5}$	$\bar{5}$	$\bar{0}$	$\bar{1}$

(1) Table 1 shows that for every $x, y \in X_1$, $x\ (+_9)\ y \in \overline{X_1}$;
(2) association property holds in $\overline{X_1}$;
(3) there exists $\bar{0} \in \overline{X_1}$, such that for every $\bar{x} \in \overline{X_1}$, $\bar{x}(+_9)\bar{0} = \bar{0}(+_9)\bar{x} = \bar{x}$;
(4) there exists $\bar{x} \in X_1$, there exists $\bar{y} \in X_1$ such that $\bar{x}(+_9)\bar{y} = \bar{0}$ or $\bar{y} = (\bar{x})^{-1}$, that is $(\bar{0})^{-1} = \bar{0} \in X_1$, $(\bar{4})^{-1} = \bar{5} \in X_1$, and $(\bar{5})^{-1} = \bar{4} \in X_1$.

Table 2. Rough Inverse Element on X_1

No	1	2	3
$\bar{x} \in X_1$	$\bar{0}$	$\bar{4}$	$\bar{5}$
Inverse of $\bar{x}$	$\bar{0}$	$\bar{5}$	$\bar{4}$

Based on Table 2, we have that every element of X_1 has a rough inverse in $\overline{X_1}$. Hence, X_1 is a rough group.

Now, let $X_2 = \{\bar{1}, \bar{3}, \bar{6}, \bar{8}\}$. We get $\overline{X_2} = E_1 \cup E_2 \cup E_3 \cup E_4 = \mathbb{Z}_9$.

Table 3. Table Cayley on X_2

$+_9$	$\bar{1}$	$\bar{3}$	$\bar{6}$	$\bar{8}$
$\bar{1}$	$\bar{2}$	$\bar{4}$	$\bar{7}$	$\bar{0}$
$\bar{3}$	$\bar{4}$	$\bar{6}$	$\bar{0}$	$\bar{2}$
$\bar{6}$	$\bar{7}$	$\bar{0}$	$\bar{3}$	$\bar{5}$
$\bar{8}$	$\bar{0}$	$\bar{2}$	$\bar{5}$	$\bar{7}$

(1) Table 3 shows that for every $x, y \in X_2$, $x\ (+_9)\ y\ \in \overline{X_2}$;
(2) association property holds in $\overline{X_2}$;
(3) there exists $\bar{0} \in \overline{X_2}$, such that for every $\bar{x} \in \overline{X_2}$, $\bar{x}(+_9)\bar{0} = \bar{0}(+_9)\bar{x} = \bar{x}$;
(4) for every $\bar{x} \in X_2$, there exist $\bar{y} \in X_2$, such that $\bar{x}(+_9)\bar{y} = \bar{0}$ or $\bar{y} = (\bar{x})^{-1}$, that is $(\bar{1})^{-1} = \bar{8} \in X_2$, $(\bar{8})^{-1} = \bar{1} \in X_2$, $(\bar{3})^{-1} = \bar{6} \in X_2$, and $(\bar{6})^{-1} = \bar{3} \in X_2$.

Table 4. Rough Inverse Element on X_2

No	1	2
$\bar{x} \in X_2$	$\bar{1}$	$\bar{3}$
Inverse of $\bar{x}$	$\bar{8}$	$\bar{6}$

Table 4 shows that every element of X_2 has a rough inverse in $\overline{X_2}$. Hence, X_2 is a rough group.

Let $X_3 = \{\bar{1}, \bar{3}, \bar{4}, \bar{5}, \bar{6}, \bar{8}\}$. We obtain $\overline{X_3} = E_1 \cup E_2 \cup E_3 \cup E_4 = \mathbb{Z}_9$.

Table 5. Table Cayley on X_3

$+_9$	$\bar{1}$	$\bar{3}$	$\bar{4}$	$\bar{5}$	$\bar{6}$	$\bar{8}$
$\bar{1}$	$\bar{2}$	$\bar{4}$	$\bar{5}$	$\bar{6}$	$\bar{7}$	$\bar{0}$
$\bar{3}$	$\bar{4}$	$\bar{6}$	$\bar{7}$	$\bar{8}$	$\bar{0}$	$\bar{2}$
$\bar{6}$	$\bar{7}$	$\bar{0}$	$\bar{1}$	$\bar{2}$	$\bar{3}$	$\bar{5}$
$\bar{8}$	$\bar{0}$	$\bar{2}$	$\bar{3}$	$\bar{4}$	$\bar{5}$	$\bar{7}$

(1) Table 5 shows that for every $x, y \in X_3$, $x\ (+_9)\ y \in \overline{X_3}$;
(2) association property holds in $\overline{X_3}$;
(3) there exists $\bar{0} \in \overline{X_3}$, such that for every $\bar{x} \in \overline{X_3}$, $\bar{x}(+_9)\bar{0} = \bar{0}(+_9)\bar{x} = \bar{x}$;
(4) for every $\bar{x} \in X_3$, there exist $\bar{y} \in X_3$, such that $\bar{x}(+_9)\bar{y} = \bar{0}$ or $\bar{y} = (\bar{x})^{-1}$, that is
$(\bar{1})^{-1} = \bar{8} \in X_3$, $(\bar{8})^{-1} = \bar{1} \in X_3$, $(\bar{3})^{-1} = \bar{6} \in X_3$, $(\bar{6})^{-1} = \bar{3} \in X_3$, $(\bar{4})^{-1} = \bar{5} \in X_3$, and $(\bar{5})^{-1} = \bar{4} \in X_3$.

Table 6. Rough Inverse Element on X_3

No	1	2	3
$\bar{x} \in X_3$	$\bar{1}$	$\bar{3}$	$\bar{4}$
Inverse of $\bar{x}$	$\bar{8}$	$\bar{6}$	$\bar{5}$

Based on Table 6, we have every element of X_3 has a rough inverse in $\overline{X_3}$. Hence, X_3 is a rough group.

Finally, we form a sequence $\overline{X_1} \xrightarrow{f} \overline{X_2} \xrightarrow{g} \overline{X_3}$ with f homomorphism rough group $f: a \bmod 9$ and g identity function. Then let $U_1 \subseteq X_3$, let $U_1 = \{\bar{4}, \bar{5}\}$ obtained $\overline{U_1} = E_1 \cup E_4 = \{\bar{0}, \bar{1}, \bar{4}, \bar{5}, \bar{8}\}$ is a rough subgroup of X_3. We have $\bar{4}(+_9)\bar{5} = \bar{0} \in \overline{U_1}$ and $(\bar{4})^{-1} = \bar{5} \in U_1$.

We will show the sequence $\overline{X_1} \xrightarrow{f} \overline{X_2} \xrightarrow{i} \overline{X_3}$ is U_1-exact in $\overline{X_3}$. Since $\overline{X_1} \xrightarrow{f} \overline{X_2}$, $f: a \bmod 9$, and $\overline{X_2} \xrightarrow{i} \overline{X_3}$, we have:

$$\begin{aligned}\text{im}\,(f) &= \{x \in \overline{X_2} | x = f(\overline{X_1})\} \\ &= \{x \in \overline{X_2} | g(x) = \overline{U_1}\} \\ &= g^{-1}(\overline{U_1}) \\ &= \{\bar{0}, \bar{1}, \bar{4}, \bar{5}, \bar{8}\}\end{aligned}$$

Hence $\overline{X_1} \xrightarrow{f} \overline{X_2} \xrightarrow{g} \overline{X_3}$ is U_1-exact in $\overline{X_3}$.
Next, we will give the properties of the rough U-exact sequence of rough groups.

Proposition 1. Let (V, θ) be an approximation space, K a rough group in V, and $U_1, U_2, \ldots U_n$ rough subgroup K. If $\overline{U_1} \cap \overline{U_2} \cap \ldots \cap \overline{U_n} = \overline{U_1 \cap U_2 \cap \ldots U_n}$ then $U_1 \cap U_2 \cap \ldots U_n$ is a rough subgroup K of the approximation space (V, θ).

Proof. Let $U_1, U_2, \ldots U_n$ rough subgroups of K with binary operation $*$. Given any $a, b \in U_1 \cap U_2 \cap \ldots \cap U_n$ then $a * b \in \overline{U_i}, \forall i = 1,2, \ldots, n$. Furthermore, $a - b \in U_i, \forall i = 1,2, \ldots, n$. Next $a * b \in \overline{U_1} \cap \overline{U_2} \cap \ldots \cap \overline{U_n}, \forall i = 1,2, \ldots, n$ and $a - b \in U_1 \cap U_2 \cap \ldots \cap U_n$. If $\overline{U_1} \cap \overline{U_2} \cap \ldots \cap \overline{U_n} = \overline{U_1 \cap U_2 \cap \ldots \cap U_n}$, then $a * b \in \overline{U_1 \cap U_2 \cap \ldots \cap U_n}, \forall i = 1,2, \ldots, n$ and $a - b \in U_1 \cap U_2 \cap \ldots \cap U_n$. In other words, $U_1 \cap U_2 \cap \ldots \cap U_n$ is a rough subgroup of K. ■

Example 2. Let $V = \{0,1,2,3,4, \ldots, 49\}$. We define the relation R in V, where aRb if and only if $a - b = 6k$, for some $k \in \mathbb{Z}$ and $a, b \in V$. It is easy to show that R is an equivalence relation on V. From this equivalence relation, we have 6 equivalence classes as follows:

$E_1 = [1] = \{1,7,13,19,25,31,37,43,49\}$,
$E_2 = [2] = \{2,8,14,20,26,32,38,44\}$,
$E_3 = [3] = \{3,9,15,21,27,33,39,45\}$,
$E_4 = [4] = \{4,10,16,22,28,34,40,46\}$,
$E_5 = [5] = \{5,11,17,23,29,35,41,47\}$,
$E_6 = [6] = \{0,6,12,18,24,30,36,42,48\}$.
Let $Y = \{2,4,5,8,10,14,15,16,20,22,23,25,27,28,30,34,35,36,40,42,45,46,48\} \subseteq V$.

Therefore, the lower approximation and the upper approximation of Y are as follows:
$\underline{Y} = E_4 = \{4,10,16,22,28,34,40,46\}$
$\bar{Y} = E_1 \cup E_2 \cup E_3 \cup E_4 \cup E_5 \cup E_6 = V$
The rough set Y is the ordered pair of the lower approximation and the upper approximation written as $Apr(Y) = (\{4,10,16,22,28,34,40,46\}, V)$.
Next, we define the binary operation $+_{50}$ on rough set Y. We will show that $\langle Y, +_{50}\rangle$ is a rough group.

1. $a+_{50}b \in \bar{Y}$, for every $a, b \in Y$.
2. Association property holds in $\bar{Y}$, i.e. $(a+_{50}b)+_{50}c = a+_{50}(b+_{50}c)$, for every $a, b \in \bar{Y}$.
3. There exist the rough identity element $0 \in \bar{Y}$, such that for every $y \in Y, y(+_{50})0 = 0(+_{50})y = y$.
4. For every $y \in Y$, there is a rough inverse element of y, i.e. $y^{-1} \in Y$ such that $y+_{50}y^{-1} = y^{-1}+_{50}y = 0$.

Hence, $\langle Y, +_{50}\rangle$ is a rough group on the approximation space (S, θ).
Next, let $I = \{2,4,20,22,28,30,46,48\}$. We have $\bar{I} = E_2 \cup E_4 \cup E_6$. Since $I \subseteq Y$ and each element of I has an rough inverse in I, then I is a rough subgroup of Y. Now, let $J = \{2,5,23,27,45,48\}$ and $\bar{J} = E_2 \cup E_3 \cup E_5 \cup E_6$. We will show that J rough subgroup Y. Since $J \subseteq Y$ and each element of J has a rough inverse in J, then J is a rough subgroup of Y.
From the two rough subgroups that have been constructed in the previous section can be obtained
$I \cap J = \{2,48\}$
$\overline{I \cap J} = \{0,2,6,8,12,14,18,20,24,26,30,32,36,38,42,44,48\}$
The same can be obtained.
$\bar{I} \cap \bar{J} = \{0,2,6,8,12,14,18,20,24,26,30,32,36,38,42,44,48\}$
Consequently $\bar{I} \cap \bar{J} = \overline{I \cap J} = E_2 \cup E_6$
$= \{0,2,6,8,12,14,18,20,24,26,30,32,36,38,42,44,48\}$
Next, it will be indicated that $I \cap J = \{2,48\}$ is a rough subgroup of Y.

i. $2(+_{50})48 = 0 \in \overline{I \cap J}$,
ii. $(2)^{-1} = 48 \in I \cap J$.

Hence {2,48} is also a subgroup rough of Y.

Proposition 2. Let (S, θ) be an approximation space, and let K, L, M be rough groups. then U_1 and U_2 are a rough subgroup of M and $U_1 \neq U_2$ where $\overline{U_1} = \overline{U_2}$. If a sequence

$$\bar{K} \xrightarrow{f} \bar{L} \xrightarrow{g} \bar{M}$$

is a rough $\overline{U_1}$-exact sequence, then the sequence $\bar{K} \xrightarrow{f} \bar{L} \xrightarrow{g} \bar{M}$ is a rough $\overline{U_2}$-exact sequence.

Proof. We assume that the sequence $\bar{K} \xrightarrow{f} \bar{L} \xrightarrow{g} \bar{M}$ is a rough U_1-exact sequence. Based on Definition 1, we have im $(f) = g^{-1}(\overline{U_1})$. Since $\overline{U_1} = \overline{U_2}$, we have im $(f) = g^{-1}(\overline{U_2})$. In other words, the sequence $\bar{K} \xrightarrow{f} \bar{L} \xrightarrow{g} \bar{M}$ is U_2-exact rough in M. ■

Example 3. Let $\mathbb{Z}_9 = \{\bar{0}, \bar{1}, \bar{2}, \bar{3}, \bar{4}, \bar{5}, \bar{6}, \bar{7}, \bar{8}\}$ is a set of integers modulo 9 and $+_9$ modulo 9 summation operations. We define $\mathbb{Z}_9$ as the relation on R is aRb where a, $b \in \mathbb{Z}_9$ if and only if $a - b = 4k$, for some $k \in \mathbb{Z}$. From this equivalence relation, we have 4 equivalence classes as follows:
$E_1 = \{\bar{1}, \bar{5}\}$,
$E_2 = \{\bar{2}, \bar{6}\}$,
$E_3 = \{\bar{3}, \bar{7}\}$,
$E_4 = \{\bar{0}, \bar{4}, \bar{8}\}$.

Next, we construct three rough groups to form a rough U-exact sequence of rough groups. Let $X_1 = \{\bar{0}, \bar{4}, \bar{5}\}$. We have $\overline{X_1} = E_1 \cup E_4 = \{\bar{0}, \bar{1}, \bar{4}, \bar{5}, \bar{8}\}$.
(1) for every $x, y \in X_1$, $x\ (+_9)\ y \in \overline{X_1}$;
(2) association property holds in $\overline{X_1}$;
(3) there exists $\bar{0} \in \overline{X_1}$, such that for every $\bar{x} \in \overline{X_1}$, $\bar{x}(+_9)\bar{0} = \bar{0}(+_9)\bar{x} = \bar{x}$;
(4) for every $\bar{x} \in X_1$, there exists $\bar{y} \in X_1$ such that $\bar{x}(+_9)\bar{y} = \bar{0}$ or $\bar{y} = (\bar{x})^{-1}$, that is
$(\bar{0})^{-1} = \bar{0} \in X_1$, $(\bar{4})^{-1} = \bar{5} \in X_1$, and $(\bar{5})^{-1} = \bar{4} \in X_1$.
Hence, X_1 is a rough group.

Now, let $X_2 = \{\bar{1}, \bar{3}, \bar{6}, \bar{8}\}$. We have $\overline{X_2} = E_1 \cup E_2 \cup E_3 \cup E_4 = \mathbb{Z}_9$.
(1) for every $x, y \in X_2$, $x\ (+_9)\ y\ \in \overline{X_2}$;
(2) association property holds in $\overline{X_2}$;
(3) there exists $\bar{0} \in \overline{X_2}$, such that for every $\bar{x} \in \overline{X_2}$, $\bar{x}(+_9)\bar{0} = \bar{0}(+_9)\bar{x} = \bar{x}$;
(4) for every $\bar{x} \in X_2$, there exist $\bar{y} \in X_2$ such that $\bar{x}(+_9)\bar{y} = \bar{0}$ or $\bar{y} = (\bar{x})^{-1}$, that is
$(\bar{1})^{-1} = \bar{8} \in X_2$, $(\bar{8})^{-1} = \bar{1} \in X_2$, $(\bar{3})^{-1} = \bar{6} \in X_2$, and $(\bar{6})^{-1} = \bar{3} \in X_2$.
Hence, X_2 is a rough group.

Let $X_3 = \{\bar{1}, \bar{3}, \bar{4}, \bar{5}, \bar{6}, \bar{8}\}$. We obtain $\overline{X_3} = E_1 \cup E_2 \cup E_3 \cup E_4 = \mathbb{Z}_9$.
(1) for every $x, y \in X_3$, $x\ (+_9)\ y \in \overline{X_3}$;
(2) operation $(+_9)$ association property holds in $\overline{X_3}$;
(3) there exists $\bar{0} \in \overline{X_3}$,such that for every $\bar{x} \in \overline{X_3}$, $\bar{x}(+_9)\bar{0} = \bar{0}(+_9)\bar{x} = \bar{x}$;
(4) for every $\bar{x} \in X_3$, there exist $\bar{y} \in X_3$ such that $\bar{x}(+_9)\bar{y} = \bar{0}$ or $\bar{y} = (\bar{x})^{-1}$, that is
$(\bar{1})^{-1} = \bar{8} \in X_3$, $(\bar{8})^{-1} = \bar{1} \in X_3$, $(\bar{3})^{-1} = \bar{6} \in X_3$, $(\bar{6})^{-1} = \bar{3} \in X_3$, $(\bar{4})^{-1} = \bar{5} \in X_3$, and $(\bar{5})^{-1} = \bar{4} \in X_3$.
Hence, X_3 is a rough group.

Next, we form a sequence $\overline{X_1} \xrightarrow{f} \overline{X_2} \xrightarrow{g} \overline{X_3}$. Let $U_1 = \{\bar{4}, \bar{5}\} \subseteq X_3$. We obtain $\overline{U_1} = E_1 \cup E_4 = \{\bar{0}, \bar{1}, \bar{4}, \bar{5}, \bar{8}\}$ is a rough subgroup of X_3. We get $\bar{4}(+_9)\bar{5} = \bar{0} \in \overline{U_1}$ and $(\bar{4})^{-1} = \bar{5} \in U_1$.
We will show the sequence $\overline{X_1} \xrightarrow{f} \overline{X_2} \xrightarrow{g} \overline{X_3}$ is U_1-exact in $\overline{X_3}$.
Since $\overline{X_1} \xrightarrow{f} \overline{X_2}$, $f: a \bmod 9$, and $\overline{X_2} \xrightarrow{g} \overline{X_3}$, g identity function, we obtain
$$\begin{aligned}\text{im}\,(f) &= \{x \in \overline{X_2} | x = f(\overline{X_1})\} \\ &= \{x \in \overline{X_2} | g(x) = \overline{U_1}\} \\ &= g^{-1}(\overline{U_1}) \\ &= \{\bar{0}, \bar{1}, \bar{4}, \bar{5}, \bar{8}\}\end{aligned}$$
Hence $\overline{X_1} \xrightarrow{f} \overline{X_2} \xrightarrow{g} \overline{X_3}$ is U_1-exact in $\overline{X_3}$.

Next, we form the second sequence: $\overline{X_1} \xrightarrow{f} \overline{X_2} \xrightarrow{g} \overline{X_3}$ with f homomorphism rough group $f: a \bmod 9$ and g identity function. Then let $U_2 = \{\bar{1}, \bar{8}\} \subseteq X_3$. We obtain $\overline{U_2} = E_1 \cup E_4 = \{\bar{0}, \bar{1}, \bar{4}, \bar{5}, \bar{8}\}$ is a rough subgroup of X_3, and $\bar{1}(+_9)\bar{8} = \bar{0} \in \overline{U_2}$ and $(\bar{1})^{-1} = \bar{8} \in U_2$.
We will show the sequence $\overline{X_1} \xrightarrow{f} \overline{X_2} \xrightarrow{g} \overline{X_3}$ is U_2- exact in $\overline{X_3}$.

Since $\overline{X_1} \xrightarrow{f} \overline{X_2}$, $f: a \bmod 9$ dan $\overline{X_2} \xrightarrow{g} \overline{X_3}$, g identity function, we have:

$$\begin{aligned} \text{im}\,(f) &= \{x \in \overline{X_2} | x = f(\overline{X_1})\} \\ &= \{x \in \overline{X_2} | g(x) = \overline{U_2}\} \\ &= g^{-1}(\overline{U_2}) \\ &= \{\overline{0}, \overline{1}, \overline{4}, \overline{5}, \overline{8}\} \end{aligned}$$

Hence $\overline{X_1} \xrightarrow{f} \overline{X_2} \xrightarrow{g} \overline{X_3}$ is U_2-exact in $\overline{X_3}$.

From Example 3, we can conclude that if the sequence $\overline{X_1} \xrightarrow{f} \overline{X_2} \xrightarrow{g} \overline{X_3}$ is a rough U_1-exact sequence and U_2 is a subgroup of rough of $\overline{X_3}$ where $U_1 \neq U_2$ and $\overline{U_1} = \overline{U_2}$, the sequence $\overline{X_1} \xrightarrow{f} \overline{X_2} \xrightarrow{g} \overline{X_3}$ is a rough U_2-exact rough in $\overline{X_3}$.

Conclusion and Suggestion

The rough U-exact sequence is a generalization of the rough exact sequence in the rough groups. If K, L, M are rough groups, U_1 and U_2 are a rough subgroups of M and $U_1 \neq U_2$ where $\overline{U_1} = \overline{U_2}$, and the sequence $\overline{K} \xrightarrow{f} \overline{L} \xrightarrow{g} \overline{M}$ is a rough $\overline{U_1}$-exact sequence, then the sequence $\overline{K} \xrightarrow{f} \overline{L} \xrightarrow{g} \overline{M}$ is a rough $\overline{U_2}$-exact sequence.

References

Aminizadeh, R., Rasouli, H., & Tehranian, A. (2017). Quasi-exact Sequences of S-Act. *Bulletin of the Malaysian Mathematical Society*. https://doi.org/https://doi.org/10.1007/s40840-017-0596-3

Davvaz, B., & Mahdavipour, M. (2006). Roughness in modules. *Information Sciences*, 176, 3658–3674.

Davvaz, B., & Parnian-Garamaleky, Y. A. (1999). A Note on Exact Sequences. *Bulletin of the Malaysian Mathematical Society*, 22, 53–56.

Elfiyanti, G., Muchtadi, I., Nasution, D., & Amartiwi, U. (2016). Abelian Property of the Category of U-Complexes Chain of U-Complexes. *International Journal of Mathematical Analysis*, 10(17), 849–853.

Faisol, A., Ftriani, & Sifriyani. (2021). Determining the Noetherian Property of Generalized Power Series Modules by Using X-Sub-Exact Sequence. *Journal of Physics: Conference Series*, 1751(1). https://doi.org/10.1088/1742-6596/1751/1/012028

Fitriani, F., Wijayanti, I. E., Surodjo, B., & Faisol, A. (2021). The Rank of U_V-Generated Modules. *Journal of Mathematics Research*, 13(4), 81. https://doi.org/10.5539/jmr.v13n4p81

Fitriani, Surodjo, B., & Wijayanti, I. E. (2016). On Sub-Exact Sequences. *Far East Journal of Mathematical Sciences (FJMS)*, 100(7), 1055–1065. https://doi.org/dx.doi.org/10.17654/MS100071055

Fitriani, Surodjo, B., & Wijayanti, I. E. (2017). On X-sub-linearly independent modules. *Journal of Physics : Conferences Series*, 893. https://doi.org/https://doi.org/10.1088/1742-6596/893/1/012008

Fitriani, Wijayanti, I. E., & Surodjo, B. (2018a). A Generalization of Basis and Free Modules Relatives to a Family of R-Modules. *Journal of Physics: Conference Series*, 1097(1). https://doi.org/10.1088/1742-6596/1097/1/012087

Fitriani, Wijayanti, I. E., & Surodjo, B. (2018b). Generalization of U -Generator and M -Subgenerator Related to Category σ [M]. *Journal of Mathematics Research*, 10(4), 101–106.

Isaac, P., & Neelima, C. A. (2013). *Rough ideals and their properties*. 1, 1–8.

Jesmalar, L. (2017). Homomorphism and Isomorphism of Rough Group. *International Journal of Advance Research, Ideas and Innovations in Technology*, 3(3), 1382–1387.

Kuroki, N. (1997). Rough ideals in semigroups. *Information Sciences*, 100(1–4), 139–163. https://doi.org/10.1016/S0020-0255(96)00274-5
Miao, D., Han, S., Li, D., & Sun, L. (2005). Rough Group, Rough Subgroup and Their Properties. In *Lecture Notes in Computer Science* (Vol. 3641, pp. 104–113). Springer-Verlag Berlin Heidelberg. https://doi.org/https://doi.org/10.1007/11548669_11
Pawlak, Z. (1982). Rough sets. *International Journal of Computer & Information Sciences*, 11(5), 341–356. https://doi.org/10.1007/BF01001956
Setyaningsih, N., Fitriani, F., & Faisol, A. (2021). Al-Jabar : jurnal pendidikan matematika. *Al-Jabar : Jurnal Pendidikan Matematika*, 12(2), 267–272. http://ejournal.radenintan.ac.id/index.php/al-jabar/article/view/134/124
Sinha, A. K. (2016). *Rough Exact Sequences of Modules*. 11(4), 2513–2517.

THE INFLUENCE OF DISTANCE BETWEEN NEEDLE TIP AND COLLECTOR ON FORMATION OF TITANIUM DIOXIDE (TIO_2) NANOFIBERS WITH ELECTROSPINNING METHOD

Intan Wandira[1, a)] and Posman Manurung[1, b)]

[1]*Postgraduate Student of Physics Program, University of Lampung, Jl. Sumantri Brojonegoro No. 1 Bandar Lampung, Indonesia*

[a)]Corresponding author: intanwandira7@gmail.com
[b)]posman.manurung@fmipa.unila.ac.id

Abstract

Synthesis of Titanium Dioxide (TiO_2) nanofibers has been successfully made using the electrospinning method. This study aims to determine the effect of distance variations on the morphology and crystal structure of TiO_2 nanofibers. The variation of the distance between tip to collector is 7, 9, 11 and 13 cm. The precursor is titanium (IV) isopropoxide (TTIP), ethanol as a solvent, acetic acid as a catalyst and polyvinylpyrrolidone (PVP) as a fiber-forming polymer. The electrospinning process is carried out at a high voltage of 20 kV with a flow rate of 1.5 ml/hour then as-prepared nanofiber annealed at a temperature of 450°C for 3 hours. TiO_2/PVP nanofibers are characterized using Scanning Electron Microscopy – Energy Dispersive X-Ray (SEM-EDS) and X-Ray Diffraction (XRD). The viscosity and surface tension TiO_2/PVP solution 2,8 Pa.s and (28,9 ± 3,7) dyn/cm. SEM result showed relatively uniform nanofiber morphology with fiber diameter ranging from 56 nm – 0,961 μm. XRD result showed that the particle size of the TiO_2 nanofibers ranged from 12 nm with the crystal structure formed are anatase phase.

INTRODUCTION

Nanofiber is one of nanotechnology applications in the form of small threads with a diameter of 100-500 nm [1]. Nanofibers have the characteristics of a high surface area, an interconnected porous structure and conductive [2]. With these characteristics, researchers are interested in developing nanofibers as filters for submicron-sized particles. With a smaller order, nanofibers enable optimization of dust filtration in the air [3].

Titanium dioxide (TiO_2) is one of the materials currently being developed for the manufacture of nanofibers. Besides TiO_2, many materials are available, such as zinc oxide (ZnO) and stannic oxide (SnO_2). However, the use of TiO_2 outperforms the two semiconductor materials. TiO_2 is better because it is cheaper and non-toxic [4,5]. As a high- performance semiconductor, TiO_2 nanofibers have superior potential applications as filter materials, photo-oxidation films, gas sensors, humidity sensors, solar cells and photocatalysts [1, 6-10].

The sol-gel method is commonly used in the synthesis of TiO_2 nanofibers. This method was used because it was believed to produce materials with high homogeneity, relatively cheap, environmentally friendly, and very pure [11]. The sol-gel method is highly dependent on the precursor used [12]. TiO_2 nanofibers are generally synthesized with various precursors such as TTIP, tetrabutyl titanate (TBOT), and titanium tetrachloride ($TiCl_4$). TTIP can produce smaller diameter fibers than other predecessors [13]. That's why TTIP has become the most widely used predecessor.

Nanofibers can be produced in several ways, including multicomponent fiber spinning [14], meltblowing spinning [15], and electrospinning. From the three methods of making fiber, electrospinning technology is the focus of researchers in this study. Electrospinning is a widely used method for obtaining nanofibers, because it is efficient and allows obtaining nanofibers in the minimum size range of 40-2000 nm [16]. In addition, electrospinning allows the fiber diameter to be controlled by adjusting various electrospinning parameters such as voltage, distance between needle tip and fiber collector, and solution viscosity [17,18]. Electrospinning is considered effective in the production of nanofibers because it is cheap, convenient, and allows the use of various materials [19].

Recently Hazem (2020) [20] has synthesized TiO_2/PVP nanofibers at the tip to collector distances of 6, 9, 12, 15 and 18 cm with TTIP as precursor, acetic acid as solution stabilizer, PVP as polymer and ethanol as solvent. Based on SEM data, the best nanofibers are at a distance of 15 cm with a diameter of 65 nm and based on XRD data, the phase formed is the anatase phase.

The above explanation underlies this research, namely the manufacture of TiO_2/PVP nanofibers whose solution was synthesized by the sol-gel method and spun by electrospinning technique. The electrospinning process is carried out by varying the distance from the tip to the electrospinning collector to see its effect on the size and uniformity of the diameter of the fibers formed. The viscosity and surface tension of the solution are monitored to show that the resulting solution can be electrically spun. Ostwald viscometer and tensiometer were used as instruments. Sample characterization was performed using SEM-EDS to determine the morphology and elemental composition of nanofibers and XRD to determine the crystal structure and particle size formed in the samples.

EXPERIMENT

Materials

TTIP ($(Ti(OCH(CH_3)_2)_4$, 97%) was found from Sigma-Aldrich. Acetic acid glacial (CH_3COOH, 100%), methanol (CH_3OH, 99,9%) and ethanol (C_2H_5OH, 99,9%) were found from Merck. PVP ($(C_6H_9NO)_n$, K-90) were purchased from RRC.

Synthesis of TiO_2/PVP Nanofibers

The synthesis process is divided into dissolving polymer and mixing TiO_2/PVP solution. The polymer was prepared by dissolving 1.3 g of PVP in 8 ml of ethanol for 30 minutes while stirring at 350 rpm. Next, a solution of TiO_2 was made by mixing 2.5 ml of TTIP with 3 ml of ethanol, then adding 2.5 ml of CH_3COOH gradually while stirring for 5 minutes at 350 rpm. Then the two solutions were mixed by adding the TiO_2 solution gradually into the polymer solution and stirred for 1 hour at 350 rpm. The exsperiment schematic can be seen in Figure 1.

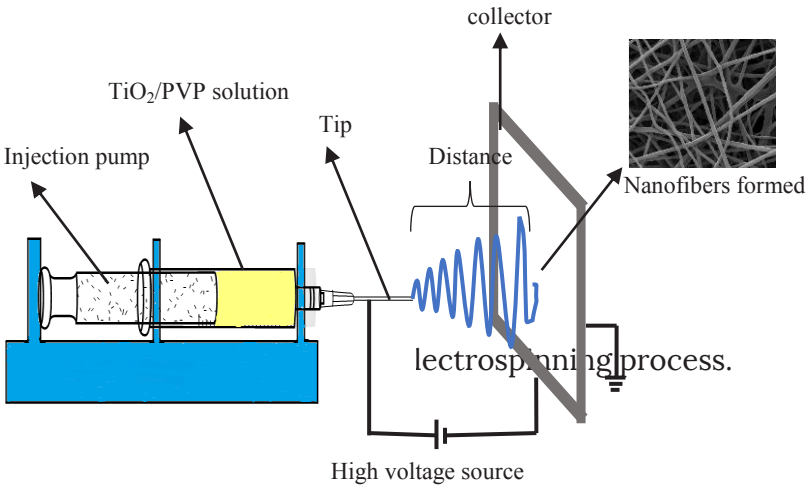

Measurement of the viscosity of the solution is done by looking at the flow rate of the solution on the Ostwald viscometer and calculated by Equation 1.

$$\frac{\eta_1}{\eta_2} = \frac{t_1 \cdot \rho_1}{t_2 \cdot \rho_2}; \eta_2 = \eta_1 \frac{t_2 \cdot \rho_2}{t_1 \cdot \rho_1} \quad (1)$$

where η_1, ρ_1, t_1, η_2, ρ_2, and t_2, respectively are viscosity (Pa.s), density (g/ml), and flow time of solutions 1 and 2 (1 is standard solution (methanol) and 2 is TiO_2/PVP solution) in seconds. Furthermore, the surface tension was measured with a tensiometer and calculated by Equation 2.

$$\gamma_n = \frac{\bar{k}\Delta X}{4\pi r} \quad (2)$$

where γ, k, ΔX, π, and r, respectively are the coefficient of surface tension of the solution (dyn.cm^{-1}), spring constant, solution spring force (mN) and ring radius can be used to make nanofibers using electrospinning techniques [21]. The electrospinning process was carried out to spin TiO_2/PVP nanofibers with a scheme as shown in Figure 1. The solution was put into a 10 ml syringe with a flattened pointed needle tip. The collector used is aluminum foil coated with glass preparations so that the fiber is easy to pick up. The tip to collector distance is varied, namely 7, 9, 11 and 13 cm. The electrospinning process was carried out for 6 hours at room temperature with a flow rate of 1.5 ml/hour. The needle is connected to a positive high voltage while the collector which has been coated with aluminum foil is connected to a negative high voltage rate with a voltage of 20 kV.

Characterization

TiO_2/PVP nanofibers produced by electrospinning were characterized by SEM-EDX (Evo MA 10 model) to obtain the morphology and elemental composition of TiO_2/PVP nanofibers. Powder XRD pattern was obtained using XRD XPERT PRO PANanalytical using Cu kα radiation (λ = 1,54060) at a voltage of 40 kV and a current of 30 mA to obtain the crystal structure and particle size formed in the samples. Particle size was calculated using the Scherrer equation:

$$D = \frac{0{,}9\,\lambda}{B\cos\theta} \quad (3)$$

where λ = X-Ray wavelength, B = full width at half maximum, and θ = scattering angle.

RESULT AND DISCUSSION

Viscosity and Surface Tension

The viscosity of the TiO_2/PVP solution based on Equation 1 is shown in Table 1. The resulting viscosity value of 2,889 Pa.s indicates that the TiO_2/PVP solution can fulfill electrospinning technique [22].

TABLE 1. TiO_2/PVP nanofiber solution viscosity

Description	Value
Methanol viscosity (Pa.s)	0,00059
Methanol mass (g/cm^3)	0,7918
Methanol flow time (s)	20,1433
TiO_2/PVP mass (g/cm^3)	0,9267
TiO_2/PVP flow time (s)	8430
TiO_2/PVP Viscosity (Pa.s)	2,889

The surface tension value of TiO_2/PVP solution obtained based on calculations using Equation 2 is (28.9 ± 3.7) dyn/cm. This value was expressed as the value of surface tension of the solution that can be used in the electrospinning process [21].

Surface Morphology Analysis

Samples characterized by SEM were TiO_2/PVP nanofibers spaced 7, 9, 11 and 13 cm apart. SEM results in the form of surface morphology images are shown in Figure 2. The results of SEM analysis show that the nanofibers have been successfully formed through the electrospinning process. Based on Figure 2, the TiO_2/PVP nanofibers have been spreaded evenly and the resulting fiber size is relatively uniform and continuous.

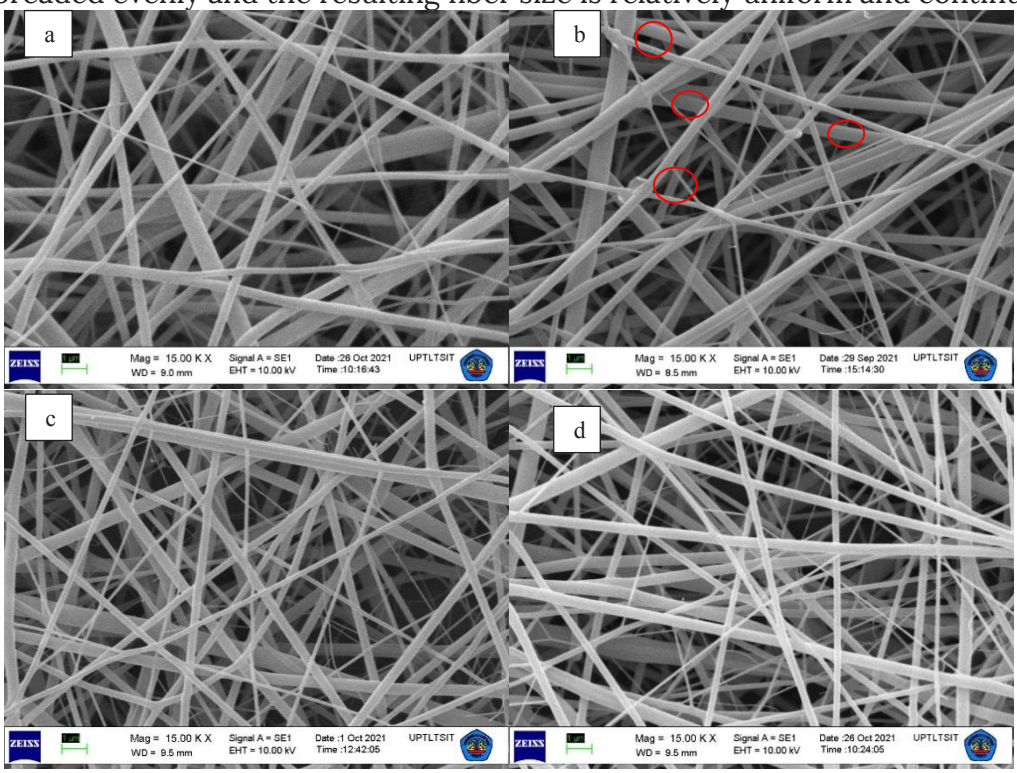

FIGURE 2. Surface morphology of TiO_2/PVP nanofibers in the sample: (a) ES7, (b) ES9, (c) ES11 and (d) ES13.

From the four samples, the fiber size of ES7 obtained appears to be larger than that of the longer distanced fiber. The fiber size is relatively smaller than other samples as seen in the ES11. However, the ES9 showed presence of beads. The presence of beads produced on the fiber is thought to be due to several contributing factors including viscosity, surface tension, and electric field forces experienced by the polymer solution [23]. The thrust at electrospinning voltage of 20 kV is insufficient to overcome the surface tension of solution. In addition, the environmental conditions of the electrospinning system during spinning process were at a temperature (31 ± 2) °C and humidity (60 ± 4) % can cause the solution to oxidize quickly. Oxidation can block the jet stream by the dried solution, so that beads are more likely to form. From the results of the diameter measurements, the observed diameters of samples ES7, ES9, ES11 and ES13 were in the range of 56 nm to 961 μm respectively. The average diameter sizes obtained by each sample were (410 ± 190) nm, (367 ± 169) nm, (286 ± 156) nm and (296 ± 164) nm. The increase in the distance between needle tip and collector obtained optimum distance at 11 cm internal homogenity.

The diameter distribution of TiO_2/PVP nanofibers is shown in Figure 3. Based on the measurements, the diameter distribution of each sample ES7, ES9, ES11 and ES13 are 350, 270, 170 and 330 nm. Accordingly diameter distribution data of TiO_2/PVP nanofibers, it can be stated that there is an optimization of fiber diameter as the distance given increases.

The distance between needle tip and collector affects the morphology and diameter of fiber because the distance can determine deposition time, evaporation rate, and instability of jet or emission of solution. Therefore, it is necessary to have an optimum tip-to-collector distance to form nanofibers with the desired fiber diameter and morphology. Based on the research of Haider et. al. (2015) [24] as the distance increases, the fiber diameter decreases but the solution jet instability increases. As the distance decreases, the fiber diameter increases with decrease jet instability. The tip-to-collector distance is applied to several solutions that have different viscosities, it will produce different fiber diameters. This is also in agreement with the average diameter of TiO_2/PVP nanofibers in the four samples produced. The average diameter of TiO_2/PVP nanofibers proves that the fibers formed are nanofibers because they are <1000 nm in size [25].

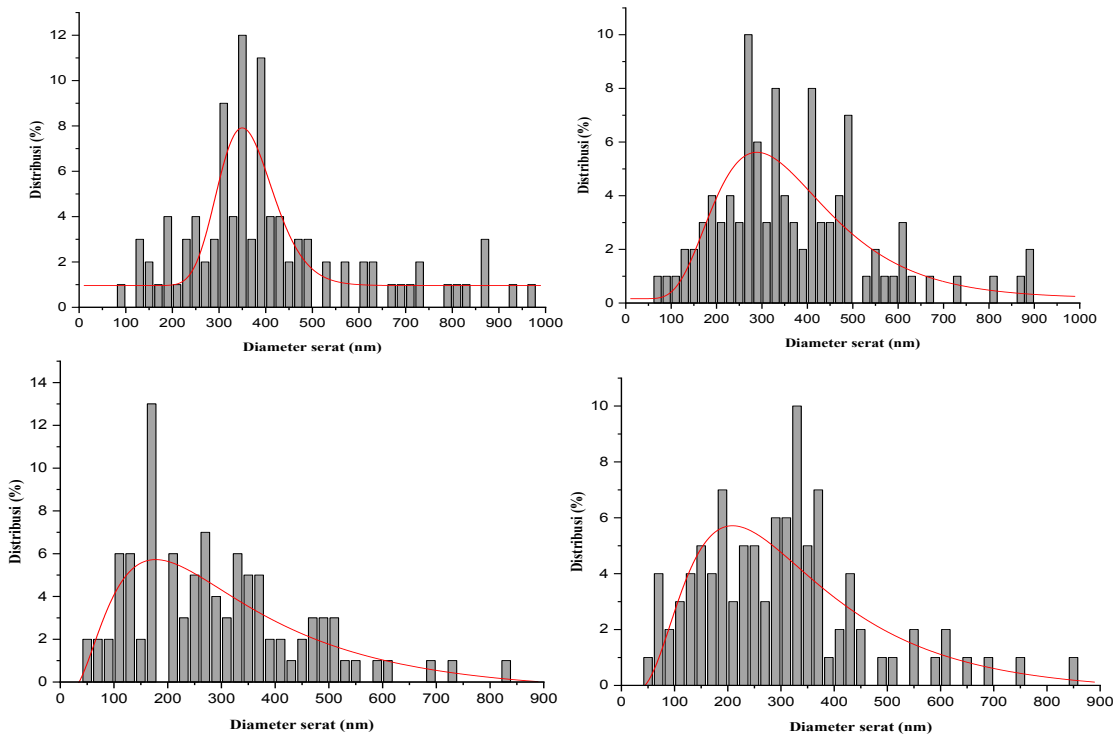

FIGURE 3. Size distribution of nanofiber diameter in the samples: (a) ES7, (b) ES9, (c) ES11, and (d) ES13.

The relationship between needle tip and collector with the average diameter of TiO_2/PVP nanofibers can be seen in Figure 4. By looking at the estimated standard deviation, it can be seen that the graph of the average diameter of TiO_2/PVP nanofibers has an optimization trend and increases with increasing distance.

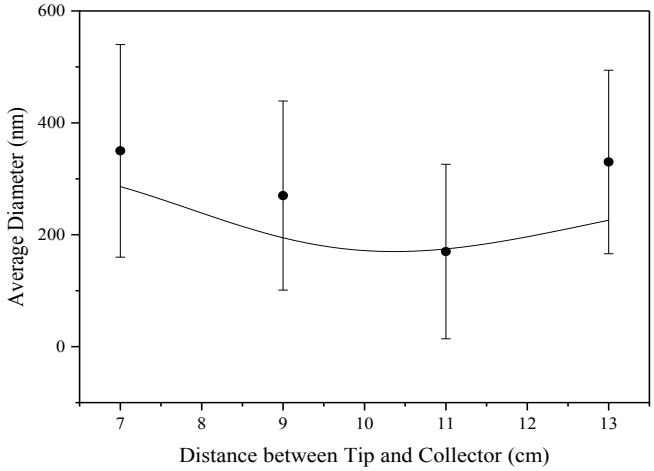

FIGURE 4. Influence of distance between needle tip and collector on the average diameter of TiO_2/PVP nanofibers.

The EDS spectrum is shown in Figure 5. EDS analysis aims to confirm the presence of Ti in TiO_2/PVP nanofibers. The EDS spectrum showed the presence of four constituent elements, namely element C with a mass of 48.80%, O with a mass of 25.29%, Ti with a mass of 17.12% and Si with a mass of 8.79%. The elements that are read in the EDS results are under the formula for the chemical compound TTIP, namely $TiC_{12}H_{28}O_4$, and PVP, namely C_6H_9NO. EDS shows less impurities such as silica in prepared TiO_2 [26].

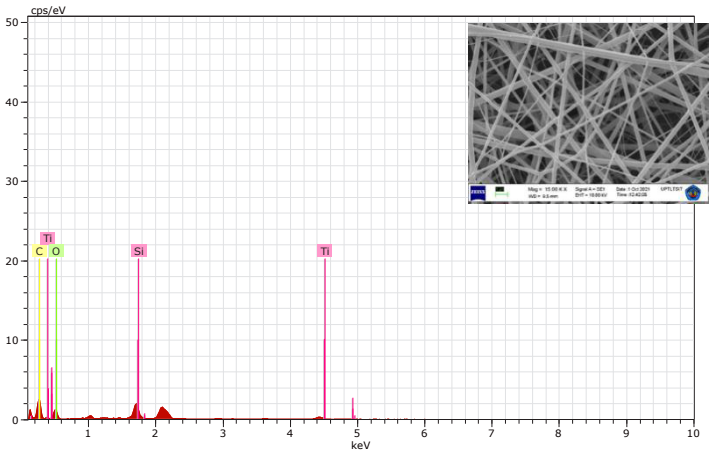

El	AN	Series	unn. C [wt.%]	norm. C [wt.%]	Atom. C [at.%]	Error (1 Sigma) [wt.%]
C	6	K-series	14.66	48.80	63.12	2.28
O	8	K-series	7.60	25.29	24.56	1.38
Ti	22	K-series	5.14	17.12	9.47	0.26
Si	14	K-series	2.64	8.79	2.85	0.17
Total:			30.05	100.00	100.00	

FIGURE 5. Elemental composition of TiO_2/PVP nanofibers sample ES11

XRD Analysis

XRD characterization was carried out to observe the presence of TiO_2/PVP nanofiber crystal phase. The results of matching sample XRD data with database are shown in Figure 6.

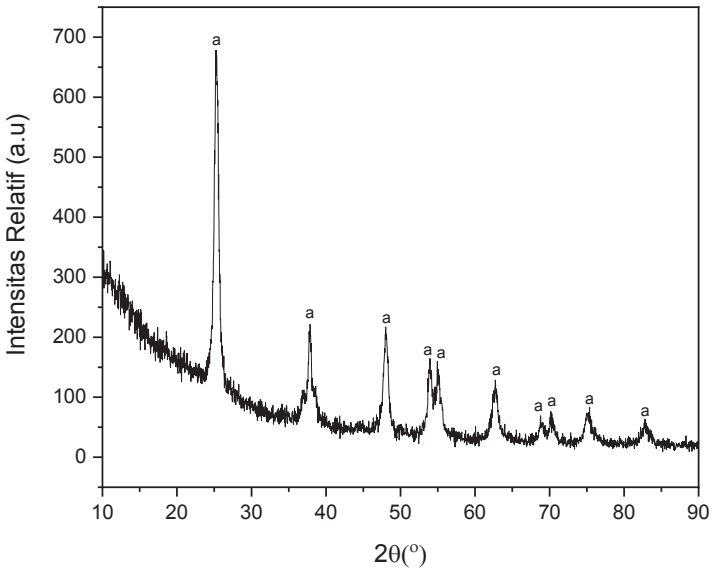

FIGURE 6. XRD diffractogram of sample ES 11. a = anatase.

The results of qualitative analysis show that diffraction peak suitable for the anatase phase is the ICDD file database 01-075-8897 [27]. Figure 6 shows that there is no significant 2θ peak shift. In this study, the highest anatase peak was at position 2θ 25.34° as found in several studies (Abdel et. al. (2014); Galkina et. al. (2011); Manurung et. al. (2020) [28-30]). As shown in Figure 6, rutile and brukit phases are not visible. This is because calcination temperature used is only 450°C. In several studies the appearance of rutile phase occurred at temperatures above 500°C and brukit appeared below 500°C [31-33]. In addition to the heating factor, this is also due to the absence of surfactants involved. The addition of surfactants in the synthesis of TiO_2 can produce a phase other than anatase [28,29].

Quantitative analysis of XRD data was carried out by the Rietveld method. Rietica software was used to refine data [34]. The refinement model used for the anatase phase was Djerdj and Tonejc [35]. The pseudo-Voight function was used to model the shape of diffraction peaks. The refinement result of sample ES11 is shown in Figure 7.

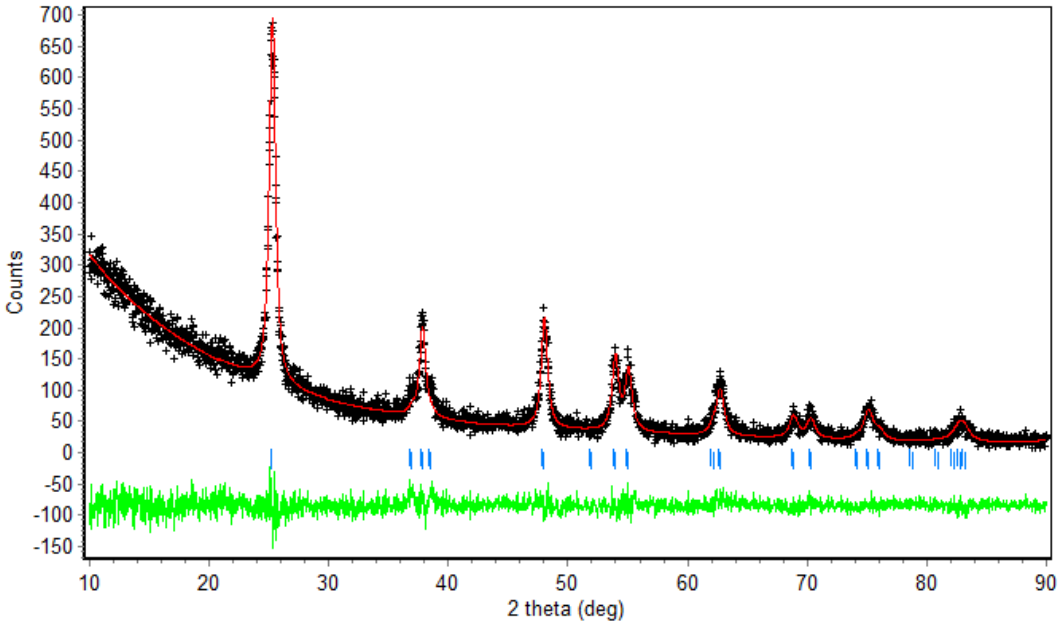

FIGURE 7. XRD plot for sampel ES11. The measured and calculated patterns are indicated by crosses and solid lines. Vertical bars represent the allowable peak position for anatase.

It can be seen from Figure 7 that the refinement result is quite adequate, indicated by the decreasing of the R factors during the calculation process. The lattice structure parameter value, criteria-of-fit (Rwp) value, goodness-of-fit (χ^2) value and the mass fraction of phase formed for sample ES11 compound are shown in Table 2.

TABLE 2. The lattice structure parameter value, criteria-of-fit (Rwp) value, goodness-of-fit (χ^2) value and the mass fraction of phase formed for sample ES11

Phase	Lattice Parameter (Å)			Fraction Wt%	Rwp (%)	Rp (%)	χ^2
	a	b	c				
Anatase	3,7871	3,7871	9,5034	100	12,42	8,88	1,347

Table 2 shows the refined data. It can be observed that the phase present is the anatase phase. In addition, it can be observed that the Rwp and Rp values obtained are less than 20% and the GoF value is less than 4. Thus, it can be said that the refining quality obtained in this study is quite good and in accordance with the indicators of success [36,37]. From data obtained, it is used to determine the particle size by finding the FWHM (Full Width Half Maximum) value from the highest peak at an angle of $2\theta(^{o})$. The FWHM value is a parameter used to calculate the width of diffraction peak of a curve by determining distance between 2 points that has a value of half maximum value of the curve. From the FWHM value, the particle size was calculated using the Scherrer equation (Equation 3). The results of the particle size calculations obtained are presented in Table 3.

TABLE 3. Particle size calculation result

Phase	k	λ (nm)	FWHM (^{o})	FWHM (rad)	2θ (^{o})	D (nm)
Anatase	0,94	0,15406	0,7128	0,0124	25,3	12,3

Based on Table 3, the particle size obtained is 12.3 nm. The results obtained are slightly different from Hazem's (2020) study, which is 65 nm [20]. The calculation results show that the size of ES11 sample of TiO_2/PVP nanofibers is nanoparticles. Thus, it can be concluded that the material prepared in this study is included in the nanomaterial category.

CONCLUSION

Based on the synthesis results, TiO_2/PVP solution with a viscosity of 2.8 Pa.s and a surface tension (28.9 ± 3.7) dyn/cm can be spun into TiO_2/PVP nanofibers by electrospinning method. The distance between tip and collector has been shown to affect the formation of TiO_2/PVP nanofibers seen through the surface morphology and fiber diameter size. The surface morphology indicates that the TiO_2/PVP nanofibers are relatively uniform and continuous. Considering the estimated standard deviation, the graph of the average fiber diameter shows the optimization trend. The results of SEM analysis showed that diameter size was in the range of 56 nm to 0.961 μm. To ensure that nanofibers contain TiO_2, it was further confirmed by XRD results which showed that the crystal structure formed on nanofibers was the anatase phase with particle sizes ranging from 12.3 nm.

ACKNOWLEDGMENTS

We would like to thank the physics department of mathematics and science faculty for providing the place and facilities to conduct this research and those who have supported and assisted in completing this research.

REFERENCE

1. T. Subbiah, G. S. Bhat, R. Tock, W. S. Parameswaran, and S. S. Ramkumar, Journal of Applied Polymer Science **96**, 557–569 (2005).
2. N. Bhardwaj and S. C. Kundu, Electrospinning, Biotechnology Advances **28**, 325–347 (2010).
3. S. Ramasundaram, H. N. Yoo, K. G. Song, J. Lee, K. J. Choi, and S. W. Hong, Journal of Hazardous Materials **258**, 124-132 (2013).
4. G. Yang, Y. Zifeng, and X. Tiancun, Journal of Applied Surface Science **258**, 4016-4022 (2012).
5. S. Hayle and G. Gonfa, Journal of Nanoscience and Nanotechnology **2**, 1-7 (2014).
6. M. Modesti, M. Roso, C. Boaretti, S. Besco, D. Hrelja, P. Sgarbossa, and A. Lorenzetti, Applied Catalysist B: Environmental **144**, 216-222 (2014).
7. Z. Li, H. Zhang, W. Zheng, W. Wang, H. Huang, C. Wang, A. G. MacDiarmid, and Y. Wei, Journal of the American Chemical Society **130**, 5036-5037 (2008).
8. J. Moon, J. A. Park, S. J. Lee, T. Zyung and I. D. Kim, Sensors and Actuators B: Chemical **149**, 301-305 (2010).
9. M.Y. Song, D.K. Kim, K.J. Ihn, S.M. Jo, D.Y. Kim, Nanotechnology **15**, 1861- 1865 (2004).
10. M. Nasikhudin, A. Diantoro, Kusumaatmaja. and K. Triyana, Journal of Physics: Conference Series **1011**, 1-7 (2014).
11. W. Yu, X. Liu, L. Pan, J. Li, J. Liu, J. Zhang, P. Li, C. Chen and Z. Sun, Applied Surface Science **319**, 107-112 **(**2014).
12. J. Bai, Y. Li, M. Li, S. Wang, C. Zhang, and Q. Yang, Applied Surface Science **254**, 4520–4523 (2008).
13. K. Nasouri, A. M. Shoushtari and M. R. M. Mojtahedi, Advances in Polymer Technology **34** (2015) 21495-21503.
14. C. Chen, A. D. Townsend, S. A. Sell, and R. S. Martin, Analytical Methods **9**, 3274-3283 (2017).
15. M.M. Hasan, Dissertation, University of Toronto, Canada (2013).
16. V.E. Kalayci, MS Thesis, University of Massachusetts, Dartmouth (2002).
17. K. Nakane and N. Ogat, Photocatalyst Nanofibers Obtained by Calcination of Organic-Inorganic hybrids. Nanofibers ISBN: 978-953-7619-86-2 (2010).
18. A.D. Vaisniene, J. Katunskis, and G. Buika, Fibers & Textiles in Eastern Europe **17**, 40-43 **(**2009).
19. X. Wang, D. G. Yu, X.-Y. Li, S. W. A. Bligh, and G. R. Williams, International Journal of Pharmaceutics **490**, 384–390 (2015).
20. N. Z. A. Hazeem, Nanomedicine & Nanotechnology Open Access **5**, 195-199 (2020).
21. S. Tungprapa, T. Puangparn, M. Weerasombut, I. Jangchud, P. Fakum, S. Semongkhol, C. Meechaisue, and P. Supaphol, Cellulose **14**, 563- 575 (2007).
22. J. Geltmeyer, L. Van der Schueren, F. Goethals, K. De Buysser, and K. De Clerck, J. Sol-Gel Sci. Technol. **67**, 188-195 (2013).
23. H. Fong, I. Chun and Reneker, D, Polymer **40**, 4585 – 4592 (1999).
24. A. Haider, S. Haider and I. K. Kang, Arabian Journal of Chemistry **11**, 1165–1188 **(**2018).
25. R. A. Chapman, Applications of Nonwovens in Technical Textiles, New Delhi: Woodhead Publishing Limited **22** (2010).
26. M. Ramazani, M. Farahmandjou and T. P. Firoozabadi, Int. J. Nanosci. Nanotechonol **11**, 115-122 (2015).
27. C. J. Howard, T. M. Sabine and F. Dickson, Acta Crystallographica Section B. **47**, 462–68 (1991).
28. S. M. Abdel-Azim, A. K. Aboul-Gheit, S. M. Ahmed, D. S. El-Desouki, and M. S. A. Abdel-Mottaleb, International Journal of Photoenergy **2014**, 1-11 (2014).

29. O. L. Galkina, V. V. Vinogradov, A. V. Agafonov, and A. V. Vinogradov, International Journal of Inorganic Chemistry **6346**, 1–8 (2011).
30. P. Manurung, R. Situmeang, P. Sinuhaji and S. Sembiring, Asian Journal of Chemistry **32**, 3019-3023 (2020).
31. S. Bakardjieva, S. Vaclav, S. Lorant, J. Subrt, J. Lukac, N. Murafa, D. Niznansky, K. Cizek, J. Jirkovsky and N. Petrova, Journal of Materials Chemistry **16**, 1709–1716 (2006).
32. D. Dastan, C. Nandu and K. Moses, Journal of Materials Science: Materials in Electronics **28**, 7784–96 (2017).
33. B. K. Mutuma, N. S. Godlisten, W. D. Kim and H. T. Kim, Journal of Colloid and Interface Science **442**, 1–7 (2015).
34. B. A Hunter dan C. J. Australian Nuclear Science and Technology Organization. Lucas Heights Research Laboratories: Australia (1997).
35. I. Djerdj and A. M. Tonejc, Journal of Alloys and Compounds **413**, 159–74 (2006).
36. E. H. Kisi, Rietveld Analysis of Power Diffraction Pattern. Material Forum (1994).
37. R. A. Young, *The Rietveld Method* (Oxford University Press Inc. New York, 1993).

ROBUST BIPLOT ANALYSIS OF NATURAL DISASTERS IN INDONESIA FROM 2019 TO 2021

Hilda Venelia[1], Khoirin Nisa[1*], Rizki Agung Wibowo[1], Mona Arif Muda[2]

[1]Department of Mathematics, Faculty of Mathematics and Natural Sciences, University of Lampung, Lampung, Indonesia
[2]Department of Informatics Engineering, Faculty of Engineering, University of Lampung, Indonesia

*Corresponding author:
khoirin.nisa@fmipa.unila.ac.id

ABSTRACT

Indonesia is one of the most natural disaster-prone countries in the world, frequently exposed to a range of hazards. Currently, Indonesia has 34 provinces and natural disasters that occur in each province are different, therefore it is necessary to analyze the mapping of natural disasters that often occur in each province to provide scientific analysis for risk management of the natural disasters. One of the quick steps in describing data that can be used is biplot analysis, as biplot analysis can describe a lot of data then summarized it into the form of a two-dimensional graph. The aim of this research is to map 34 provinces in Indonesia based on the incidence of natural disasters from 2019 to 2021 using robust biplot analysis to see which provinces that have a high risk of natural disaster. Based on the result, robust biplot analysis can explain 87,9% of the information on natural disasters in every province in Indonesia. Lampung, Bengkulu, Bangka Belitung, Special Region of Yogyakarta, North Sulawesi, West Sulawesi, Southeast Sulawesi, Gorontalo, East Nusa Tenggara, Bali, Maluku, West Maluku, Papua, and West Papua are provinces that have similar natural disaster characteristics. Flood, tornado and forest and land fires are natural disasters that often occur in Indonesia. The provinces that have the highest risk of flood, landslide, and tornado were West Java, Central Java, and East Java. Then, the provinces with the highest risk of forest and land fires were Aceh and South Kalimantan.

Keywords: Natural disasters, risk management, biplot.

INTRODUCTION

Based on Law of Republic of Indonesia number 24 of 2007 concerning Disaster Management, disaster is an event or series of events that threaten and disrupt people's lives and livelihoods, caused by natural and/or non-natural and human factors that result in human casualties, environmental damage, property losses, and psychological impacts. Natural disaster is a catastrophic event with atmospheric, geological, and hydrological origin (e.g., droughts, earthquakes, floods, hurricanes, landslides) that can cause fatalities, property damage and social environmental disruption (Xu, *et al.*, 2016). Every country in the world has been hit by natural disaster, either high, medium, or low

risk. Indonesia is one of the countries with a high disaster-prone level in most of its territory. Geographically, Indonesia is an archipelagic country located at the confluence of four tectonic plates, namely Asian Continent plate, Australian Continent plate, Indian Ocean plate and Pacific Ocean. These conditions are potential disaster-prone such as volcanic eruptions, earthquakes, tsunamis, floods and landslides (Arnold, 1986).

Indonesian National *Agency* for *Disaster Management* (*Indonesian*: Badan Nasional Penanggulangan Bencana (BNPB)) noted that the annual trend of natural disasters in Indonesia tends to increase. In period of 2010 until 2020, the highest number of annual disasters occurred in 2019, which was 3.814 incidents. Disasters that hit Indonesia are generally caused by hydrometeorology. Flood, landslide, and tornado have dominated the natural disasters that have occurred over the past decade. The number of missing and dead victims annually reaches hundreds to thousands of people. The peak occurred in 2018 with 3.397 disasters which caused the number of victims to reach 6.240 people. That year, Indonesia experienced a series of major disasters, such as Lombok earthquake (West Nusa Tenggara), Palu earthquake and tsunami (Central Sulawesi), and Sunda Strait tsunami. Meanwhile, from 31 December 2019 to 1 January 2020 there was rain in the Greater Jakarta (i.e. Jakarta Bogor Tangerang Bekasi, abbreviated to Jabodetabek) which resulted in flooding on 1-3 January 2020. The incident killed at least 48 people, and more than 31.000 people were evacuated. Then, floods and landslides also occurred in East Nusa Tenggara in early April 2021 due to Cyclone Seroja which killed 183 people.

Therefore, many provinces in Indonesia are affected by natural disasters in terms of social, economic, environmental, and other aspects. This is due to the lack of readiness of government and society in disaster management before the disaster occurs or better known as Disaster Risk Reduction (DRR). The main objective of DRR is to reduce losses due to disaster impacts by increasing society capacity and reducing exposure and increasing community resilience through preparedness, emergency response, and recovery. The first thing that must be considered in DRR is to map the province in Indonesia based on the level of risk from the natural disaster and find out what natural disasters often occur in each province in Indonesia. This is because, by mapping the provinces in Indonesia based on their level of natural disaster risk, it can be seen which provinces that have high, medium, and low risk of natural disaster. Thus, natural disaster management can be prioritized to provinces that have a high risk of being affected by natural disasters.

There is one of descriptive statistical methods that can be used for mapping purposes, namely biplot analysis. Biplot analysis is one of descriptive statistical methods that can simultaneously present plots of n observations and p variables in two-dimensional graph (Jolliffe, 2002). Biplot analysis has been used in various research fields, one can see e.g. (Makhya, *et al.*, 2020; Fitry, *et al.*, 2021; Suryowati, JP and Nasution, 2021; Ghazvini, 2021). However, the classical biplot is sensitive to the presence of outliers in the data, therefore when data contain outliers it is recommended to use robust biplot.

METHODOLOGY

The data used in this study is Natural Disasters in Indonesia data from January 1st 2019 until August 14th 2021 obtained from Indonesian National Disaster Mitigation Agency (BNPB). The data consists of $n = 34$ provinces and $p = 6$ natural disasters in Indonesia. The variables used in this study are the types of natural disasters, namely Flood (F), Landslide (LS), Earthquake (EQ), Tidal Wave/Abrasion (TW), Forest and Land Fires (FF), and Tornado (T).

The computation of biplot analysis based on Singular Value Decomposition (SVD) (Gabriel, 1971) that can be written as follows:

$$\mathbf{X} = \mathbf{U}\,\mathbf{\Lambda}\,\mathbf{V}^{\mathrm{T}}, \qquad (1)$$

where $\mathbf{X}$ is data matrix with rank r, $\mathbf{U}_{(n\times r)}$ and $\mathbf{V}_{(p\times r)}$ are columnar orthonormal matrices $\left(\mathbf{U}^{\mathrm{T}}\mathbf{U} = \mathbf{V}^{\mathrm{T}}\mathbf{V} = \mathbf{I}_{\mathbf{r}}\right)$ and $\mathbf{\Lambda}_{(r\times r)} = \mathrm{diag}\left(\sqrt{\lambda_1, \lambda_2, \dots, \lambda_{\mathrm{r}}}\right)$ with $\sqrt{\lambda_1} \geq \sqrt{\lambda_2} \geq \cdots \geq \sqrt{\lambda_{\mathrm{r}}}$ and $r \leq p \leq n$. The element λ_i, $i = 1, 2, \dots, r$ are eigenvalues of $\mathbf{X}^{\mathrm{T}}\mathbf{X}$ (Johnson and Wichern, 2014). Matrix $\mathbf{V}$ is a matrix whose columns consist of eigenvectors $\boldsymbol{v_i}$ corresponding to λ_i of $\mathbf{X}^{\mathrm{T}}\mathbf{X}$. The columns of $\mathbf{U}$ can be calculated as:

$$\mathbf{U} = \frac{1}{\sqrt{\lambda_{\mathrm{i}}}} \times \boldsymbol{v_i}.$$

Define $\mathbf{\Lambda}^{\alpha} = \mathrm{diag}\left(\sqrt{\lambda_1^{\alpha}}, \sqrt{\lambda_2^{\alpha}}, \dots, \sqrt{\lambda_{\mathrm{r}}^{\alpha}}\right)$ with $\alpha \in [0,1]$ and suppose $\mathbf{G} = \mathbf{U}\,\mathbf{\Lambda}^{\alpha}$, $\mathbf{H} = \mathbf{V}\,\mathbf{\Lambda}^{1-\alpha}$ than (1) can be written as (Gabriel, 1971):

$$\begin{aligned}\mathbf{X} &= \mathbf{U}\,\mathbf{\Lambda}\,\mathbf{V}^{\mathrm{T}} \\ &= (\mathbf{U}\,\mathbf{\Lambda}^{\alpha})\left(\mathbf{\Lambda}^{1-\alpha}\,\mathbf{V}^{\mathrm{T}}\right) \\ &= \mathbf{G}\,\mathbf{H}^{\mathrm{T}}.\end{aligned}$$

Therefore, element (i, j) of data matrix $\mathbf{X}_{(n\times p)}$ can be expressed as:

$$\boldsymbol{x}_{ij} = \boldsymbol{g}_{\boldsymbol{i}}^{\boldsymbol{T}}\,\boldsymbol{h}_{\boldsymbol{j}}$$

where $\boldsymbol{g}_{\boldsymbol{i}}^{\boldsymbol{T}}, i = 1, 2, \dots, n$ and $\boldsymbol{h}_{\boldsymbol{j}}, j = 1, 2, \dots, p$ are row vectors of $\mathbf{G}$ and $\mathbf{H}$, respectively, with r elements. Here, n rows of $\mathbf{G}$ correspond to rows of $\mathbf{X}$ and p rows of $\mathbf{H}$ correspond to columns of $\mathbf{X}$.

Outliers are data points that deviate far from the majority of the data (Filzmoser, 2004). Multivariate outliers can be identified using Mahalanobis distance (Majewska, 2015) as follows:

$$D_i(\boldsymbol{x_i}, \bar{\mathbf{X}}) = \sqrt{(\boldsymbol{x_i} - \bar{\mathbf{X}})^{\mathrm{T}}\mathbf{S}^{-1}(\boldsymbol{x_i} - \bar{\mathbf{X}})},$$

where $\boldsymbol{x_i}$ represents the i-th object, $\bar{\mathbf{X}}$ is the mean vector and $\mathbf{S}$ is the sample covariance matrix (Ghorbani, 2019). If $D_i^2(\boldsymbol{x_i}, \bar{\mathbf{X}}) > \chi^2_{p;1-\alpha}$ with p the number of variable in the data and α the significant level, then the object can be identified as outlier.

However, not all outliers can be removed from data because it can cause the loss of information contained in data. Furthermore, the covariance matrix also very sensitive to outliers (Islami and Sihombing, 2021; Larasati, *et al.*, 2021). To overcome this problem, biplot analysis can be generated using a robust covariance matrix by estimating eigenvalues and eigenvectors of $\mathbf{U}$ and $\mathbf{V}$ such that the predicted results are resistant to outliers (Hawkins, *et al.*, 2001). In this case the calculation of SVD uses robust estimator of mean vector $\bar{\mathbf{X}}$ and covariance matrix $\mathbf{S}$. Here we used the Minimum Covariance Determinant (MCD) estimator which is knows as a very robust method for mean vector and covariance matrix estimation (Hubert and Debruyne, 2010). The MCD estimator with the fast-MCD algorithm proposed by Rousseeuw and Van Dreissen (1999) can be done with the following steps:

1. Take a random subset of matrix $\mathbf{X}$, suppose the subset as $\mathbf{K}_1$ with the number of elements as much as h, where n and p are the sample size and the number of variables in the data respectively.

$$h = \frac{(n+p+1)}{2}$$

2. Calculate the mean vector $\bar{\mathbf{X}}_1$ and the covariance matrix $\mathbf{S}_1$ of $\mathbf{K}_1$ using:

$$\bar{\mathbf{X}}_1 = \frac{1}{h}\sum_{i\in H} \boldsymbol{x}_i$$

$$\mathbf{S}_1 = \frac{1}{h-1}\sum_{i=1}^{h} (\boldsymbol{x}_i - \bar{\mathbf{X}}_1)^T(\boldsymbol{x}_i - \bar{\mathbf{X}}_1)$$

3. Calculate the determinant of $\mathbf{S}_1$.
4. Calculate the relative distance of each observation to $\bar{\mathbf{X}}_1$ and covariance $\mathbf{S}_1$ using Mahalanobis distance.
5. Sort the observation by the distance of Mahalanobis, from the smallest to largest.
6. Take the elements of h observations with the smallest distance based on step 5 to become subset of $\mathbf{K}_2$, repeat steps 2 until 5 so that it is found the subsets are converge and have the smallest determinant of the covariance matrix, namely:

$$|\mathbf{S}_{n+1}| < |\mathbf{S}_n|$$

7. Based on the elements of h, the next data is weighted as:

$$w_i = \begin{cases} 1, & (\boldsymbol{x}_{ij} - \bar{\mathbf{X}})^T \mathbf{S}^{-1} (\boldsymbol{x}_{ij} - \bar{\mathbf{X}}) < \chi^2_{p;1-\alpha} \\ 0, & \text{others} \end{cases}$$

8. Based on the weighted above, the fast-MCD estimators are:

$$\bar{\mathbf{X}}_{MCD} = \frac{\sum_{i=1}^{n} w_i \boldsymbol{x}_{ij}}{\sum_{i=1}^{n} w_i}$$

$$\mathbf{S}_{MCD} = \frac{\sum_{i=1}^{n} w_i \left(\boldsymbol{x}_{ij} - \bar{\mathbf{X}}_{MCD}\right)^T \left(\boldsymbol{x}_{ij} - \bar{\mathbf{X}}_{MCD}\right)}{\left(\sum_{i=1}^{n} w_i\right) - 1}$$

Robust biplot analysis in this research was carried out using R software, the analysis procedure can be described as follows:

1. data screening to detect outliers by using Mahalanobis distance;
2. performing robust biplot analysis based on the covariance matrix $\mathbf{S}_{MCD}$ using *robustbase* package;
3. plotting data using *ggbiplot* package;
4. interpretation of the result.

RESULT & DISCUSSION

In this research, the first step was to detect outliers in data based on the robust Mahalanobis distance. The plot of the robust squared Mahalanobis distances and the chi-square quantiles is shown in Figure 1.

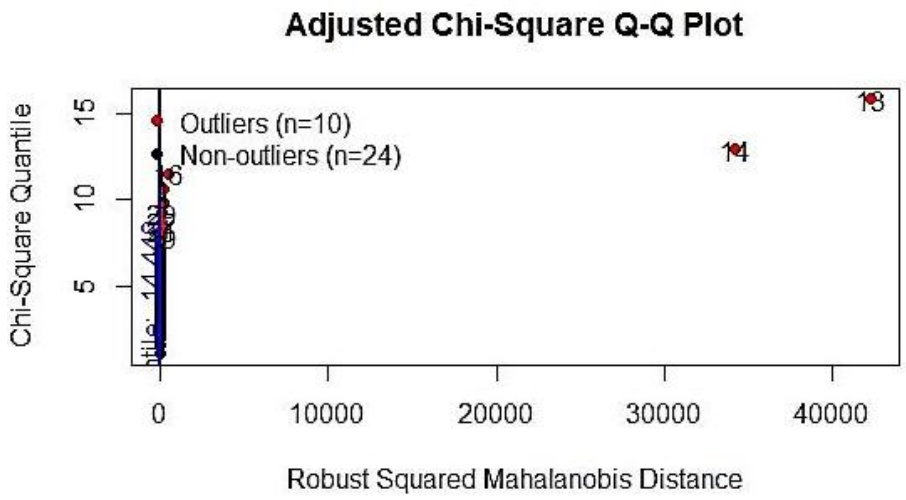

Figure 1. Outlier detection based on robust Mahalanobis distance.

The result showed that there were ten provinces that were identified as outliers as can be seen in Figure 1. The list of data that identified as outliers is presented in the following table.

Table 1. Provinces that are considered as outliers and their number of natural disasters

Province	Flood	Landslide	Earthquake	Tidal Wave	Forest and Land Fires	Tornado
Aceh	217	33	4	13	245	193
North Sumatra	108	22	1	1	27	96
West Sumatra	133	68	1	7	24	164
West Java	452	883	26	3	83	895
Central Java	446	788	3	11	95	791
East Java	344	99	30	2	195	394
South Kalimantan	110	17	0	3	168	112
East Kalimantan	41	37	0	1	105	13
Bali	14	48	5	4	14	79
South Sulawesi	119	54	1	7	28	159

In Table 1, Aceh, North Sumatra, West Sumatra, South Kalimantan, and South Sulawesi are provinces that experience flood and tornado with high risk, especially in West Java, Central Java, and East Java that experience flood, landslide, and tornado with very high risk than other provinces. While East Kalimantan and Bali are provinces that experience flood and tornado with low risk than others.

Based on the report above it can be concluded that the data of natural disasters in Indonesia from 2019 until 2021 contains outliers. Therefore, it is appropriate to use robust biplot analysis in this research. The resulted robust biplot describes the characteristics of object (Provinces) against the variables (Natural Disasters) as can be seen in the following figure.

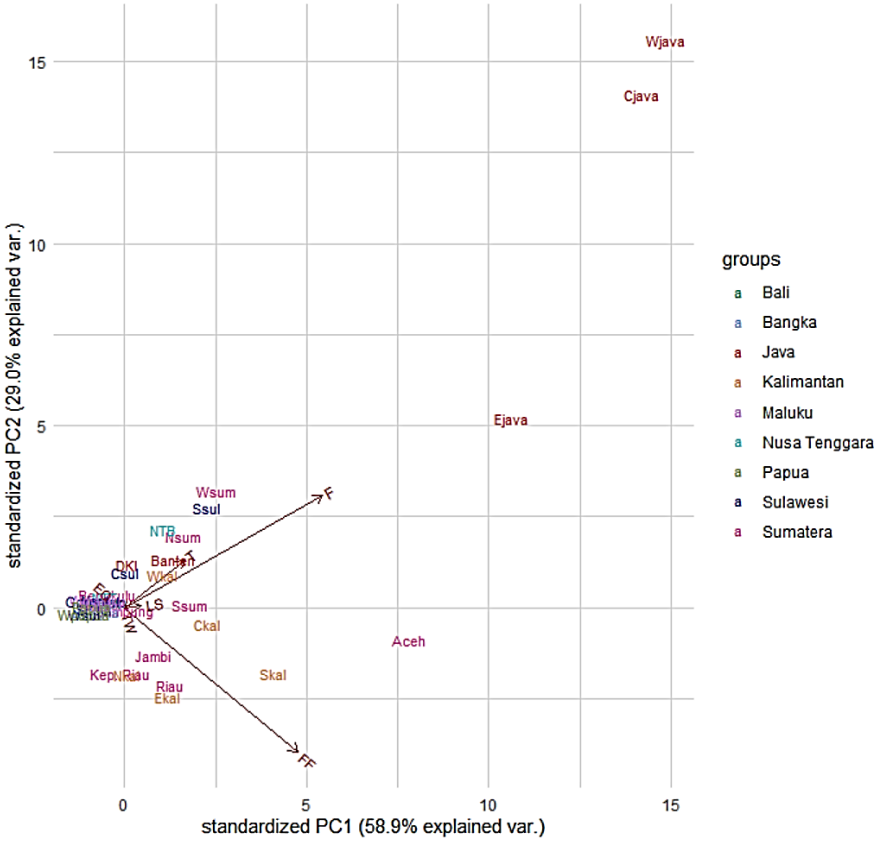

Figure 2. Robust biplot charts of natural disasters.

The important thing that needs to be considered in biplot analysis is how good the biplot can explain the information contained in data. Based on Figure 2, it can be explained that the information in component 1 was 58,9% and component 2 was 29%. Therefore, the cumulative information that can be explained by biplot against data based on two components was 87,9%. It means that the resulted biplot was very capable in describing the characteristics of natural disaster data in Indonesia. Furthermore, there are four information obtained from biplot in Figure 2 as described as follows.

Proximity Between Objects

This information can be used as a guide to identifying objects that have similar characteristics to other objects. Two objects that have similar characteristics will be described as two points with adjacent positions. Based on Figure 2, West Sumatra and South Sulawesi are two provinces with similar characteristics. West Nusa Tenggara and North Sumatra are two provinces with similar characteristics. DKI Jakarta and Central Sulawesi are two provinces with similar characteristics. Then, Banten and West Kalimantan are two provinces with similar characteristics. Also with Riau and East Kalimantan have similar characteristics. Jambi, Riau Islands, and North Kalimantan are three provinces with similar characteristics. Meanwhile, Lampung, Bengkulu, Bangka Belitung, Special Region of Yogyakarta, North Sulawesi, West Sulawesi, Southeast Sulawesi, Gorontalo, East Nusa Tenggara, Bali, Maluku, West Maluku, Papua, and West Papua form their own group and have similar characteristics.

Variability of Variables

This information is used to see if there are variables that have almost the same diversity. Variables with small variance are represented by short vectors, whereas if the variance is high, they are represented by long vectors. Based on Figure 2, flood and forest fire are variables with the highest variance compared to other variables because they have the longest vector. It means that the level of risk of flood and forest fires varies widely in each province in Indonesia. Then, tidal wave is variable with the smallest variance represented by the shortest vector. This means, tidal wave was a natural disaster with the lowest risk in every province in Indonesia from 2019 until August 2021.

Correlation Between Variables

Correlation between variables shows how one variable is related to another. In biplot, variables are presented as vector lines. If two vectors form an acute angle ($< 90^{\circ}$) or have the same direction, then it can be stated that the two variables are positively correlated. Whereas if two vectors form obtuse angles ($> 90^{\circ}$) or have opposite directions, it can be stated that the two variables are negatively correlated. Then, if the angle formed between two vectors is a right angle, then it can be stated that the two variables are not correlated.

Based on Figure 2, flood has positive correlation with forest and land fires, tornado, and landslide. This means that from 2019 until August 2021, the level of flood risk in each province in Indonesia was directly proportional to the level of risk of forest and land fires, tornado, and landslide. Earthquake has negative correlation with flood, landslide, and forest and land fires which means from 2019 until August 2021, the level of earthquake risk was inversely proportional to the level of risk of flood, landslide, and forest and land fires. But earthquake, tornado, and forest and land fires have no correlation.

Relative Position of Object to Variable

This information is used to see the advantages of each object. Objects that are in the same direction as the variable vector, indicate that the value of the object is above the average, if it is in the opposite direction, it means that the value is below the average, if it is almost in the middle, it means that the value is close to the average. Based on Figure 2, information about natural disasters in Indonesia from 2019 until August 2021 shows that West Java, Central Java, and East Java are provinces with the highest risk of flood, tornado, and landslide than other provinces. Whereas, West Sumatra, North Sumatra, South Sumatra, Banten, DKI Jakarta, West Kalimantan, West Nusa Tenggara, South Sulawesi, and Central Sulawesi are provinces with a medium risk of flood and tornado.

Aceh and South Kalimantan were at the highest risk of forest and land fires. Meanwhile, South Sumatra, Jambi, Riau, Riau Islands, Central Kalimantan, North Kalimantan, and East Kalimantan have a medium risk of forest and land fires and a lower risk of earthquake. Meanwhile, Lampung, Bengkulu, Bangka Belitung, Special Region of Yogyakarta, North Sulawesi, West Sulawesi, Southeast Sulawesi, Gorontalo, East Nusa Tenggara, Bali, Maluku, West Maluku, Papua, and West Papua are provinces with a medium risk of earthquake and a lower risk of forest and land fires.

CONCLUSION

Based on results and discussion, there are several points that can be concluded as follow:

1. The information obtained from robust biplot analysis is 87,9% which means very good to describe the characteristics of natural disasters in Indonesia.
2. Flood, tornado, and forest and land fires are natural disasters that often occur in Indonesia. Meanwhile, tidal wave is a natural disaster that is very rare occurrence in Indonesia.
3. Lampung, Bengkulu, Bangka Belitung, Special Region of Yogyakarta, North Sulawesi, West Sulawesi, Southeast Sulawesi, Gorontalo, East Nusa Tenggara, Bali, Maluku, West Maluku, Papua, and West Papua are provinces that have similar natural disaster characteristics and have medium risk of earthquake.
4. West Java, Central Java, and East Java have the highest risk of being affected by flood, tornado, and landslide. Meanwhile, Aceh and South Kalimantan are provinces at high risk of being affected by forest and land fires.

Based on these information, it is recommended for further research to examine the factors and impacts of natural disasters that occur in Indonesia.

REFERENCES

Arnold, E.P. 1986. Series on Seismology Volume V: Indonesia. *South-East Asia Association of Seismology and Earthquake Engineering.*

Filzmoser, P. 2004. *Multivariate Outlier Detection Method*. Austria: Department of Statistics and Probability Theory.

Filzmoser, P. and Gregorich, M. 2020. Multivariate Outlier Detection in Applied Data Analysis: Global, Local, Compositional, and Cellwise Outliers. *Mathematical Geosciences*, Vol. 52 (8), 1049-1066.

Fitry, R., Rostini, N., Hersanti and Zubair, A. 2021. Biplot and Correlation Analysis of 189 Superior F2 Genotypes Chili-Unpad in Indonesia. *Advances in Biological Sciences Research*, Vol. 9, 10-14.

Gabriel. K. R. 1971. The biplot graphic display of matrices with application to principal component analysis. *Biometrika*, Vol. 58 (3), 453–467.

Ghazvini, H., Bagherikia, S., Pour-Aboughadareh, A., Sharifalhossaini, M., Razavi, S.A., Mohammadi, S., Ghasemi, K. M., Fathihafshejani, A. and Khakizade, G. 2021. GGE Biplot Analysis of Promising Barley Lines in the Cold Regions of Iran. *Journal of Crop Improvement*, Vol. 35, 1–12.

Ghorbani, H. 2019. Mahalanobis Distance and Its Application for Detecting Multivariate Outliers. *Facta Universitatis: Mathematics and Informatics*, Vol. 34, 583.

Hawkins, D. M., Liu, L. and Young, S. S. 2001. Robust Singular Value Decomposition. *Linear Algebra and its Applications*, Vol. 417 (122), 370-380.

Hubert, M. and Debruyne, M. 2010. Minimum covariance determinant. *Wiley Reviews: Computational Statistics*, Vol. 2 (1), 36-43.

Islami, R. L. and Sihombing, P. R. 2021. Application Biplot and K-Medians Clustering to Group Export Destination Countries of Indonesia's Product. *Advance Sustainable Science, Engineering and Technology*, Vol. 3 (1), 0210105.

Johnson, R. and Wichern D. 2014. *Applied Multivariate Statistical Analysis 6th ed.* England: Pearson Education Limited.

Jolliffe, I. T. 2002. *Principal Component Analysis, Second Edition*. New York: Springer-Verlag.

Larasati, S.D.A., Nisa, K. and Herawati, N. 2021. Robust Principal Component Trimmed Clustering of Indonesia Provinces Based on Human Development Index Indicators. *Journal of Physics: Conference Series*, Vol. 1751 (1).

Mahalanobis, P. C. 1936. On the generalised distance in statistics. *Proceedings of the National Institute of Sciences of India*, Vol. 2 (1), 49-55.
Majewska, J. 2015. Identification of Multivariate Outliers Problems and Challenges of Visualization Methods. *Informatyka i Ekonometria* 247, 69-83.
Mattjik, A. A. and Sumertajaya, I. M. 2011. *Sidik Peubah Ganda dengan Menggunakan* SAS. Bogor: IPB Press.
Rousseeuw, P. J. and Driessen, K. V. 1999. A Fast Algorithm for the Minimum Covariance Determinant Estimator. *Technometrics*, Vol. 41 (3), 212-223.
Suryowati, K, Titah, J.P., and Nasution, N. 2021. Application Biplot Analysis on Mapping of Non-Convertive Diseases in Indonesia. *Parameter*: *Journal of Statistics*, Vol. 1 (2), 11-20.
Syarief, M., Nisa, K., Larasati, S., Suripto and Suprihatin, A. 2020. Government policy in the case of provision of commercial bank loans based on business fields per Sumatra region. *TEST Engineering and Management*, Vol. 82, 6843-6851.
Xu, J., Wang, Z., Shen, F., Ouyang, C. and Tu, Y. 2016. Natural disasters and social conflict: A systematic literature review. *Int. J. Disaster Risk Reduct*, Vol. 17, 38–48.

BIRD SPECIES DIVERSITY IN LIWA BOTANICAL GARDEN, WEST LAMPUNG

Indah Fitri Sari*, Nuning Nurcahyani, M. Kanedi, dan Tugiyono

Jurusan Biologi Fakultas Matematika dan Ilmu Pengetahuan Alam Universitas Lampung
Jl. Prof. Soemantri Brodjonegoro, No 1, Bandar Lampung 35145

*Email: IndahFitri1998@gmail.com

Abstract

The diversity of bird species can reflect the high biodiversity of an area. it means that birds can be used as a bio-indicator of environmental quality. Determining the quality and level of environmental damage can be seen from the diversity of bird species in the region. Environmental quality will be better if the diversity of bird species in the region is diverse. Birds have an important role in protecting the ecosystem in the Liwa Botanical Garden. The presence of birds in the Liwa Botanical Garden has not been well identified. Therefore this research needs to be done. This research was conducted on 12 October 2019 to 20 October 2019 in the Liwa Botanical Garden, West Lampung. Data collection of bird species is conducted in the morning at 06.30.00-08.30 West Indonesia Time and afternoon at 16.30-18.00 West Indonesia Time, with a combination of the count point and the transect method then all encounters with birds are recorded and identified directly at the study site. After the birds are identified, data is processed to find out Shannon's level index and diversity index. The species diversity index uses the Shannon and Weiner formula. The level of diversity is determined based on the species diversity index. The results showed that there were 15 bird species with a total of 466 individuals with a moderate diversity index and an evenness index indicating a distressed community.

Keywords: Liwa Botanical Garden, bird species diversity, environmental quality

PENDAHULUAN

Kebun Raya Liwa terletak di Way Mengaku, Balik Bukit, Kabupaten Lampung Barat. Kebun Raya Liwa merupakan salah satu destinasi wisata yang ada di Lampung Barat yang sedang dikembangkan untuk dijadikan objek wisata dan upaya pelestarian alam. Salah satu habitat tempat beraktivitas satwa termasuk burung yaitu Kebun Raya.

Burung merupakan salah satu bioindikator lingkungan yang memiliki peran penting bagi suatu ekosistem maupun kehidupan manusia (Rusmendro, 2009). Tingginya keanekaragaman hayati suatu kawasan dapat dilihat dari keanekaragaman jenis burung. Artinya bioindikator kualitas lingkungan dapat dilihat dari populasi burung di wilayah tersebut. Burung merupakan jenis hewan vertebrata yang memiliki jumlah paling banyak di antara hewan vertebrata lainnya. Sebanyak 9.040 jenis burung tercatat di dunia (Sulistyadi, 2010). Sebanyak 1.666 jenis diantaranya terdapat di Indonesia dengan 397 jenis (26%) endemik (Ramadhani, 2018). Habitat burung perlu dijaga karena digunakan

sebagai tempat untuk mencari makan, minum, istirahat, dan berkembang biak bagi satwa.

Untuk menentukan kualitas dan tingkat kerusakan lingkungan dapat dilihat dari keanekaragaman jenis burung yang ada di wilayah tersebut. Jika keanekaragaman jenis burung di wilayah tersebut beraneka ragam maka kualitas lingkungan akan semakin baik. Informasi ini perlu diperhatikan sebagai upaya pengembangan Kebun Raya Liwa.

Burung berperan penting dalam menjaga kestabilan ekosistem di Kebun Raya Liwa, namun keberadaan burung di Kebun Raya Liwa belum teridentifikasi dengan baik. Oleh karena itu, perlu dilakukan penelitian ini. Tujuan penelitian ini yaitu identifikasi jenis burung yang ada di Kebun Raya Liwa dan mengetahui keanekaragaman jenis burung yang ada di Kebun Raya Liwa.

METODE PENELITIAN

Waktu dan Tempat Penelitian

Penelitian ini dilaksanakan pada tanggal 12 - 20 Oktober 2019 di Kebun Raya Liwa, Lampung Barat. Penelitian ini merupakan tindak lanjut kerja sama jurusan Biologi dengan Kebun Raya Liwa.

Alat dan Bahan Penelitian

Alat yang digunakan untuk penelitian ini yaitu *work sheet*, teropong binoculler Nikon Trailblazer, alat tulis, kamera dengan sensor 32 MP, jam digital, serta buku panduan lapangan Jenis Burung di Sumatera,Kalimantan, Jawa, dan Bali (MacKinnon *et.al*., 2010).

Work sheet atau lembar kerja digunakan sebagai tempat mencatat jenis burung yang ditemukan saat dilakukan pengamatan. Isi dari *work sheet* yaitu keterangan tempat pengamatan, keterangan waktu pengamatan, keterangan kondisi cuaca saat pengamatan, dan tabel pengamatan yang terdiri dari nomor, jenis burung yang teramati, nama lokal burung, nama ilmiah burung, jumlah individu, waktu ditemukannya burung, dan keterangan. Teropong binoculler digunakan sebagai alat bantu untuk melihat burung agar terlihat lebih jelas dan fokus. Alat tulis digunakan untuk mencatat. Kamera digunakan untuk mengambil gambar jenis burung yang ditemukan saat melakukan pengamatan. Jam digital digunakan untuk melihat waktu saat burung ditemukan. Serta buku panduan lapangan Jenis Burung di Sumatera, Jawa, Bali, dan Kalimantan (MacKinnon *et.al*., 2010) yang digunakan sebagai alat bantu dalam melakukan identifikasi jenis burung apa saja yang didapat saat melakukan pengamatan.Objek pengamatan pada penelitian ini yaitu burung yang terdapat di Kebun Raya Liwa.

Pelaksanaan Penelitian

Observasi Lapangan

Penentuan lokasi pengamatan dilakukan dengan metode *purposive sampling* (salah satu teknik sampling *non random*) saat melakukan observasi pendahuluan. Hal ini bertujuan untuk mengenal lokasi atau habitat yang akan dijadikan sebagai tempat untuk pengamatan. Penentuan lokasi pengamatan dibagi menjadi tiga titik tempat pengamatan yaitu lokasi A sekitar kantor, lokasi B taman *araceae* dan lokasi C perbatasan kantor dengan kumpulan pohon berkayu.

Cara Kerja

Pengamatan burung dilakukan pada pagi hari pukul 06.30-08.30 WIB menjelang matahari terbit dan sore hari pukul 16.30-18.00 WIB menjelang matahari terbenam. Pengamatan dilakukan selama 9 hari. Pengamatan pada masing- masing lokasi dilakukan pengulangan hingga mendapatkan data yang tidak berubah (maksimal tiga kali pengulangan). Pengamatan jenis burung dilakukan dengan menggunakan metode

kombinasi antara metode titik hitung (*point count*) atau IPA (*Index Point Abundance* – Indeks Kelimpahan pada Titik) dan metode transek jalur yang di setiap lokasi terdapat tiga stasiun (Bibby, Jones dan Marsden, 2000).

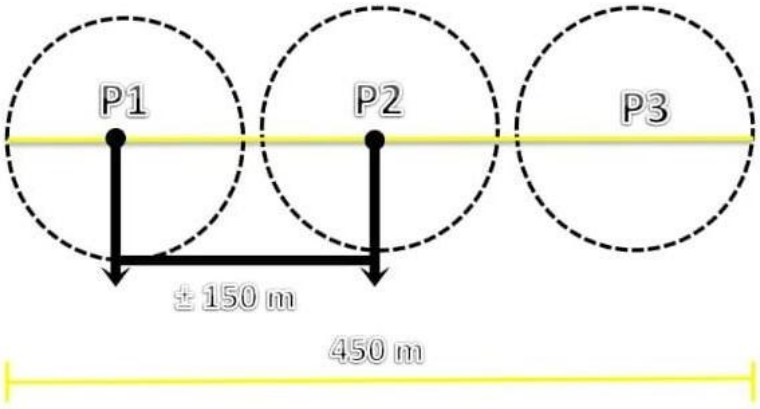

Gambar 1. Titik pengamatan burung menggunakan metode kombinasi antara titik hitung atau IPA dan metode jalur.
Jalur transek: sepanjang jalur transek di tiga stasiun pengamatan

Analisis Data

Indeks Keanekaragaman Jenis Keanekaragaman jenis dapat diketahui dengan Indeks Keanekaragaman Jenis Shannon-Wienner yaitu dengan rumus:

H^'	=	-∑pi ln pi
Keterangan:		
H^'	=	Indeks Keanekaragaman Jenis
pi	=	Jumlah proporsi kelimpahan satwa spesies ke-i
ln	=	Logaritma natural

Kriteria nilai indeks keanekaragaman Shanon – Wienner (Odum, 1993) adalah sebagai berikut.

H^' ≤ 1	:	Keanekaragaman rendah
1 < H^' < 3	:	Keanekaragaman sedang
H^' ≥ 3	:	Keanekaragaman tinggi

Indeks Kesamarataan

Indeks kesamarataan digunakan untuk mengetahui kesamarataan setiap spesies dalam setiap komunitas yang dijumpai, dengan menggunakan rumus :

J = H^' / H max atau J = - ∑Pi ln (Pi)/ln(S) Keterangan :
J = Indeks kesamarataan,
S = Jumlah spesies.
Kriteria indeks kesamarataan (Daget, 1976) adalah sebagai berikut.

0,75 < J ≤ 1 : Komunitas stabil
0 < J ≤ 0,5 : Komunitas tertekan
0,5 < J ≤ 0,75 : Komunitas labil

HASIL DAN PEMBAHASAN

Hasil penelitian yang telah dilakukan di Kebun Raya Liwa, menunjukkan adanya 15 spesies burung dari 9 famili dengan total 466 individu (Tabel 1). Selain pengamatan terhadap jenis burung yang ada, juga dilakukan pengamatan terhadap tumbuhan yang ada di Kebun Raya Liwa. Keberadaan tumbuhan sangat penting untuk keberlangsungan hidup burung-burung yang ada di Kebun Raya Liwa. Terdapat 8 jenis tumbuhan yang ditemukan di Kebun Raya Liwa yang dijadikan sebagai tempat beraktivitas burung (Tabel 2).

Berdasarkan data yang diperoleh, semakin banyak spesies burung yang ditemukan maka semakin tinggi indeks keanekaragamannya. Perbandingan indeks keanekaragaman pada tiga lokasi pengamatan menunjukkan bahwa lokasi C (perbatasan kantor dengan hutan Kebun Raya Liwa) memiliki indeks keanekaragaman jenis lebih tinggi dibandingkan dengan lokasi A (sekitar kantor Kebun Raya Liwa) dan lokasi B (taman *Araceae* Kebun Raya Liwa). Hal tersebut disebabkan lokasi C yang merupakan perbatasan kantor dengan hutan Kebun Raya Liwa lebih banyak terdapat pepohonan dan semak-semak sebagai habitat burung (tabel 3). Untuk menjamin kelangsungan hidupnya burung memerlukan habitat. Menurut

Alikodra (1990) habitat mempunyai fungsi dalam penyediaan makanan, air dan pelindung. Salah satu habitat yang ada yaitu Kebun Raya Liwa. Salah satu bagian yang penting dalam habitat burung yaitu pelindung. Pelindung dapat berupa pepohonan ataupun semak-semak. Pelindung berfungsi untuk tempat berkembang biak ataupun untuk berlindung. Tipe habitat seperti faktor struktur habitat dan ketersediaan pakan perlu diperhatikan agar keanekargaman jenis burung meningkat (Rusmendro, 2004).

Di Kebun Raya Liwa dapat ditemukan beberapa jenis pepohonan yang menjadi tempat burung mencari makan, air, dan perlindungan. Pada pohon pulai (*Alstonia scholaris*) saat pengamatan dijumpai banyak burung sedang bertengger, bersuara, makan, dan berlindung karena daunnya rimbun dan melebar ke samping. Di bulan Oktober bunga pada pohon ini bermekaran dan memiliki aroma yang harum. Pohon pulai menyediakan biji pulai yang merupakan pakan burung seperti perkutut, uncal buau, dan punai gading. Hal yang utama bagi keberadaan burung pada suatu habitat yaitu sumber pakan (Napitu,2007).

Beluntas (*Pluchea indica*) adalah tumbuhan semak yang berbunga bonggol. Berdasarkan hasil pengamatan di lapangan terlihat burung walik jambu sedang bertengger dan memakan madu tumbuhan beluntas. Baobab (*Adansonia digitata*) adalah pohon yang besar yang memiliki buah dan biji. Pada saat pengamatan, terdapat burung punai gading sedang bertengger, bermain dan mencari makan. Pada tumbuhan kelapa sawit (*Elaeis guineensis*) ditemukan beberapa spesies burung yang bertengger. Pohon ini dapat dijadikan sebagai tempat berlindung burung untuk menghindari pemangsa ataupun untuk berkembang biak. Pada pohon Ki Tenjo (*Anisoptera costata*) saat diamati terlihat burung sedang bertengger dan burung pemakan serangga seperti cekakak sungai, cinenen kelabu sedang mencari makan karena pohon ini menjulang sangat tinggi dengan jarak pandang yang lebih luas dan tidak terhalang vegetasi yang rapat *sehingga* memudahkan burung untuk mencari mangsa seperti serangga (Winarsih, 2015). Paku Andam (*Dicranopteris linearis*) adalah pohon yang beranting kecil dan perdu. Di pohon ini ditemukan burung kutilang dan merbah cerukcuk bertengger. Alang-alang (*Imperata cylindrica*) adalah tumbuhan liar yang dapat dijadikan tempat berlindung burung dan mencari mangsa. Loleba (*Bambusa atra lindl*) memiliki ranting – ranting yang kecil dan saat pengamatan terlihat burung merbah cerukcuk bertengger dan bermain di pohon ini.

Kondisi habitat di Kebun Raya Liwa sangat berpotensi untuk mendatangkan banyak jenis burung. Hanya saja, Kebun Raya Liwa belum tertata dengan rapih dibandingan dengan Kebun Raya lainnya seperti Kebun Raya Bogor yang sudah memiliki banyak taman koleksi yang bisa menjadi habitat bagi burung seperti Taman Meksiko

yang berisikan koleksi kaktus dan koleksi tanaman air, Taman Astrid yang berisikan kolam teratai raksasa yang biasa disebut *giant lotus* yang didalamnya terdapat banyak spesies teratai, Jalan Tasbih yang berisikan bunga-bunga tasbih, Jalan Kenari 2 yang berisikan pohon-pohon kenari, Rumah Anggrek yang berisikan spesies bunga anggrek. Selain itu, di Kebun Raya Bogor juga terdapat koleksi tanaman palem, koleksi tanaman kayu dan juga koleksi tanaman obat yang sudah tertata dengan rapih (Ratna *et al*., 2018).

Kondisi habitat ini sangat mempengaruhi keanekaragaman jenis burung di Kebun Raya Liwa, habitat adalah tempat burung beraktivitas dan memenuhi kebutuhan hidupnya seperti makan, minum dan tempat tinggal atau tempat berlindung. Untuk meningkatkan keanekaragaman jenis burung yang ada di Kebun Raya Liwa perlu dilakukan penanaman tanaman yang berpotensi untuk mendatangkan burung. Tanaman berbunga dan berbuah berpotensi tinggi untuk mendatangkan burung-burung terutama bagi burung pemakan bunga dan buah. Jika banyak tanaman yang berbunga akan mendatangkan banyak serangga pula. Hal ini dapat mendatangkan burung pemakan serangga. Pemilihan habitat khususnya di daerah urban harus menyediakan kebutuhan burung khususnya untuk pakan burung (Slaterry *et.al*., 2003).

Tabel 1. Spesies-spesies burung yang terdapat di Kebun Raya Liwa

No.	Nama Jenis	Nama Ilmiah	Lokasi A	Lokasi B	Lokasi C
1.	Cekakak Sungai	*Todirhamphus chloris*	0	9	7
2.	Walet Sapi	*Collocalia esculenta*	79	107	23
3.	Perkutut	*Geopelia striata*	5	2	34
4.	Cucak Kutilang	*Pycnonotus aurigaster*	26	27	25
5.	Cucak Kuning	*Pycnonotus melanicterus*	2	1	1
6.	Punai Gading	*Treron vernans*	6	15	27
7.	Punai Jambu / Walik Jambu	*Ptilinopus jambu*	0	0	1
8.	Uncal Buau	*Macropygia emiliana*	15	2	8
9.	Merbah Cerukcuk	*Pycnonotus goiavier*	6	6	13
10.	Bentet Kelabu	*Lanius schach*	1	1	5
11.	Tekukur	*Streptopelia chinensis*	0	0	4
12.	Kicuit Batu	*Motacilla cinerea*	3	0	0
13.	Kareo Padi	*Amaurornis phoenicurus*	2	0	1
14.	Cabai Bunga Api	*Dicaeum trigonostigma*	1	0	0
15.	Cinenen Kelabu	*Orthotomus ruficeps*	0	1	0
Jumlah Spesies (S)			11	10	12
Jumlah Individu (N)			146	171	149
Indeks Keanekaragaman (H')			1,51	1,02	2,16
Indeks Kesamarataan (J)			0,30	0,23	0,41

Tabel 2. Daftar Jenis Tumbuhan yang Dijadikan Tempat Beraktivitas Burung

No	Nama Lokal	Nama Ilmiah	Aktivitas Burung
1	Pulai	*Alstonia scholaris*	Bertengger dan bermain
2	Beluntas	*Pluchea indica*	Bertengger dan makan
3	Baobab	*Adansonia digitata*	Bertengger dan bermain
4	Kelapa Sawit	*Elaeis guineensis*	Bertengger
5	Ki Tenjo	*Anisoptera costata*	Bertengger dan bermain
6	Paku Andam	*Dicranopteris linearis*	Mencari makan
7	Alang-alang	*Imperata cylindrical*	Bermain dan mencari makan
8	Loleba	*Bambusa atra lindl*	Bertengger

Tabel 3. Indeks keanekaragaman jenis dan indeks kesamarataan burung di Kebun Raya Liwa, Lampung Barat.

Titik Pengamatan	Jumlah Spesies	Indeks Keanekaragaman	Indeks Kesamarataan
A	11	1,51**	0,30*
B	10	1,02**	0,23*
C	12	2,16**	0,41*

Ket: **indeks keanekaragaman sedang; *indeks kesamarataan menunjukkan komunitas

KESIMPULAN

Terdapat 15 spesies burung dengan total 466 individu. Lokasi pengamatan A (sekitar kantor Kebun Raya Liwa), lokasi pengamatan B (taman *Araceae* Kebun Raya Liwa), lokasi pengamatan C (perbatasan kantor dengan kumpulan pohon berkayu) memiliki tingkat keanekaragaman yang sedang yaitu berturut-turut sebesar 1,51 ; 1,02 dan 2,16.

UCAPAN TERIMAKASIH

Terimakasih kepada Badan Penelitian dan Pengembangan Daerah Kabupaten Lampung Barat dan kepada Bapak Sukimin, S.IP. MM. selaku Kepala UPTD Pengelolaan Kebun Raya Liwa beserta seluruh staff Kebun Raya Liwa yang telah membantu selama penelitian.

DAFTAR PUSTAKA

Alikodra, H. S. (1990). *Pengelolaan Satwa Liar*. Departemen Pendidikan dan Kebudayaan. IPB. Bogor.

Bibby, C., M. Jones., S. Marsden. (2000). *Teknik Ekspedidi Lapangan: Survey Burung*. SKMG Mardi Yuana. Bogor.

Daget. (1976). *Kriteria Kesamarataan*. http;//www.elib.pdii.lipi.go.id/katalog/indeks.php/searchkatalog/./8212/8218.p. Diakses pada tanggal 10 Desember 2019 pukul 19.30 WIB.

Mac Kinnon, J., K. Phillips, dan B. Van Balen. (2010). *Seri Panduan Lapangan Burung-burung di Sumatera, Jawa, Bali, dan Kalimantan*. LIPI. Bogor.

Napitu. (2007). *Pengelolaan Lapangan Konservasi*. Gadjah Mada University Press. Yogyakarta.

Odum, E. P. (1993). *Dasar-dasar Ekologi*. Terjemahan. Gadjah Mada University Press. Yogyakarta.

Ramadhani. (2018). Hubungan Keanekaragaman Jenis Burung dengan Komposisi Pohon di Kampus Universitas Lampung. Skripsi. Jurusan Biologi. Universitas Lampung. Bandar Lampung.

Ratna SH, Tubagus UN. Rangga M. (2018). *Jalur Interpretasi Birdwatching di Kebun Raya Bogor*. Bogor. *Media Konservasi*, 23:28-36.

Rusmendro, H. (2004). *Bahan Kuliah Ornithology*. Jakarta. Universitas Nasional.

Rusmendro, H. (2009). Perbandingan Keanekaragaman Burung pada Pagi dan Sore Hari di Empat Tipe Habitat di Wilayah Pengandaran. Jawa Barat. *Jurnal Vit Vitalis*. 2(1):8-1.

Slaterry BE, Reshetiloff K, Zwicker SM. (2003). *Native Plants for Wildlife Habitat and Conservation Landscaping*. Native Plant Center.

Sulistyadi, E. (2010). Kemampuan Kawasan Nir-Konservasi dalam Melindungi Kelestarian Burung Endemik Dataran Rendah Pulau Jawa Studi Kasus di Kabupaten Kebumen. *J. Biologi. Indonesia*. Perhimpunan Biologi Indonesia. 237-253 (245).

Winarsih, A. (2015). *Komunitas Burung di Pulau Tidung Kecil, Kepulauan Seribu*. Jakarta. Universitas Islam Negeri Syarif Hidayatullah.

IMOBILISASI BAKTERI ASAM LAKTAT DENGAN MENGGUNAKAN ALGINAT

Kinasih Cahyono[1], Endang Nurcahyani[2], Sri Wahyuningsih[2], Bambang Irawan[2], dan Sumardi[2*]

[1]Mahasiswa Program Studi Magister Biologi, Fakultas MIPA, Universitas Lampung
Jl. Prof. Dr.Ir. Sumantri Brojonegoro No. 1, Gedong Meneng, Bandar Lampung 35141
[2]Jurusan Biologi, Fakultas MIPA, Universitas Lampung
Jl. Prof. Dr.Ir. Sumantri Brojonegoro No. 1, Gedong Meneng, Bandar Lampung 35141

Email: sumardi_bio@yahoo.co.id

ABSTRAK

Lactobacillus sp. merupakan bakteri asam laktat, salah satu spesies yang sering digunakan sebagai probiotik, namun kelemahan dari bakteri tersebut adalah tidak toleran terhadap pH rendah (asam), di cairan empedu, serta pada suhu yang tinggi. Bakteri probiotik harus tetap hidup sejak mereka dikonsumsi hingga menetap di usus. Hal ini sulit karena bakteri harus melewati pH asam ekstrim di saluran pencernaan. Imobilisasi dengan enkapsulasi bakteri probiotik adalah alternatif yang memberikan perlindungan bagi sel-sel hidup (bakteri) yang berada pada kondisi yang merugikan. Berdasarkan hasil uraian tersebut maka tujuan imobilisasi adalah untuk meningkatkan jumlah kelangsungan hidup (viabilitas) bakteri *Lactobacillus* sp dalam kondisi simulasi asam lambung dan garam empedu (*ox bile* 0,5%) dengan menggunakan imobilisasi matriks alginat. Metode yang digunakan dalam imobilisasi bakteri adalah ekstrusi. Teknik ini melibatkan persiapan larutan hidrokoloid, penambahan mikroorganisme, dan ekstrusi suspensi sel melalui jarum *syringe*. Tetesan tersebut diteteskan ke larutan pengeras $CaCl_2$. Perbandingan bakteri yang diimobilisasi dengan bakteri bebas adalah imobilisasi dengan penyalut alginat metode ekstrusi mampu meningkatkan viabilitas bakteri asam laktat dibandingkan dengan bakteri yang tidak diimobilisasi.

Kata kunci : Imobilisasi, alginat, bakteri asam laktat, viabilitas

ABSTRACT

Lactobacillus sp. is a lactic acid bacteria, one of the species that is often used as a probiotic, but the weakness of these bacteria is they are not intolerant of low pH (acid), in bile, and also at high temperatures. Probiotic bacteria must stay alive from the time they are consumed until they settle in the intestines. This is difficult because the bacteria have to pass through the extreme acidic pH in the digestive tract. Immobilization with probiotic bacterial encapsulation is an alternative that provides protection for living cells (bacteria) that are in adverse conditions. Based on the results of the description, the objective of the study is to increase the number of survival of *Lactobacillus* sp bacteria in simulated conditions of gastric acid and bile salts (*ox bile* 0,5%) by using the immobilization of the alginate matrix. Extrusion is the method used

in bacterial immobilization. This technique involves the preparation of a hydrocolloid solution, addition of microorganisms. and extrusion of the cell suspension through a syringe needle. The comparison between immobilized bacteria and free bacteria is that immobilization with alginate coatings extrusion method can increase the viability of lactic acid bacteria compared to bacteria that are not immobilized.

Keywords : Immobilization, alginate, lactic acid bacteria, viability

PENDAHULUAN

Probiotik menurut Suryani et, al. (2019) didefinisikan sebagai mikroorganisme hidup, yang jika diberikan atau dikonsumsi dalam jumlah tertentu akan memberikan manfaat kepada inang. Kelompok bakteri spesies *Lactobacillus* sp. merupakan bakteri asli pada pencernaan manusia, sehingga menjadi pilihan utama produk probiotik, selain itu juga bakteri ini bersifat nonpatogen dan aman. *Lactobacillus* sp. memiliki kelemahan dalam mempertahankan diri di lingkungan yang sangat asam, di cairan empedu, serta pada suhu yang tinggi. Nilai pH optimum yang dapat ditoleransi *Lactobacillus* sp berada di kisaran 3-5.

Permasalahan utama Bakteri *Lactobacillus* sp adalah rawan dalam kondisi lingkungan yang ekstrim, sehingga dapat menyebabkan hilangnya kehidupan fungsional bakteri tersebut. Strategi terbaik untuk mengatasi masalah ini adalah dengan cara imobilisasi dan menjebak sel-sel bakteri. Bakteri probiotik harus tetap hidup sejak dikonsumsi hingga menetap di usus. Hal ini sulit karena bakteri harus melewati pH asam di saluran pencernaan. Imobilisasi dengan enkapsulasi bakteri probiotik adalah alternatif yang memberikan perlindungan bagi sel-sel hidup yang berada pada kondisi yang merugikan (Burgin, *et al*., 2011).

Imobilisasi merupakan suatu metode untuk mengurung atau menempatkan sel mikroba secara fisik pada suatu ruang tertentu dimana sel masih memiliki aktivitas katalitik serta dapat dipergunakan secara berkelanjutan dan berulang kali, dalam proses imobilisasi sel-sel biasanya tumbuh dipermukaan atau terperangkap di dalam model, karena banyak mikroorganisme yang mampu melekat pada berbagai permukaan alami. Mikroorganisme dapat distabilkan pada matriks yang berbeda seperti menjebak dalam bahan berpori, penyerapan atau adehsi, penghambatan sel, dan ikatan kovalen serta ikatan ion (Hassanzadeh, *et al*., 2017).

Produk probiotik dapat digunakan dengan cara enkapsulasi bakteri. Enkapsulasi bakteri juga merupakan suatu cara yang dapat melindungi dan membawa mikroorganisme sampai ke usus. Mikroenkapsulasi dengan bead hidrokoloid telah di uji dapat meningkatkan viabilitas probiotik di dalam makanan dan saat di saluran pencernaan. Mikroenkapsulasi membantu ketidakstabilan inti di lingkungan, meningkatkan stabilitas, dan memperpanjang umur simpan bakteri. Mikroenkapsulasi bakteri probiotik sering menggunakan matriks berupa alginat. Alginat telah diuji dapat meningkatkan ketahanan hidup probiotik 80-95% . Preparasi mikrokapsul alginat sebagai matrik bakteri, dapat dilakukan dengan cara ekstrusi dan emulsi. Penggunaan ekstrusi sebagai metode enkapsulasi bakteri memiliki beberapa keuntungan, diantaranya metode ekstrusi merupakan metode yang mudah dan murah dalam pengoperasian, memberikan viabilitas yang tinggi pada bakteri, dan tidak merusak sel probiotik seperti halnya ketika menggunakan teknik *spray-drying* (Suryani, *et al*., 2019). Berdasarkan uraian di atas artikel ini bertujuan untuk meningkatkan kelangsungan hidup (viabilitas) bakteri probiotik dalam kondisi simulasi cairan asam lambung (pH rendah) dan simulasi garam empedu (*ox bile* 0,5%) dengan menggunakan imbolisasi alginate.

1. ISI

1.1 Karakterisasi Alginat

Alginat menurut Wulandari, et.al (2019) merupakan polimer alami yang berasal dari alga coklat (Phaeophyta). Alginat adalah garam dari asam alginat yang merupakan kopolimer dari blok β-d-mannuronic acid (M) dan epimer C-5, asam α-l-guluronic (G), dihubungkan bersama untuk membentuk polisakarida linier dengan ikatan (1,4) -glikosidik yang terlihat pada Gambar 1. berikut:

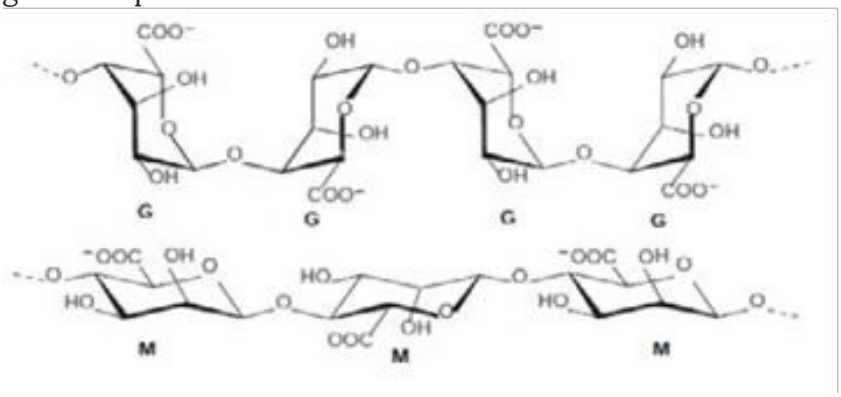

Gambar 1. Struktur Blok Alginat (blok G, blok M dan blok MG) (Imeson, 2010 dalam Wulandari, et.al 2019).

Alginat merupakan salah satu jenis hidrokoloid, yaitu suatu sistem koloid oleh polimer organik di dalam air. Alginat dapat membentuk gel yang stabil terhadap panas dimana dapat disimpan pada suhu kamar (Herawati, 2018). Pemanfaatan alginat didasarkan pada tiga sifat utamanya yaitu yang pertama kemampuannya dalam menaikkan viskositas larutan apabila alginat dilarutkan dalam air. Kedua adalah kemampuan alginat untuk membentuk gel, gel akan terbentuk jika pada larutan natrium alginat ditambahkan garam Ca. Gel terbentuk karena adanya reaksi kimia, pada proses tersebut Ca akan menggantikan posisi natrium dari alginat dan mengikat molekul alginat yang panjang. Proses ini tidak memerlukan panas dan gel yang terbentuk tidak akan meleleh jika dipanaskan. Berbeda dengan gel agar yang memerlukan pemanasan untuk pembentukan gelnya, sehingga air harus dipanaskan sampai suhu 80°C untuk membentuk *swelling*/gelatinisasi agar dan gel terbentuk pada suhu di bawah 40° C. Sifat ketiga dari alginat adalah kemampuannya untuk membentuk film dari natrium atau kalsium alginat dan fiber dari kalsium alginat.

Pemanfaatan alginat sebagai bahan prebiotik yang merupakan substrat bagi mikroba untuk menghasilkan asam lemak rantai pendek juga tidak mudah dilakukan karena polimernya yang panjang, sehingga kurang sesuai bagi bakteri probiotik seperti *Bifidobakteria* dan *Lactobacillus* (Subaryono, 2010). Struktur mikroenkapsulasi mengggunakan alginat yaitu bakteri probiotik diselimuti oleh kapsul berupa alginat, dapat dilihat pada gambar (2) dibawah ini.

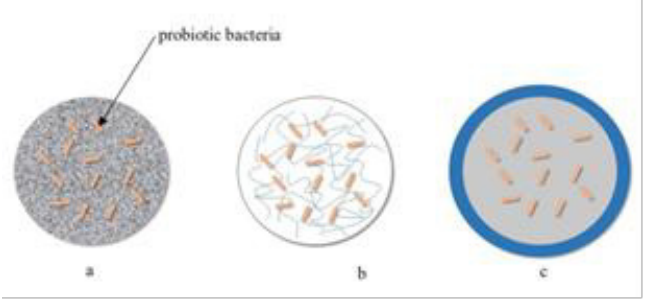

Gambar 2. Skema Struktur mikroenkapsulasi (a) struktur matrik, (b) struktur cross-link, (c) struktur pelapisan bagian luar dengan alginat (Liu, *et al.*, 2017).

1.2 Teknik Ekstrusi

Teknik tertua dan paling umum untuk menghasilkan kapsul dengan hidrokoloid (misalnya, alginat dan karagenan) terdiri dari menyiapkan larutan hidrokoloid, menambahkan mikroorganisme dan membentuk tetesan dengan mengekstrusi suspensi melalui jarum suntik (*syringe*) ke dalam larutan pengerasan (misalkan kalsium klorida) atau dengan cara menambahkan mikroba probiotik ke dalam larutan hidrokoloid alginat, kemudian diteteskan ke dalam larutan pengeras ($CaCl_2$) menggunakan *syringe* (Gambar 3). Ukuran dan bentuk mikrokapsul yang terbentuk tergantung pada diameter nosel dan jarak antara nosel dan $CaCl_2$ larutan. Metode ini sederhana dan hemat biaya, tidak menyebabkan kerusakan sel dan menghasilkan viabilitas sel yang tinggi. Teknologi ini tidak menggunakan pelarut berbahaya dan dapat dilakukan di bawah kondisi aerobik dan anaerobik (Krasaekoopt *et al*., 2003).

Hasil penelitian Krasaekoopt *et al*., (2006) dalam Cock-Serna dan Castillo-Vallejo (2013) menunjukkan bahwa kelangsungan hidup bakteri probiotik yang dienkapsulasi lebih besar dibandingkan dengan bakteri bebas (tidak di enkapsulasi) dalam sekitar 1 siklus log, selama penyimpanan dan jumlah bakteri probiotik. Kapsul disimpan pada suhu 4 ° C dan viabilitasnya dicatat selama 63 hari. Hasil penelitian Soto *et al*. (2011). menunjukkan bahwa kapsul yang didinginkan memiliki viabilitas yang lebih besar dibandingkan dengan kapsul yang disimpan pada suhu kamar. Disimpulkan bahwa probiotik memiliki umur simpan minimal 2 bulan dan dapat digunakan sebagai inisiator kultur. Berikut dibawah ini merupakan diagram metode ekstrusi dapat di lihat pada Gambar 3.

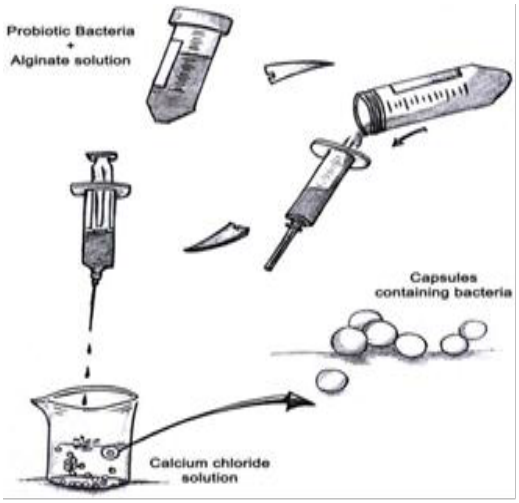

Gambar 3. Diagram skematis dari metode enkapsulasi ekstrusi (Cock-Serna dan Castillo-Vallejo, 2013).

1.3 Karakterisasi Bakteri Probiotik Hasil Imobilisasi

Viabilitas sel probiotik merupakan parameter penting terkait manfaatnya terhadap kesehatan. Manfaat probiotik bisa dirasakan ketika ia mampu bertahan hidup di saluran cerna dalam jangka waktu yang lama, laporan Vos et al., (2010) menyebutkan bahwa sel probiotik dalam kondisi bebas cenderung memiliki survival yang rendah dibandingkan dengan yang diimobilisasi dengan alginat. Morfologi kapsul diukur dengan SEM dan mikroskop optik, semua mikrokapsul berbentuk bulat dapat dilihat pada (Gambar 4 dan 5). Teknik ekstrusi menurut Solanki et al. (2013) akan menghasilkan mikrokapsul yang lebih beragam daripada teknik emulsifikasi. Umumnya, diameter yang terbentuk antara 2-5 mm lebih besar dari yang dibentuk dalam metode emulsi. Ukuran dan bentuk mikrokapsul dipengaruhi oleh konsentrasi dan viskositas larutan polimer, jarak antara jarum suntik dan larutan pembentuk mikrokapsul serta ukuran diameter ekstruder yang digunakan.

Temuan ini sesuai dengan Sultana *et al.* (2000), yang melaporkan bahwa bentuk mikrokapsul berbentuk bulat. Bentuk serupa dari mikrokapsul juga ditunjukkan oleh banyak peneliti (Zanjani *et al.*, 2012). Berikut merupakan bentuk kapsul yang dilapisi alginat:

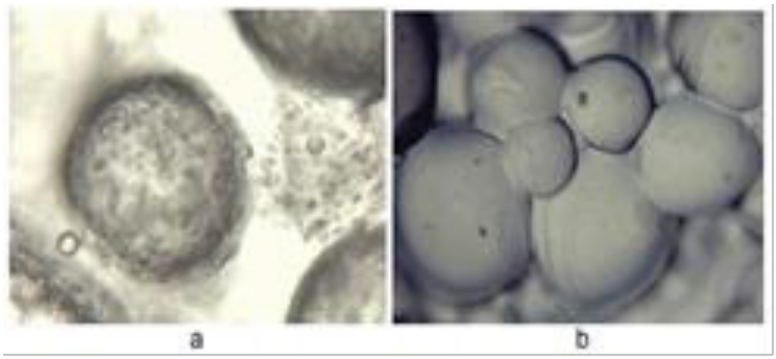

Gambar 4. Gambar mikroskop optik dari kapsul alginat (a dan b) pada perbesaran 40x. (Zanjani *et al.*, 2012).

Berikut merupakan bentuk kapsul yang dilapisi natrium alginat-zeolit-pati:

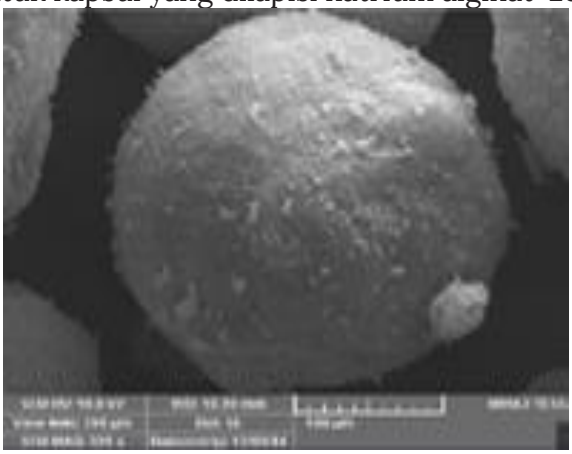

Gambar 5. Pengamatan dengan mikroskop elektron yang menunjukkan mikroenkapsulasi dari *L.casei* dengan natrium alginat-zeolit-pati (Hassanzadeh, *et al*, 2017).

1.4 Viabilitas Mikroenkapsulasi *Lactobacillus* sp. pada Simulasi Asam Lambung

Berdasarkan hasil penelitian Purnasari (2015) mengenai ketahanan strain *Lb. plantarum* terhadap pH rendah (pH 2) Salah satu syarat bakteri termasuk dalam probiotik adalah mampu bertahan hidup pada kondisi saluran pencernaan yang meliputi keasaman tinggi dan sekresi garam empedu. Penurunan jumlah bakteri probiotik bebas yang diinkubasi dengan pH 2 berbeda nyata lebih banyak dengan probiotik terenkapsulasi. *Lb. plantarum* BSL dan *Lb. plantarum* 2C12 masing-masing mengalami penurunan sebesar 2,6 dan 2,5 Log CFU mL-1 . Hasil berbeda nyata ditunjukkan pada *Lb. plantarum* BSL dan *Lb. plantarum* 2C12 terenkapsulasi masing-masing hanya mengalami penurunan sebesar 1,3 dan 1,2 Log CFU mL-1 (Gambar 6).

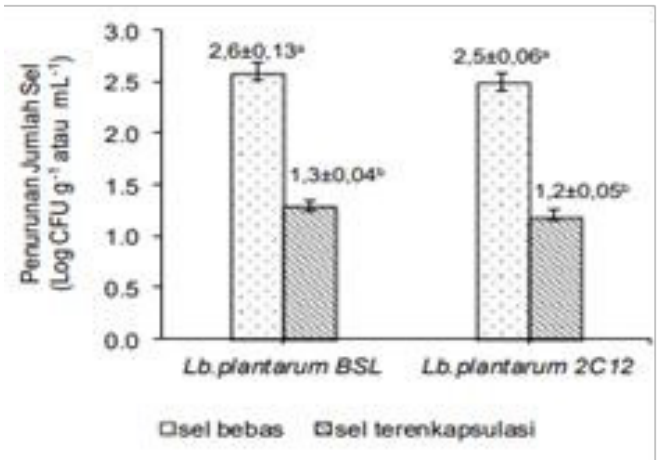

Gambar 6. Ketahanan sel strain *Lb. plantarum* bebas dan terenkapsulasi terhadap pH rendah (pH 2) (Purnasari, *et.al.* 2015).

Pada percobaan ini, ketahanan sel probiotik terhadap pH rendah dilakukan dengan inkubasi pada kondisi pH rendah (pH 2) selama 5 jam, sesuai dengan lamanya makanan berada di dalam lambung (2-6 jam). Chandramouli et al. (2004) dalam Purnasari, *et.al.* (2015) melaporkan kenaikan viabilitas *Lb. acidophilus* secara nyata pada pH 2 setelah dienkapsulasi dengan alginat. Kim *et al.* (2008) melaporkan bahwa sintasan *Lb. acidophilus* ATCC 43121 pada kondisi pH rendah (pH 1,2 dan 1,5) berbeda nyata lebih tinggi dibandingkan dengan sel bebas. Pada pH 1,2 *Lb. acidophilus* ATCC 43121 bebas mengalami kematian setelah inkubasi selama 1 jam, sedangkan Lb. acidophilus ATCC 43121 terenkapsulasi mengalami penurunan dari 6 menjadi 3 Log CFU g -1 . Dengan demikian enkapsulasi dengan alginat mampu meningkatkan sintasan probiotik setelah dipapar dengan pH rendah.

1.5 Viabilitas Mikroenkapsulasi *Lactobacillus* sp. pada Simulasi Garam Empedu

Viabilitas Bakteri asam laktat terhadap garam empedu merupakan salah satu persyaratan penting untuk probiotik. Dalam hal ini Hermana *et al.* (2015) menyebutkan semua mikroba yang berhasil hidup setelah ditumbuhkandalam de Man, Rogosa, Sharpe Agar (MRSA) yang ditambah 0,5% *ox bile* dinyatakan bersifat tahan terhadap garam empedu. Hasil simulasi ketahanan bakteri probiotik BN12 pada media *ox bile* (garam empedu 0,5%) memperlihatkan bahwa pada awalnya jumlah bakteri probiotik BN12 setelah proses pengeringan cukup tinggi kecuali kitosan, namun setelah diinkubasi dalam media garam empedu mengalami penurunan. Penurunan jumlah bakteri pada media garam empedu berkaitan dengan sifat garam empedu yang merupakan racun bagi bakteri. Konsentrasi garam empedu yang tinggi merupakan racun sekaligus zat antimikroba yang sangat keras. Cairan empedu di dalam usus halus bersifat menghambat pertumbuhan mikroba (Bezkorovainy, 2001).

Namun setelah masa inkubasi 6 jam, jumlah bakteri cenderung mengalami kenaikan, kecuali bakteri probiotik dengan penyalut kitosan yang sejak awal disimulasikan tidak tumbuh. Adanya kenaikan jumlah bakteri menunjukkan bahwa bakteri tersebut mampu beradaptasi dalam media garam empedu yang selanjutnya bereproduksi melalui pembelahan sel. Dilaporkan bahwa fase adaptasi bakteri asam laktat *Streptococcus* terjadi pada jam ke-0 hingga jam ke-4. Sementara fase adaptasi *Lactobcillus* sp. RED4 terjadi pada jam ke-0 hingga jam ke-2. Bakteri probiotik BN12 selama masa inkubasi 6 jam dalam media garam empedu mengalami pertumbuhan. Pertumbuhan bakteri tersebut lebih rendah dibandingkan pertumbuhan 99 strain *Lactobacillus plantarum* yang memiliki rata-rata pertumbuhan sebesar 40% dengan persentase pertumbuhan terendah 12,21% dan tertinggi 95,98% (Zago et al., 2011). Hal ini

terlihat dari persentase kenaikan jumlah bakteri probiotik BN12 terenkapsulasi dengan penyalut alginat, xanthan gum dan kontrol (tanpa penyalut) berturut-turut sebesar 25,68; 10,65; dan 1,12% (Tabe1).

Tabel 1. Ketahanan bakteri probiotik terenkapsulasi terhadap garam empedu

Penyalut	**Log Jumlah Bakteri (cfu/g)**			**% kenaikan BAL setelah 6 jam inkubasi.**
	Setelah Spraay Drying	Masa Inkubasi dalam Garam Empedu		
		0jam	6Jam	
Alginat	7.99	5.88[a]	7.39[a]	25.68
Xanthan Gum	8.36	6.95[a]	7.69[a]	10.65
Kitosan	2.04	0[b]	0[b]	0
Kontrol	8.18	6.24[a]	6.31[a]	1.12

Keterangan : Huruf yang sama pada kolom yang sama kolom yang sama menunjukkan tidak berbeda nyata (p>0,05) (Hermana, *et al.*, 2015).

Sementara hasil penelitian dari Purnasari, et.al. (2015) ketahanan strain *Lb. plantarum* terhadap garam empedu (0,5%) Kemampuan bakteri probiotik untuk bertahan pada kondisi saluran pencernaan diperlukan untuk dapat memberikan efek kesehatan. Ketahanan bakteri probiotik terhadap garam empedu merupakan salah satu sifat penting yang harus dimiliki agar mampu tumbuh dan bertahan hidup selama berada pada bagian usus kecil. Ketahanan sel *Lactobacillus plantarum* bebas dan terenkapsulasi dalam simulasi larutan garam empedu 0,5 % dapat dilihat pada Gambar 7.

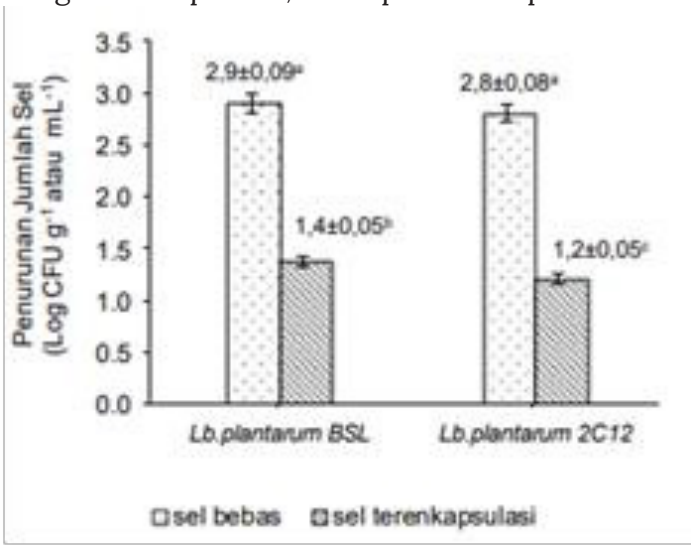

Gambar 7. Ketahanan sel strain *Lb. plantarum* bebas dan terenkapsulasi terhadap garam empedu (0,5%) (Purnasari, et.al. 2015).

Penurunan jumlah bakteri probiotik bebas yang diinkubasi dengan MRSB yang mengandung garam empedu 0,5% berbeda nyata lebih banyak dibandingkan dengan probiotik terenkapsulasi. *Lb. plantarum* BSL dan *Lb. plantarum* 2C12 terenkapsulasi masing-masing hanya mengalami penurunan sebesar 1,4 dan 1,2 Log CFU mL-1 (Gambar 10) atau sekitar separuh dari penurunan sel bebas setelah dipapar dengan kondisi garam empedu 0,5%. *Lb. plantarum* BSL dan *Lb. plantarum* 2C12 masing-masing mengalami penurunan sebesar 2,9 dan 2,8 Log CFU mL-1.

2. KESIMPULAN

Berdasarkan uraian di atas maka dapat disimpulkan bahwan imobilisasi dengan penyalut alginat mampu meningkatkan viabilitas bakteri *Lactobacillus* sp. dalam kondisi simulasi asam lambung dan garam empedu (*ox bile* 0,5%). Hasil berbeda nyata ditunjukkan pada *Lb. plantarum* BSL dan *Lb. plantarum* 2C12 terenkapsulasi masing-masing hanya mengalami penurunan sebesar 1,3 dan 1,2 Log CFU mL^{-} pada pH rendah (simulasi asam lambung) dan penurunan sebesar 1,4 dan 1,2 Log pada simulasi garam empedu (*ox bile* 0,5%). Berdasarkan data tersebut maka dapat disimpulkan bahwa imobilisasi dengan penyalut alginate metode ekstrusi mampu meningkatkan viabilitas bakteri asam laktat.

DAFTAR PUSTAKA

Bezkorovainy, A. 2001. Probiotics: Determinants of survival and growth in the gut. *Am.Clin. Nutr*., 73: 399S–405S.

Burgin, C., Gaiani, C., Linder, M., and Scher, J. 2011. Enkapsulasi dari sel hidup probiotik: Dari skala laboratorium hingga aplikasi industri. *J. Makanan Eng*. 104: 467-483.

De Vos, P., Faas, M.M., Spasojevic, M., and Sikkema, J. 2010. Encapsulation forpreservation of functionality and targeted delivery of bioactive foodcomponents. *International Dairy Journal*, 20(4): 292–302

Hassanzadeh, A.M., Khiabani, M.S., Sadrnia, M., Divband, B., Rahmanpour, O., Jabbari, V., Gholizadeh, P., dan Kafil, H.S. 2017. Immobilization and microenc-apsulation of *Lactobacillus caseii* and *Lactobacillus plantarum* using zeolite base and evaluating their viability in gastroesophageal-intes-tine simulated. *Ars Pharm*, 58 (4): 163-170.

Herawati, Heny. 2018. Potensi Hidrokoloid Sebagai Bahan Tambahan pada Produk Pangan dan Nonpangan Bermutu. Jurrnal Litbang Pertanian. 37(1): 17-25.

Hermana, I, Kusmarwati, A., dan Indriati, N. 2015. Mikroenkapsulasi Strain Probiotik *Leuconostoc mesenteroides* Ssp. *Cremonis* Bn12 Menggunakan Berbagai Penyalut. *JPB Kelautan dan Perikanan*, 10 (2): 133–141.

Imeson, A. 2010. *Food Stabilisers, Thickeners, and Gelling Agents*. United Kingdom: Wiley-Blackwell.

Kim, S.J., Cho, S.Y., Kim, S.H., Song, O.J., Shin, I.S., Cha, D.S., dan Park, H.J. 2008. Effect of microencapsulation on viability and other characteristics in *Lactobacillus acidophilus* ATCC 43121. *LWT-Food Sci. Technol.* 41: 493–500. DOI: 10.1016/j.lwt.2007.03.025

Krasaekoopt, W., Bhandari, W., and Deeth, H. 2003. Evaluation of encapsulation techniques of probiotics for yoghurt. *Int. Dairy Journal*. 13:313

Liu, H., Steve W. Cui, Chen,M., Li, Y., Liang, R., Xu, F., dan Zhong, F. 2017. Protective approaches and mechanisms of microencapsulation to the survival of probiotic bacteria during processing, storage and gastrointestinal digestion. *Journal Food Science and Nutrition*. 1(1): 1-7

Purnasari, N., Jenie, B.Sl., dan Nuraida, L. 2015. Karakteristik Mikrokapsul *Lactobacillus Plantarum* dan Stabilitasnya dalam Produk Selai Salak. *Jurnal Teknologi dan Industri Pangan*. 26(1): 90-99.

Serna-cock, L., and Vallejo-calello, V. 2013. Probiotic encapsulation, *Global Journal of Medical Microbiology*, 7(40): 4744-4751.

Soto, L.P., Frizzo, L.S., Avataneo, E., Zbrun, M.V., Bertozzi, E., Sequeira, G., Signorini, M.L., and Rosminia, M.R. 2011. Design of macrocapsules to improve bacterial viability and supplementation with a probiotic for young calves. *Anim. Sci. Technol*. 165:176-183.

Subaryono. 2010. Modifikasi Alginat dan Pemanfaatan Produknya. *Balai Besar Riset Pengolahan Produk dan Bioteknologi Kelautan dan Perikanan.* 5(1): 1-7

Suryani, N., Betha, O.F., Mawaddana, Q. 2019. Uji Viabilitas Mikroenkapsulasi *Lactobacillus Case*i Menggunakan Matrik Natrium Alginat. *Jurnal Farmasi Lampung* , 8(1): 1-7.

Zago, M., Fornasari, M.E., Carminati, D., Burns, P., Suarez, V., Vinderola, G., Reinheimer, J., and Giraffa, G. 2011. Characterization and probiotic potential of Lactobacillus plantarum strains isolated from cheeses. *Food Microbiology*, 28: 1033-1040.

Zanjani, M.A.K., Tarzi, B.G., Sharifan, A., Mohammadi, N., Bakhoda, H., Madanipour, M.M. 2012. Microencapsulation of *Lactobacillus casei* with calcium alginate-resistant starch and evaluation of survival and sensory properties in cream-filled cake, *African Journal of Microbiology Research.* 6 (26): 5511-5517.

ADSORPTION KINETICS AND ISOTHERM OF CRYSTAL VIOLET BY CARBON MODIFIED WITH MAGNETITE (Fe_3O_4) AND TRIETHOXYPHENYLSILANE (TEPS) FROM RUBBER FRUIT SHELL

Nadya S. Fajriyah[1], Buhani[2,*] and Suharso[2]

[1]Postgraduate Student of Master Program in Chemistry, Department of Chemistry, University of Lampung, Jl. Sumantri Brojonegoro No 1, Bandar Lampung 35145, Indonesia

[2]Department of Chemistry, Faculty of Mathematic and Natural Sciences, University of Lampung, Jl. Soemantri Brojonegoro No. 1 Bandar Lampung 35145, Indonesia

[*] Corresponding author: Tel.: +62-81278152368, Email: buhani_s@yahoo.co.id

ABSTRACT

Carbon modified with magnetite (MC) and triethoxyphenylsilane (TEPS) (SC) made from rubber fruit shells were used to effectively adsorb crystal violet (CV) dye. The carbon was successfully modified by magnetite and TEPS, according to characterization of the adsorbent utilizing Fourier transform infrared (FTIR) spectroscopy, X-ray diffraction (XRD), and scanning electron microscopy-energy-dispersive X-ray (SEM-EDX) showed that the carbon was successfully modified by magnetite and TEPS. Several adsorption process parameters were investigated, and the ideal results were obtained with an adsorbent dose of 0.1 g, pH 10, contact time of 15 minutes, and initial concentration of CV 250 mg L^{-1}. The MC and SC adsorption capacities are 47.01 and 54.63 mg g^{-1}, respectively. The adsorption kinetics tends to follow pseudo-second order model with MC and SC rate constants of 3.403 and 0.827 g mg^{-1} min^{-1}, respectively. The Freundlich adsorption isotherm is suitable for CV dye adsorption using MC and SC with K_F values are 1.362 and 1.761 mg g^{-1} L mg^{-1} which gives R^2 0.943 and 0.932, respectively.

***Keywords*:** Magnetite carbon; Silane carbon; Adsorption; Crystal violet; Rubber fruit shell

INTRODUCTION

Environmental issues, especially in Indonesia, are still a problem that needs attention. Water pollution that is commonly found can be in the form of dyes, herbicides, heavy metals, and other contaminants that accumulate in the environment [1].

One of the most common industrial pollutants is the textile industry. The textile industry produces a lot of dye waste in the environment. Dyes used in the textile industry are classified into three categories, namely cationic, anionic and non-ionic dyes

[2,3]. Cationic dyes, are very dangerous compared to others and are most widely used in the textile industry. Crystal violet (CV) is a triphenyl methane and one of the cationic dyes used in various industries such as pharmaceuticals, paper, textiles, and printer inks [4]. CV if it is in the water can reduce the penetration of sunlight and interfere with the photosynthesis process [5]. If CV enters the human body in a certain amount, it can cause various diseases such as respiratory problems, eye and skin irritation, increased heart rate, blindness and mutagenesis [4,6].

Considering the impact caused by the presence of CV dye can be harmful to humans, several steps to reduce or even eliminate CV dye waste have been carried out such as chemical degradation, adsorption, and photocatalysis [7-9]. Adsorption is the cheapest method, easy to do and proven effective in removing various contaminants such as dyes in the aquatic environment [1,6].

Carbon material is one of the most commonly used adsorbents for the process of adsorption because of its abundant source, good stability and wide application [10]. The carbon material used in this study was modified using magnetite to overcome the lack of effectiveness on carbon [1]. Carbon magnetite has magnetic properties and a larger molecular weight than ordinary carbon so that the filtration process runs more effectively [11].

In this study, the carbon used came from rubber fruit shells. Besides, it was modified using magnetite, the carbon modification was also carried out using a triethoxyphenylsilane (TEPS) coupling agent [12]. This is due to the nature of the organosilane which has two different active groups that can form chemical bonds between organic and inorganic materials. In the silanization process, TEPS forms silanol and siloxane groups which are expected to increase the carbon adsorption ability of CV dyes [12,13]. The magnetite carbon (MC) and silane carbon (SC) adsorbents obtained were tested for their ability to CV covering several parameters including; adsorbent dose, the influence of pH, the influence of contact time, and the concentration of adsorbate.

EXPERIMENTAL

Materials

Some materials used in this study were crystal violet (CV), $FeSO_4 \cdot 7H_2O$, $FeCl_3 \cdot 6H_2O$, $NaNO_3$, HCl, NaOH, ethanol, triethoxyphenylsilane (TEPS) and buffer solution from Merck (Darmstadt Germany). Rubber fruit shells obtained from East Lampung Regency.

Instrumentation

The adsorbent material was characterized by X-ray diffraction (XRD) (LabX XRD-6000 Shimadzu) to recognize the magnetite's phase after modification, scanning electron microscope-energy-dispersive X-ray (SEM-EDX) (Zeiss EVO MA 10) to discover the surface structure of adsorbents, and FTIR (IRPrestige-21) is used to determine the functional groups of adsorbents. The CV concentration in solution was determined using UV-Vis Spectrophotometer (Agilent Cary 100).

Procedure

Preparation of carbon from rubber fruit shell

The rubber fruit shells were cleaned and dried in the sun. Furthermore, it was burned in a drum made of the iron plate for approximately 6 hours to obtain the carbon of the rubber fruit shell. The carbon obtained from carbonization was then pulverized by grinding and then sieved through a 100-mesh sieve.

Carbon modification with magnetite

The MC was obtained by putting 6.5 g of carbon in 300 mL of distilled water and subsequently heating it to 70 °C. Then added iron salt consisting of 7.6 g $FeCl_3 \cdot 6H_2O$ and 3.9 g $FeSO_4 \cdot 7H_2O$ diffused in 300 mL of distilled water. The mixture was then stirred for 30 minutes while adding 100 mL of 5 M NaOH dropwise. The precipitate obtained was separated and neutralized to pH 6. Afterwards it was dried at 100 °C for 3 hours [14].

Carbon modification with TEPS

A total of 4 g of carbon was mixed with 200 mL of ethanol. Next, 0.4 mL of triethoxyphenylsilane (TEPS) was put into the mixture hereafter stirred using a magnetic stirrer for 7 hours at 70 °C in a water bath. The resulting carbon was then separated and cleanse by using ethanol subsequently dried at 60 °C for 1 hours [12].

Determination of zeta potential

A total of 0.1 g MC and SC was put into 20 mL 0.1 M $NaNO_3$, respectively. A pH range of 3 to 12 was used for the initial pH. The pH was adjusted by adding 0.1 M HCl and NaOH. Then, the pH was maintained by the addition of buffer solution. The mixture was stirred using a shaker for 24 hours. After that, the final pH was observed and measured using a pH meter [15].

Adsorption experiment

CV adsorption by MC and SC was carried out by batch method with using several parameters such as adsorbent dose (0.1 - 0.5 g), solution pH (3 - 12), contact time (15 - 120 minutes), and CV dye concentration (10 - 250 mg L^{-1}). For each experiment, a certain amount of MC and SC were added to 20 mL CV solution with an initial concentration at the appropriate pH value. 0.1 M NaOH and HCl solution were used to alter the initial pH solution. At a steady speed of 100 rpm, the mixture was agitated in an orbital shaker. CV residues were analyzed on λ_{max} 590 nm using Spectrophotometer UV Vis. The CV dye adsorption percentage and adsorption capacity were calculated by Eq. (1) and (2), respectively:

$$\text{Adsorption (\%)} = \frac{C_o - C_e}{C_o} \text{ x } 100 \qquad (1)$$

$$q = \frac{(C_o - C_e)v}{w} \qquad (2)$$

Where w (g) is the amount of adsorbent, v (L) is the volume of the solution, q (mg g^{-1}) is the amount of CV dye adsorbed per unit mass, C_o and C_e (mg L^{-1}) are the initial CV concentration and CV concentration after the adsorption, respectively.

RESULTS AND DISCUSSION

Adsorbent Characterization

The MC modification was carried out through a magnetite coating process using $FeCl_3 \cdot 6H_2O$ and $FeSO_4 \cdot 7H_2O$ which were mixed to form Fe_3O_4 which then coats the carbon surface. The SC modification was carried out through the silanization process using a silane coupling agent, namely TEPS. TEPS has two different active groups, namely the phenyl group which is can bind organic materials and ethoxy to bind inorganic materials [12]. The obtained MC and SC adsorbents were characterized by FTIR to identify the functional groups, XRD to identify magnetite crystals and SEM-EDX to recognize the carbon's surface pattern and analyze its constituent elements.

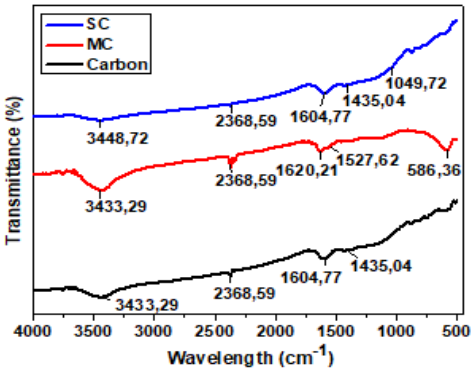

Fig 1. IR Spectrum of Carbon, MC and SC

Fig. 1 shows a hydroxyl group (OH) as seen by the peaks at wavenumber 3433.29 cm^{-1} and Fe-O is indicated by absorption at wavenumber 586.36 cm^{-1} [12]. Peak at 2931.80, 1620.21, and 1165 cm^{-1} are corresponding to C-H vibration, carbonyl group (C=O), and C-O band. These peaks indicate that Fe_3O_4 has coated the carbon [16]. In addition, the presence of Si-O-Si is indicated by the absorption at wavenumber 1049.72 cm^{-1} which indicates the carbon has been coated with TEPS [17].

The XRD pattern (Fig. 2) on the carbon shows a wide asymmetric peak at 2θ 20-45° which is characteristic of amorphous carbon. Fig. 2 on magnetite carbon shows sharp peaks compared to carbon at 2θ 35.46, 43.04, 57.22, and 62.58° [18]. The asymmetrical carbon peaks turn into sharp peaks in the XRD MC pattern, this indicates that the carbon has been coated with magnetite so that the peaks appear with sharp intensity.

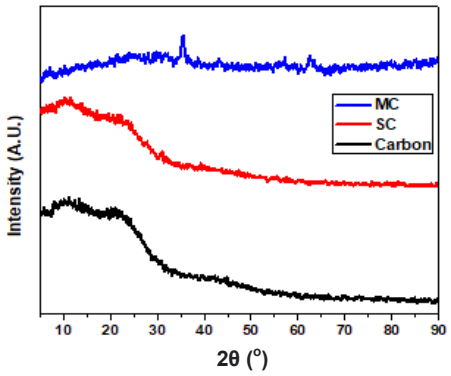

Fig 2. Diffractogram of Carbon, MC and SC

The SC diffraction pattern at 2θ 20-30° showed wide peaks indicating the presence of amorphous silica formed on carbon. Amorphous silica obtained by hydrolysis of TEPS [12].

The morphology of MC can be seen in Fig. 3(b). The MC surface looks rougher than the carbon surface. Magnetite grains have completely coated the carbon surface. This is supported by EDX data. The elemental compositions of C, O and Fe are 65.97, 30.95, and 3.08%, respectively. In addition, the pore diameter of MC is around 2.051-6.447 μm, smaller than the diameter of carbon which has a pore diameter of around 3.517-9.378 μm. This indicates that Fe_3O_4 has been perfectly attached to the carbon surface.

The surface morphology of SC in Fig. 3(c) shows the presence of small white particles which are silica from TEPS modification and stick to the carbon pores but do not completely cover the carbon pores. The results of the EDX analysis showed the elemental compositions of C, O and Si were 90.43, 9.45, and 0.13 %, respectively. From the EDX data, it can be seen that TEPS has coated the carbon.

Adsorption Study

Adsorbent dosage

The adsorbent dose can affect the adsorption ability. Fig. 4 shows the adsorption percentage depending on the adsorbent dose. Based on Fig. 4 the adsorption efficiency decreased while the adsorbent dose increased. This is due to the fact that adsorption will occur more quickly as the adsorbent's mass increase. Because of the superficial adsorption, the contact between the adsorbent and adsorbate happens quickly on the adsorbent's surface [19].

Influence of pH

Based on Fig. 5, the influence of pH on a CV is not significant, starting from pH 4-12 the efficiency tends to go up and down. pH 12 at MC gave the highest adsorption percentage, but the CV solution became saturated. Thus, the optimum pH obtained is pH 10 for both MC and SC.

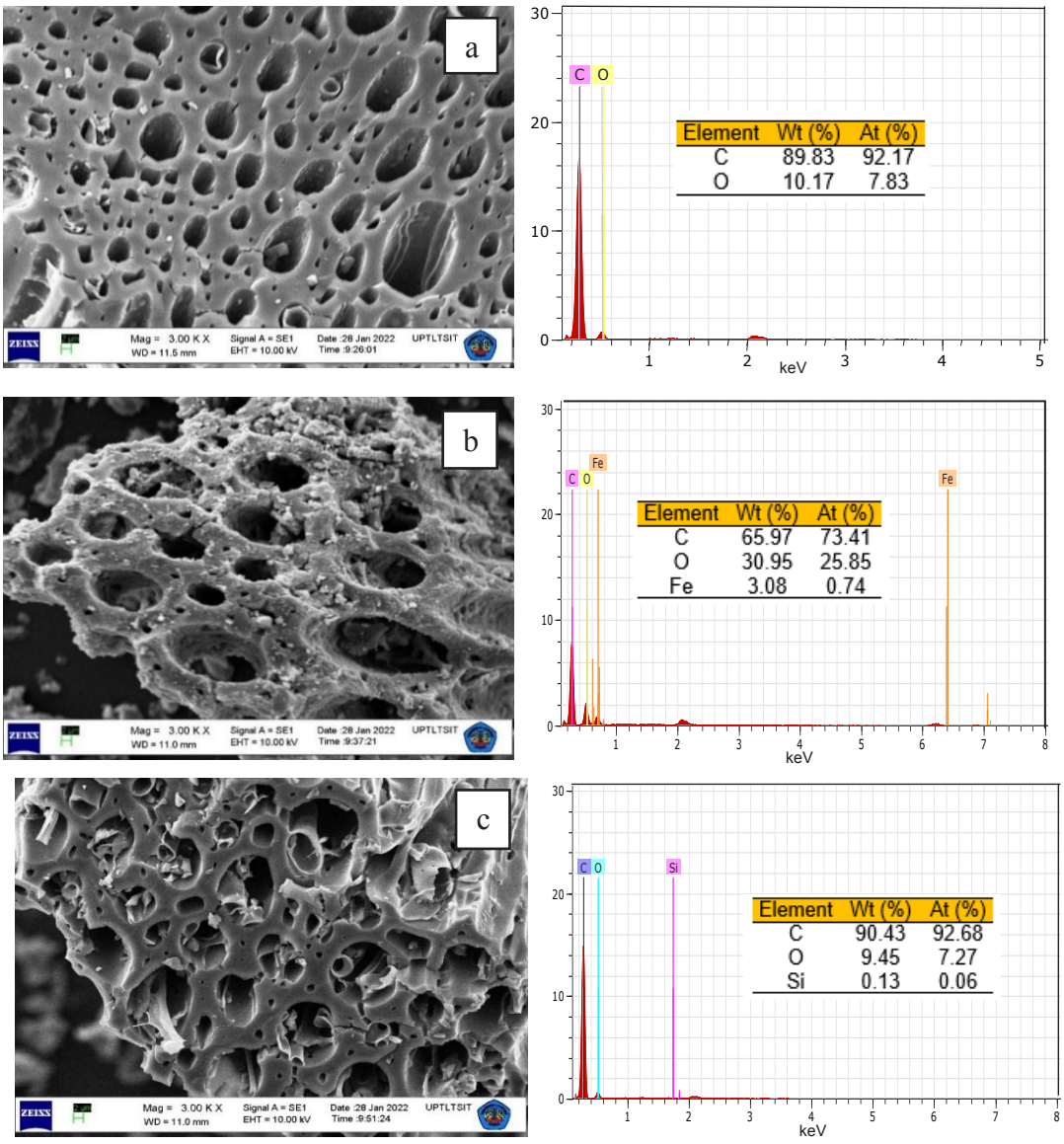

Fig 3. Micrograph of (a) Carbon, (b) MC and (c) SC

At pH 10 the adsorption process worked effectively because it was following the previously obtained ZPC pH, namely at pH 8 and the adsorbent had a negative surface charge so that it could interact with a CV which is a cationic dye. Due to competition between CV molecules and H^+ ions on the surface of the adsorbent at pH<7, the adsorption process is not ideal, and a repulsion reaction will take place between the adsorbate and adsorbent.

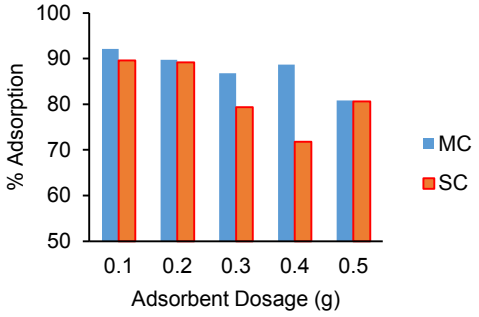

Fig 4. Influence of adsorbent dosage on adsorbed CV

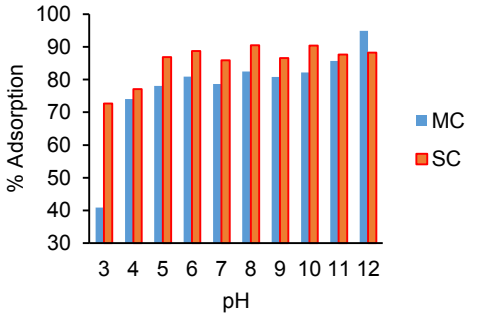

Fig 5. Influence of pH solution on adsorbed CV

The amount of H^+ ions on the adsorbent's surface will decrease in alkaline conditions (pH>7) so that the adsorbate is effectively adsorbed by the adsorbent. The more negative the surface charge on the adsorbent, the more electrostatic interactions that occur between the adsorbent and adsorbate will increase. At an increasingly alkaline pH (pH>10), there is an increase in the concentration of OH^- which will cause precipitation in the solution and the adsorption ability will be inhibited [20].

Influence of contact time and the kinetic studies

Based on Fig. 6, the contact time of 15 minutes gave the highest efficiency for both MC and SC adsorbents, which means the adsorption process is faster. This can occur because of the empty and available part of the surface (active site) from the adsorbent that can interact with CV dyes. The brief contact time suggests that the interaction between MC or SC and CV that takes place is a physical interaction [21]. The highest adsorption percentages obtained by MC and SC were 91.51 and 90.36 %, respectively, where the results obtained were greater than CV adsorption carried out using Raw *Parthenium hysterophorus* and Raw *Saccharum munja* which gave the respective adsorption percentages 84.2 and 86 % [22].

Utilizing the contact time data gathered for this study, the kinetics that happened throughout the adsorption process were computed. Pseudo-first order and pseudo-second order kinetics are determined using Eq. (3) and (4), respectively:

$$ln(q_e - q_t) = ln(q_e)k_1 t \quad (3)$$

$$\frac{t}{q_t} = \frac{1}{k_2 q_e^2}\frac{1}{q_e} \quad (4)$$

Where q_t and q_e (mg g^{-1}) represent the total adsorption capacity of CV at time t and equilibrium k_1 and k_2 represent the first-order and second-order rate constants of adsorption, respectively.

Table 1. Kinetic parameters for CV adsorption on MC and SC

Adsorbents	Pseudo-first order		Pseudo-second order	
	k_1 (min^{-1}) (10^{-3})	R^2	k_2 (g mg^{-1} min^{-1})	R^2
MC	3.4	0.301	3.403	0.991
SC	2.9	0.230	0.827	0.982

In Table 1, kinetic information, adsorption rate constants, and regression coefficients are shown. The results demonstrated that CV adsorption by MC and SC had a pseudo-second-order kinetic model because the correlation coefficient (R^2) value was closer to 1 [20].

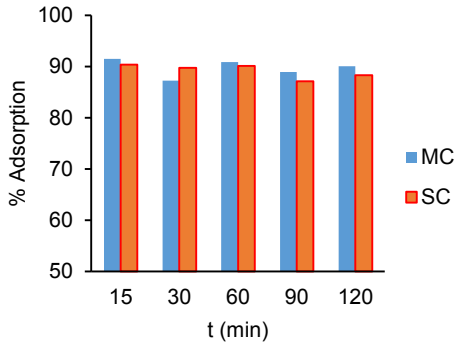

Fig 6. Influence of contact time on adsorbed CV

Influence of Concentration and Adsorption Isotherm

The increase in adsorbate concentration increased the adsorption capacity of CV from 2.14 to 47.01 mg g^{-1} for MC adsorbent and from 2.27 to 54.63 mg g^{-1} for SC adsorbent. This is due to the adsorbent's high affinity, which enables the active site to better adsorb the adsorbate [1].

Judging from the adsorption capacity data, SC adsorbent has a larger adsorption capacity than MC. This can be due to the narrowing of the pores of the magnetite coating so that the surface's active site of the carbon becomes slightly reduced.

The result data of the influence of concentration were then analyzed using the Langmuir Eq. (5) and Freundlich adsorption isotherm pattern Eq. (6).

$$\frac{1}{q_e} = \frac{1}{q_m K_l C_e} + \frac{1}{q_m} \quad (5)$$

$$log\ q_e = log\ K_F + \frac{1}{n} log\ C_e \quad (6)$$

Where, C_e (mg L^{-1}) is the equilibrium concentration of CV in solution, q_e (mg g^{-1}) is the equilibrium adsorption capacity, q_m is the adsorption capacity of a single layer, K_L (L mg^{-1}) is the equilibrium constant incorporating the binding site affinity, K_F ((mg g^{-1})(L mg^{-1})$^{1/n}$) is the adsorption capacity factor and n is the adsorption intensity factor which has a value between 1 to 10 [20].

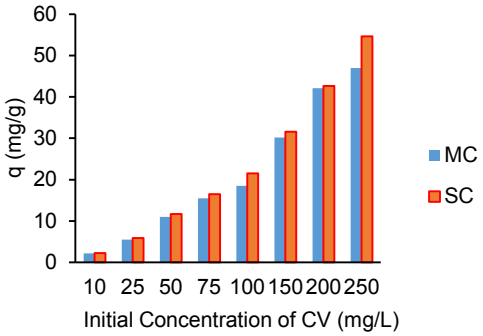

Fig 7. Influence of initial concentration of adsorbate on the amount of CV dye adsorbed.

The Langmuir isotherm model assumes that there are a certain number of active sites on the adsorbent's surface that are proportional to the surface area [23,24]. When the active site of a surface has been filled with adsorbate, there will be no additional adsorption at that site [25]. Thus, the maximum saturation point of adsorption on the adsorbent surface will be reached [26]. As a result, the occurrence of the adsorption process is known as monolayer adsorption. Freundlich's isotherm model is an empirical formula that used to illustrate a heterogeneous system which is conveyed through Eq. (6) [27].

Table 2. Isotherm parameters for adsorption of CV onto MC and SC

Adsorbents	Langmuir			Freundlich		
	q_m (mg g^{-1})	K_L (L mg^{-1})	R^2	n	K_F (mg g^{-1}) (L $mg^{-1})^{1/n}$)	R^2
MC	71.429	0.025	0.428	1.093	1.362	0.943
SC	69.93	0.049	0.549	1.026	1.761	0.932

According to Table 2, the adsorption of CV by MC and SC tends to follow the Freundlich isotherm pattern. This is because the R^2 value for the adsorbent's Freundlich isotherm pattern is closer to 1 than the Langmuir isotherm pattern. This shows that the adsorption occurs on a CV is because not all active surfaces of the adsorbent have the potential to adsorb therefore the adsorption that occurs is heterogeneous. The heterogeneous adsorption process is distinguished by the formation of a multilayer on the adsorbent's surface [28].

CONCLUSION

In this research, modified carbon with magnetite (MC) and TEPS (SC) has been made which is used as an effective and inexpensive adsorbent for CV dye solution. The adsorption capacity of MC and SC is influenced by several parameters including adsorbent dose (0.1 g), pH (10), contact time (15 minutes), and initial CV concentration (250 mg L^{-1}) with excellent results. The adsorption capacity obtained at MC was 47.01 and at SC was 54.63 mg g^{-1}. The rate of adsorption kinetics tends to follow pseudo-second order kinetics. The Freundlich isotherm is suitable for this adsorption compared to the Langmuir model, indicating that the adsorption that occurs is multilayer with physical interactions. MC and SC modified carbon can be used as an effective adsorbent to remove CV dye solution.

ACKNOWLEDGEMENT

The authors are grateful to the Research and Community Service Institute of the University of Lampung (LPPM Universitas Lampung) has funded this project with contract number: 819/UN26.21/PN/2022 and the Ministry of Education, Culture, Research, and Technology, Republic of Indonesia (Kemendikbud-Ristek) for the support of this research.

CONFLICT OF INTEREST

The authors declares that there is no conflict of interest.

AUTHOR CONTRIBUTIONS

Nadya S. Fajriyah conducted the experiment. Nadya S. Fajriyah wrote the manuscript with support and supervised by Buhani and Suharso. All authors approved the final version of the manuscript.

REFERENCES

[1]. Buhani, Suharso, Luziana, F., Rilyanti, M., and Sumadi, 2019, Production of Adsorbent from Activated Carbon of Palm Oil Shells Coated by Fe_3O_4 Particle to Remove Crystal Violet in Water, *Desalination and Water Treatment*, 171, 281-293.

[2]. Foroutan, R., Peighambardoust, S. J., Aghdasinia, H., Mohammadi, R., and Ramavandi, B., 2020, Modification of Bio-Hydroxyapatite Generated from Waste Poultry Bone with Mgo for Purifying Methyl Violet-Laden Liquids, *Environmental Science and Pollution Research International*, 35, 44218-44229.

[3]. Peighambardoust, S. J., Aghamohammadi-Bavil, O., Foroutan, R., and Arsalani, N., 2020, Removal of Malachite Green using Carboxymethyl Cellulose-g-polyacrylamide/montmorillonite Nanocomposite Hydrogel, Int. J. Biol. Macromol, 159. 1122–1131.

[4]. Pashaei-Fakhri. S.. Peighambardoust. S.J.. Foroutan. R.. Arsalani. N.. and Ramavandi. B.. 2021. Crystal Violet Dye Sorption Over Acrylamide/Graphene Oxide Bonded Sodium Alginate Nanocomposite Hydrogel. *Chemosphere*. 270. 129419.

[5]. Mittal. H.. Alili A. A.. Morajkar. P.P.. and Alhassan. S.M.. 2021. Graphene Oxide Crosslinked Hydrogel Nanocomposites of Xanthan Gum for The Adsorption of Crystal Violet Dye, *Journal of Molecule Liquids*, 323, 115034.

[6]. Foroutan, R., Peighambardoust, S. J., Peighambardoust, S. H., Pateiro, M., and Lorenzo, J. M., 2021, Adsorption of Crystal Violet Dye Using Activated Carbon of Lemon Wood and Activated Carbon/Fe_3O_4 Magnetic Nanocomposite from Aqueous Solutions: A Kinetic, Equilibrium and Thermodynamic Study, *Molecules*, 26(8), 2241.

[7]. Abdi, M., Balagabri, M., Karimi, H., Hossini, H., and Rastegar, S. O., 2020, Degradation of Crystal Violet (CV) from Aqueous Solutions Using Ozone, Peroxone, Electroperoxone, and Electrolysis Processes: A Comparison Study, 2020, *Applied Water Science*, 10(168), 1-10.

[8]. Thuong, N. T., Nhi, N. T. T., Nhung, V. T. C., Bich, H. N., Quynh, P., Bach, L. G., and Nguyen, T. D., 2019, A fixed-bed column study for temoval of organic dyes from aqueous solution by pre-treated durian peel waste, *Indonesian Journal of Chemistry*, 19(2), 486-494.

[9]. Thattil, P. P and Rose, A. L., 2020, Enhanced Removal of Crystal Violet Dye using Zinc Oxide Nanorods and Air Oxidation under Sunlight Radiation, *Rasayan Journal of Chemistry*, 13(2), 1166-1173.

[10]. Li, H., Qi, H., Yin, M., Chen, Y., Deng, Q., dan Wang, S., 2020, Carbon tubes from biomass with prominent adsorption performance for paraquat, *Chemosphere*, 262, 1-27.

[11]. Zulaicha, A. S., Buhani, and Suharso, 2021, Modification of Activated Carbon from *Elaeis Guineensis* Jacq Shell with Magnetite (Fe_3O_4) Particles and Study Adsorption-Desorption on Ni(II) Ions in Solution, *Journal of Physics: Conference Series*, 1751, 1-11.
[12]. Wong, K. T., Yoon, Y., Snyder, S. A., and Jang, M., 2016, Phenyl-functionalized Magnetic Palm-based Powdered Activated Carbon for the Effective Removal of Selected Pharmaceutical and Endocrine-disruptive Compounds, *Chemosphere*, 152, 71-80.
[13]. Kausar, R. A., Buhani, and Suharso, 2020, Methylene Blue Adsorption Isotherm on *Spirulina* sp. Microalgae Biomass Coated by Silica-Magnetite, *IOP Conf Series: Materials Science and Engineering*, 857, 1-7.
[14]. Buhani, Suharso, Rilyanti, M., Sari, M., and Sumadi, 2021, Removal of Cd (II) Ions in Solution by Activated Carbon from Palm Oil Shells Modified with Magnetite, *Desalination and Water Treatment*, 218, 352-362.
[15]. Buhani, Suharso, Miftahza, N., Permatasari, D., and Sumadi, 2021, Improved Adsorption Capacity of *Nannochloropsis* sp. through Modification with Cetyltrimethylammonium Bromide on the Removal of Methyl Orange in Solution, *Adsorption Science and Technology*, 2021, 1-14.
[16]. Dalali, N., Habibizadeh, M., Rostamizadeh, K., and Nakisa, S., 2014, Synthesis of Magnetite Multi-Walled Carbon Nanotubes Composite and Its Application for Removal of Basic Dyes from Aqueous Solutions, *Asia-Pacific Journal of Chemical Engineering*, 9, 552-561.
[17]. Permatasari, D., Buhani, Rilyanti, M., and Suharso, 2021, Adsorption Kinetic and Isotherm of Solution Pair of Methylene Blue and Crystal Violet by Algae-Silica-Magnetite Hybrid Adsorbent on *Porphyridium* sp. Algae, *Journal of Physics: Conferense Series*, 1751, 1-7.
[18]. Harimu, L., Wahyuni, S., Nasrudin, N., Baari, M. J., and Permana, D., 2022, Fabrication of Chitosan/Fe_3O_4 Nanocomposite as Adsorbent for Reduction Methylene Blue Contents, *Indonesian Journal of Chemistry*, 22(3), 878-886.
[19]. R. H. Khuluk, A. Rahmat, Buhani, and Suharso, 2019, Removal of Methylene Blue by Adsorption onto Activated Carbon From Coconut Shell (*Cocous Nucifera* L.), *Indonesian Journal of Science and Technology*, 4(2), 229-240.
[20]. Buhani, Halimah, S. N., Suharso, and Sumadi, 2022, Utilization of Activated Carbon from Candlenut Shells (*Aleurites Moluccana*) as Methylene Blue Adsorbent, *Rasayan Journal of Chemistry*, 15(1), 124-131.
[21]. Kakavandi, B., Javari, A. J., Kalantary, R. R., Nasseri, S., Esrafili, A., Gholizadeh, A., and Azari, A., 2016, Simultaneous Adsorption of Lead and Aniline onto Magnetically Recoverable Carbon: Optimization, Modeling, and Mechanism, *Journal of Chemical Technology and Biotechnology*, 91(12), 3000-3010.
[22]. Singh, A., Kumar, S., Panghal, V., Arya S. S., and Kumar, S., 2019, Utilization of Unwanted Terrestrial Weeds for Removal of Dyes, *Rasayan Journal of Chemistry*, 12(4), 1956-1963.
[23]. Toan, N. C., Binh, Q. A., Tungtakanpoung, D., and Kajitvichyanukul, P., 2020, Kinetic, Istherm and Mechanism in Paraquat Removal by Adsorption Process Using Biochar, *Lowland Technology International*, 22(2), 200-211.
[24]. Iryani, A., Nur, H., Santoso, M., and Hartanto, D., 2020, Adsorption Study of Rhodamine B and Methylene Blue Dyes with ZSM-5 Directly Synthesized from Bangka Kaolin without Organic Template, *Indonesian Journal of Chemistry*, 20(1), 130-140.

[25]. Damiyine, B., Guenbour, A., and Boussen, R., 2020, Comparative Study on Adsorption of Cationique Dye onto Expanded Perlite and Natural Clay, *Rasayan Journal of Chemistry*, 13(1), 448-463.
[26]. P. Pranoto, C. Purnawan and T. Utami, 2018, Application of bekonang clay and andisol soil composites as copper (II) metal ion adsorbent in metal crafts wastewater, *Rasayan Journal of Chemistry*, 11(1), 23-31.
[27]. Shao, Y., Zhou, L., Bao, C., Ma, J., Liu, M., and Wang, F., 2016, Magnetic Responsive Metal–Organic Frameworks Nanosphere with Core–Shell Structure for Highly Efficient Removal of Methylene Blue, *Chemical Engineering Journal*, 283, 1127–1136.
[28]. Buhani, Narsito, Nuryono, E. S. Kunarti, and Suharso, 2015, Adsorption Competition of Cu (II) Ion in Ionic Pair and Multi-metal Solution by Ionic Imprinted Amino-Silica Hybrid Absorbent, *Desalination and Water Treatment*, 55(5),1240-1252.

STOMATA CHARACTER OF COMMERCIAL SUGARCANE ON 21 MUTANTS OF GMP3 VARIETY AT PT GUNUNG MADU PLANTATIONS, INDONESIA

Putri Kendari [1], Mahfut [2] *, Endang Nurcahyani [2], Bambang Irawan [2], Sri Wahyunigsih [2], Alhuda Niftakul Ahyar [3], Endah Susiyanti [3]

[1] Post Graduate, Faculty of Mathematics and Natural Sciences, University of Lampung. Jl. Prof., Dr. Ir. Soemanri Brodjonegoro, No. 1. Gedong Meneng, Kec. Rajabasa, Bandar Lampung, Lampung, 35145 Tel// Fax : +62-812-6061-5502, *email : putrikendari2810@gmail.com

[2] Department of Biology, Faculty of Mathematics and Natural Sciences, University of Lampung. Jl. Prof., Dr. Ir. Soemanri Brodjonegoro, No. 1. Gedong Meneng, Kec. Rajabasa, Bandar Lampung, Lampung, 35145. Tel// Fax : +62-812-6061-5502, *email : mahfut.mipa@fmipa.unila.ac.id .

[3] Division of Agronomy, Research and Development, PT. Gunung Madu Plantations. KM 90 Terbanggi Besar, Gunung Batin Udik, Terusan Nunyai, Lampung, 34167

Abstract

One breeding effort can be made using the induction of colchicine mutations. PT Gunung Madu Plantations has induced mutations of the GMP3 variety, but studies on the effect of colchicine on stomatal characters are still limited. This study aimed to analyze the stomata character of 21 sugarcane mutants of the GMP3 variety. This research method involves the preparation of microscopic incisions. The observed characters were stomatal opening width, stomata length, stomata width, number of stomata, stomatal density, and stomata index. Analysis of the mean of each stomatal character using cluster and Principal Component Analysis (PCA) through MVSP software. This study showed that the stomata of all GMP3 mutants were Graminae. The results of stomata length and width, the average size of the GMP3 variety mutant was greater than that of the GMP3 variety. The diversity of stomata characters in 21 varieties of GMP3 mutants showed greater stomata opening width (2.26 µm), longer stomata length (21.31 µm), large stomata width (12.82 µm), high stomata density (499 µm), high number of stomata (97 µm), and high stomata index (0.45%). Meanwhile, the phenetic analysis of 21 mutants showed a similarity index between 0.20-1.00 which indicated that the relationship between mutants and controls was far. This study showed that the character of the width of the aperture and the length of the stomata are the two stomata characters that determine the grouping of mutants of the GMP3 variety.

Keywords : Colchicine, GMP3, Stomata, Sugarcane (*Saccharum officinarum* L.), UPGMA.

INTRODUCTION

Sugarcane (*Saccharum officinarum* L.) is a monocotyledonous plant with has the highest sucrose and the lowest fiber content (Lubis et al., 2015). Therefore, it is widely used as the main raw material in the sugar industry. Sugar consumption in Indonesia continues to increase following the increase in population. However, the increase in sugar consumption has not been matched by an increase in sugar production. Based on sugarcane production data from 2017-2021, it is currently around 2.1 -2.3 tons/ha with sugar recovery (*sugar recovery*) of around 7-8% (Central Bureau of Statistics, 2021).

PT Gunung Madu Plantations (PT GMP) is one of the sugar industries attempting to increase production by assembling high-yielding sugar cane varieties through its research and development department. The commercial varieties at PT. GMP consists of GMP1, GMP2, GMP3, GMP4, GMP5, GMP6, and GMP7. GMP3 is the most commercial and dominant variety, comprising approximately 30% of the total land area. However, according to the field data, its variety has a low quality, low sugar yield, an agronomic appearance on small stems, and narrow leaf width (Central Bureau of Statistics, 2021).

Plant breeding is one of the ways to improve the quality of a variety. The primary principle of a sugarcane breeding program is to obtain transgressive segregation that exhibits maximum heterosis from across. Furthermore, adequate genetic diversity is essential to producing superior sugarcane varieties (Carsono et al., 2022). Therefore, plant breeding can be conducted through mutation induction using the chemical mutagen colchicine (Kamwean et al., 2017). Colchicine can be used to induce mutations to obtain polyploid plants. Colchicine in breeding programs can improve the characteristics of plants with better traits (Sivakumar, 2017). Cansian et al. (2016), showed that corn induced by colchicine experienced an increase in stomata density, and increase in stomata length and width. Polyploidy plants are defined anatomically by their bigger cell sizes and the high number of chromosomes. Additionally, the anatomical types of each species of sugarcane exhibit distinct traits. The cells are larger and more visible, especially that of the epidermis, with a nucleus, transport reeds, and the larger size of the stomata (Bagheri and Mansouri, 2014).

PT GMP induced mutations with the colchicine mutagen in sugarcane GMP3, but this effect of colchicine has not been tested further, and information on the anatomical characteristics of sugarcane remains limited. Due to these problems, this research on the anatomical characteristics of sugarcane that have been induced by colchicine needs to be tested further. This information on genetic diversity and the relationship between plant accessions will provide important input in determining appropriate management strategies and assisting plant improvement through plant breeding programs, especially in facilitating the selection of breeding materials (Restykania et al. 2019). So, the purpose of this study was to analyze the stomata character of 21 sugarcane mutants of the GMP variety.

MATERIALS AND METHODS

Plant Material

The plant materials used included 21 varieties of GMP3 mutant, colchicine at concentrations 0.1 % and 0.2%, aquadest, immersion oil, glycerin, and clear nail polish. This research was conducted in the botanical laboratory, PT GMP, Gunung Batin Baru, Lampung.

Procedure

Leaf stomata characters were observed from the paradermal part. Making microscopic incisions on the paradermal part of the leaf according to Munir et al. (2011), Arzani et al. (2013), Chikmawati (2013), and Arofatun et al. (2020). The first step is to take the leaf and clean it using 70% alcohol, then the bottom of the leaf is placed on a slide.

Then covered with transparent nail polish, then dripped with glycerin and covered with a cover glass. Light microscopic observations (Model: Olympus, magnification 10 x for the ocular and 40 x for the objective) were used to observe the specimens (Pitoyo et al. 2018). The stomata characters observed were stomata type, stomata opening width, guard cell length and width, number of stomata, stomata density, and stomata index (Arofatun et al., 2020).

Data Analysis

Stomata characters were analyzed quantitatively and qualitatively. Quantitative data are presented in the shape of stomata tables by the number, and qualitative data presented in descriptive forms supported by quantitative data and relative analysis, by scoring from quantitative data (6 character stomata) into binary data, then continued with grouping for relationships between species. The grouping is further illustrated in dendogram by using a Multivariate Statistical Package (MVSP) ersion 3.2 and a genetic distance for cluster analysis using nweighted Pair-Group With Arithmetic Average (UPGMA) method and using the Jaccard coefficient. Quantitative determination that affects the grouping used Principal Component Analysis (PCA) using software Multivariate Statistical Package (MVSP) version 3.2.

The formula for calculating stomata density is as follows: (Suhaimi, 2017).

$$Stomata\ density\ (\mu m) = \frac{Count\ of\ stomata}{Broad\ field\ of\ view}$$

Meanwhile, the formula for calculating the stomata index is as follows: (Tambaru, 2015).

$$Stomata\ index\ (\mu m) = \frac{Count\ of\ stomata}{Count\ of\ epidemal\ cells + Count\ of\ stomata} \times 100\%$$

RESULTS AND DISCUSSION

Stomata Shape Character Analysis

Based on the anatomical observations of **Figure 1**. shows that the GMP3 variety has Graminae stomata type, which shows the length of the axis of the neighboring cell is parallel to the stomata axis. The type of stomata of GMP3 mutants obtained in each 0.1% and 0.2% colchicine treatment did not show changes in the shape of the stomata. This indicates that colchicine has no effect on the stomata's shape. According to Moghbei et al. (2015), the type of olive leaf stomata obtained on each treatment, is submersion and drops at various concentrations (0.25%: 0.5%: 0.75%: 1%) did not change the shape of the stomata. This is because colchicine doesn't affect all parts of the cell, just a few cells or random cell mutations. According to the research of Syukur et al. (2011), colchicine does not affect all cells or cause random cell mutations. Cells that are actively dividing are sensitive to colchicine, whereas differentiated cells are less sensitive to this mutagen. According to Moghbei et al. (2015), the sensitivity of each plant species to colchicine application will be different even from the existing plant parts.

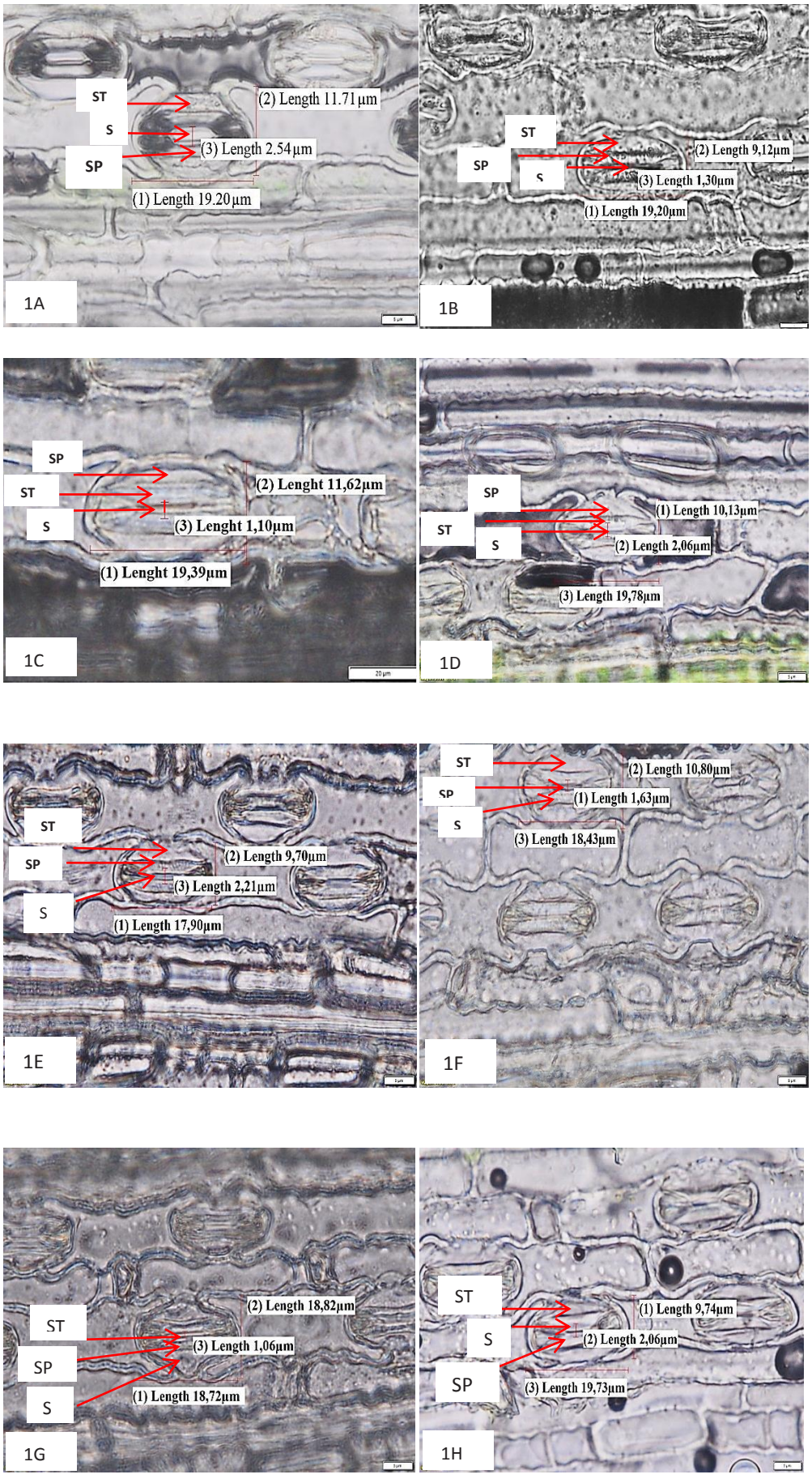
ST
S
SP
(2) Length 11.71 µm
(3) Length 2.54 µm
(1) Length 19.20 µm
1A
ST
SP
S
(2) Length 9,12µm
(3) Length 1,30µm
(1) Length 19,20µm
1B
SP
ST
S
(2) Lenght 11,62µm
(3) Lenght 1,10µm
(1) Lenght 19,39µm
1C
SP
ST
S
(1) Length 10,13µm
(2) Length 2,06µm
(3) Length 19,78µm
1D
ST
SP
S
(2) Length 9,70µm
(3) Length 2,21µm
(1) Length 17,90µm
1E
ST
SP
S
(2) Length 10,80µm
(1) Length 1,63µm
(3) Length 18,43µm
1F
ST
SP
S
(2) Length 18,82µm
(3) Length 1,06µm
(1) Length 18,72µm
1G
ST
S
SP
(1) Length 9,74µm
(2) Length 2,06µm
(3) Length 19,73µm
1H

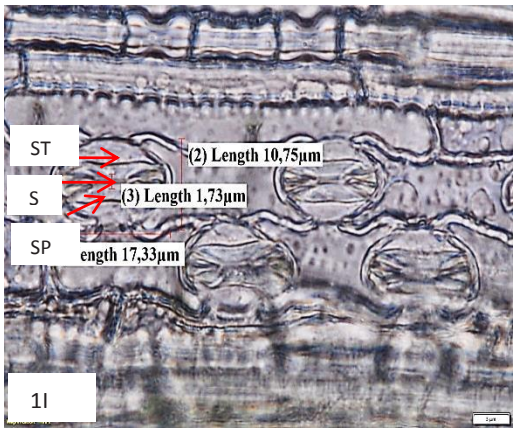
ST
S
SP
(2) Length 10,75µm
(3) Length 1,73µm
ength 17,33µm
1I

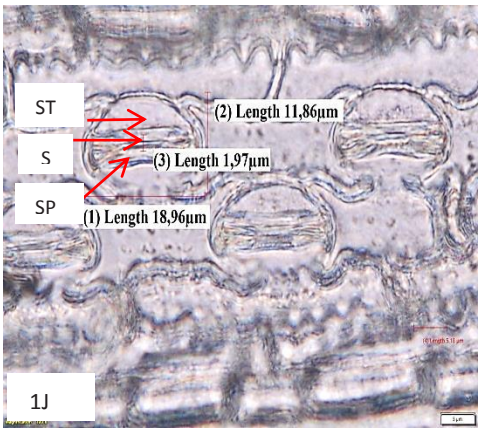
ST
S
SP
(2) Length 11,86µm
(3) Length 1,97µm
(1) Length 18,96µm
1J

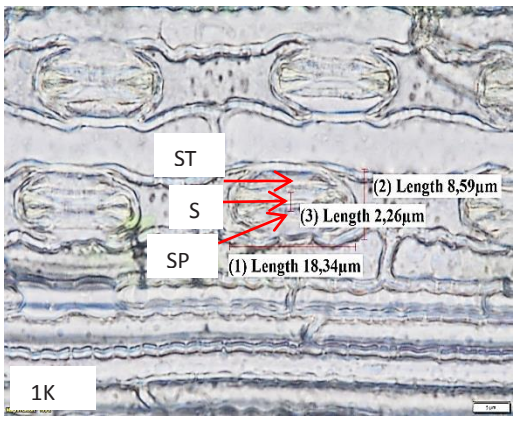
ST
S
SP
(2) Length 8,59µm
(3) Length 2,26µm
(1) Length 18,34µm
1K

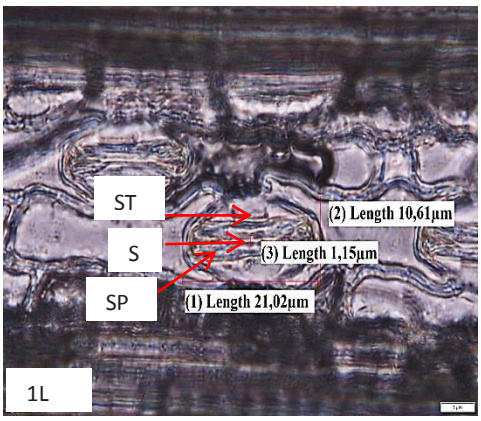
ST
S
SP
(2) Length 10,61µm
(3) Length 1,15µm
(1) Length 21,02µm
1L

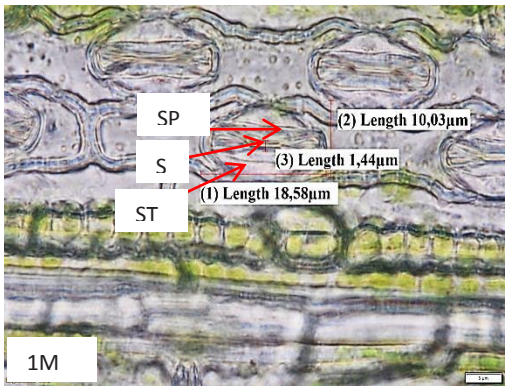
SP
S
ST
(2) Length 10,03µm
(3) Length 1,44µm
(1) Length 18,58µm
1M

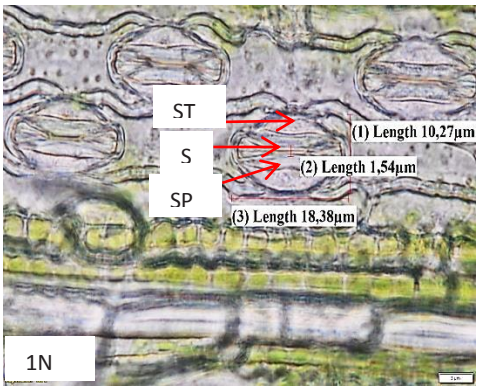
ST
S
SP
(1) Length 10,27µm
(2) Length 1,54µm
(3) Length 18,38µm
1N

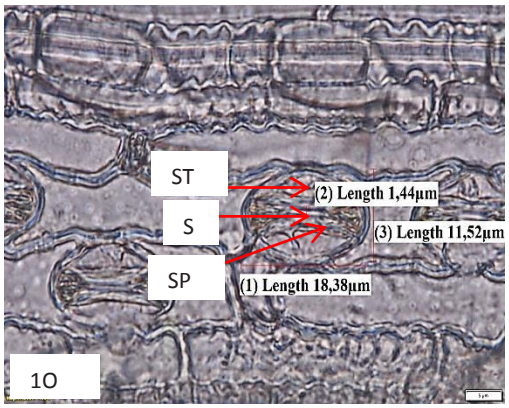
ST
S
SP
(2) Length 1,44µm
(3) Length 11,52µm
(1) Length 18,38µm
1O

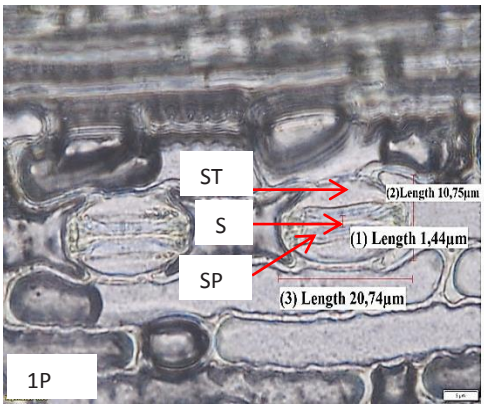
ST
S
SP
(2)Length 10,75µm
(1) Length 1,44µm
(3) Length 20,74µm
1P

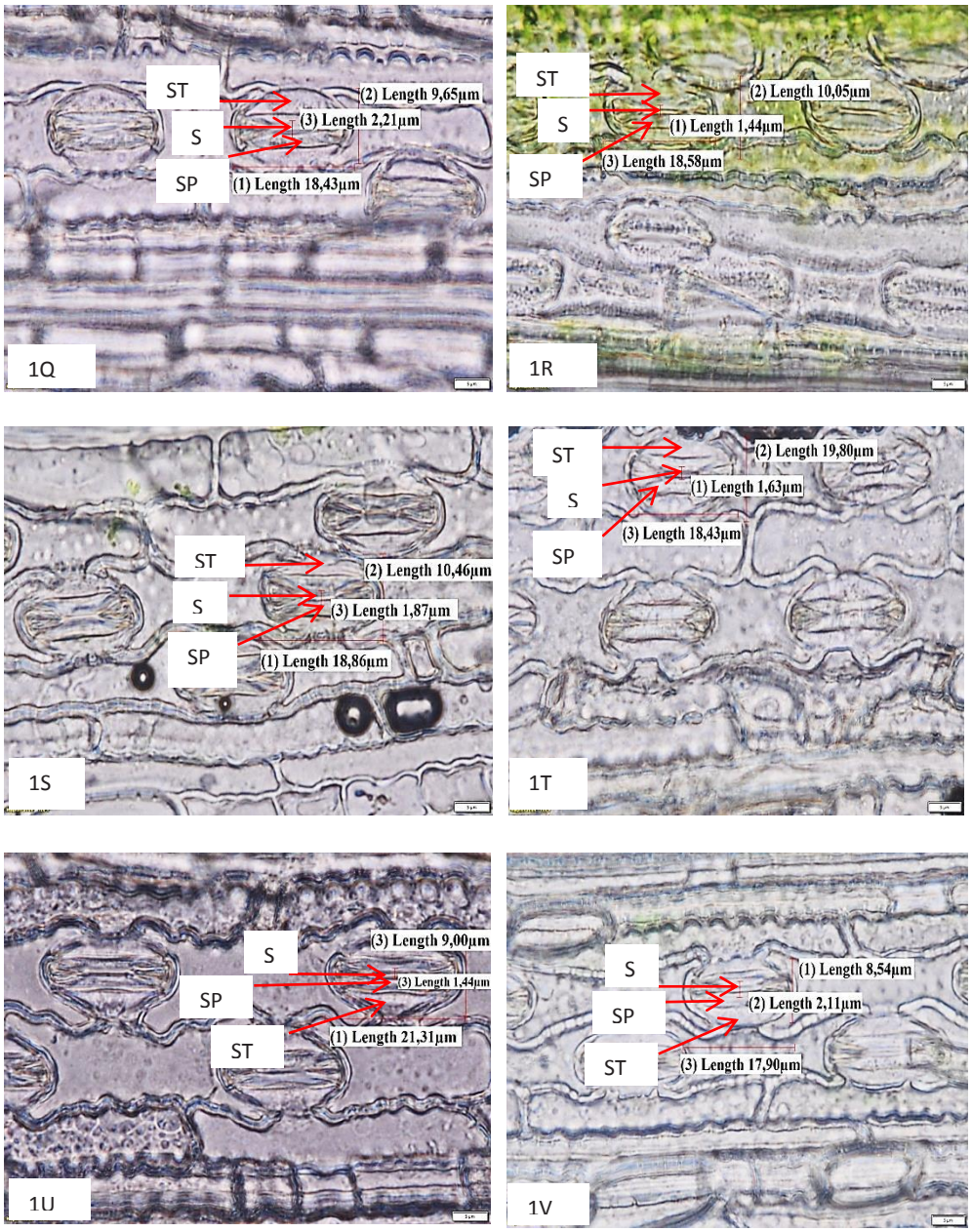

Figure 1. Stomata shape in GMP3 varieties and GMP3 . mutants
Description : 1: length of stomata, 2: width of stomata, 3: width of stomata opening; ST: neighboring cell, SP: guard cell, S: Stoma, M: Mutant; 1A:GMP3, 1B-1V: M1-M24.

Table 1. The average value of stomata characters in the GMP3. variety and 21 GMP3. mutant varieties based on stomata size.

No.	Varieties	Stomata Aperture Width (µm)	Stomata Length (µm)	Stomata Width (µm)	Number of Stomata	Stomata Density (µm)	Stomata Index (%)
6.	GMP3	2.54	19,20	11,71	77	392	0,32
1.	M / C 0,1/ 2H/01	1,30	18,72	9,12	95	484	0,41
2.	M / C 0,1/3H/15	1,10	19,39	11,62	87	443	0,39
3.	M / C 0,1/3H/16	2,06	19,78	10,13	74	377	0,30
4.	M / C 0,1/ 3H/02	2,21	17,90	9.07	97	494	0.38
5.	M/C 0.1/3H/10	1.63	18,43	10,80	77	392	0.32
7.	M / C 0,1/ 3H/04	1.06	18,72	12,82	79	402	0.34
8.	M/C 0,1/3H/07	2.06	19,73	9.74	89	453	0.41
9.	M/C 0,1/3H/06	1.73	17,33	10.75	59	300	0.30
10.	M / C 0,1/ 3H/03	1.97	18,96	11.86	72	366	0.34
11.	M/C 0.1/3H/14	2.26	18,34	8.59	91	463	0.38
12.	M / C 0,1/ 3H/02	1.15	21.02	10,61	93	473	0.40
13.	M / C 0,1/ 3H/08	1,44	18,58	10,03	84	428	0,41
15.	M / C 0,1/3H/05	1,54	18,38	10,27	88	448	0,42
16.	M / C 0,1/ 3H/01	1,44	18,38	11,52	84	428	0,39
17.	M / C 0,1/1H/01	1,44	20,74	10,75	82	417	0,39
18.	M / C 0,1/ 2H/01	2,21	18,43	9,65	97	494	0,45
19.	M / C 0,2/1H/04	1,44	18,58	10,05	95	484	0,41
21.	M / C 0,1/3H/09	1,87	18,86	10,46	98	499	0,42
22.	M / C 0,2/3H/10	1,63	18,43	10,80	80	407	0,44
23.	M/C 0.1/3H/12	1.44	21.31	9.00	73	371	0.30
24.	M/C 0.1/3H/11	2.11	17.9	8.54	89	453	0.43

Description: M; Mutant, C: Colchicine, 0.1-0.2; Colchicine concentration, 1H: 1 day of immersion, 2H: 2 days immersion, 3H: 3 days of immersion

Based on **Table 1**, the character of stomata's width has been smaller size in several varieties of GMP3 mutants (1.06-2.06µm) than in the control (2.54µm). Meanwhile, stomata's size of the GMP3 mutant variety increased in length and stomata width compared to the GMP3 variety. This suggests that colchicine has an influence on the character of length and width stomata. However, colchicine induction at a concentration of 0.1-0.2% has not been able to produce superior sugarcane varieties as polyploid plants. In accordance with the results of Miguel and Leonhardt's research (2011), plants of the Orchidaceae family with larger stomata than 1.25 times the length of a control plant are thought to be polyploid plants. The enlargement of stomata size occurs due to the doubling of chromosomes, which causes the enlargement of plant cells (Chen et al., 2011). According to Miguel and Leonhardt (2011), plants with stomata length and width greater than the control were thought to be polyploid plants. Polyploidy plants with stomatal character can be characterized by the size of their cells getting bigger and clearly visible in the epidermal cells, cell nucleus, and stomata (Suryo, 2009).

Based on the results of **Table 1** shows that some GMP3 mutants have more stomata than GMP3 varieties. while stomata density in some mutants also has higher stomata density. than the GMP3 variety. Based on this. it can be said that colchicine can induce polyploidy formation in GMP3 varieties. Gantait et al (2011) explained that the stomata density of Gerberea jamesonii Bolus cv. higher than that of diploid plants because the stomata and epidermal cells of polyploid plants are larger. The value of olive leaf stomata density obtained in the colchicine treatment has increased stomata density (Rohmah et al., 2017). Stomata density in plants is closely related to plant resistance to drought stress, while stomata size and stomata density are closely related to plant resistance to water stress (Yanny et al., 2022).

Table 1 shows that some mutants had a higher stomata index than controls. This is because colchicine with a concentration of 0.1-0.2% causes the stomatal index to increase, and in accordance with the results of research by Mogbei et al. (2015) which showed that the stomata index in olive leaves treated with colchicine 0.2-05% increased the size of the stomata index from 0.21-0.24%. An increase in stomata size indicates a decrease in the frequency of stomata in plant mutations. The number of stomata affects the density of stomata. If the number of stomata increases, so the stomata density is high.

Colchicine induction in GMP3 mutant varieties showed larger stomata size. increased number of stomata. and high stomata index. Cansian et al (2016) stated that colchicine-induced maize plants experienced an increase in stomatal density. length. and width. This indicates that colchicine provides good quality changes in the GMP3 variety. This is because plants with larger stomata can increase the rate of photosynthesis where the effect of this rate of photosynthesis is able to increase the growth and productivity of sugarcane plants (Prabowo et al., 2022).

Table 2. Similarity Index on GMP3 varieties and 21 sugarcane mutants of GMP3 . varieties

	GMP3	M1	M2	M3	M4	M5	M7	M8	M9	M10	M11	M12	M13	M15	M16	M17	M18	M19	M21	M22	M23	M24
GMP3	1																					
M1	0.16	1																				
M2	0.33	0.40	1																			
M3	0.75	0	0.40	1																		
M4	0.16	0.50	0.40	0.20	1																	
M5	0.25	0	0.25	0.33	0	1																
M7	0.20	0.25	0.50	0.25	0.25	0.50	1															
M8	0.50	0.60	0.50	0.33	0.60	0	0.16	1														
M9	0.25	0	0.25	0.33	0	1	0.50	0	1													
M10	0.75	0	0.40	1	0.20	0.33	0.25	0.33	0.33	1												
M11	0.16	0.50	0.40	0.20	1	0	0.25	0.60	0	0.20	1											
M12	0.33	0.75	0.60	0.16	0.40	0.25	0.50	0.50	0.25	0.16	0.40	1										
M13	0.33	0.75	0.60	0.16	0.40	0.25	0.50	0.50	0.25	0.16	0.40	1	1									
M15	0.33	0.75	0.60	0.16	0.40	0.25	0.50	0.50	0.25	0.16	0.40	1	1	1								
M16	0.16	0.50	0.75	0.20	0.50	0.33	0.66	0.33	0.33	0.20	0.50	0.75	0.75	0.75	1							
M17	0.33	0.40	1	0.40	0.40	0.25	0.50	0.50	0.25	0.40	0.40	0.60	0.60	0.60	0.75	1						
M18	0.33	0.75	0.33	0.16	0.75	0	0.20	0.80	0	0.16	0.75	0.60	0.60	0.60	0.40	0.33	1					
M19	0.33	0.75	0.60	0.16	0.40	0.25	0.50	0.50	0.25	0.16	0.40	1	1	1	0.75	0.60	0.60	1				
M21	0.33	0.75	0.60	0.16	0.40	0.25	0.50	0.50	0.25	0.16	0.40	1	1	1	0.75	0.60	0.60	1	1			
M22	0.33	0.75	0.60	0.16	0.40	0.25	0.50	0.50	0.25	0.16	0.40	1	1	1	0.75	0.60	0.60	1	1	1		
M23	0.25	0	0.25	0.33	0	0	0	0.20	0	0.33	0	0	0	0	0	0.25	0	0	0	0	1	
M24	0.33	0.75	0.33	0.16	0.75	0	0.20	0.80	0	0.16	0.75	0.60	0.60	0.60	0.40	0.33	1	0.60	0.60	0.60	0	1

Based on the similarity index values shown in **Table 2**, the similarity index of 21 GMP3 mutant varieties and GMP3 varieties ranged from 0.20-1.00. The higher similarity index indicates the results of the phenetic analysis between samples are getting closer, while the lower similarity index indicates the results of the phenetic analysis are getting farther away (Hamidah et al., 2016).

The highest similarity index (1.00) is owned by M9, M5, M24, M18, M11, M4, M17, M2, M22, M21, M19, M15, M13, M12, M10 and M3. Due to this proximity kinship, the GMP3 and GMP3 mutants have the same stomata characteristics. According to Purnomo et al. (2012), the similarity index of 1.00 indicates no difference between the objects being compared. Based on the results of this study, 16 varieties of GMP3 mutants were closely related and had the same stomata character in common, the similarities were found in the characters of stomata length, stomata width, and stomata index. A cluster analysis based on the character stomata is presented in the dendrogram in **Figure 3.**

Phenetic Analysis

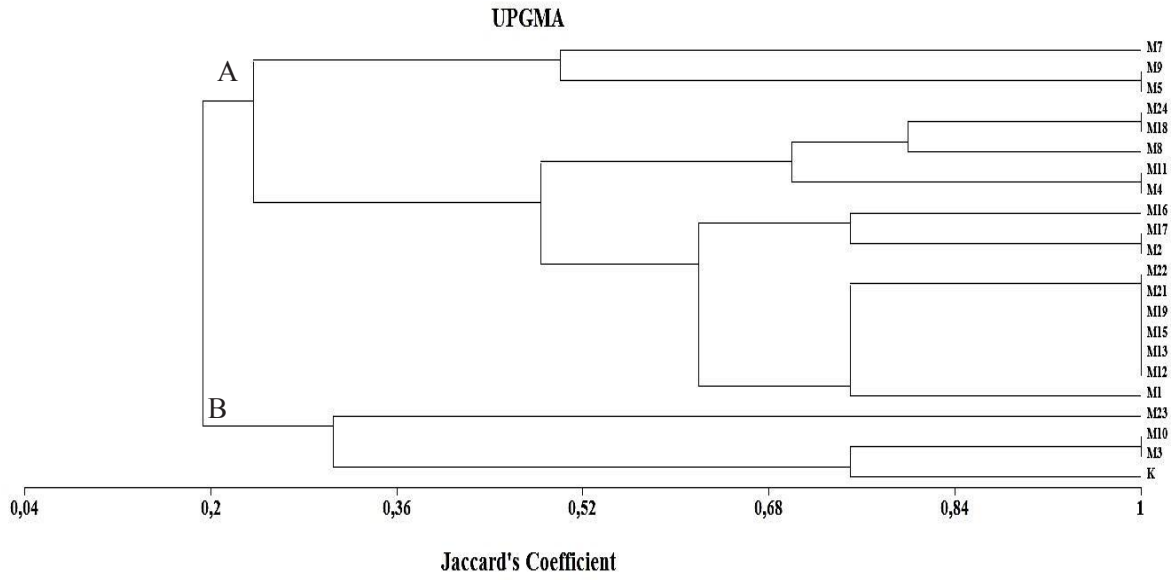

Figure 2. Dendrogram of phenetic relationship of 21 GMP3 mutants and GMP3 varieties using Jaccard's coefficient

The results of the cluster analysis in Figure 2 show that the accessions of GMP3 mutant variety can be grouped into 2 major groups, namely cluster A and cluster B. Cluster A has a similarity index of 0.23, the closeness of this kinship relationship is based on the similarity of the characters of the width of the stomata opening and the length of the stomata consisting of the 18 accessions are M7, M9, M5, M24, M18, M8, M11, M4, M16, M17, M2, M22, M21, M19, M15, M13, M13, and M1. Cluster A is divided into 2 sub-clusters, namely Sub Cluster I consisting of M7, M9, and M5, while Sub Cluster II consists of M24, M18, M8, M11, M4, M16, M17, M2, M22, M21, M19, M15, M13, M13, and M12. Cluster B has a similarity value of 0.30. The closeness of this kinship relationship is based on the similarity of the characteristics of the width of the stomata opening, the number of stomata, and the density of stomata which consists of 4 accessions, namely varieties GMP3, M23, M10, and M3. Cluster B is divided into 2 sub-clusters, Sub-Cluster I which only consists of M23, whereas Sub-Cluster II consists of GMP3, M10, and M3.

The similarity of character stomata overall with the closest kindship and the value of the similarity index of 0.80 is found in cluster A, this similarity index value was found in M24, M18, and M8. This indicates possible duplication of species in the

collection. Based on the research in the field, it is also known that the three accessions have very similar characters and are difficult to distinguish. Based on the phenetic analysis (**Figure 2**), there were differences in the stomata characters of the GMP3 mutant variety with the GMP3 variety, those are the width of the stomata opening, the length of the stomata, and the width of the stomata found in M23, M1, and M7. This is supported by the low similarity index value in the three mutants.

Principal Component Analysis (PCA)

Principal Component Analysis (PCA) results based on stomata characters are presented in **Figure 3**.

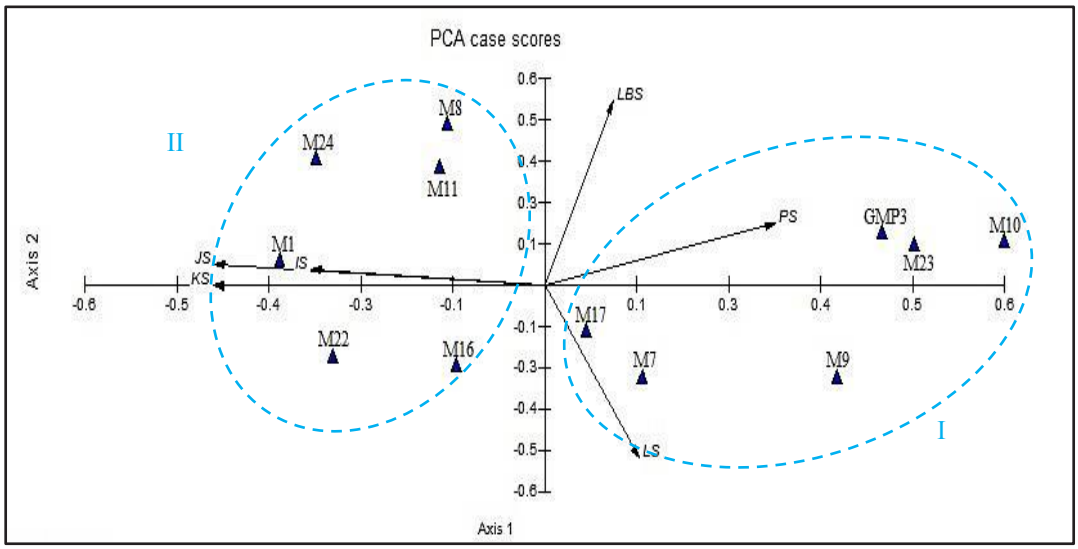

Figure 3. Principal Component Analysis on 21 varieties of GMP3 and mutants GMP3 varieties based on the character of the stomata.

Based on the results of the main component analysis in **Figure 3**, the grouping of GMP3 varieties and GMP3 mutant varieties are divided into 2 clusters, Cluster I consisting of GMP3, M7, M9, M10, M17, and M23 based on the characters of stomata length and stomata width. Cluster II consists of M2, M8, M11, M16, M22, and M24 which are grouped based on the character of the number of stomata, stomata index, and stomatal density. According to Sari et al. (2016), the length and direction of the arrows indicate the stomata characters that most influence the grouping. Arrows pointing to a particular group indicate the most influential anatomical character. The length of the arrow is directly proportional to the character of the stomata. The characters that play a role in the grouping of GMP3 mutant accessions are presented in **Table 3.**

Table 3 . Characters that play a role in grouping GMP3 . mutant varieties

Code	Character	PC1	PC2
LBS	Stomata Aperture Width	0.117	**0.706**
PS	Stomata Cell Length	**0.395**	**0.235**
LS	Guard Cell Width	0.162	-0.661
JS	Number of Stomata	-0.567	0.081
KS	Stomata Density	-0.568	-0.003
IS	Stomata Index	-0.401	0.061
	Eigenvalues	**2,433**	1,141
	Percentage	40,544	19.023
	cum. Percentage	40,544	19.023

Based on the results of **Table 3,** there are two characters that play an important role in grouping GMP3 mutant varieties. These two characters, namely stomata aperture width (LBS) and stomata cell length (PS) were simultaneously able to separate all samples on PC1 and PC2.

In the main component analysis, there is an eigenvalue that shows the percentage value of the contribution of each grouping (Sultan et al., 2010). Eigenvalue >2 indicates the most important character in cluster grouping (Steven and Tello, 2014). So that based on the results in **Table 3** the total variation on axis 1 contributes 40.54% variation of the six anatomical characters used with an eigenvalue of 0.395 while the total variation on axis II is 19 0.02% variation with eigenvalues of 0.706 and 0.235.

The size of the eigenvalues shows the influence of each character, which can be seen from the short length of the projection formed. Sari et al (2016), explained that the length and direction of the projection arrows indicate the stomata characters that most influence the grouping. The longer the arrow, the more influential the stomata character. PCA is used to show the distance between groups in the specimens studied in addition, according to Adebisi et al (2013) and Hamidah et al (2016) that PCA can show the magnitude of the influence of stomata characters in the grouping.

Based on the results of this study, apart from the cluster grouping pattern (I and II), the characteristics that play a role in sample separation between cluster analysis and principal component analysis have similarities. Jalil et al. (2020) stated that there is congruence between the results of cluster analysis and principal component analysis. Both analyzes are commonly used methods for identifying cluster structures in numeric taxonomy and can distinguish a number of closely related plants.

The conclusion of this study is that the diversity of stomata characters in the GMP3 mutant variety has a larger stomata size, has a high stomata density, a large number of stomata and a high stomata index.

ACKNOWLEDGMENT

We thank to LPPM, University of Lampung through Applied Research number 777/UN26.21/PN/2022 for financial support. The authors also thank PT. Gunung Madu Plantations, Lampung, Indonesia, contract number 023-00/GMP/I/2021 and 013-00/GMP/I/2022 for collaboration the research.

REFERENCE

Adebisi MA, Okelola FS, Ajala MO, Kehinde TO, Daniel IO, and Ajani O. 2013. Evaluation of variation in seed vigor character of the West African rice genotype (*Oryza sativa* L.) using multivariate technique. Am J Plant Sci 4: 356-363. DOI:10.4236/ajps.2013.42047.

Arofatun IN, Rugayah R, and Chikmawati T. 2020. Leaf anatomical variation in *Desmos* Lour. and *Dasymaschalon* (Hook. F. & Thomson) Dalla Torre & Harms species (Annonaceae). J Biodiversitas 21(7):3317-3330. DOI: 10.13057/biodiv/d210756.

Arzani K, Ghasemi M, Yadollahi A, and Hokmabadi H. 2013. Study of foliar epidermal anatomy of four pistachio rootstocks under water stress. Idesia (Chile). 31(1):101-107. DOI: 10.4067/S0718-34292013000100012.

Bagheri M, and Mansouri H. 2014. Effect of induced polyploidy on some biochemical parameters in *Cannabis sativa* L. J Appl Biochem Biotechnol 175(5):2366-75. DOI: 10.1007/s12010-014-1435-8.

Cansian MS, Roberto CC, Ronildo WC. 2016. The polyploidy and its key role in plant breeding. J Planta 243(2):281-296. DOI: 10.1007/s00425-015-2450-x.

Carsono N, Ibnu GR, Sari S, Rachmadi M. 2022. Agronomic characteristics and genetic relationship of putative transgenic rice lines of cv. Fatmawati with the *Glu-IDx5* Transgene. J Biodiversitas 23(1):291-298. DOI:10.13057/biodiv/d230135.

Central Bureau of Statistics. 2021. Indonesian Sugarcane Statistics. Central Bureau of Statistics. Jakarta.

Chen WH, Tang CY, and Kao YL. 2009. *Ploidy doubling by in vitro culture of excised protocorms or protocorm–like bodies in Phalaenopsis species. Plant Cell, Tissue and Organ Culture.* Columbia University Press. New York.

Chikmawati, T. 2013. Anatomical and cytological features of *Spatthoglottis plicata* from Java Island J Trop Life Sci. 3(2): 87-92. DOI: 10.11594/JTLS.03.02.03.

Gantait S, Mandal N, and Bhattacharyya S. 2011. Induction and identification of tetraploids using in vitro colchicine treatment of *Gerbera iamesonii* Bolus cv. Sciella. Plant Cell Tissue and Organ Culture. 106(2):485–493. DOI: 10.1186/ s43141-021-00269-1.

Hamidah H, Tsawab, and Rosmanida. 2016. Analysis of Hylocereus spp. diversity based on phonetic methods. AIP Conf. proc. 1854: 1-8. DOI:10.1063/1.4985403.

Jalil M, Purwantoro A, Setiadi BD, Purnomo. 2020. Distribution, variation, and relationship of *Curcuma soloensis* Valeton in Java, Indonesia based on morphological caharacters.

Kamwean P, Chaisan T, Thobunluepop P, Phumichai C, and Bredemeir M. 2017. Chaging of morphological Characteristic and Biomass Properties in *Pennisetum* grassland soil. J Soil Sci Society of America. 68: 1429-1436. DOI:10.3923/JA.2017.23.31.

Lubis MM, Mawarni L, and Husni Y. 2 015. Response to growth of Sugarcane (Saccharum officinarum L.) Against Tillage on Two Conditions of Drainage. J Agro 3(1):214 - 220. DOI: 10.32734/jaet.v3i1.9385.

Miguel TP, and Leonhart KW. 2011. In vitro polyploid induction of orchids using oryzalin. Scie Horror. 130:314-319. DOI: 10.1016/J.SCIENTA.2011.07.002 .

Moghbei N, Khalili MB, and Bernard F. 2015. Colchicine effect on the DNA content and stomata size of *Glycyrrhiza glabra* var. glandulifera and *Carthamus tinctorius* L. J of Genetic Engineering and Biotecnology 13(1):1-6. DOI: 10.1016/ j.jgeb.2016.02.002.

Munir M, Khan MA, Ahmad M, Bano A, Ahmed SN, Tariq K, Tabassum S, Mukhtar T, Ambreen M, and Bashir S. 2011. Foliar epidermal anatomy of some ethnobotanically important species of wild edible fruits of northern Pakistan. J Med Plants Res. 5(24):5873-5880. ISSN 1996-0875.

Pitoyo A, Prameta AA, Marussi, Suratman, and Suranto. 2018. Morphological, anatomical, and isozyme variability among taro (*Colocasia esculenta*) accessions from the southeastern part of Central Java, Indonesia. J Biodiv 19(5):1811-1819. DOI: 10.13057/biodiv/d190532.

Prabowo H, Tri BR, Mudjiono G, Rizali A. 2022. Stable isotope analysis to assess the trophic level of arthropod in sugarcane ratoon agroecosystem. J. Biodiversitas 23(6):2871-2881. DOI:10.13057/biodiv/d230613.

Purnomo, Daryono BS, Rugayah I, Sumardi H, and Shivachi. 2012. Phenetic analysis and intraspecific classification of Indonesian water yam (*Dioscorea alata* L.) germplasm based on morphological characters. SABRAO J. Breed. genetics 44(2): 277-291. ISSN: 1029-7073.

Restykania S, Pitoyo A, dan Suranto. 2019. Morphology and isozyme variation among Madeira vine (*Anredera cordifolia*) accessions from the southeastern part of Central Java, Indonesia. Biodiv 20(10): 3024-3032. DOI: 10.13057/biodiv/d201035.

Sari N, Purnomo, Daryono BS, Suryadiantina M, Setyowati. 2016. Variation and intraspecies classification of edible canna (*Canna indica* L.) based on morphological characters. AIP. Conf. Proc. 1744: 1-8. DOI:10.1063/1.4953515.

Sivakumar, G. 2017. *Upstream biomanufacturing of pharmaceutical colchicine. Critical Review in Biotechnology*. Houston. USA.

Stevens, RD, and Tello JS. 2014. On the Measurement of Dimensionality of Biodiversity. Global Ecology and Biogeography 23 (2):1115-1125. DOI: 10.1111/geb.12192.

Suhaimi, S. 2017. Evaluation of Morphology, Anatomy, Physiology and Anatomy of Forage Plants Obtained by Colchiisin Treatment. *Thesis*. Master of Animal Husbandry Study Program, Faculty of Animal Husbandry. Diponegoro University.

Sultan HA, Elreish SB, and Yagi SM. 2010. Anatomical and phytochemical studies of the leaves and roots of Urginea grandiflora Bak. and Pancratium tortuosum Herbert. Ethnobotanical Leaflets 14: 826-835. DOI: 10.1.1.1.683.9435.

Suryo, 2009. *Cytogenetics*. Gadjah Mada University Press. Yogyakarta.

Yanny DL, Sukma D, Syukur M, Ngurah DS, Nurcholis W, and Iis SA. 2022. Increasing the diversity of marigold (*Tagetes* sp.) by acute and chronic chemical induced mutation of EMS (Ethyl Methane Sulfonate). J Biodiversitas. 23(3):1399-1407. DOI:10.13057/biodiv/d230326.

THE INFLUENCE OF MIXTURE FROM GAMBIER EXTRACT AND LIQUID SMOKE OF COCONUT SHELL AS INHIBITOR OF MAGNESIUM CARBONATE (MGCO3) SCALE FORMATION

Restu Dwi Aprian[a]*, Suharso[a], Buhani[a]

[a]*Department of Chemistry, Faculty of Mathematic and Natural Sciences, University of Lampung, Jl. Soemantri Brojonegoro No. 1 Bandar Lampung, Indonesia, 35145*

ABSTRACT

In this this research, an inhibitors was added to the growth of magnesium carbonate (MgCO3) scale using the unseeded experiment method. The MgCO3 growth solution used was 0.050 M interacted with mixed inhibitors of gambier extract and liquid smoke of coconut shell grade 2 (GA) with varying concentrations. Analysis using the Particle Size Analyzer (PSA) showed that the particle size distribution of the MgCO3 scale became smaller with the addition of an inhibitors. Analysis using Scanning Electron Microscopy (SEM) showed that the surface morphology of the MgCO3 crust with the addition of the inhibitors turned into a thin and small sheet compared to that without the addition of the inhibitors in the form of granules.

***Keywords*:** MgCO3, inhibitor, gambier extract, liquid smoke of coconut shell.

1. Introduction

Pipes are construction components that are always used for various industrial purposes, especially oil and gas companies, drinking water, and other chemical industries that function as fluid flow transportation from one area to another [1-6]. One of the problems that often occurs in the pipeline of the oil and gas industry is the formation of deposits called crust. The build-up of scale causes corrosion, changes in ionic composition, pH, pressure and temperature of the salt water. Non-productive expenditures related to slag deposits are estimated at 1.5 billion Euros per year in France, 0.8 billion USD in the UK, and 9 billion USD in the United States [7-11]. A common method for controlling scale deposition is the use of addictives that act as anti-scalers so that the negative impact of scale formation can be reduced [12-16].

Gambier extract from *Uncaria Gambier Roxb* contains chemical compounds such as tannic acid, catechins, and quarcetin which have been reported as green scale growth inhibitors [9]. However, gambier extract has disadvantages such as easy to mold and cannot be stored for a long time [8]. To overcome this problem, gambier extract will be mixed with liquid smoke of coconut shell which is known to contain phenolic compounds, acids, aldehydes, and ketones [17-19]. These compounds are believed to play a role in preventing the growth of fungi so that they can be used for a long time as a scale inhibitor. In addition, inhibitors of a mixture of gambier extract and liquid smoke of coconut shell have a cheaper price and are environmentally friendly.

In this research, we will study the effect of using a mixture of gambir extract and liquid smoke of coconut shell in inhibiting the growth of magnesium carbonate ($MgCO_3$) crust with variations in the concentration ratio of gambier extract and coconut shell liquid smoke in a solution of 0.050 M $MgCO_3$ growth using the unseeded experiment method. The growth rate of $MgCO_3$ scale was calculated from the amount of sediment formed over time. The precipitate formed will be characterized using scanning electron microscopy and particle size analyzer to provide an overview of its composition, size, and morphology.

2. Experimental Procedure

2.1 Materials

The instrument used in this experiment consisted of analytical balance (Kenr & Sohn GMBH ABT 220-4M, Germany), oven (Thermo Fisher Scientific, United Kingdom), water bath (Haake S21, Thermo Fisher Scientific, USA), plastic bottles, magnetic stirrer, beaker, Fourier Transform Infrared (FTIR) spectrophotometer (Shimadzu FTIR-8400, Japan), gas Chromatography–Mass Spectrometry (GC-MS, Shimadzu GC2010 MSQP 2010S, made in Japan), Scanning Electron Microscopy (SEM, JSM 6360 LA, JEOL, Japan), and Particle Size Analyzer (PSA, The Beckman Coulter LS 13 320 MW, manufactured in USA). The materials used in this experiment were $MgCl_2$ and $NaHCO_3$ (Merck, Germany), gambier extract obtained from a traditional market in Bandarlampung, and liquid smoke of coconut shell used was grade 2 obtained from the coconut waste processing center in Bandar Jaya, Central Lampung.

2.2 Preparation of gambier extract and liquid smoke of coconut shell grade 2

Gambier extract is made by smoothing solid gambier with a cup until smooth, so that gambier powder is obtained. A total of 0.25 grams of gambier powder was dissolved in 1 L of distilled water. The solution was stirred using a magnetic stirrer for 3 hours at 90^{o}C and then the solution was filtered using filter paper. The filtrate obtained is gambier extract with a concentration of 250 ppm [9]. Liquid smoke of coconut shell grade 2 with a concentration of 50 ppm was prepared by diluting 50 mL liquid smoke of coconut shell grade 2 with distilled water in a measuring flask to the mark, then homogenized. The same treatment was carried out for the manufacture of inhibitor solutions with concentrations of 150, 250, 350, 450 ppm [20].

2.3 Testing the use of a mixture of gambier extract and liquid smoke of coconut shell grade 2 as an inhibitors of $MgCO_3$ crystal formation with the unseeded experiment method

2.3.1 Without the addition of inhibitors

A growth solution of 0.050 M $MgCO_3$ was prepared by mixing a solution of 0.2 M $MgCl_2$ and 0.2 M $NaHCO_3$ each in 200 mL of distilled water, then placed in a magnetic stirrer and stirred using a magnetic stirrer at 60^{o}C for 15 minutes. After the two solutions were mixed, the solution was divided into 6 plastic bottles where each bottle contained 50 mL of growth solution. The solution is then placed into a water bath at a temperature of 60^{o}C. Observations were made for 65 minutes (15 minutes the first one glass was taken, then taken every 10 minutes) then weighed the weight of the crystals formed by filtering the solution in the bottle using filter paper, washed with distilled water, and dried in an oven at 105^{o}C for 3 hours. The precipitate formed was weighed, then selected the most effective and analyzed using SEM to determine the crystal morphology and particle size distribution in the precipitate using PSA.

2.3.2 *With the addition of inhibitors*

The inhibitors solution was made by mixing 200 mL of gambier extract with 200 mL of coconut shell liquid smoke grade 2 with varying concentration ratios. The combination of gambier extract and liquid smoke of coconut shell grade 2 was tested for effectiveness by varying the concentration of the mixture of gambier extract with liquid smoke of coconut shell grade 2 where the concentration of gambier extract was kept constant. Comparison of the concentrations of the liquid smoke of coconut shell grade 2 mixture can be seen in Table 1. The mixed solution of gambier extract and liquid smoke of coconut shell grade 2 was stirred using a magnetic stirrer for 15 minutes and cooled and then stored in a dark bottle. Each mixture was tested for effectiveness in inhibiting the formation of $MgCO_3$ scale in 0.050 M $MgCO_3$ growth solution.

Growth solution of 0.050 M $MgCO_3$ was prepared by mixing 0.2 M $MgCl_2$ solution and 0.2 M $NaHCO_3$ solution in a mixture inhibitors of gambier extract and liquid smoke of coconut shell grade 2 with a concentration ratio of 5:1. The mixture was placed in a magnetic stirrer and stirred using a magnetic stirrer at 60^{o}C for 15 minutes. After the two solutions were mixed, the solution was divided into 6 plastic bottles where each bottle contained 50 mL of growth solution. The solution is then placed into a water bath at a temperature of 60^{o}C. Observations were made for 65 minutes (15 minutes the first one glass was taken, then taken every 10 minutes) then weighed the weight of the crystals formed by filtering the solution in the bottle using filter paper, washed with distilled water, and dried in an oven at 105^{o}C for 3 hours. This experiment was repeated with variations in the concentration ratio of gambier extract and coconut shell liquid smoke grade 2 of 5:3, 5:5, 5:7, 5:9. The precipitate formed was weighed, then selected the most effective and analyzed using SEM to determine the crystal morphology and particle size distribution in the precipitate using PSA.

2.4 *Data analysis*

To find out the effectiveness of inhibitors in inhibiting the scale formation of $MgCO_3$, Eq. (1) [21] given as follows can be used:

$$\text{Effectiveness of inhibitors (\%)} = 100\% \times \frac{(C - C)}{(C - C)} \quad (1)$$

where :
Ca = Precipitation amount of $MgCO_3$ after added inhibitor at equilibrium (g/L)
Cb = Precipitation amount of $MgCO_3$ without inhibitor at equilibrium (g/L)
Cc = Initial precipitation amount of $MgCO_3$ (g/L)

3. Results and Discussion

3.1 *Quality of the inhibitors mixtures*

Gambier can be used as an inhibitor of scale growth, but gambier has a weakness that is quickly damaged due to fungal growth. Therefore, a combination of inhibitors of gambier extract and liquid smoke of coconut shell grade 2 was used so that the gambier extract was not easily molded and increased its effectiveness as an inhibitor of $MgCO_3$ scale. The resistance of the inhibitor solution can be seen in Fig. 1. In Fig. 1 shows the gambir extract which is not added with liquid smoke of coconut shell grade 2 within 2 weeks has started to grow fungus that look like there are impurities, while the gambier extract is mixed with liquid smoke of coconut shell grade 2 has not grown fungus and looks still clear without any impurities. Liquid smoke of coconut shell grade 2 can slow down the damage of gambier extract by slowing the growth of fungi because it contains benzoic acid and cinnamic acid which can be used as antimicrobials and fungi [20].

3.2 *Characterization of inhibitor using FTIR spectrophotometer*

Characterization using an IR spectrophotometer serves to determine the functional groups contained in gambier extract and liquid smoke of coconut shell grade 2. The IR spectrum obtained for gambier extract and liquid smoke of coconut shell grade 2 is presented in Fig. 2. In Fig. 2(a) it can be observed the appearance of a number of absorption bands related to the functional groups possessed by the organic components in the gambier extract. The presence of a hydroxyl group (-OH) can be observed by the appearance of an absorption band in the area 3,417.86 to 3,363.86 cm^{-1} with a very wide intensity. In Fig. 2(a) the wave number appears in the 3,324.8 cm^{-1} area forming a stretching vibration which indicates the presence of a hydroxyl group (-OH) contained in tannic acid (tannin) which is very rich in hydroxyl groups. At a wave number of 1,640 cm^{-1}, it forms a stretching vibration which indicates the presence of a carbonyl functional group (C=O) present in tannic acid. The presence of a C=C group in aromatic compounds was seen by the appearance of peaks at wave numbers 2,109.7 and 2,363.1 cm^{-1}. From these data, it can be concluded that gambier extract contains several chemical compounds such as tannic acid which can function as an MgCO3 inhibitor.

Figure 2(b) observes the appearance of a number of absorption bands related to functional groups possessed by organic components in liquid smoke of coconut shell grade 2. The absorption band appears at a wave number of 3,339.7 cm^{-1} indicating the hydroxyl (-OH) stretching vibration. The (-OH) functional group corresponds to the component that is widely found in liquid smoke of coconut shell grade 2, namely phenol. The absorption band at wave number 1,640 cm^{-1} forms stretching vibrations indicating the presence of a carbonyl group (C=O) with a sharp intensity derived from carboxylic compounds (acetic acid) and ketones. In addition, at a wave number of 1,274.7 cm^{-1} with a bending vibration, a peak appears as a sign of the presence of an alcohol group (C-O). Based on this description, it can be stated that liquid smoke of coconut shell grade 2 has chemical compounds that can function as MgCO3 scale inhibitors. In addition to these components, liquid smoke of coconut shell grade 2 also has absorption bands at wave numbers 2,117.1 cm^{-1} and 2,363.1 cm^{-1} with stretching vibrations indicating the presence of a C=C group of alkenes.

In this research, the inhibitor with the highest effectiveness was a mixture of gambir extract and liquid smoke of coconut shell grade 2 (GA) with a concentration ratio of 5 : 9 respectively so that this GA inhibitor was also analyzed using an IR spectrophotometer as shown in Fig. 2(c). Based on this analysis, the absorption band of the hydroxyl group (-OH) is seen at the wave number 3,339.7 cm^{-1}, the carbonyl functional group (C=O) is seen at the wave number 1,640 cm^{-1}, the functional group (C = C) of the alkene is seen at the wave number. waves of 2,117.1 cm^{-1} and 2,363.1 cm^{-1} and at wave numbers of 1,274.7 cm^{-1} with bending vibrations, a peak appears as a sign of the presence of alcohol groups (C-O). The characterization results show that in the mixed GA inhibitor (5 : 9) there is an active group that can be used as an MgCO3 inhibitor.

3.3 *Characterization of inhibitor using chromatography–mass spectrometry* (GC-MS)

Chemical analysis from gambier extract using GC-MS is shown in Table 2. This table shows the separation of chemical components displayed from chromatogram peaks in GC. The peaks start at a retention time of 2.86 to 17.36 min. The results of chromatogram peak analysis show that gambier extract has 8 chemical components as listed in Table 2. The most abundant content of gambier extract is (2-Methylphenoxy) acetic acid (33.04%) and 1,3-Benzenedicarboxylic acid (15.83%). Chemical analysis from

liquid smoke of coconut shell grade 2 using GC-MS is shown in Table 3. This table shows the separation of chemical components displayed from chromatogram peaks in GC. The peaks start at a retention time of 3.30 to 14.63 min. The results of chromatogram peak analysis show that liquid smoke of coconut shell grade 2 has 8 chemical components as listed in Table 3. The most abundant content of coconut shell liquid smoke is phenol (45.04%) and acetone (8.19%). This result is consistent with IR data (Fig. 2) obtained with the functional groups found in gambier extract and liquid smoke of coconut shell grade 2, namely hydroxyl, aldehyde, ketone, carboxylic, or ester group.

3.4 Testing of inhibitor mixtures in inhibiting MgCO3 scale formation

Determination of the effectiveness of the Inhibitor mixture of gambir extract (G) and liquid smoke of coconut shell grade 2 (A) on the growth rate of $MgCO_3$ scale with various inhibitor concentrations at a concentration of 0.050 M $MgCO_3$ growth solution using the unseeded experiment method can be seen in Fig. 3. Fig. 3 shows that the growth of 0.050 M $MgCO_3$ scale with mixed GA inhibitor at various concentration ratios was able to reduce the growth of $MgCO_3$ scale. Based on the observational data, calculations can be made using Eq. (1) to obtain the effectiveness of the mixed GA inhibitor shown in Table 4. This is in accordance with previous studies which reported that the higher the concentration of the added inhibitor, the greater the inhibitor's ability to inhibit the formation of $MgCO_3$ scale [29]. The greatest decrease occurred in the mixed GA inhibitor with a concentration ratio of 5 : 9 in a 0.050 M $MgCO_3$ growth solution of 95.44%.

The crystal morphology of $MgCO_3$ was observed using SEM and can be seen in Fig. 4 and 5. The results of the SEM analysis shown in Fig. 4 and 5 showed that there was a change in the surface morphology of the 0.050 M $MgCO_3$ crystal using a mixed GA inhibitors (5 : 9) at 1000x and 5000x magnification. The results of the SEM analysis showed that the $MgCO_3$ crystals before the addition of the GA inhibitors (5 : 9) were in the form of plates that fused to form granules. Meanwhile, the $MgCO_3$ crystals which had been added with GA inhibitors (5 : 9) turned into thin and small sheets. The same thing also happened to the results of previous studies which reported that magnesium carbonate crystals were in the form of a sphere composed of small plates that fused like an arrangement on flower petals [22]. So it can be concluded that the addition of inhibitors causes significant morphological changes of $MgCO_3$ crystals.

To further prove changes in the size of $MgCO_3$ crystals without and with the addition of GA inhibitors, an analysis using a particle size analyzer (PSA) was performed on $MgCO_3$ crystals obtained as seen in Fig. 6. The graph in Fig. 6 shows a comparison of the distribution of 0.050 M $MgCO_3$ scale particles without and with the addition of a GA inhibitor (5 : 9) which shows that there is a shift in the graph between without an inhibitors and with the addition of an inhibitors. The graph shows that the $MgCO_3$ scale without inhibitor has a median value of 12.87 μm and a mean value of 16.09 μm. After the addition of the GA inhibitor (5 : 9) the size of the $MgCO_3$ scale particles had a median value of 5.38 μm and an average value (mean) of 8.04 μm. $MgCO_3$ scale without the addition of inhibitors and with the addition of inhibitors has a difference in particle size distribution based on the median value of 7.49 μm and based on the mean value of 8.05 μm. The particle size distribution can describe the effectiveness of the inhibitor in inhibiting the rate of crystal growth by comparing the crystal growth in the growth medium with the addition of an inhibitor and without the addition of an inhibitor. Crystal growth will generally be stunted in the presence of inhibitors in the growth solution medium [23].

The shift in the mean and median values in the $MgCO_3$ crust with the addition of an initiator is due to the bond between Mg^{2+} metal and the active groups contained in GA inhibitor compounds such as hydroxyl groups (-OH) and carbonyl (C=O) so that the particle size is the diameter of the $MgCO_3$ crystals. In gambier extract, compounds that play a role in inhibiting the growth rate of magnesium carbonate crystals are tannic acid, while in liquid smoke of coconut shell grade 2 compounds that play a role in inhibiting the growth rate of magnesium carbonate crystals are phenol and acetic acid. The growth solution was prepared from magnesium chloride ($MgCl_2$) and sodium bicarbonate ($NaHCO_3$) which were dissolved in a GA inhibitor, respectively. This means that Mg^{2+} ions will interact with inhibitors before reacting with CO_3^{2-} ions to form $MgCO_3$ crystals. The Mg^{2+} ion will bind to the hydroxyl group (-OH) and carbonyl group (C=O) which are the active groups of compounds derived from GA inhibitors.

3.4 Inhibition mechanism

Morphological changes that occur in $MgCO_3$ crystals without and with inhibitors are caused by crystal distortion. In the crystal distortion mechanism, scale inhibitors affect the arrangement reaction and crystal growth causing irregular and non-crystalline forms. The inhibitor molecule adsorbs to the active crystal growth site, consequently the inhibitor molecule blocks and prevents further crystal growth. In addition, distortions (defects in the crystal lattice) create internal stresses, making the crystal brittle and fine. These fine crystals cannot withstand the mechanical forces exerted by water and are thus removed easily from the surface [24–28]. The mechanism of GA inhibitors in inhibiting the rate of crystal growth of $MgCO_3$ can be illustrated in Fig. 7 which provides an illustration of how GA inhibitors work in adsorption on the crystal growth sides of crystal seedlings which results in inhibited crystal growth and irregular crystal shape.

4. Conclusion

A mixture of gambier extract and liquid smoke of coconut shell grade 2 can be used as an alternative to $MgCO_3$ scale inhibitor. This can be seen by the decreased growth of $MgCO_3$ scale after adding a mixture of gambier extract and liquid smoke of coconut shell grade 2. Gambier extract and liquid smoke of coconut shell grade 2 at a mixture concentration ratio of 5 : 9 as an inhibitor of scale formation $MgCO_3$ has the highest effectiveness of 95.41 %. The results of observations with SEM showed a significant change between the $MgCO_3$ scale without the addition of inhibitors and with the addition of GA inhibitors (5 : 9). The scale morphology of $MgCO_3$ with the addition of GA inhibitor (5 : 9) was smaller and thinner than the scale morphology of $MgCO_3$ without the addition of inhibitor.

Acknowledgments

The authors would like to appreciate the Directorate of Research and Community Services, Directorate General of Strengthening Research and Development, Ministry of Research, Technology and Higher Education of the Republic of Indonesia (Kemristekdikti).

Table 1 Concentration comparisons of gambier extract (G) and liquid smoke of coconut shell grade 2 (A) mixtures.

Ratio of concentration	Concentration of gambier extract (ppm)	Concentration of liquid smoke of coconut shell
(G:A)		grade 2 (ppm)
5 : 1	250	50
5 : 3	250	150
5 : 5	250	250
5 : 7	250	350
5 : 9	250	450

Table 2 Chemical analysis of gambier extract by GC-MS.

No	Retention time (min)	% Area	Chemical compound
1.	2,86	15,83	1,3-Benzenedicarboxylic acid
2.	4,68	33,04	(2-Methylphenoxy)acetic acid
3.	7,82	1,2	(4-Fluorophenyl)-(2'-thienyl)methanol
4.	10,03	8,83	5H-benzothiophene
5.	12,46	7,6	Pentanoic acid
6.	14,65	6,83	Benzoic acid
7.	16,59	2,98	1H-Purin-6-amine
8.	17,36	1,84	Patchouli alcohol

Table 3 Chemical analysis of liquid smoke of coconut shell grade 2 by GC-MS.

No	Retention time (min)	% Area	Chemical compound
1.	3,30	8,19	Acetone
2.	4,86	0,31	Butanoic Acid
3.	5,05	2,66	3-furaldehyde
4.	7,61	45,04	Phenol
5.	9,36	4,57	Phenol, 2-methoxy
6.	12,25	0,30	2,5-dimethylfuran
7.	13,28	2,93	2,4-dimethoxyphenol
8.	14,63	1,22	Methyl salicylic acid

Effectiveness of inhibitor (%) at the concentration of growth solution of 0.05 M with the various concentration of inhibitor added.

Effectiveness of inhibitor (%)	Ratio of concentration (G:A)
5 : 1	91.34
5 : 3	92.19
5 : 5	93.29
5 : 7	94.00
5 : 9	95.44

References

[1] H. Wang, M. Gao, Y. Guo, Y. Yang, R. Hu, A natural extract of tobacco rob as scale and corrosion inhibitor in artificial seawater, Desalination, 398 (2016) 198–207.

[2] Y. Gao, L. Fan, L. Ward, Z. Liu, Synthesis of polyaspartic acid derivative and evaluation of its corrosion and scale inhibition performance in seawater utilization, Desalination, 365 (2015) 220–226.

[3] K.D. Demadis, E. Mavredaki, A. Stathoulopoulou, E. Neofotistou, C. Mantzaridis, Industrial water systems: problems, challenges and solutions for the process industries, Desalination, 213 (2007) 38–46.

[4] R. Ikeda, A. Ueda, Experimental field investigations of inhibitors for controlling silica scale in geothermal brine at the Sumikawa geothermal plant, Akita Prefecture, Japan, Geothermics, 70 (2017) 305–313.

[5] M.K. Nayunigari, A. Maity, S. Agarwal, V.K. Gupta, Curcumin–malic acid based green copolymers for control of scale and microbiological growth applications in industrial cooling water treatment, J. Mol. Liq., 214 (2016) 400–410.

[6] M.K. Jensen, M.A. Kelland, A new class of hyperbranched polymeric scale inhibitors, J. Pet. Sci. Eng., 94–95 (2012) 66–72.

[7] R. Rosset, Les procédés physiques antitartre: mythe ou réalité, Actual. Chim., (1992) 125-148.

[8] Suharso, T. Reno, T. Endaryanto, Buhani, Modification of gambier extracts as green inhibitor of calcium carbonate ($CaCO_3$) scale formation, J.Water Process Eng., 18 (2007) 1-6.

[9] Suharso, Buhani, S. Bahri, T. Endaryanto, Gambier extracts as an inhibitor of calcium carbonate ($CaCO_3$) scale formation, Desalination, 265 (2011) 102-106.

[10] Suharso, Buhani, S.D. Yuwono, Tugiyono, Inhibition of calcium carbonate ($CaCO_3$) scale formation by celix[4] resorcinarene compounds, Desalin. Water Treat., 68 (2017) 32-39.

[11] J. MacAdam and S.A. Persons, Calcium carbonate scale control, effect of material and inhibitors, Water Sci. Technol., 49 (2004) 153-159.

[12] Y. Zhao, L. Jia, K. Liu, P. Gao, H. Ge, L. Fu, Inhibition of calcium sulfate scale by poly (citric acid), Desalination, 392 (2016) 1–7.

[13] L. Yang, W. Yang, B. Xu, X. Yin, Y. Chen, Y. Liu, Y. Ji, Y. Huan, Synthesis and scale inhibition performance of a novel environmental friendly and hydrophilic terpolymer inhibitor, Desalination, 416 (2017) 166–174.

[14] Suharso, Buhani, L. Aprilia, Influence of calix[4]arene derived compound on calcium sulphate scale formation, Asian J. Chem., 26 (2014) 6155–6158.

[15] G. Liu, M. Xue, Q. Liu, Y. Zhou, Linear-dendritic block copolymers as a green scale inhibitor for calcium carbonate in cooling water systems, Des. Monomers Polym., 20 (2017) 397–405.

[16] A.A. Al-Hamzah, C.M. Fellows, A comparative study of novel scale inhibitors with commercial scale inhibitors used in seawater desalination, Desalination, 359 (2015) 22–25.

[17] J. Towaha, A. Aunillah, E.H. Purwanto, Utilization of rubber wood liquid smoke and coconut shell liquid smoke to reduce air pollution in the lump processing, Bul. RISTRI, 4 (2013) 71–80.

[18] F. Swastawati, Quality and safety of smoked catfish (Aries talassinus) using paddy chaff and coconut shell liquid smoke, J. Coast. Dev., 12 (2008) 47–55.

[19] R. Simon, B. de la Calle, S. Palme, D. Meier, E. Anklam, Composition and analysis of liquid smoke flavoring primary products, J. Sep. Sci., 28 (2005) 871–882.

[20] Suharso, Eka Setiosari, Kiswandono, A. A., Buhani, Heri Satria, Liquid smoke of coconut shell as green inhibitor of calcium carbonate scale formation, Desalin. Water Treat., 169 (2019) 29-37.

[21] S. Patel, M.A. Finan, New antifoulants for deposit control in MSF and MED plants, Desalination, 124 (1999) 63–74.
[22] C. Unluer, A. Al-Tabbaa, Characterization of light and heavy hydrated magnesium carbonates using thermal analysis. J. Therm. Anal. Calorim.,35 (2013) 393-406.
[23] H. Wang, Y. Zhou, Q. Yao, W. Sun, Calcium sulfate precipitation studies with fluorescent tagged scale inhibitor for cooling water systems, Polym. Bull., 72 (2015) 2171–2188.
[24] M.D. Sikirić, H.F. Milhofer, The influence of surface active molecules on the crystallization of biominerals in solution, Adv. Colloid Interface Sci., 128–130 (2006) 135–158.
[25] Y.W. Wang, F.C. Meldrum, Additives stabilize calcium sulfate hemihydrate (bassanite) in solution, J. Mater. Chem., 22 (2012) 22055–22062.
[26] N.B. Singh, B. Middendorf, Calcium sulphate hemihydrate hydration leading to gypsum crystallization, Prog. Cryst. Growth Charact. Mat., 53 (2007) 57–77.
[27] T. Rabizadeh, C.L. Peacock, L.G. Benning, Carboxylic acids: effective inhibitors for calcium sulfate precipitation?, Mineral. Mag., 78 (2014) 1465–1472.
[28] M.P. Alvarez, R.O. Roa, E.S. Castruita, E.B. González, R.C. Dévora, D.N. Álvarez, M.P. Jiménez, L.S.Z. Rivera, Growth inhibition in calcium sulfate crystal using a copolymer in oil fields: theoretical study and experimental evaluations, Iran. Polym. J., 27 (2018) 927–937.
[29] Suharso, Buhani, Utami, H.R.., Tugiyono, Heri Satria, Influence of gambier extract modification as inhibitor of calcium sulfate scale formation, Desalin. Water Treat., 169 (2019) 22-28.

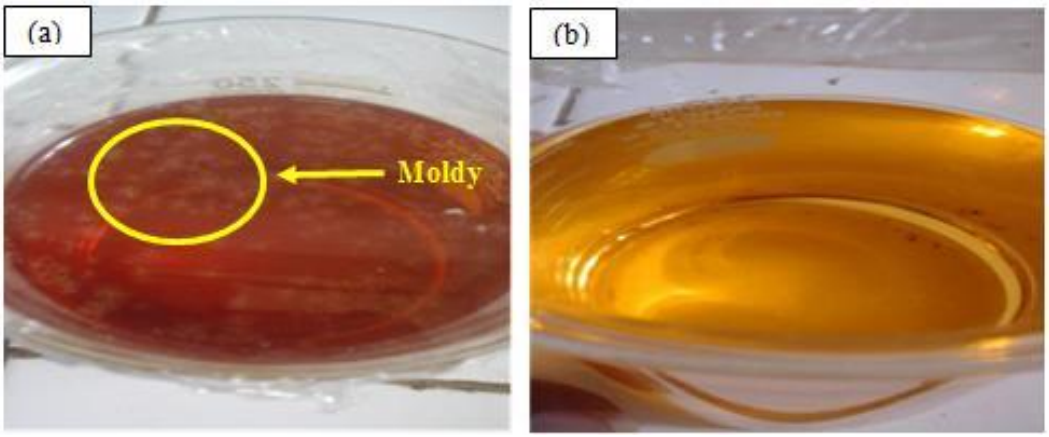

Fig. 1. Changes in gambier extract (a) without the addition of liquid smoke of coconut shell grade 2 and (b) with the addition of liquid smoke of coconut shell grade 2 after being kept for 2 weeks.

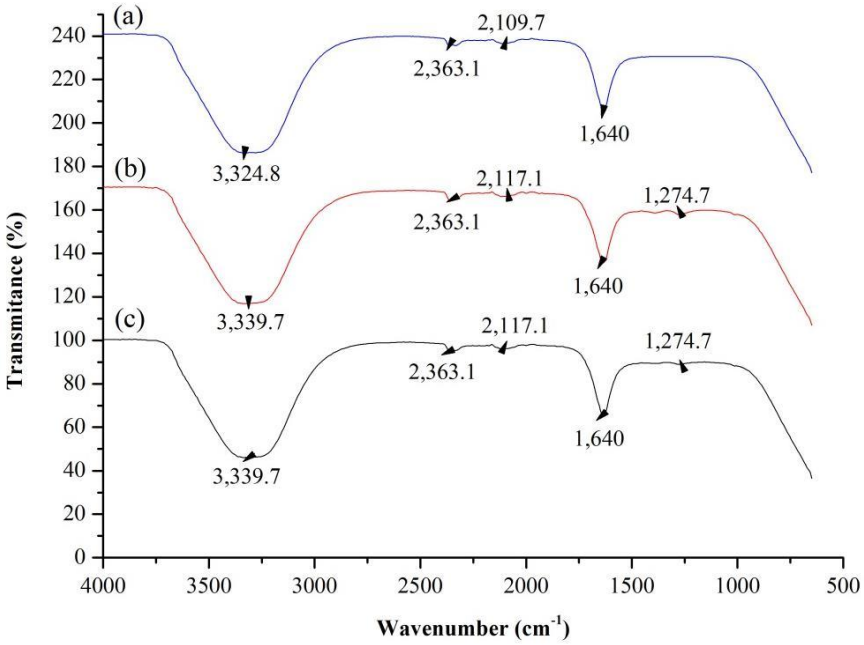

Fig. 2. IR spectrum of (a) gambier extracts, (b) liquid smoke of coconut shell grade 2, and (c) gambier- liquid smoke of coconut shell grade 2 (5:9).

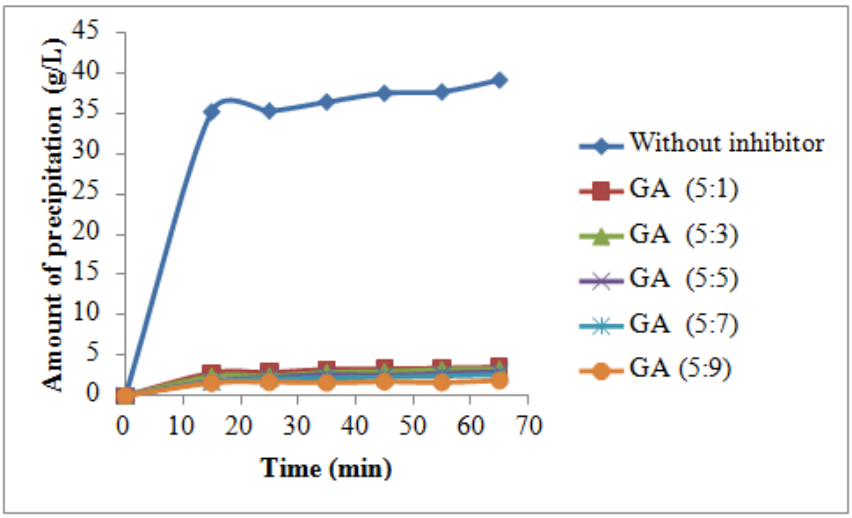

Fig. 3. The growth of MgCO3 scale at a growth solution concentration of 0.050 M versus time at various ratios of GA inhibitor concentrations.

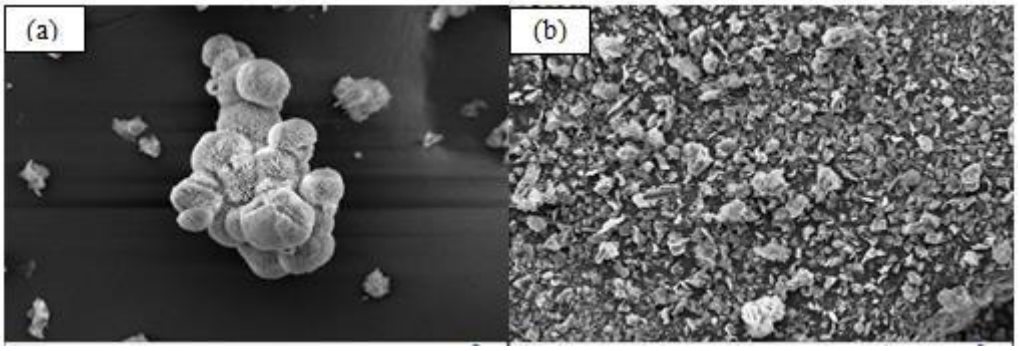

Fig. 4. Morphology of MgCO3 crystals (a) without inhibitors and (b) with inhibitors of the mixture of gambier extracts and liquid smoke of coconut shell with a ratio of 5:9 at magnification of 1,000×.

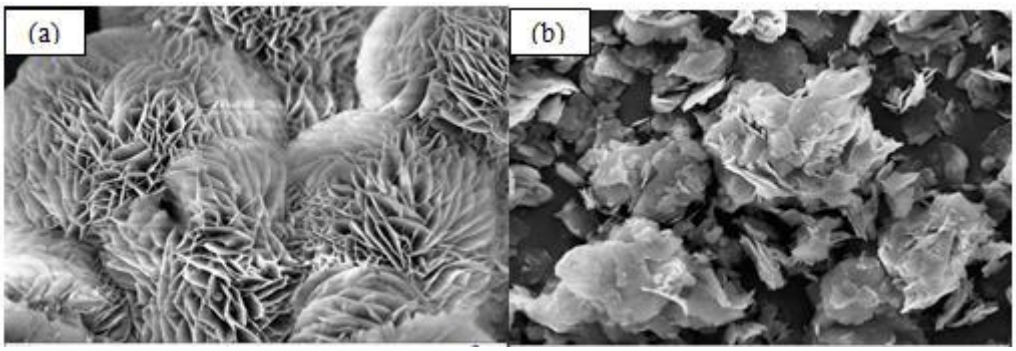

Fig. 5. Morphology of MgCO3 crystals (a) without inhibitors and (b) with inhibitors of the mixture of gambier extracts and liquid smoke of coconut shell with a ratio of 5:9 at magnification of 5,000×.

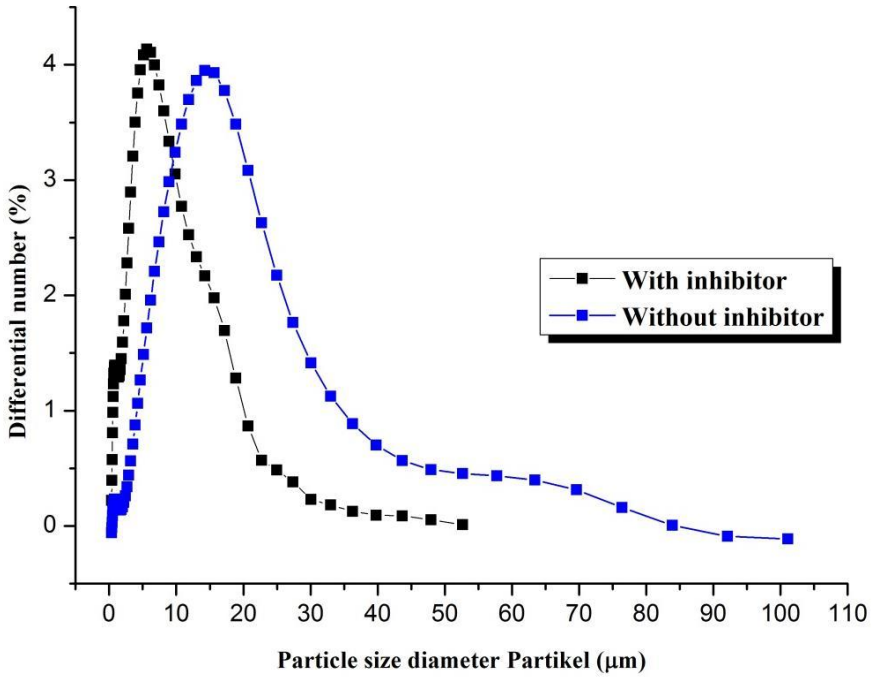

Fig. 6. Particle size distribution of MgCO3 crystals with and without inhibitor of G:A (5:9) at the concentration of MgCO3 growth solution of 0.05 M.

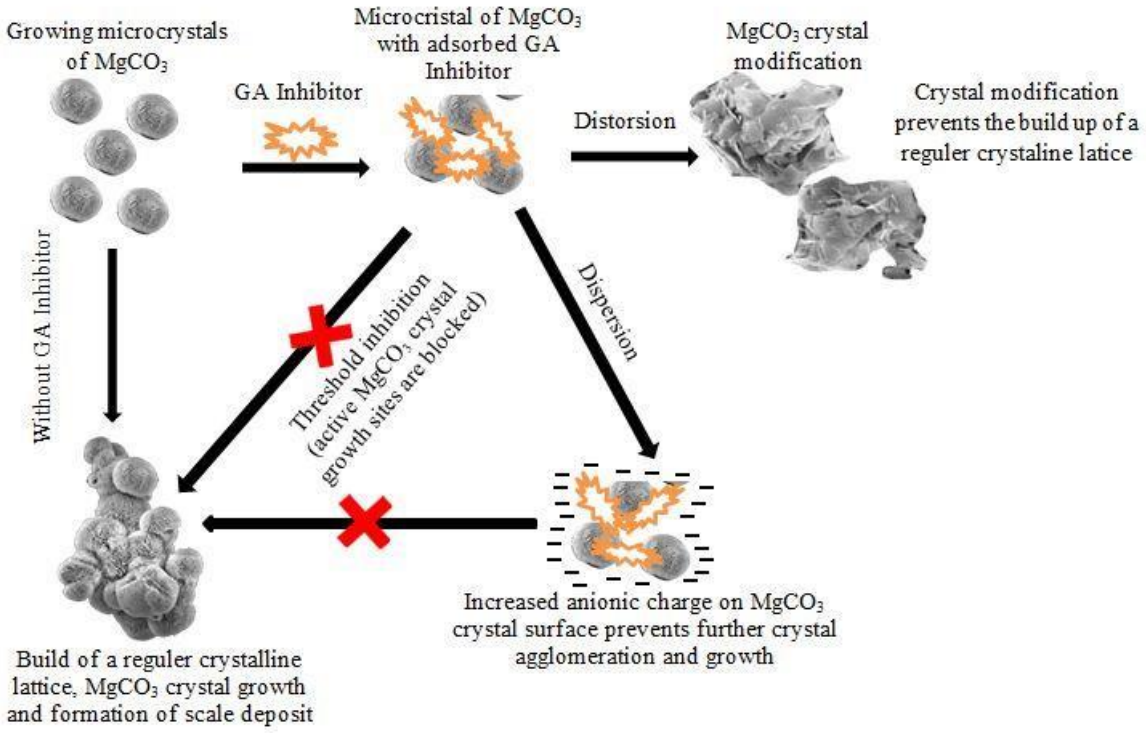

Fig. 7. The mechanism of GA inhibitors in inhibiting the growth rate of MgCO3 crystals in the growth solution.

ROBUST CLUSTERING OF COVID-19 PANDEMIC WORLDWIDE

Rizki Agung Wibowo[1], **Khoirin Nisa**[2*], **Hilda Venelia**[3], **Warsono**[4]

[1,2,3,4]*Department of Mathematics, Faculty of Mathematics and Natural Sciences, University of Lampung*
Jl. Prof. Dr. Soemantri Brodjonegoro No. 1, Bandar Lampung, 35145, Indonesia

Corresponding author e-mail: [2*] *khoirin.nisa@fmipa.unila.ac.id*

Abstract

COVID-19 pandemic is described as the most challenging crisis that human have faced *since* World War II. From December 2019 until August 2021 based on the dataset provided by WHO, globally there are 219 countries in the world that are affected by this virus. There are 205.338.159 case cumulative total and 4.333.094 death cumulative total caused by this virus. In this paper the data of 219 countries are analyzed using a robust clustering method namely K-Medoids cluster analysis. Based on the result, 219 countries in the world can be divided into five clusters based on four COVID-19 related variables, i.e. the number of case cumulative total, death cumulative total, positive cases per capita and case fatality rate. The distribution of the countries to five clusters was as follows; the first cluster contained 48 countries, the second cluster contained 3 countries, the third and fourth clusters contained 16 and 89 countries respectively, and the last cluster contained 63 countries. The largest cluster is the fourth one containing countries that form cluster with centroid below the world average, and the smallest cluster is the second cluster with the high cases in all attributes consists of USA, India and Brazil.

Keywords: *COVID-19, Cluster Analysis, K-Medoids.*

1. INTRODUCTION

In December 2019, an outbreak of pneumonia of unknown origin was reported in Wuhan, Hubei, China, this case were epidemiologically linked to the Huanan Seafood Wholesale Market [1]. The pneumonia *then was known as Coronavirus* Disease 19 (COVID-19) and spread across the world becoming a lethal pandemic. The effects of the pandemic were operationalized in terms of mobility, economy, and healthcare system. The mobility affected includes restructions on travel by airplane, ship and land transportation. Pandemics affect the economy in terms of demand and supply, decelerating the economic growth of affected countries, leading to reduction in trade and increase in poverty [2]. From December 2019 until August 2021 based on the dataset provided by World Health Organization (WHO), globally there are 219 countries in the world affected by this virus. There are 205338159 case cumulative total and 4333094 death cumulative total caused by this virus. To observe the spread of the pandemic among countries around the world, it is necessary to group countries with

homogeneous characteristics of COVID-19 related variables as a basis for the United Nations (UN), particularly WHO, to analysis COVID-19 situation worldwide.

Cluster analysis is a statistical technique for finding groups of objects from multivariate data. The aim of cluster analysis is to construct groups with homogeneous properties out of heterogeneous large samples [3]. An assumption that must be fulfilled in performing cluster analysis is the independencies between variables [4]. However, correlation between variables commonly occurs in research data. When the variables in the data are correlated, one should handle the problem by performing principal component analysis (PCA) to obtain new uncorrelated variables called "principal components" (PCs) [5]. The PCs are built as linear combinations of the original variables.

Clustering algorithms are designed to identify an underlying structure of data and use the detected relationships within the structure to group the objects into distinct groups. One of the most commonly used algorithms among the partitioning methods in cluster analysis is the K-means algorithm [6], [7]. K-means starts by assigning K initial cluster centroids, either randomly or by an initialization algorithm. All objects are distributed into each cluster based on their distance to the centroids. The solution is refined by first electing a new cluster centroid, based on the mean values of each object in the cluster, and then redistributing the object accordingly. K-means refines the solution until changes are no longer made or until a maximum limit of iterations has been reached [8]. However, K-means is very sensitive to outliers. Even one outlier can affect the result of K-means clustering [9], [10]. Therefore a robust cluster algorithm is needed when we deal with data containing outliers. One of the efficient robust clustering techniques is the K-medoids, also simply referred to as Partitioning Around Medoids (PAM) algorithm [11].

2. RESEARCH METHODS

This research was conducted in August 2021. The data used in this research sourced from WHO's website, with variables used are case cumulative total (CCT), death cumulative total (DCT), positive case per capita (PCC) and case fatality rate (CFR) caused by coronavirus. The dataset collected from December 2019 until August 2021.

Algebraically, principal components are particular linear combination of the p random variables $X_1, X_2, \dots, X_p$ [4]. Let $\boldsymbol{X}' = [X_1, X_2, \dots, X_p]$ be random vector, and $\boldsymbol{\Sigma}$ is the covariance matrix of $\boldsymbol{X}$ with eigenvalues $\lambda_1 \geq \lambda_2 \geq \lambda_3 \geq \dots \geq \lambda_p \geq 0$ and eigenvectors $\boldsymbol{a'_i}$, i = 1, 2, ..., p. Consider the linear combinations:

$$Y_i = \boldsymbol{a_i'X} = a_{i1}X_1 + a_{i2}X_2 + a_{i3}X_3 + \dots + a_{ip}X_p \; ; \quad i = 1,2,\dots,p \tag{1}$$

with variance and covariance:

$$Var(Y_i) = \boldsymbol{a_i' \Sigma a_i} \quad ; i = 1,2,\dots,p \tag{2}$$

$$Cov(Y_i, Y_k) = \boldsymbol{a_i' \Sigma a_k} \quad ; i,k = 1,2,\dots,p \tag{3}$$

The principal components are those uncorrelated linear combinations $Y_1, Y_2, \dots, Y_p$ whose variances in (2) are as large as possible [4]. In general, the i-th principal component is a linear combination $\boldsymbol{a_i'X}$ which maximizes $Var(\boldsymbol{a_i'X})$ subject to $\boldsymbol{a_i'a_i} = \boldsymbol{1}$ and $Cov(\boldsymbol{a_i'X}, \boldsymbol{a_k'X}) = 0$ for $k < i$. If the variables in the data have different units, the correlation matrix is used instead of the covariance matrix.

K-Medoids clustering algorithm is also a partition-based clustering algorithm [12]. Many studies to improve K-Medoids algorithm have been done in decades (see e.g. [13]–[15]). The uses of the K-medoids have been also applied in various research fields, one can see e.g. [10], [11], [16]–[19]. The procedure of PAM algorithm can be summarized as follows:

1. Determine initial medoids
   - Calculate the distance between every pair (i, j) of all objects using Euclidean distance:

$$d(i,j) = d_{ij} = \sqrt{\sum_{k=1}^{p}(x_{ik} - x_{jk})^2} \quad (4)$$

   - Calculate v_i for object i as follows

$$v_i = \sum_{j=1}^{n} \frac{d_{ij}}{\sum_{l=1}^{n} d_{jl}} \qquad ; j = 1,2, \dots, n \quad (5)$$

   - Sort v_i in ascending order, then select k objects having the first k smallest values as initial medoids.
   - Obtain the initial cluster result by assigning each object to the nearest medoid
   - Calculate the sum of distance from all objects to their medoids
2. Update medoids
   - Find a new medoid from each cluster by minimizing the total distance to other objects in cluster
   - Update new medoid in each cluster
3. Assign objects to medoids
   - Set each object to the nearest medoid and obtain the cluster result
   - Calculate the sum distance of all objects to their medoids,
   - Repeat from step 2, if the sum is equal to the previous iteration then stop algorithm [20].

The performance of cluster result is necessarily evaluated to see the level of homogenity of each cluster and determine the optimal number of clusters underlying the data. One of the most widely used statistics for cluster evaluation is the R-Squared (RS). R-Squared is computed as:

$$RS = \frac{SS_B}{SS_T} = \frac{SS_T - SS_W}{SS_T} = \frac{\{\sum_{j=1}^{n}(x_j - \bar{x})^2\} - \{\sum_{i=1}^{n_c}\sum_{j=1}^{r_i}(x_{ij} - \bar{x})^2\}}{\{\sum_{j=1}^{n}(x_j - \bar{x})^2\}} \quad (6)$$

The value of RS ranges from 0 to 1, with 0 indicating no differences among cluster and 1 indicating maximum differences among cluster.

Processed resulted are analyzed using the help of Rstudio software. The analysis procedure can be described as follow:

a) Outliers detection by using the Mahalanobis distance:

$$d_i(\boldsymbol{x_i}, \bar{x}) = \sqrt{(\boldsymbol{x_i} - \bar{x})' \boldsymbol{S}^{-1} (\boldsymbol{x_i} - \bar{x})},$$

$\boldsymbol{x_i}$ is an outlier if $d_i^2(\boldsymbol{x_i}, \bar{x}) > \chi^2_{p,1-\alpha}$, where p is the number of variables and α is a significance level with the default cut off *commonly* used is α=0.05.

b) Calculate the correlations among variables CCT, DCT, PCC, and CFR
c) If the variables are correlated, PCA is performed
d) Clustering the countries using PAM algorithms based on the principal components scores.
e) Evaluate the cluster result

3. RESULTS AND DISCUSSION

The correlations between variables are presented in Table 1. Based on Table 1 it has been shown that correlation value between CCT and DCT is very high as much as 0,932, although other correlations are mild we have to perform PCA to obtain independent new variables.

Table 1. Correlation between four variables

	CCT	DCT	PCC	CFR
CCT	1	0.932	0.156	0.035
DCT	0.932	1	0.164	0.156
PCC	0.156	0.164	1	-0.126
CFR	0.035	0.156	-0.126	1

The following table shows the eigenvalues of the sample correlation matrix above. The percentage of variances contained in each eigenvalue is described graphically in Figure 1.

Table 2. Eigen value

Eigen	Eigenvalue	Variance Percent	Cumulative Variance Percent
λ_1	1.995	49.868 %	49.868 %
λ_2	1.126	28.138 %	78.006 %
λ_3	0.820	20.490 %	98.496 %
λ_4	0.060	1.504 %	100 %

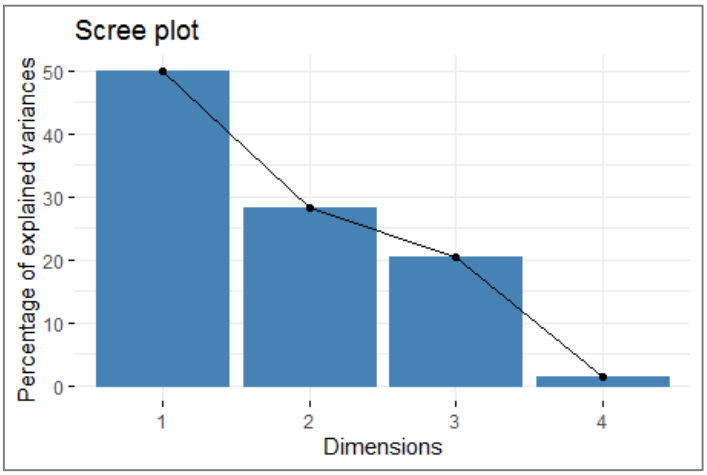

Figure 1. Scree plot of eigen values

Based on Table 2, we only use two initial eigenvalues for further analysis since both eigenvalues already contain 78 % of cumulative variance, and scree plot in Figure 1 also suggests that two components be retained. The scatter plot of objects using the first and the second Principal Component Scores (PC_1 and PC_2) is presented in Figure 2.

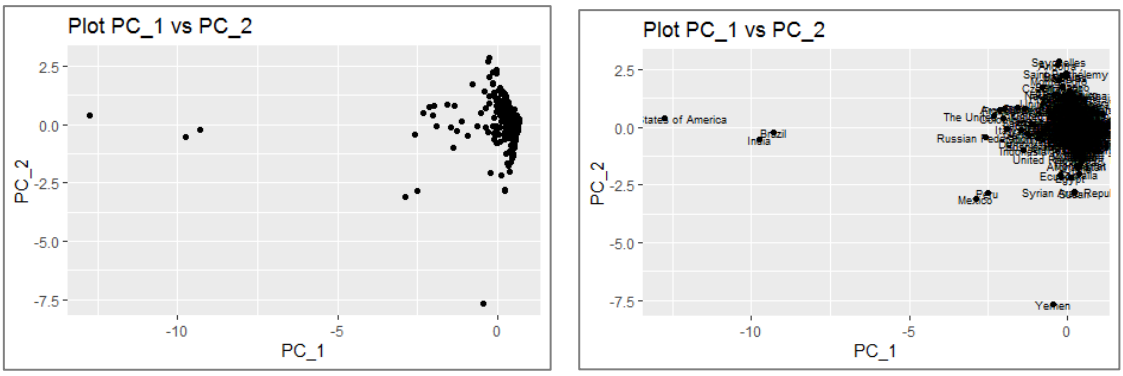

Figure 2. Plot PC_1 vs PC_2

Based on Figure 2, both variables form a stationary pattern, which means the two variables are uncorrelated, then the assumption of mutually uncorrelated variables is satisfied. However, it is indicated that there are outliers in the data. We conducted outlier detection using robust squared of Mahalanobis distance and the result is shown in Figure 3.

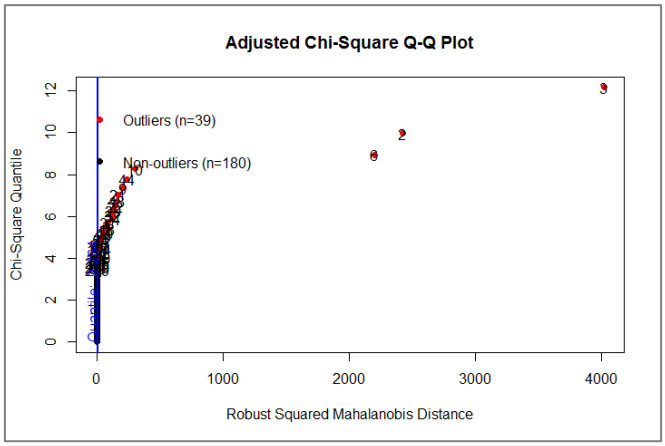

Figure 3. Outlier detection

The result shows that the number of outlier in the data is 39, then a robust clutering algorithm is required. The robust cluster analysis used is based on the principal component scores that have been obtained. Using K-Medoids algorithm we obtained the optimal number of cluster according to silhouette width is equal to 5 as presented in the following figure 4.

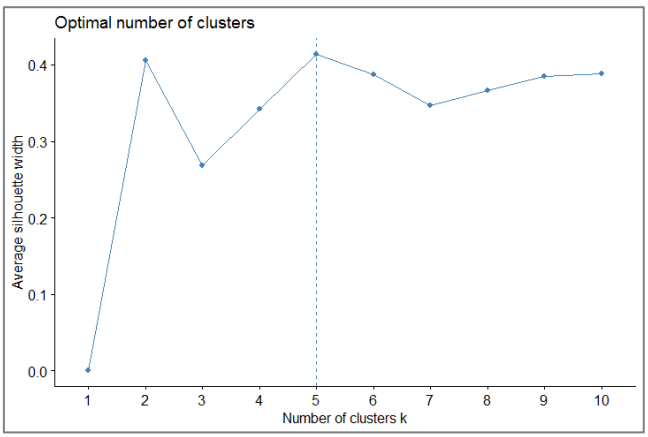

Figure 4. Optimal number of clusters

The result of K-medoids algorithm for five clusters yields the R-Square value as much as 0,8105, which means that 81,05 % of characteristics between clusters are different from each other. The resulted clusters graphically are shown in Figure 5, and the members of each cluster are presented in Table 3.

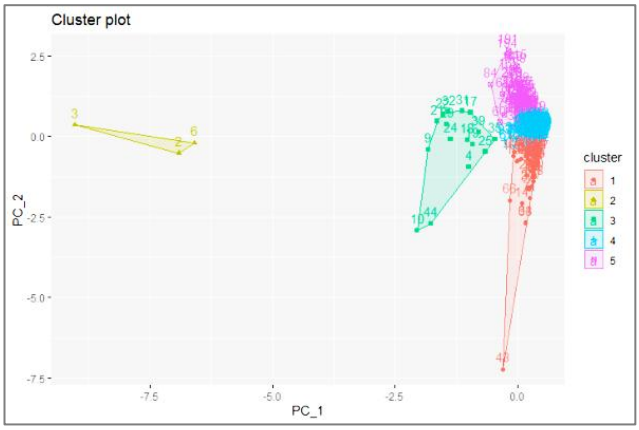

Figure 5. Cluster plot result

To determine cluster characteristics based on each variables and paid more attention to in each cluster, it is necessary to carry out a descriptive analysis. From all countries in the data, the average value of each variables are $\bar{X}_{CCT} = 933380{,}584$, $\bar{X}_{DCT} = 19755{,}571$, $\bar{X}_{PCC} = 0{,}042$ and $\bar{X}_{CFR} = 0{,}019$. These average values are compared to the cluster centers $(\bar{X}_{c,j})$, if $\bar{X}_{c,j} \leq \bar{X}_j$ (where j is the variable: CCT, DCT, PCC, CFR), it is interpreted sequentially as "medium", "low", "very low", if $\bar{X}_{c,j} > \bar{X}_j$, it is interpreted sequentially as "high", "very high". Details of the result are described in Table 4 and Table 5.

Table 3. Cluster result

Cluster	Countries	Cluster size
Cluster 1	Madagascar, Australia, Nigeria, Mali, Malawi, Syrian Arab Republic, Guatemala, Ecuador, Senegal, Cambodia, Chad, Somalia, Zimbabwe, Tunisia, Bolivia, Haiti, Honduras, Sierra Leone, Bulgaria, Nicaragua, El Salvador, Liberia, Mauritania, Bosnia and Herzegovina, Jamaica, Gambia, Lesotho, Guinea-Bissau, Trinidad and Tobago, Eswatini, Comoros, Antigua and Barbuda, Montserrat	48
Cluster 2	India, United States of America (USA), Brazil	3
Cluster 3	Indonesia, Russian Federation, Mexico, Turkey, Iran , Germany, The United Kingdom, France, Italy, South Africa, Colombia, Spain, Argentina, Ukraine, Poland, Peru	16
Cluster 4	Nigeria, Japan, Ethiopia, Philippines, Thailand, Republic of Korea, Canada, Morocco, Saudi Arabia, Uzbekistan, Mozambique, Ghana, Nepal, Venezuela, Côte d'Ivoire, Cameroon, Sri Lanka, Burkina Faso, Romania, Kazakhstan, Zambia, Guinea, Rwanda, Benin, Burundi, South Sudan, Dominican Republic, Greece, Azerbaijan, Tajikistan, Hungary, Jersey, Papua New Guinea, Togo, Lao People's Democratic Republic, Paraguay, Libya, Kyrgyzstan, Singapore, Congo, Finland, Norway, Slovakia, Central African Republic, New Zealand, Republic of Moldova,	89

	Eritrea, Albania, Puerto Rico, Namibia, Botswana, Gabon, North Macedonia, Kosovo, Equatorial Guinea, Timor-Leste, Mauritius, Djibouti, Fiji, Guyana, Bhutan, Solomon Islands, Suriname, Brunei Darussalam, Belize, Bahamas, Iceland, Vanuatu, New Caledonia, Barbados, Sao Tome and Principe, Samoa, Saint Lucia, Guam, Grenada, Saint Vincent and the Grenadines, Dominica, Cayman Islands, Guernsey, Bermuda, Marshall Islands, Northern Mariana Islands, Greenland, Saint Kitts and Nevis, Faroe Islands, Anguilla, Wallis and Futuna, Saint Pierre and Miquelon, Falkland Islands	
Cluster 5	Iraq, Malaysia, Chile, Netherlands, Belgium, Cuba, Czechia, Jordan, Portugal, Sweden, United Arab Emirates, Belarus, Austria, Switzerland, Serbia, Lebanon, Denmark, Oman, Palestine, Costa Rica, Ireland, Panama, Kuwait, Croatia, Georgia, Uruguay, Mongolia, Armenia, Qatar, Lithuania, Slovenia, Latvia, Bahrain, Estonia, Cyprus, Réunion, Luxembourg, Montenegro, Cabo Verde, Maldives, Malta, Guadeloupe, Martinique, French Guiana, French Polynesia, Mayotte, Curaçao, Aruba, United States Virgin Islands, Seychelles, Isle of Man, Andorra, Sint Maarten, Monaco, Saint Martin, Turks and Caicos Islands, Liechtenstein, San Marino, Gibraltar, British Virgin Islands, Bonaire, Saint Barthélemy, Holy See.	63

Table 4. Cluster Centre $(\bar{X}_{c,j})$

Cluster	CCT	DCT	PCC	CFR
1	167364.94	5315.25	0.011	0.037
2	29487418.33	536756.33	0.075	0.019
3	4300364.50	116061.13	0.066	0.031
4	182017.34	3350.18	0.020	0.012
5	363638.11	4855.95	0.091	0.011

Table 5. Cluster Characteristics

Cluster	CCT	DCT	PCC	CFR
1	Very low	Medium	Low	Very high
2	Very high	Very high	High	Medium
3	High	High	High	High
4	Low	Very low	Medium	Low
5	Medium	Low	Very high	Very low

Table 5 shows that the members in Cluster 1 have very low COVID-19 number of cases, medium COVID-19 death cases, low spread (postive case per capita) of COVID-19 and very high COVID-19 fatality rate. Cluster 2 has very high confirmed and death cases, high postive case per capita and medium fatality rate. Cluster 3 have high characteristics in all variables. Cluster 4 have low COVID-19 cases and fatality rate, very low death cases and medium spread. The last cluster (Cluster 5) has medium COVID-19 cases, low death cases, very high spread and very low fatality rate.

4. CONCLUSIONS

In this paper, we applied combination of robust clustering use K-Medoids algorithm and principal component analysis for grouping 219 countries in the world based on COVID-19 pandemic case. Based on result and discussion it can be concluded that 219 countries in the world can be divided into five clusters by using k-medoid algorithm. Each cluster has unique characteristic and different form other cluster. Most countries in the world have the COVID-19 related conditions below the world average. However, Madagascar, Australia, Nigeria, Mali and 44 other countries in Cluster 1 have a very low COVID-19 number of cases but very high fatality rate. Indonesia, Mexico, Turkey, Iran, Germany, and 11 other countries in Cluster 3 have high COVID-19 related conditions. While India, USA and Brazil have a very high COVID-19 confirmed and death cases , high COVID-19 spread and medium fatality rate.

AKNOWLEDGEMENT

The abstract of this paper has been presented in **16th APRU Multi-Hazards Symposium 2021** hosted by Disaster Risk Reduction Center Universitas Indonesia in collaboration with Association of Pacific Rim Universities.

REFERENCES

[1] M. Ciotti, M. Ciccozzi, A. Terrinoni, W. C. Jiang, C. Bin Wang, and S. Bernardini, "The COVID-19 pandemic," *Crit. Rev. Clin. Lab. Sci.*, vol. 57, no. 6, pp. 365–388, 2020.

[2] N. Shrestha *et al.*, "The impact of COVID-19 on globalization," *One Heal.*, vol. 11, p. 100180, 2020.

[3] J. F. Hair, W. C. Black, and R. E. Anderson, *Multivariate Data Analysis: Pearson New International Edition*, 7th ed. England: Pearson Education Limited, 2014.

[4] R. A. Johnson and D. W. Wichern, *Applied Multivariate Statistical Analysis*, 6th ed. Pearson Education Limited, 2014.

[5] S. D. A. Larasati, K. Nisa, and N. Herawati, "Robust Principal Component Trimmed Clustering of Indonesian Provinces Based on Human Development Index Indicators," *J. Phys. Conf. Ser.*, vol. 1751, no. 1, pp. 0–8, 2021.

[6] R. Shang, B. Ara, I. Zada, S. Nazir, Z. Ullah, and S. U. Khan, "Analysis of Simple K-Mean and Parallel K- Mean Clustering for Software Products and Organizational Performance Using Education Sector Dataset," *Sci. Program.*, vol. 2021, 2021.

[7] C. Wu *et al.*, "K -Means Clustering Algorithm and Its Simulation Based on Distributed Computing Platform," *Complexity*, vol. 2021, 2021.

[8] B. Suharjo and M. S. U. Utama, "K-Means Cluster Analysis of Sex, Age, and Comorbidities in the Mortalities of Covid-19 Patients of Indonesian Navy Personnel," *JISA(Jurnal Inform. dan Sains)*, vol. 4, no. 1, pp. 17–21, Jun 2021.

[9] X. Jin and J. Han, "K-Means Clustering," in *Encyclopedia of Machine Learning and Data Mining*, C. Sammut and G. I. Webb, Eds. Boston, MA: Springer US, 2017, pp. 695–697.

[10] P. Devi and K. Kaur, "A Robust Cluster Head Selection Method Based on K-Medoids Algorithm to Maximize Network Life Time and Energy Efficiency for Large WSNs," *Int. J. Eng. Res. Technol.*, vol. 3, no. 5, pp. 1430–1432, 2014.

[11] M. A. Ramdani and S. Abdullah, "Application of partitioning around medoids cluster for analysis of stunting in 100 priority regencies in Indonesia," *J. Phys. Conf. Ser.*, vol. 1722, no. 1, p. 012097, Jan 2021.

[12] S. Vishwakarma, P. S. Nair, and D. S. Rao, "A Comparative Study of K-means and K-medoid Clustering for Social Media Text Mining," *Int. J.*, vol. 2, no. 11, pp. 297–302, 2017.

[13] R. P. A, K. S. Vani, J. R. Devi, and D. . N. Rao, "An Efficient Density based Improved K- Medoids Clustering algorithm," *Int. J. Adv. Comput. Sci. Appl.*, vol. 2, no. 6, 2012.
[14] E. Schubert and P. J. Rousseeuw, "Faster k-Medoids Clustering: Improving the PAM, CLARA, and CLARANS Algorithms," in *Lecture Notes in Computer Science (including subseries Lecture Notes in Artificial Intelligence and Lecture Notes in Bioinformatics)*, Oct 2019, vol. 11807 LNCS, pp. 171–187.
[15] R. K. Dinata, S. Retno, and N. Hasdyna, "Minimization of the Number of Iterations in K-Medoids Clustering with Purity Algorithm," *Rev. d'Intelligence Artif.*, vol. 35, pp. 193–199, 2021.
[16] G. Ghufron, B. Surarso, and R. Gernowo, "The Implementations of K-medoids Clustering for Higher Education Accreditation by Evaluation of Davies Bouldin Index Clustering," *J. Ilm. Kursor*, vol. 10, no. 3, pp. 119–128, Jul 2020.
[17] K. Nakagawa, M. Imamura, and K. Yoshida, "Stock price prediction using k-medoids clustering with indexing dynamic time warping," *Electron. Commun. Japan*, vol. 102, no. 2, pp. 3–8, Feb 2019.
[18] R. Hajlaoui, E. Alsolami, T. Moulahi, and H. Guyennet, "An adjusted K-medoids clustering algorithm for effective stability in vehicular ad hoc networks," *Int. J. Commun. Syst.*, vol. 32, no. 12, p. e3995, Aug 2019.
[19] I. H. Rifa, H. Pratiwi, and R. Respatiwulan, "Clustering Of Eartquake Risk in Indonesia Using K-Medoids and K-Means Algorithms," *MEDIA Stat.*, vol. 13, no. 2, pp. 194–205, Dec. 2020.
[20] S. Gultom, S. Sriadhi, M. Martiano, and J. Simarmata, "Comparison analysis of K-Means and K-Medoid with Ecluidience Distance Algorithm, Chanberra Distance, and Chebyshev Distance for Big Data Clustering," *IOP Conf. Ser. Mater. Sci. Eng.*, vol. 420, no. 1, 2018.

ANTIBACTERIAL ACTIVITY OF ETOAC EXTRACT FROM MARINE-DERIVED FUNGUS *ASPERGILLUS NOMIAE* A12-RF AGAINST CLINICAL PATHOGEN BACTERIA, *STAPHYLOCOCCUS AUREUS*

[1]Andi Setiawan, [1]Rosyidatul Lutfiah, [1]Ni L. G. R. Juliasih, [2]Wawan A. Setiawan, [1]John Hendri, [3]Masayoshi Arai

[1] Department of Chemistry, Faculty of Mathematics and Natural Sciences, Lampung University, Bandar Lampung, Indonesia; [2] Department of Biology, Faculty of Mathematics and Natural Sciences, Lampung University, Bandar Lampung, Indonesia; [3] Graduate School of Pharmaceutical Sciences, Osaka University, Suita, Osaka, Japan.
Corresponding author: A. Setiawan, andi.setiawan@fmipa.unila.ac.id

Abstract

Sponge-derived fungi are a potential source for obtaining bioactive secondary metabolites. The aim of the study was to evaluate the *in vitro* antibacterial activity extract from sponge-derived fungi that could inhibit clinical pathogenic bacteria. In this study, nine isolated fungi were selected from deposite of Integrated Laboratory of Innovation and Technology Center, Lampung University. All isolates were maintained in malt extract media. Based on phylogenetic sequencing results, isolate 18A12RF was *Aspergillus nomius* (603 bp) using ITS1-5.8-ITS2. The isolate A12RF was cultivated and co-cultivated on rice solid media in 4 L Erlenmeyer flask to obtain 4.2 g of ethyl acetate extract (EtOAc). After that, the extract was subjected to several chromatographic steps based on bioassay-guided separation. The results of the fractionation of 2.4 g of EtOAc extract obtained 33.8 mg of the active fraction of A12RFBF3. The minimum inhibition concentration (MIC) test for the A12RFBF3 fraction showed inhibition of the growth of clinical bacteria *Staphylococcus aureus* at a concentration of 6.25 μg mL^{-1}. The findings of this study concluded that the crude extract prepared from the A12RF has antibacterial properties against clinical bacteria. This study is an important work as initial information for further studies in the search for new bioactive compounds.

Key Words: antibacterial agent, *Aspergillus nomiae*, bacterial pathogen, marine fungi.

Introduction

The decline in the quality of marine ecosystems due to human activities has serious ecological, social and economic implications. Over the past 4 decades, there has been a 58% decline in the global population of vertebrate species and 31% of marine fauna (WWF 2016). This decrease affects the quality of ecosystem diversity and endangers the sustainability of existing ecosystems. On the other hand, marine ecosystems are a potential source for substances with pharmacological properties (Rateb & Ebel 2011). However, the data that has been reported has not been comparable to the potential that should have been obtained based on the existing biological wealth.

Therefore, it is necessary to make more intensive efforts to obtain information on bioactive compounds contained in marine organisms before damage occurs to marine ecosystems.

Based on the results of studies since 1985, more than 15,000 new secondary metabolites have been identified from marine organisms, many of which having interesting bioactivities (Blunt et al 2009; Al-Dhabi et al 2019). Sponges are the most studied animals among marine invertebrates as a source of diverse bioactive compounds (Varijakzhan et al 2021). However, problems arise in obtaining bioactive compounds in marine biota such as sponges, one of which is a difficult cultivation process. So that a search for bioactive compounds was carried out through the microorganisms found in the sponge. Sponges are famous for their filter feeder properties so there are various kinds of microorganisms that are diverse and specific (Kiran et al 2018). Marine microorganisms have been reported to be able to produce new compounds and are easier to culture than marine macroorganisms (Blunt et al 2015). The utilization of marine microorganisms as a new source of bioactive compounds is able to avoid overexploitation of marine resources and the practice of over-taking marine biota (Romano et al 2017). Furthermore, the large amount of fungal biodiversity derived from sponges has not been fully investigated. This indicates that there are still many undiscovered metabolites.

Sponges are invertebrate animals that are filter feeders so they can contain various kinds of microorganisms. As much as 40% of the sponge's volume consists of microorganisms (Vacelet & Donadey 1977). The presence of microorganisms in the body of a sponge can be varied and specific. This is a consideration for the development of the search for bioactive compounds through marine microorganisms. As recently reported, epidithiodiketopiperazine DC1149B which has cytotoxic activity was obtained from the sponge-derived fungus *Trichoderma lixii* (Tang et al 2020). However, new problems arise in the fungi cultivation process to get bioactive compounds such as dereplication and loss of fungi ability to produce target compounds. To overcome this problem, it is necessary to carry out a fungal co-cultivation process with different microorganisms. Co-cultivation technique is a simple method that aims to increase the production of bioactive secondary metabolites. As has been successfully reported by Jomori et al (2020), the co-culture of *Aspergillus niger* originating from the sea with *Mycobacterium smegmatis* produced malforming C and TMC-256A1 which have cytotoxic properties.

In this study, we aimed to evaluate the *in vitro* antibacterial activity of EtOAc extract from sponge-derive fungi that could inhibit clinical pathogenic bacteria with resistance to several antibiotics. Moreover, we report a new method for the efficient production of antibacterial extracts from fungi cultured using solid fermentation technique using rice media. This initial information is very important for further development of the search for new antibiotic compounds that can inhibit the growth of resistant bacteria.

Material and Method

Isolation of fungi from marine sponges.

Marine organisms, especially sponges, were selected for fungal isolation. Sponge samples were collected from Singaraja, Buleleng, Bali, Indonesia in August 2018. Samples were collected along the sea coast (8°07'20.9"S 114°34'03.8"E) at depths of 5-20 m by SCUBA diving. A small piece of sponge was rinsed and homogenized in sterile seawater. The homogenate was submitted to serial dilution and spread on plates of Malt Extract (ME) (105397, Merck kGAa Germany) and Trypthic Soy Broth (TSB) (105459, Merck kGAa Germany) agar prepared with 50% (v/v) seawater and cultured at 28°C for 7 days. Fungi were isolated and purified on ME TSB agar medium prepared with 50% (v/v) seawater.

The purified isolate was streaked on slants of ME TSB agar at 4°C and in glycerol 20% (v/v) suspensions at -20°C.

Cultivation and co-cultivation

Cultivation. Fungal isolates were grown on ME media and TSB (10 mL) and then cultivated for 2-4 days with shaking at 100 rpm. After the fungus grows, the fungi inoculum was poured into the rice medium consisting of 100 g of rice in 110 mL of sterile artificial seawater (ASW). After that, it was cultivated at 30°C for 1 week under static conditions.

Co-cultivation. For co-cultivation, 10 mL inoculum bacterial broth (1.0 x 10^8 CFU mL^{-1} Mc Farland) was prepared in TSB (Tryptic Soy Broth) (Merck, KGaA) medium and incubated overnight at 37°C. Then, *S. aureus* inoculum was added to the fourth day of fungal cultivation. Co-cultivation was carried out at 30°C for 14 days (Frank et al 2019; Jomori et al 2020). The cultivation and co-cultivation processes were repeated three times. The fungal biomass from cultivation and co-cultivation was then extracted with EtOAc. The extraction results were then concentrated under reduced pressure using a vacuum rotary evaporator (Büchii RA 210 with vacuum pump V-100, Switzerland) to obtain the crude EtOAc extract for further experiments.

Clinical pathogenic multidrug resistance (MDR) bacteria.

The clinical pathogenic *S. aureus* and *Pseudomonas aeruginosa* which were used in this study were collected from General Hospital Abdoel Moeloek, Bandar Lampung. For inoculum preparation, *S. aureus* and *P. aeruginosa* were re-cultured on nutrient agar (105450 Merck KGaA, Germany) at 37°C for 18 h, and then inoculated in TSB. Turbidity was adjusted to 0.5 standard McFarland (equal to 5 x 10^8 CFU mL^{-1}). The disc diffusion method (Kwasny & Opperman 2010) was used to determine the sustainability of *S. aureus* and *P. aeruginosa* to several commercial antibiotics. According to the CLSI guidelines (2017), test results showed *S. aureus* was resistant to amoxicillin (25 µg), ciprofloxacin (5 µg), and clindamycin (2 µg), while *P. aeruginosa* was resistant to amoxicillin (25 µg), ciprofloxacin (5 µg), clindamycin (2 µg), and chloramphenicol (30 µg).

Screening antibacterial activity against clinical pathogen.

The fungi extract was screened using a 96-well plate assay according to CLSI guidelines (CLSI 2017). Briefly, serial two-fold dilutions of the extract were prepared by dissolving 2 mg of fungi extract in 1 mL of 12.5% methanol (range, 500 to 3.9 µg mL^{-1}) and 50 µL of extract solution and 25 µL of bacterial suspension added to each well. The bacterial suspension was prepared from 12 h pure colonies of *S. aureus* and *P. aeruginosa*. Suspensions were adjusted to 0.5 McFarland standard turbidity (10^6 CFU mL^{-1}) and subsequently incubated for 18-24 h at 37°C. Wells with 12.5% MeOH were used as solvent control and wells without bacteria were used as contamination control. An extract control was also included. The plates were prepared in triplicates, and placed in an incubator for 18 hours at 37°C. After that, resazurin was added and incubated for 8 hours, and the absorbance (Abs) values were measured at 630 nm using Hospitex reader (Italy). Furthermore, the minimum inhibition concentration (MIC) test was carried out on only the active extract (Elsikh et al 2016).

Morphology of fungus A. nomiae.

Fungi were spotted on slides and covered with coverslips and then were identified morphologically as fungi with light microscopy, using an Observer A1 Zeiss microscope. ME and TSB agar was poured on sterile slides and allowed to solidify. Then organisms were streaked on it and incubated at 37°C for 2-3 days (Goodfellow et al

2012). Scanning Electron Microscopy (SEM) was performed to study the mycelial and spore arrangements of isolated fungi. Fungi were grown on standard media after 4 days, and a small part of the coverslip was cut off using a microtome SLEE Disposable Blades to obtain a piece of 0.5 cm x 0.5 cm with a thickness of 0.1 cm. Prepared samples were placed on stubs, which were fixed with carbon adhesive tabs. Prepared samples were placed on stubs, which fixed with carbon adhesive tabs. The upper surface of each stub was then coated, under vacuum, with a film of gold. The gold coating (Quorum Q150R ES, Germany) process was completed in ~ 20 min. The gold-coated metal stubs were viewed on the SEM (Zeiss EVO MA10, Germany) at an accelerating voltage of 20 kV.

DNA extraction and PCR amplification.

Fungal genomic DNA was extracted as previously described by Landum et al (2016), in accordance to the manufacturer's instructions, using the QIAamp DNA Minikit (Qiagen, Germany). The nuclear ribosomal DNA internal transcribed spacer (ITS) of the fungal isolates was amplified using the forward primer, ITS1-F (5′-TCCGTAGGTGAACCTGCGG-3′) and the reverse primer, ITS4-R (5′-TCCTCCGCTTATTGATATGC-3′) (White et al 1990). The final reaction volume was 20.5 µL, containing 10 µL of PCR kit NEXpro TM (PCR Biosystems, UK), 0.25 µL of forward, 0.25 µL reverse primers, 5 µL ddH_2O, and 5 µL of genomic DNA template. For negative control, the DNA was replaced with distilled water to verify the absence of contamination. PCR was carried out using Sensoquest Sensodirect Gradient Termo block 96 (SensoQuest, Germany), programmed for 5 min at 94°C; 35 cycles for 1 min at 94°C, 1 min at 52°C, and 1 min at 72°C; and a final 5 min extension at 72°C. The PCR products were separated using 2% agarose gel in 1X TAE buffer (40 mM Tris-acetate and 1 mM EDTA, pH 8.0), stained with ethidium bromide (0.5 µg mL^{-1}) and documented using Qiaxcell Advanced (Qiagen, Germany). PCR products were sent for direct bi-directionally sequencing using ABIPRISM3730 × 1 Genetic Analyzer (Applied Biosystems, USA) at the First BASE Laboratory Sdn. Bhd., Selangor, Malaysia.

Sequence and phylogenetic analysis.

The resulting DNA sequences were aligned using MUSCLE software embedded in MEGA 7 (Kumar et al 2016), manually trimmed and edited to obtain complete sequences. Homology searches were carried out using the BLASTn program against the NCBI *GenBank* database (https://blast.ncbi.nlm.nih.gov/ Blast.cgi). The appropriate DNA substitution models for the ITS gene was assessed using the "find best DNA/Protein Models" function embedded in the software MEGA 7. Futhermore the maximum likelihood (ML) statistical method was used to test the goodness of fit against various models of evolution. According to the estimated values of all parameters for each model, the model best fitting to the dataset from the ITS sequences was general time reversible (GTR) model and gamma distributed (+G) with invariant sites (+I) (=GTR+G+I) model. ML tree was constructed using MEGA 7 with all positions containing gaps and missing data were included for analysis. Clade supports were calculated based on 1,000 bootstrap resamplings.

Extraction, fractionation and MIC test.

Fungi biomass was harvested using EtOAc extraction. Filtrate of the EtOAc extract was concentrated by evaporation under reduced pressure. The EtOAc extract was partitioned into a water–ButOH mixture (1:1). Fractionation was carried out on the basis of bioassay-guided separation. The MIC test was carried out on the active fraction obtained following the Elsikh et al (2016) method.

Results and Discussion

Sample collection and isolation of fungus.

Marine organisms were collected at Singaraja, Buleleng, Bali, Indonesia. During a one-week collection trip, nine sponges were collected along the coast (8°07'20.9"S 114°34'03.8" E) at a depth of 5-25 meters. Identification of marine organisms based on their physical form and the presence of spicules showed that all specimens were sponges belonging to the genus *Desmospongiae*. After going through the process of enrichment and purification on agar media, nine fungi were isolated from the sample of sponges as shown in Table 1.

Table 1 Isolate fungi from marine organisms

No.	*Sponge code*	*Species*	*Isolate fungus*	*Color*
1	18A02	*Callyspongia armigera*	18A02RF	White
2	18A12	Unidentified	18A12RF	White-orange
3	18B15	*Plakina jamaicensis*	18B15RF	White
4	18B20	*Cinachyrella kuekenthali*	18B20RF	White
5	18B21	*Niphates alba*	18B21RF	White
6	18B23	*Diplastrella* sp.	18B23RF	White
7	18C24	*Batzella* sp.	18B24RF	White
8	18E41	*Niphates erecta*	18E41RF	White
9	18E42	*Aplysina cauliformis*	18E42RF	White

The presence of microorganisms in the body of the sponge is certainly related to its filter feeder nature (Müller 2003). Furthermore, the presence of fungi in marine organisms such as sea fans, corals, and macroalgae (Loque et al 2009; Amend et al 2012) has also been reported. However, studies show that the fungi originating from the sea have a relatively small number, which is about 0.6% of the total number of fungi globally. It is estimated that there are still many fungi that have not been isolated (Burgaud et al 2009). In addition, fungi have a role in marine ecosystems as saprophytes in dead organisms, and symbionts (parasites, commensals, and mutualists) in living marine organisms (Raghukumar 2017).

Screening antibacterial activities.

Antibacterial screening tests have been carried out on nine extracts of fungal isolates prepared from cultivation and co-cultivation on rice media. The test results on clinical pathogenic bacteria, *S. aureus*, and *P. aeruginosa* are shown in Figures 1 and 2. Crude extracts from cultivation and co-cultivation results show differences in antibacterial activity. The test results of fungal extracts prepared from co- cultivation against *S. aureus* (Figure 1) showed a significant increase in the inhibitory activity, especially in the 18A12RF extract. Meanwhile, the co-cultivation process had no significant effect on the other isolates.

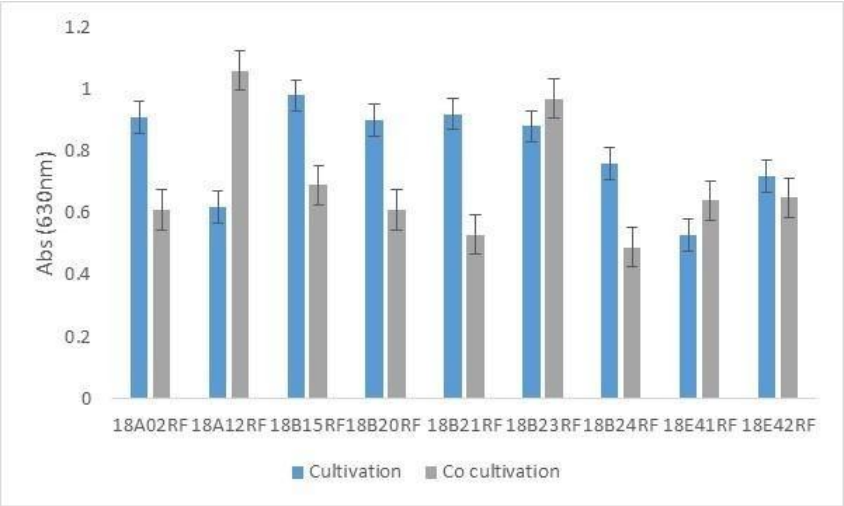

Figure 1. Screening extract EtOAc (cultivation and co cultivation) of isolate fungus against S. *aureus.*

Different results also occurred in the screening tests for *P. aeruginosa*. Nine extracts of co-cultivated fungal isolates that were tested showed an increase in the ability to inhibit the growth of *P. aeruginosa* (Figure 2). The increase in antibacterial activity in the co- cultivation process could be due to competition between different microorganisms for self-defence, thereby triggering the formation of secondary metabolites through activation and transcription under stress conditions. The competition or antagonism experienced during co-cultivation was shown to lead to significantly enhanced compound production and the accumulation of undetectable cryptic compounds in axenic cultures of the producing strains. Co-cultivation proves that this experimental approach increases chemical productivity (Li et al 2011).

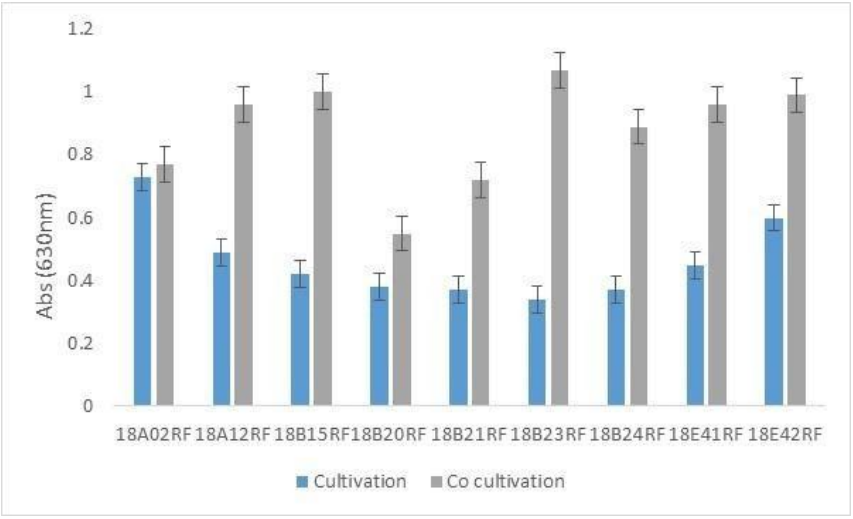

Figure 2. Screening extract EtOAc (cultivation and co cultivation) of isolate fungus against *P. aeruginosa.*

Morphology of fungus 18A12RF.

Visual observation of fungi cultivated in media showed mycelia penetrating the substrate, while mycelia grew vertically at the media-air interface. Under microscopic observation, all isolated fungi had an average mycelium diameter of ~5 microns. This is larger than many fungi which have mycelia of 1-2 microns (Toledo-Hernandez et al 2008).

The microscopic characteristics of 18A12RF are shown in Figure 3. Under the microscope, the conidiophores of 18A12RF were colourless, thick-walled, roughed, and bearing vesicles. The diameter of the conidiophores ranged from 2.5 to 3 µm. The vesicle shape of 18A12RF was globose to sub-globose. The diameter of the vesicles ranged from 20 to 30 µm. The cells were uniseriate or biseriate. In the biseriate cells, the phialides grew on the metulae whereas, in uniseriate cells, they grew on the vesicles. The metulae enclosed the vesicles surface and emitted in all directions. The conidia were globose, thin walled, slightly roughed, and oblong ranged from 2.5 to 3 µm in diameter.

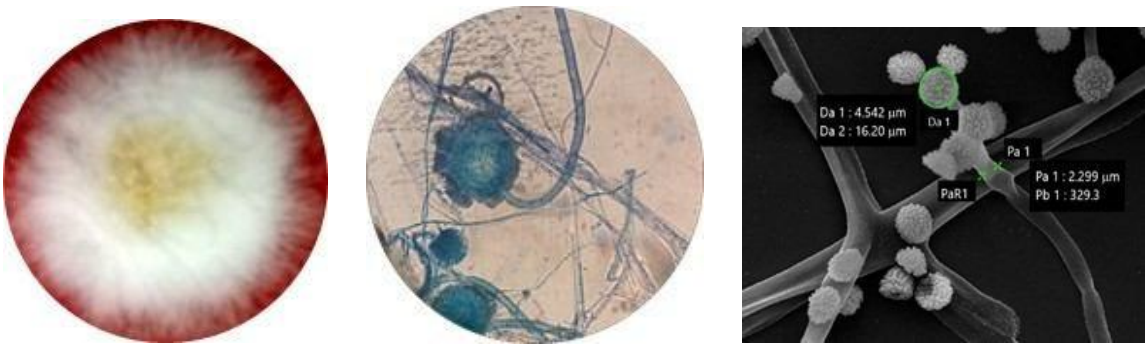

(a) (b) (c)

Figure 3. (a). Isolate 18A12RF in standard media; (b) Visualization of 18A12RF, scale 400x; (c) SEM (Scanning Electron Microscope) image.

Scanning electron microscopy (SEM) revealed that the mycelia were composed of branched, septate, smooth-walled hyphae 1.3 to 2.7 µm wide (mean = 2.1 µm). Conidial heads radiated, normally splitting into two to four dense columns (up to 500 µm long) with age. Stipes were 69 to 242 µm long (mean = 181 µm), were 3.7 to 6.0 µm wide (mean = 5.3 µm), had rough walls, and were light orange pigmented. Vesicles were globose, 6.8 to 10.9 µm in diameter (mean = 8.9 µm), and biseriate. Metulae were smooth walled and cylindrical, measuring 1.7 to 3.1 (mean = 2.6) × 1.7 to 2.1 (mean = 1.9) µm. Phialides were smooth walled and flask shaped, measuring 4.3 to 5.7 (mean = 4.8) × 1.2 to 1.3 (mean = 1.2) µm, with 0.6 to 1.4 µm-long collula. Conidia were middle orange-yellow and globose to subglobose when mature, measuring 1.4 to 1.7 (mean = 1.5) µm (Figures 3a to 3c), and roughened. A teleomorphic state was not observed. Based on the observations and descriptions above, isolate 18A12RF is a fungus that belongs to the *Aspergillus* group.

Phylogenetic analysis.

ITS1-5.8S-ITS4 sequence region (603 base pairs (bp)), deposited in GenBank with accession number LC638671) of strain 18A12RF was amplified by PCR and sequenced. A phylogenetic tree was constructed, using the maximum- likelihood method and Tamura 3-parameter model based on the similarity of a 603-bp consensus length of the ITS1-5.8S-ITS4 sequence. Thirty *Aspergillus* representatives along with *Emericella nidulans* (Acc. No. HQ026740) as an outgroup were used (Figure 4). Strain 18A12RF was found to belong to a clade related to A. *nomiae* in the tree, with sequence identities of 99% respectively. The properties of culture and morphology of strain 18A12RF were

consistent with those of A. *nomiae* as previously. The ITS phylogenetic analyses confirmed that the fungus strain A12-RF belonged to A. *nomiae*, and was designated as A. *nomiae* A12-RF.

Fractionation and MIC test.

An EtOAc extract 18A12RF (2.4 g) that exhibited antibacterial activity against S. *aureus* and P. *aeruginosa* at 250 µg mL^{-1} was partitioned into a ButOH-water mixture to obtain a ButOH soluble portion A12RFB (0.8 g). The ButOH soluble portion showed growth inhibition at 62.5 µg mL^{-1} against S. *aureus*. This fraction A12RFB was subjected to SiO_2 gel open column chromatography eluted with n- hexane and isopropanol, affording four fractions: 252.2 mg A12RFBF1 (eluted with n-hexane: isopropanol 5:1), 35.4 mg A12RFBF2 (eluted with n-hexane: isopropanol 5:1), 33.8 mg A12RFBF3, and 107.9 mg A12RFBF4 (eluted with n-hexane: isopropanol 7:3). Each fraction was subjected to a MIC assay. The fractions A12RFBF3 and A12RFBF2 inhibited growth of S. *aureus* and P. *aeruginosa* most effectively at a concentration of
6.25 and 125 µg mL^{-1} respectively (Figure 5).

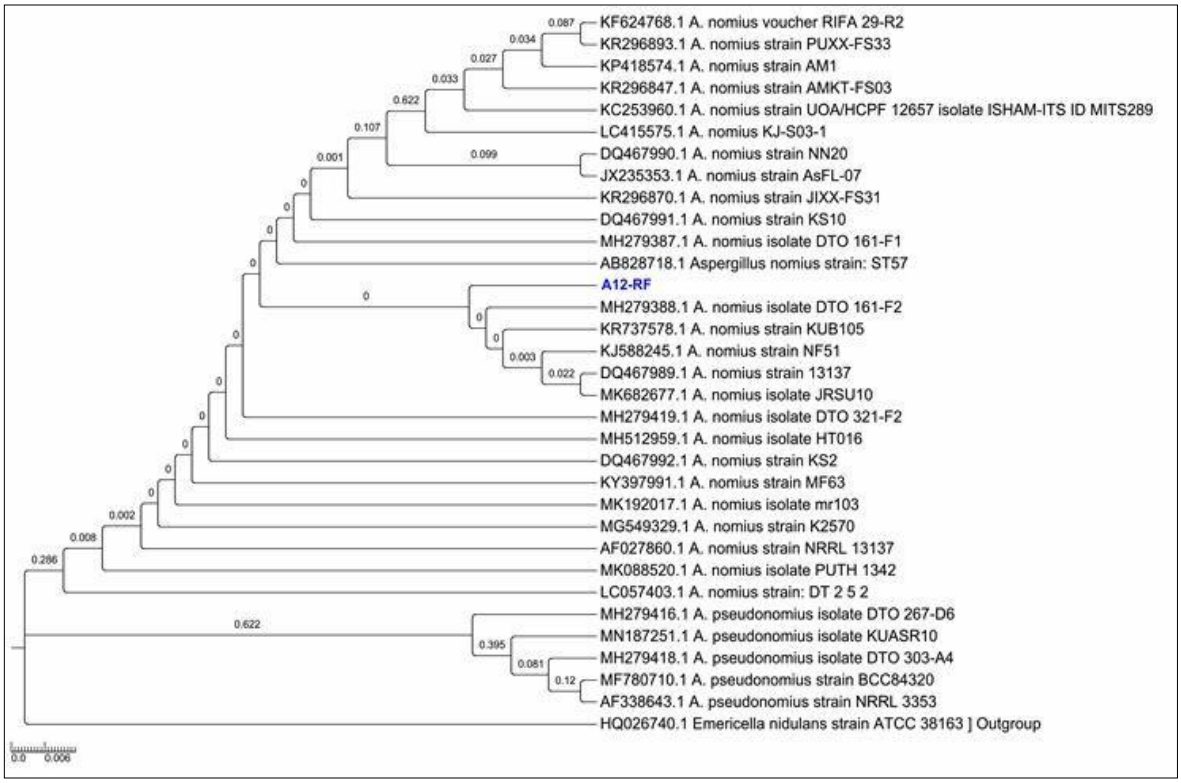

Figure 4. Phylogenetic tree strain A12-RF.

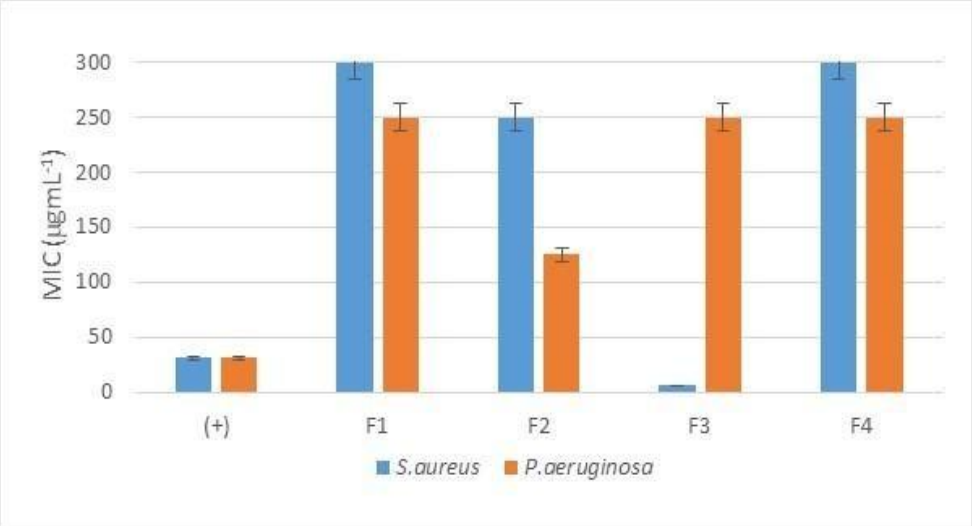

Figure 5. Minimum inhibitory concentration of fraction A12RFB (F1-F4) control (+) = chloramphenicol).

Conclusions.

The finding of the present study concluded that the extract prepared from *Aspergillus nomiae* A12-RF had bioactive metabolites with antibacterial properties. The extract fraction A12-RFBF3 inhibited the growth of clinical bacteria *S. aureus* (6.25 µg mL^{-1}) and the fraction A12-RFBF2 inhibited the growth of clinical bacteria *P. aeruginosa* (125 µg mL^{-1}), both of which were resistant to several antibiotics. This study builds on the work for further studies on the development of antibacterial agents.

Acknowledgements.

The authors would like to thank The Deputy of Research Strengthening and Development, The Ministry of Research and Technology/National Agency for Research and Innovation of the Republic of Indonesia, for Basic Research with Grand No. 3972/UN26.21/PN/2021. This research was also partially supported by the Platform Project for Supporting Drug Discovery and Life Science Research (Basis for Supporting Innovative Drug Discovery and Life Science Research (BINDS)) from the Japan Agency for Medical Research and Development (AMED) (grant no. JP21am0101084), the Kobayashi International Scholarship Foundation, and a Grant-in- Aid for Scientific Research B (grant nos. 18H02096, 17H04645 and 21H02069) from the Japan Society for the Promotion of Science (JSPS) to MA. The authors also thank the Technical Service Unit, Integrated Laboratory of Innovation and Technology Center, Lampung University for providing scanning electron microscopy facilities.

Conflict of interest. The authors declare that there is no conflict of interest.

References

Al-Dhabi N. A., Ghilan A. K. M., Esmail G. A., Arasu M. V., Duraipandiyan V., Ponmurugan K., 2019 Bioactivity assessment of the Saudi Arabian marine *Streptomyces* sp. Al-Dhabi-90, metabolic profiling and its *in vitro* inhibitory property against multidrug resistant and extended-spectrum beta-lactamase clinical bacterial pathogens. Journal of Infection and Public Health 12(4):549-556.

Amend A. S., Barshis D. J., Oliver T. A., 2012 Coral-associated marine fungi form novel lineages and heterogeneous assemblages. The ISME Journal 6:1291-1301.

Blunt J. W., Copp B. R., Hu W. P., Munro M. H. G., Northcote P. T., Prinsep M. R., 2009 Marine natural products. Natural Product Reports 26:170-244.

Blunt J. W., Copp B. R., Keyzers R. A., Munro M. H. G., Prinsep M. R., 2015 Marine natural products. Natural Product Reports 32(2):116-211.

Burgaud G., Le Calvez T., Arzur D., Vandenkoornhuyse P., Barbier G., 2009 Diversity of culturable marine filamentous fungi deep-sea hydrothermal vents. Environmental Microbiology 11(6):1588-1600.

CLSI, 2017 Performance standards for antimicrobial susceptibility testing. ^{27}th edition. CLSI supplement M100. Wayne, PA: Clinical and Laboratory Standards Institute, pp. 162-168.

Elshikh M., Ahmed S., Funston S., Dunlop P., Mc-Gaw M., Marchant R., Banat I. M., 2016 Resazurin-based 96-well plate microdilution method for the determination of minimum inhibitory concentration of biosurfactants. Biotechnology Letters 38(6): 1015-1019.

Frank M., Ozkaya F. C., Muller W. E. G., Hamacher A., Kassack M. U., Lin W., Liu Z., Proksch P., 2019 Cryptic secondary metabolites from the sponge-associated fungus *Aspergillus ochraceus*. Marine Drugs 17(2):99.

Goodfellow M., Kampfer P., Dusse H. J., 2012 Bergey's manual of systematic bacteriology. 2nd edition. Springer, New York, USA, pp. 785-787.

Jomori T., Hara Y., Sasaoka M., Harada K., Setiawan A., Hirata K., Kimishima A., Arai M., 2020 *Mycobacterium smegmatis* alters the production of secondary metabolites by marine-derived *Aspergillus niger*. Journal of Natural Medicines 74(1):76-82.

Kiran G. S., Sekar S., Ramasamy P., Thinesh T., Hassan S., Lipton A. N., Ninawe A. S., Selvin J., 2018 Marine sponge microbial association: towards disclosing unique symbiotic interactions. Marine Environmental Research 140:169-179.

Kumar S., Stecher G., Tamura K., 2016 MEGA7: molecular evolutionary genetics analysis Version 7.0 for bigger datasets. Molecular Biology and Evolution 33(7):1870-1874.

Kwasny S. M., Opperman T. J., 2010 Static biofilm cultures of Gram-positive pathogens grown in a microtiter format used for anti-biofilm drug discovery. Current Protocols in Pharmacology. Chapter 13:Unit 13A.8. doi: 10.1002/0471141755.ph13a08s50.

Landum M. C., do Rosário Félix M., Alho J., Garcia R., Cabrita M. J., Rei F., Varanda C. M. R., 2016 Antagonistic activity of fungi of *Olea europaea* L. against *Colletotrichum acutatum*. Microbiological Research 183:100-108.

Li C., Zhang J., Shao C., Ding W., She Z., Lin Y., 2011 A new xanthone derivative from the co-culture broth of two marine fungi (strain No. E33 and K38). Chemistry of Natural Compounds 47(3):382-384.

Loque C. P., Medeiros A. O., Pellizarri F. M. Oliveira E. C., Rosa C. A., Rosa L. H., 2009 Fungal community associated with marine macroalgae from Antarctica. Polar Biology 33:641-648.

Müller W. E. G., 2003 Sponges (Porifera). Berlin, Springer, 258 pp.

Raghukumar S., 2017 The marine environment and the role of fungi. In: Fungi in coastal and oceanic marine ecosystems. Springer, Cham., pp. 17-38.

Rateb M. E., Ebel R., 2011 Secondary metabolites of fungi from marine habitats. Natural Product Reports 28(2):290-344.
Romano G., Costantini M., Sansone C., Lauritano C., Ruocco N., Ianora A., 2017 Marine microorganisms as a promising and sustainable source of bioactive molecules. Marine Environmental Research 128:58-69.
Tang R., Kimishima A., Ishida R., Setiawan A., Arai M., 2020 Selective cytotoxicity of epidithiodiketopiperazine DC1149B, produced by marine-derived *Trichoderma lixii* on the cancer cells adapted to glucose starvation. Journal of Natural Medicines 74(1):153-158.
Toledo-Hernandez C., Zuluaga-Montero A., Bones-Gonzales A., Rodriguez J. A., Sabat A. M., Bayman P., 2008 Fungi in healthy and diseased sea fans (*Gorgonia ventalina*): is *Aspergillus syndowii* always the pathogen? Coral Reefs 27(3):707-714.
Vacelet J., Donadey C., 1977 Electron microscope study of the association between some sponges and bacteria. Journal of Experimental Marine Biology and Ecology 30(3): 301-314.
Varijakzhan D., Loh J. Y., Yap W. S., Yusoff K., Seboussi R., Lim S. H. E., Lai K. S., Chong C. M., 2021 Bioactive compounds from marine sponges: fundamentals and applications. Marine Drugs 19(5):246.
White T. F., Bruns T. D., Lee S. B., Taylor J. W., 1990 Amplification and direct sequencing of fungal ribosomal RNA genes for phylogenetics. In: PCR protocols: a guide to methods and applications. Innis M. A., Gelfand D. H., Sninsky F. S., White T. T. (eds), Academic Press, New York, pp. 315-322.
WWF, 2016 Living planet report 2016. Risk and resilience in a new era. Gland: WWF International, 144 pp.

BILANGAN KROMATIK LOKASI GRAF SPLIT LINTASAN

Siti Rahmatalia, Asmiati[1]*, Notiragayu

Jurusan Matematika, Fakultas MIPA, Universitas Lampung
Jl. Brodjonegoro No. 1 Bandar Lampung, Indonesia 35145
Email* : asmiati.1976@fmipa.unila.ac.id

Abstrak

Bilangan kromatik lokasi graf merupakan pengembangan dari konsep dimensi partisi dan pewarnaan titik suatu graf. Banyaknya warna minimum pada pewarnaan lokasi dari graf G disebut bilangan kromatik lokasi graf G. Pada paper ini dibahas tentang bilangan kromatik lokasi graf split lintasan dan graf barbel split lintasan. Metode yang digunakan untuk mendapatkan bilangan kromatik lokasi dari graf tersebut adalah dengan menentukan batas atas dan batas bawahnya. Hasil yang diperoleh bahwa bilangan kromatik lokasi dari graf split lintasan dan barbelnya adalah sama yaitu 4.

Kata kunci: bilangan kromatik lokasi, graf split lintasan, graf barbel split lintasan.

Abstrak

The locating chromatic number of a graph extends the partition dimension and vertex coloring of a graph. The minimum number of locating coloring of graph G is called the locating chromatic number of graph G. This paper will discuss the locating chromatic number of path split graph and barbell path split graph. The method used to obtain the locating chromatic number of the graph is to determine the upper and lower bound. The results obtained are that the path split graph's locating chromatic number and the barbell are the same, namely 4.

Keywords: *locating-chromatic number of graph, path split graph, barbell path split graph*

1. Pendahuluan

Konsep pewarnaan graf muncul sebagai model dalam menyelesaikan permasalahan pewarnaan peta. Pada tanggal 23 Oktober 1852, Frederick Guthri (1833-1886), mahasiswa di University College London, mengunjungi professor matematika, Augustus De Morgan (1806-1871), untuk menyampaikan penemuan matematika dari kakak lelakinya, Francis Guthrie (1831-1899). Beliau mendapatkan konjektur empat warna (*The Four Color Conjecture*) yang menyatakan: Semua negara di peta dapat diwarnai dengan menggunakan maksimal emapat warna sedemikian sehingga dua negara yang berbatasan mempunyai warna berbeda. Keinginan yang kuat dari para matematikawan untuk menyelesaikan permasalahan empat warna tersebut menginspirasi munculnya konsep pewarnaan daerah, titik, sisi, dan graf planar. Konsep inilah yang digunakan untuk mewarnai graf secara umum.

Bilangan kromatik lokasi yang diperkenalkan oleh Chartrand, dkk.[1], pada tahun 2002 merupakan penggabungan dari konsep dimensi partisi graf [2] dan pewarnaan graf. Dimensi metric pertama kali diperkenalkan oleh Harary dan Melter [3] pada tahun 1976. Banyak aplikasi yang dapat diterapkan menggunakan konsep dimensi metrik graf diantaranya adalah navigasi robotik [4], optimisasi penempatan sensor kebakaran [5], dan klasisfikasi data senyawa kimia [6]. Bilangan kromatik lokasi suatu graf merupakan pengelompokan titik berdasarkan warnanya yang disebut kelas-kelas warna dengan syarat setiap titik pada graf tersebut mempunyai kode warna berbeda.

Berikut ini diberikan definisi bilangan kromatik lokasi graf yang diambil dari Chartrand, dkk. [1]. Misalkan G graf terhubung dan berhingga. Misalkan c suatu pewarnaan titik pada graf G dengan $(c(u) \neq c(v))$ untuk setiap u,v yang bertetangga di G. Partisi $\Pi = \{C_1, C_2, \ldots, C_k\}$ adalah himpunan yang terdiri dari kelas - kelas warna $C_i, 1 \leq i \leq k$dari $V(G)$ yang menginduksi pewarnaan titik c. Jarak suatu titi v ke titik x dinotasikan dengan $d(v,x)$ adalah panjang lintasan terpendek dari kedua titik tersebut. Kode warna,$c_\Pi(v)$ dari v adalah$k$-ordinat terurut $(d(v,C_1), d(v,C_2), \ldots, d(v,C_k))$ dengan $d(v,C_i) = \min\{d(v,x)|x \in C_i\}$ untuk $1 \leq i \leq k$. Jika setiap titik di $V(G)$ mempunyai kode warna yang berbeda, maka c disebut pewarnaan lokasi dari graf G. Banyaknya warna minimum yang digunakan untuk pewarnaan lokasi disebut bilangan kromatik lokasi dari G, dan dinotasikan dengan $\chi_L(G)$.

Kajian tentang bilangan kromatik lokasi pada suatu graf masih menarik hingga saat ini karena belum terdapatnya suatu teorema yang dapat digunakan untuk menentukan bilangan kromatik lokasi sebarang graf. Chartrand, dkk. [1] telah berhasil menentukan bilangan kromatik lokasi beberapa kelas graf, diantaranya pada graf lengkap, siklus, lintasan, dan pohon. Setahun setelahnya Chartrand, dkk. [7] telah mengkarakterisasi graf berorde n dengan bilangan kromatik lokasi $(n-1)$. Asmiati, dkk. [8] telah berhasil mendapatkan bilangan kromatik lokasi amalgamasi bintang. Kemudian Behtoei, dkk. [9] berhasil menentukan bilangan kromatik lokasi graf kneser. Welyyanti, dkk. [10] telah mendapatkan hasil bilangan kromatik untuk graf dengan titik dominan. Selanjutnya, Asmiati [11] telah mendapatkan bilangan kromatik lokasi pada graf ulat dan kembang api yang tidak seragam. Setahun kemudian, Asmiati [12] memperoleh bilangan kromatik lokasi n amalgamasi bintang yang dihubungkan oleh suatu lintasan.

Hal menarik lainnya adalah karakterisasi graf berbilangan kromatik lokasi tertentu yang telah dikajioleh Chartrand, dkk.[7]. Mereka telah mengkarakterisasi graf berbilangan kromatik lokasi $(n-1)$ atau $(n-2)$. Selanjunya Asmiati dan Baskoro [13] tahun 2012, telah berhasil mengkarakterisasi graf memuat siklus berbilangan kromatik lokasi tiga. Baskoro dan Asmiati [14] telah menentukan karakterisasi graf pohon berbilangan kromatik lokasi 3. Pada tahun 2017, Asmiati, dkk. [15] telah memperoleh karakterisasi graf Petersen berbilangan kromatik lokasi 4 atau 5.

Kajian bilangan kromatik lokasi dan variannya juga terus berkembang sampai saat ini. Pada tahun 2018, Asmiati, dkk. [16] telah mendapatkan bilangan kromatik lokasi dari graf barbel dengan graf pembentuknya adalah graf lengkap dan graf Petersen diperumum. Kemudian Asmiati, dkk.[17] juga telah berhasil melanjutkan bilangan kromatik lokasi untuk subdivisi dari graf barbel memuat graf Petersen diperumum. Pada graf origami, Irawan, dkk.[18] telah berhasil menentukan bilangan kromatik lokasinya dan menganalisis graf barbelnya dan dilanjutkan oleh Irawan, dkk.[15] untuk subdivisinya. Selanjutnya, pada tahun 2021, Asmiati, dkk.[19] telah berhasil menganalisis bilangan kromatik lokasi graf shadow lintasan dan graf barbelnya. Prawinasti, dkk. [20] telah menentukan bilangan kromatik lokasi graf split siklus dan Damayanti, dkk. [21] untuk bilangan kromatik lokasi dari beberapa modifikasi graf lintasan dengan siklus.

Sejauh penelusuran literatur belum terdapat kajian tentang bilangan kromatik lokasi dari graf split lintasan. Berdasarkan hal tersebut, maka pada paper ini didiskusikan tentang bilangan kromatik lokasi dari graf split lintasan dan graf barbel split lintasan.

Graf split lintasan yang dinotasikan dengan $spl(P_n)$ adalah graf dengan himpunan titik $V(spl(p_n)) = \{u_i, v_i\ ;\ 1 \le i \le n\}$, dan himpunan sisi $E(spl(P_n)) = \{u_i n_{i+1}\ ; i \in [1, n-1]\} \cup \{v_i u_{i+1}\ ;\ i \in [1, n-1]\}$. Graf barbel split lintasan $B_{spl(P_n)}$ adalah graf sederhana yang diperoleh dari tiruan graf split lintasan yang dihubungkan oleh suatu jembatan, yaitu sisi $\left(\frac{u_{n+1}}{2}\frac{u'_{n+1}}{2}\right)$ untuk n ganjil dan $\left(\frac{u_n}{2}\frac{u'_n}{2}\right)$ untuk n genap, dengan himpunan titik tiruan graf splitnya adalah $\{u'_i, v'_i\ ;\ 1 \le i \le n\}$.

Teorema berikut merupakan batas bawah dari bilangan kromatik lokasi graf yang telah dibuktikan oleh Chartrand, dkk. [1].

Teorema 1.1. (Chartrand, dkk. [1]) Untuk setiap graf terhubung G berorde $n \ge 3$ memenuhi $3 \le \chi_L(G) \le$ n.

2. Hasil dan Pembahasan

Pada bab ini dibahas bilangan kromatik lokasi pada graf split lintasan yang dinotasikan dengan $spl(P_n)$ dan graf barbel dari graf split lintasan yang dinotasikan dengan $B_{spl(P_n)}$.

2.1 Bilangan Kromatik Lokasi Graf Split Lintasan

Berikut ini diberikan contoh penentuan bilangan kromatik lokasi graf $spl(P_6)$ akan ditentukan terlebih dahulu batas bawah bilangan kromatik lokasi dari graf. Karena graf split lintasan $spl(P_6)$ berorde $n \ge 3$, sehingga berdasarkan Teorema 1.1 membutuhkan sekurang-kurangnya 3 warna. Andaikan c pewarnaan lokasi pada $(spl(P_n))$ menggunakan 3 warna. Tanpa mengurangi perumuman, misalkan $c(u_1) = c(v_1) = 1$ maka, $\{c(u_2), c(v_2)\} = \{2,3\}$. Akibatnya $c(u_3) = 1$, mengakibatkan $c_\pi(u_1) = c_\pi(u_3)$, suatu kontradiksi. Oleh karena itu $\chi L(spl(p_6)) \ge 4$. Selanjutnya, diberikan pewarnaan lokasi untuk mengetahui bilangan kromatik lokasi graf $spl(P_6)$.

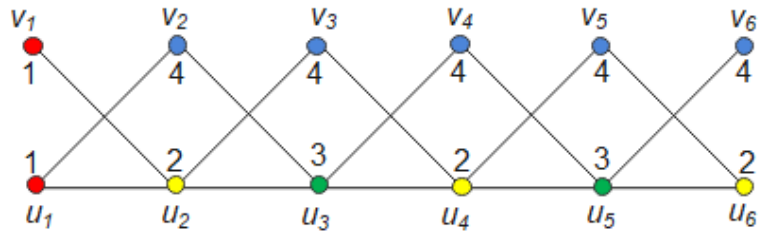

Gambar 1. Pewarnaan lokasi minimum $Spl(P_6)$

Misalkan c pewarnaan titik yang diberikan dengan menggunakan 4 warna. Pada graf split lintasan $spl(P_6)$ diberikan kelas warna sedemikian sehingga diperoleh $C_1 = \{u_1, v_1\},\ C_2 = \{u_2, u_4, u_6\},\ C_3 = \{u_3, u_5\},\ C_4 = \{v_2, v_3, v_4, v_5, v_6\}$. Maka diperoleh kode warna sebagai berikut:
$c_\pi(u_1) = (0,1,2,1)$; $c_\pi(u_2) = (1,0,1,1)$; $c_\pi(u_3) = (2,1,0,1)$; $c_\pi(u_4) = (3,0,1,1)$; $c_\pi(u_5) = (4,1,0,1)$; $c_\pi(u_6) = (5,0,1,1)$; $c_\pi(v_1) = (0,1,2,2)$; $c_\pi(v_2) = (1,2,1,0)$; $c_\pi(v_3) = (2,1,2,0)$; $c_\pi(v_4) = (3,2,1,0)$; $c_\pi(v_5) = (4,1,2,0)$; $c_\pi(v_6) = (5,2,1,0)$. Karena setiap titik pada graf tersebut mempunyai kode warna yang berbeda, maka c adalah pewarnaan lokasi. Akibatnya $\chi_L(Spl(P_6)) \le 4$. Jadi $\chi_L(Spl(P_6)) = 4$.

Berikut ini diberikan contoh penentuan bilangan kromatik lokasi graf $spl(P_7)$ akan ditentukan terlebih dahulu batas bawah bilangan kromatik lokasi dari graf. Karena graf split lintasan $spl(P_7)$ berorde $n \geq 3$, sehingga berdasarkan Teorema 1.1 membutuhkan sekurang-kurangnya 3 warna. Andaikan c pewarnaan lokasi pada $(spl(P_n))$ menggunakan 3 warna. Tanpa mengurangi perumuman, misalkan $c(u_1) = c(v_1) = 1$ maka, $\{c(u_2), c(v_2)\} = \{2,3\}$. Akibatnya $c(u_3) = 1$, mengakibatkan $c_\pi(u_1) = c_\pi(u_3)$, suatu kontradiksi. Oleh karena itu $\chi L(spl(p_7)) \geq 4$. Selanjutnya, diberikan pewarnaan lokasi untuk mengetahui bilangan kromatik lokasi graf $spl(P_7)$ sebagai berikut :

76 Rahmatalia dkk, JMI Vol 18 No 1 April 2022, pp. 73-80,doi:10.24198/jmi.v18.n1.36091.73-80

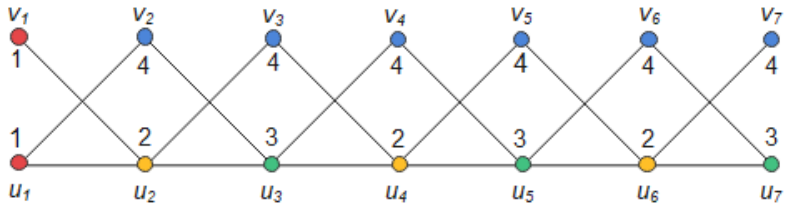

Gambar 2. Pewarnaan lokasi minimum $Spl(P_7)$

Misalkan c pewarnaan titik yang diberikan dengan menggunakan 4 warna. Pada graf split lintasan $spl(P_7)$ diberikan kelas warna sedemikian sehingga diperoleh $C_1 = \{u_1, v_1\}$, $C_2 = \{u_2, u_4, u_6\}$, $C_3 = \{u_3, u_5, u_7\}$, $C_4 = \{v_2, v_3, v_4, v_5, v_6, v_7\}$. Maka diperoleh kode warna sebagai berikut:
$c_\pi(u_1) = (0,1,2,1)$; $c_\pi(u_2) = (1,0,1,1)$;$c_\pi(u_3) = (2,1,0,1)$; $c_\pi(u_4) = (3,0,1,1)$; $c_\pi(u_5) = (4,1,0,1)$;$c_\pi(u_6) = (5,0,1,1)$; $c_\pi(u_7) = (6,1,0,1)$; $c_\pi(v_1) = (0,1,2,2)$; $c_\pi(v_2) = (1,2,1,0)$; $c_\pi(v_3) = (2,1,2,0)$; $c_\pi(v_4) = (3,2,1,0)$; $c_\pi(v_5) = (4,1,2,0)$; $c_\pi(v_6) = (5,2,1,0)$; $c_\pi(v_7) = (6,1,2,0)$. Karena setiap titik pada graf tersebut mempunyai kode warna yang berbeda, maka c adalah pewarnaan lokasi. Akibatnya $\chi_L(Spl(P_7)) \leq 4$. Jadi $\chi_L(Spl(P_7)) = 4$.

Teorema 2.1. Bilangan kromatik lokasi graf split lintasan $spl(P_n)$ untuk $n \geq 3$ adalah 4
Bukti.

Pertama-tama ditentukan batas bawah bilangan kromatik lokasi dari graf $spl(P_n)$. Berdasarkan Teorema 1.1 $\chi_L(spl(P_n)) \geq 3$. Andaikan c pewarnaan lokasi pada $(spl(P_n))$ menggunakan 3 warna. Tanpa mengurangi perumuman, misalkan $c(u_1) = c(v_1) = 1$ maka, $\{c(u_2), c(v_2)\} = \{2,3\}$. Akibatnya $c(u_3) = 1$, mengakibatkan $c_\pi(u_1) = c_\pi(u_3)$, suatu kontradiksi. Akibatnya, dibutuhkan sekurang – kurangnya 4 warna. Jadi, $\chi_L(spl(P_n)) \geq 4$.

Selanjutnya, untuk menetukan batas atas dari graf $spl(P_n)$. Misalkan c pewarnaan titik menggunakan 4 warna sebagai berikut :

$$c(u_i) = \begin{cases} 1, \text{ untuk } i = 1; \\ 2, \text{ untuk } i = 2n,\ n \geq 1; \\ 3, \text{ untuk } i = 2n+1,\ n \geq 1. \end{cases}$$

$$c(v_i) = \begin{cases} 1, \text{ untuk } i = 1; \\ 4, \text{ untuk } i > 1. \end{cases}$$

Kode warna dari $(Spl(P_n))$ adalah :

$$c_\pi(u_i) = \begin{cases} i-1, & \text{ordinat ke} - 1, \text{ untuk } i \geq 1; \\ 0, & \text{ordinat ke} - 2, \text{ untuk } i \text{ genap }, 2 \leq i \leq n; \\ 0, & \text{ordinat ke} - 3, \text{ untuk } i \text{ ganjil }, 3 \leq i \leq n; \\ 2, & \text{ordinat ke} - 3, \text{ untuk } i = 1; \\ 1, & \text{lainnya.} \end{cases}$$

$$c_\pi(v_i) = \begin{cases} i-1, & \text{ordinat ke} - 1, \text{ untuk } i \geq 1; \\ 0, & \text{ordinat ke} - 4, \text{ untuk } i \geq 2; \\ 2, & \text{ordinat ke} - 2, \text{ untuk } i \text{ genap}, 2 \leq i \leq n; \\ 2, & \text{ordinat ke} - 3, \text{ untuk } i \text{ ganjil}, 3 \leq i \leq n; \\ 2, & \text{ordinat ke} - 4, \text{ untuk } i = 1; \\ 1, & \text{lainnya.} \end{cases}$$

Karena semua titik di $V(Spl(P_n))$ untuk $n \geq 3$ memiliki kode warna yang berbeda, maka c merupakan pewarnaan lokasi menggunakan 4 warna. Akibatnya $\chi_L(Spl(P_n)) \leq 4$. Oleh karena itu $\chi_L(Spl(P_n)) = 4$. □

2.2 Bilangan Kromatik Lokasidari Graf Barbel yang memuat Split Lintasan

Berikut ini diberikan contoh penentuan bilangan kromatik lokasi graf $B_{spl(P_6)}$ akan ditentukan terlebih dahulu batas bawah bilangan kromatik lokasi dari graf. Karena graf barbel split lintasan $B_{spl(P_6)}$ memuat graf split lintasan $spl(P_n)$, sehingga berdasarkan Teorema 2.1 jelas bahwa $\chi_L(B_{spl(P_6)}) \geq 4$. Selanjutnya, diberikan pewarnaan lokasi untuk mengetahui bilangan kromatik lokasi graf $B_{spl(P_6)}$sebagai berikut :

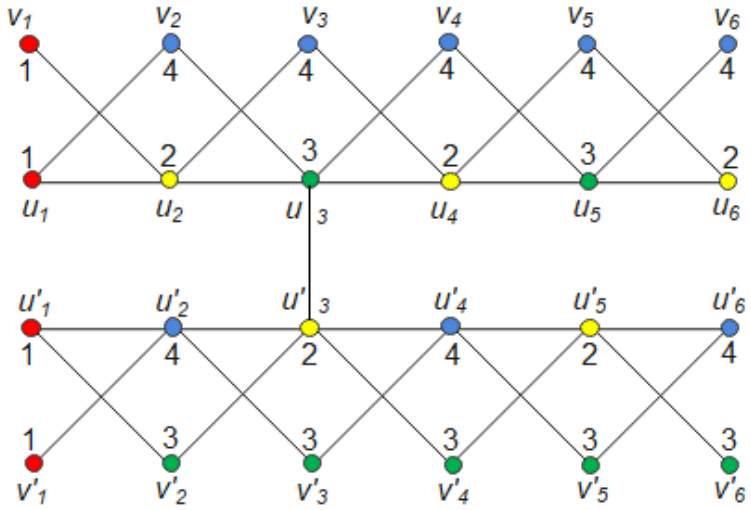

Gambar 3. Pewarnaan lokasi minimum $B_{spl(P_6)}$

Misalkan c pewarnaan titik yang diberikan dengan menggunakan 4 warna. Pada graf barbel split lintasan $B_{spl(P_6)}$ diberikan kelas warna sedemikian sehingga diperoleh $C_1 = \{u_1, u'_1, v_1, v'_1\}$, $C_2 = \{u_2, u_4, u_6, u'_3, u'_5\}$, $C_3 = \{u_3, u_5, v'_2, v'_3, v'_4, v'_5, v'_6\}$, $C_4 = \{v_2, v_3, v_4, v_5, v_6, u'_2, u'_4, u'_6\}$ Maka diperoleh kode warna sebagai berikut:
$c_\pi(u_1) = (0,1,2,1)$; $c_\pi(u_2) = (1,0,1,1)$; $c_\pi(u_3) = (2,1,0,1)$; $c_\pi(u_4) = (3,0,1,1)$; $c_\pi(u_5) = (4,1,0,1)$; $c_\pi(u_6) = (5,0,1,1)$; $c_\pi(v_1) = (0,1,2,2)$; $c_\pi(v_2) = (1,2,1,0)$; $c_\pi(v_3) = (2,1,2,0)$; $c_\pi(v_4) = (3,2,1,0)$; $c_\pi(v_5) = (4,1,2,0)$; $c_\pi(v_6) = (5,2,1,0)$; $c_\pi(u'_1) = (0,2,1,1)$; $c_\pi(u'_2) = (1,1,1,0)$; $c_\pi(u'_3) = (2,0,1,1)$; $c_\pi(u'_4) = (3,1,1,0)$; $c_\pi(u'_5) = (4,0,1,1)$; $c_\pi(u'_6) = (5,1,1,0)$; $c_\pi(v'_1) = (0,2,2,1)$; $c_\pi(v'_2) = (1,1,0,2)$; $c_\pi(v'_3) = (2,2,0,1)$; $c_\pi(v'_4) = (3,1,0,2)$; $c_\pi(v'_5) =$

(4,2,0,1); $c_\pi(v'_6) = (5,1,0,2)$. Karena setiap titik pada graf tersebut mempunyai kode warna yang berbeda, maka c adalah pewarnaan lokasi. Akibatnya $\chi_L(B_{spl(P_6)}) \leq 4$. Jadi $\chi_L(B_{spl(P_6)}) = 4$.

Selanjutnya, diberikan contoh penentuan bilangan kromatik lokasi graf $B_{spl(P_7)}$ akan ditentukan terlebih dahulu batas bawah bilangan kromatik lokasi dari graf. Karena graf barbel split lintasan $B_{spl(P_7)}$memuat graf split lintasan $spl(P_n)$, sehingga berdasarkan Teorema 2.1 membutuhkan sekurang-kurangnya 4 warna. Oleh karena itu$\chi_L(B_{spl(P_7)}) \geq 4$. Selanjutnya, diberikan pewarnaan lokasi untuk mengetahui bilangan kromatik lokasi graf $B_{spl(P_7)}$sebagai berikut :

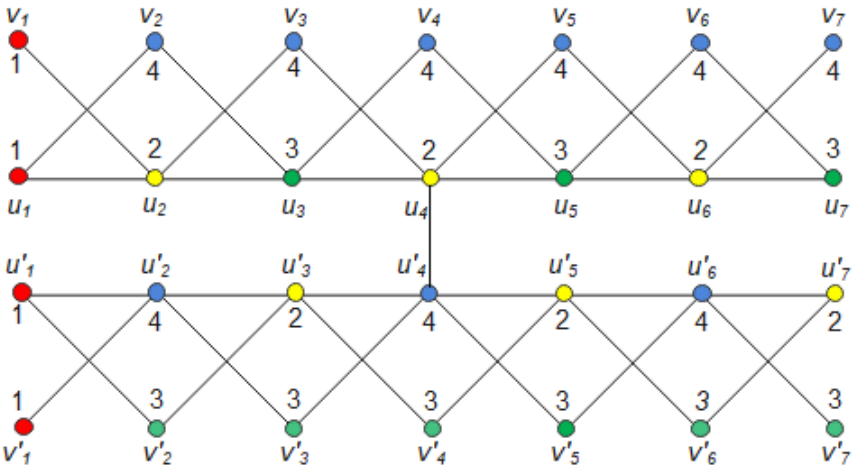

Gambar 4. Pewarnaan lokasi minimum $B_{spl(P_7)}$.

Misalkan c pewarnaan titik yang diberikan dengan menggunakan 4 warna. Pada graf barbel split lintasan $B_{spl(P_7)}$ diberikan kelas warna sedemikian sehingga diperoleh $C_1 = \{u_1, u'_1, v_1, v'_1\}, C_2 = \{u_2, u_4, u_6, u'_3, u'_5, u'_7\}, C_3 = \{u_3, u_5, u_7, v'_2, v'_3, v'_4, v'_5, v'_6, v'_7\}, C_4 = \{v_2, v_3, v_4, v_5, v_6, v_7, u'_2, u'_4, u'_6\}$ Maka diperoleh kode warna sebagai berikut:
$c_\pi(u_1) = (0,1,2,1)$; $c_\pi(u_2) = (1,0,1,1)$; $c_\pi(u_3) = (2,1,0,1)$; $c_\pi(u_4) = (3,0,1,1)$; $c_\pi(u_5) = (4,1,0,1)$; $c_\pi(u_6) = (5,0,1,1)$; $c_\pi(u_7) = (6,1,0,1)$; $c_\pi(v_1) = (0,1,2,2)$; $c_\pi(v_2) = (1,2,1,0)$; $c_\pi(v_3) = (2,1,2,0)$; $c_\pi(v_4) = (3,2,1,0)$; $c_\pi(v_5) = (4,1,2,0)$; $c_\pi(v_6) = (5,2,1,0)$; $c_\pi(v_7) = (6,1,2,0)$; $c_\pi(u'_1) = (0,2,1,1)$; $c_\pi(u'_2) = (1,1,1,0)$; $c_\pi(u'_3) = (2,0,1,1)$; $c_\pi(u'_4) = (3,1,1,0)$; $c_\pi(u'_5) = (4,0,1,1)$; $c_\pi(u'_6) = (5,1,1,0)$; $c_\pi(u'_7) = (6,0,1,1)$; $c_\pi(v'_1) = (0,2,2,1)$; $c_\pi(v'_2) = (1,1,0,2)$; $c_\pi(v'_3) = (2,2,0,1)$; $c_\pi(v'_4) = (3,1,0,2)$; $c_\pi(v'_5) = (4,2,0,1)$; $c_\pi(v'_6) = (5,1,0,2)$; $c_\pi(v'_7) = (6,2,0,1)$

Karena setiap titik pada graf tersebut mempunyai kode warna yang berbeda, maka c adalah pewarnaan lokasi. Akibatnya $\chi_L(B_{spl(P_7)}) \leq 4$. Jadi $\chi_L(B_{spl(P_7)}) = 4$.

Teorema 2.2. Bilangan kromatik lokasi graf barbel split lintasan, $B_{spl(P_n)}$untuk $n \geq 3$ adalah 4.

Bukti.
Graf $B_{spl(P_n)}$ memuat graf $spl(P_n)$, maka berdasarkan Teorema 2.1 diperoleh $\chi_L(B_{spl(P_n)}) \geq 4$.

Misalkan c adalah pewarnaan titik pada $B_{spl(P_n)}$mengunakan 4 warna sebagai berikut :

$$c(u_i) = \begin{cases} 1, & \text{untuk } i = 1; \\ 2, & \text{untuk } i = 2n; \\ 3, & \text{untuk } i = 2n+1. \end{cases}$$

$$c(u_i') = \begin{cases} 1, & \text{untuk } i = 2n+1; \\ 2, & \text{untuk } i = 2n+1; \\ 4, & \text{untuk } i = 2n. \end{cases}$$

$$c(v_i) = \begin{cases} 1, & \text{untuk } i = 1; \\ 4, & \text{untuk } i > 1. \end{cases}$$

$$c(v_i') = \begin{cases} 1, & \text{untuk } i = 1; \\ 3, & \text{untuk } i > 1. \end{cases}$$

Kode warna titik-titik dari$B_{spl(P_n)}$ adalah :

$$c_\pi(u_i) = \begin{cases} i-1, & \text{ordinat ke} -1, \text{untuk } i \geq 1; \\ 0, & \text{ordinat ke} -2, \text{untuk } i \text{ genap}, 2 \leq i \leq n; \\ 0, & \text{ordinat ke} -3, \text{untuk } i \text{ ganjil}, 3 \leq i \leq n; \\ 2, & \text{ordinat ke} -3, \text{untuk } i = 1; \\ 1, & \text{lainnya.} \end{cases}$$

$$c_\pi(u_i') = \begin{cases} i-1, & \text{ordinat ke} -1, \text{untuk } i \geq 1; \\ 0, & \text{ordinat ke} -2, \text{untuk } i \text{ genap}, 3 \leq i \leq n; \\ 0, & \text{ordinat ke} -4, \text{untuk } i \text{ ganjil}, 2 \leq i \leq n; \\ 2, & \text{ordinat ke} -2, \text{untuk } i = 1; \\ 1, & \text{lainnya.} \end{cases}$$

$$c_\pi(v_i) = \begin{cases} i-1, & \text{ordinat ke} -1, \text{untuk } i \geq 1; \\ 0, & \text{ordinat ke} -4, \text{untuk } i > 2; \\ 2, & \text{ordinat ke} -2, \text{untuk } i \text{ genap}, 2 \leq i \leq n; \\ 2, & \text{ordinat ke} -3, \text{untuk } i \text{ ganjil}, 3 \leq i \leq n; \\ 2, & \text{ordinat ke} -4, \text{untuk } i = 1; \\ 1, & \text{lainnya.} \end{cases}$$

$$c_\pi(v_i') = \begin{cases} i-1, & \text{ordinat ke} -1, \text{untuk } i \geq 1; \\ 0, & \text{ordinat ke} -3, \text{untuk } i > 1; \\ 2, & \text{ordinat ke} -2 \text{ untuk } i \text{ ganjil}, 3 \leq i \leq n; \\ 2, & \text{ordinat ke} -3 \text{ untuk } i \text{ genap}, 2 \leq i \leq n; \\ 2, & \text{ordinat ke} -4 \text{ untuk } i = 1; \\ 1, & \text{lainnya.} \end{cases}$$

Karena semua titik di $V(B_{spl(P_n)})$ untuk $n \geq 3$ mempunyai kode warna yang berbeda, maka c merupakan pewarnaan lokasi menggunakan 4 warna. Akibatnya $\chi_L(B_{spl(P_n)}) \leq 4$. Oleh karena itu $\chi_L(B_{spl(P_n)}) = 4$. □

5. Simpulan

Pada penelitian telah diperoleh bahwa bilangan kromatik lokasi untuk graf split lintasan dan graf barbel split lintasan adalah sama, yaitu 4. Penelitian lanjutan yang dapat dilakukan adalah menentukan operasi lain pada graf split lintasan yang mempertahankan bilangan kromatik lokasinya.

Daftar Pustaka

[1] F Harary, and Melter, RA., 1976, On the metric dimension of a graph, *Ars Combinatori*, 2:191-195.

[2] Chartrand, G., Salehi, E., and Zhang, P., 1998, On the partition dimension of graph, *Congr. Numer*, 130:157-168.

[3] Chartrand, G., Erwin, D., Henning, M.A., Slater, P.J., and Zhang, P., 2002, The Locating – Chromatic Number of a Graph, *Bull. Inst. Combin. Appl*, 36:89- 101.

[4] Saenpholphat, V., and Zhang, P., 2004, Conditional resolvability: a survey. Internat. *J. Math. Math. Sci.*, 38:1997-2017.

80 Rahmatalia dkk, JMI Vol 18 No 1 April 2022, pp. 73-80,doi:10.24198/jmi.v18.n1.36091.73-80

[5] Chartrand, G., and Zhang, P., 2003, The theory and appllications of resolvability in graphs, *a survey. Congr. Numer*, 160:47-68.

[6] Johnson, M.A., 1993, Structure-activity maps for visualizing the graph variables arising in drug design. *J. Biopharm. Statist*, 3:203-236.

[7] Chartrand, G., Edwin, D., Henning, M. A., Slater, P.J., and Zhang, P., 2003, Graphs of Order n with Locating-Chromatic Number $n-1$, *Discrete Mathematics*, 269:65–79.

[8] Asmiati, Assiyatun, H., and Baskoro, E.T., 2011, Locating Chromatic Number of Amalgamation of Stars, *ITB J. Sci*,43(1):1-8.

[9] Behtoei, A., dan Omoomi, B., 2011, On The Locating Chromatic Number of KneserGraphs. *Discrete Appl. Math*,159(18):2214–2221.

[10] Welyyanti, D., Baskoro, E. T., Simanjuntak, R., and Uttunggadewa, S., 2015, On Locating Chromatic Number for Graphs with Dominant Vertices, *Procedia Comput.Sci.*,74:89-92.

[11] Asmiati., 2016, On The Locating-Chromatic Numbers of Non-Homogeneous Caterpillars and Firecracker Graphs, *Far East Journal Of Mathematical Sciences*, 100(8):1305-1316.

[12] Asmiati., 2017,Bilangan Kromatik Lokasi *n* Amalgamasi Bintang yang Dihubungkan oleh suatu Lintasan, *Jurnal Matematika Integratif*, 13(2):115-121.

[13] Asmiati, and Baskoro, E.T., 2012, Characterizing of Graphs Containing Cycle with Locating-Chromatic Number Three, AIP *Conf. Proc*, 1450: 351-357.

[14] Baskoro, E.T., and Asmiati, 2013, Characterizing all trees with locating-chromatic number 3, *Elec. J. of Graph Theory and Applications*, 1(2):109-117.

[15] Irawan, A., Asmiati., Zakaria, L., Muludi, K., and Bernadhita, U., 2021, *Subdivision of Certain Barbell Operation of Origami Graphs has Locating-Chromatic Number Five. International ournal of Computer Science and Network Security*, 21 (9):1738-7906.

[16] Asmiati., Yana, I.K.D.C., and Yulianti, L., 2018, On the Locating Chromatic Number of Certain Barbell Graphs, *International Journal of Mathematics and Mathematical Sciences*, 100(8):1-5.

[17] Asmiati., Yana, I.K.S.G., and Yulianti, L., 2019, On the Locating Chromatic Number of subdivision of Barbell Graphs containing generalized Petersen graphs, International *Journal of Computer Science and Network Security*, 19(7):45-50.

[18] Irawan, A., Asmiati, Zakaria, L., and Muludi, K., 2021,The Locating Chromatic Number of Origami Graphs. Algorithms, 14(167):1-15.

[19] Asmiati., Damayanti, M., and Yulianti, 2021, On the locating chromatic number of barbell shadow path graphs, *Indonesian Journal of Combinatorics*. 5(2):82-93.
[20] Prawinasti, K., Ansori, M., Asmiati, Notiragayu, Gesti, N.R., 2021, The Locating Chromatic Number for Split Graph of Cycle,*J.Phys. Conf. Ser*, 1751:1-5.
[21] Damayanti, M., Asmiati., Fitriani., Ansori., dan Faradila, A., 2021,The Locating Chromatic Number of Some Modified Path with Cycle having Locating Number Four,*J.Phys. Conf. Ser*, 1751:1-5.

ANALYSIS OF REDUCING SUGAR LEVELS OF CATTLEYA SP. ORCHID PLANTLET AFTER INDUCTION FUSARIC ACID IN VITRO

Endang Nurcahyani [1, *], Yuliana Permata Sari [2], Elsi Diana [2], Sumardi [2], Hardoko Insan Qudus [3] and Sri Wahyuningsih [4]

[1] *Applied Biology Study Program, Faculty of Mathematics and Natural Sciences, University of Lampung, Bandar Lampung, Lampung, Indonesia.*

[2] *Master of Biology Study Program, Faculty of Mathematics and Natural Sciences, University of Lampung, Bandar Lampung, Lampung, Indonesia.*

[3] *Master of Chemistry Study Program, Faculty of Mathematics and Natural Sciences, University of Lampung, Bandar Lampung, Lampung, Indonesia.*

[4] *Biology Study Program, Faculty of Mathematics and Natural Sciences, University of Lampung, Bandar Lampung, Lampung, Indonesia.*

World Journal of Advanced Research and Reviews, 2022, 14(02), 095–099
Publication history: Received on 22 March 2022; revised on 02 May 2022; accepted on 04 May 2022
Article DOI: https://doi.org/10.30574/wjarr.2022.14.2.0369

Abstract

Cattleya sp. orchid is one type of orchid plant that is widely known in Indonesia. The queen of orchids is the nickname given to the *Cattleya* sp. orchid because of the elegant shape and color of the flowers of the *Cattelya* sp. orchid. This research was conducted to determine the level of reducing sugar produced by plantlets of *Cattleya* sp. after the addition of fusaric acid in *in vitro* media. Determination of reducing sugar content was carried out using the Nelson – Somogyi method. This study used a completely randomized design (CRD), with five levels of treatment and five replications for each level. The treatment consisted of adding fusaric acid with concentrations of fusaric acid in the medium: 0 ppm, 10 ppm, 20 ppm, 30 ppm and 40 ppm. Data analysis used Anova analysis, and continued with Tukey's test at 5% significance level. Based on the analysis, there was an increase in reducing sugar levels in the plantlets of *Cattleya* sp. orchids after adding fusaric acid to the growing media.

Keywords: Orchid; Fusaric Acid; *Cattleya* sp.; Sugar Reduction; *in vitro*

1. Introduction

Orchid plants are included in the Orchidaceae family, are one of the most popular commercial ornamental plants in Indonesia and the world, because they have very beautiful and unique types, variations in shape, color, and flower characters, and have high economic and aesthetic value. *Cattleya*, *Vanda*, *Phalaenopsis*, *Dendrobium*,

Oncidium, and *Aranthera* are some of the orchid species that are in great demand [1]. The *Cattleya* orchid itself is part of the Kingdom Plantae, Spermatophyta Division, Class Monocotyledoneae, Order Asparagales, Family Orchidaceae, and Genus *Cattleya* [2]. The beauty and beauty of the flowers make this plant called the queen of flowers. In Indonesia, *Cattleya* sp orchid is a plant that has high economic value. Conventional propagation of orchids takes a long time and gets a limited number of seeds, because it is done by separating the tillers. By means of *in vitro* seeds will be obtained in large quantities in a relatively short time and uniform [3].

Reducing sugar is the ability of sugar to reduce, which is caused by the presence of free aldehyde or ketone groups [4]. Compounds that oxidize or are reducing agents are oxidizing metals such as Cu (II). Examples of su gars including reducing sugars are glucose, fructose, lactose, maltose, and others. Monosaccharides have the ability to reduce a compound. The reducing property of a sugar is determined by the presence or absence of a reactive free hydroxyl group. The principle of analysis is based on monosaccharides which have the ability to reduce a compound, the presence of monosaccharide polymerization affects its reducing properties [5].

The analysis that can be used to determine the reducing sugar group is the Nelson-Somogyi method [6]. In this analysis, the sample will be reacted with arsenomolybdate which will produce blue molybdine, this blue material will then be measured its absorbance value. The intensity of the blue color formed is equivalent to the amount of reducing sugar in the sample. The higher the absorbance value, the more reducing sugar content in the sample. This study aims to determine the level of reducing sugar produced after the addition of fusaric acid in plantlet media of *Cattleya* sp. orchids *in vitro*

2. Material and methods

The research was conducted from October 2021 to January 2022 in the *in vitro* culture room of the Botany and tissue culture laboratory, Department of Biology, FMIPA, and University of Lampung. This study used a completely randomized design with 5 treatments of fusaric acid administration on Vacint & Went medium as much as 0 ppm, 10 ppm, 20 ppm, 30 ppm, 40 ppm with each treatment 5 repetitions.

2.1. Planting *Cattleya* sp plantlets in Vacin and Went medium that has been given Fusaric Acid

Vacint & Went medium in sterilized culture bottles was added with fusaric acid with concentrations of 0 ppm (control), 10 ppm, 20 ppm, 30 ppm, and 40 ppm. Prior to use, fusaric acid was dissolved with distilled water until the specified concentration was obtained, then filtered. Filtering using a 0.45 m diameter filter twice and with a 0.22 m diameter filter once. Filtration is carried out in a sterile room in Laminar Air Flow in sterilized culture bottles. Prior to use, the medium was incubated for 7 days at room temperature of 25 ^{0}C to ensure that the fusaric acid was well filtered. If within 7 days there is no contamination in the medium, then the medium can be used.

Plantlets of *Cattleya* sp. were carried out in a sterile room in Laminar Air Flow (LAF) Cabinet plantlets from culture bottles were removed with a sterile scalpel and one by one placed on a 10 cm diameter petri dish, then the plantlets were sorted one by one, after that they were planted in each Each culture bottle containing 3 plantlets of medi um. Plantlet selection was carried out for 30 days. On day 30, an evaluation was carried out to determine the tolerant concentration of AF for the selection of *Cattleya* sp plantlets *in vitro*.

2.2. Analysis of Reducing Sugar Levels

2.2.1. Preparation of Standard Sugar Solution

Analysis of reducing sugar was carried out by making a standard glucose solution [7] (10 mg glucose/100mL), carried out 5 dilutions of glucose solution with a concentration of 2ml, 4ml, 6ml, 8ml, and 10 mg/100 ml, each of which was added to each concentration. Each test tube and 1 tube containing distilled water as a blank. Add 1 mL of Nelson's reagent (Nelson A 25 parts Nelson B 1 part) into each tube. The solution to which Nelson was added was then heated for 20 minutes. The solution was cooled in a beaker until the tube temperature was 25 ^{0}C, then 1 ml of arsenomolybdate reagent was added, shaken until all the precipitate dissolved again. After homogenizing again, 7 ml of distilled water was added and shaken until homogeneous. The solution was measured with a Vis spectrophotometer at a wavelength of 695 nm, then a calibration curve was made for the relationship between glucose concentration and absorbance.

2.2.2. Determination of Reducing Sugar Content

Determination of reducing sugar content using the Nelson – Somogyi method [8]. Fresh *Cattleya* sp. orchid leaf extract (extract solution must be clear), each concentration of 1 ml is taken. put into each test tube and add 1 ml of Nelson's reagent into each tube, the solution to which Nelson has been added is then heated for 20 minutes. The solution was cooled in a beaker until the tube temperature was 25 ^{0}C, then 1 ml of arsenomolybdate reagent was added, shaken until all the precipitate dissolved again. After homogenizing again, 7 ml of distilled water was added and shaken until homogeneous. The solution was measured with a Vis spectrophotometer at a wavelength of 695 nm, then a calibration curve was made for the relationship between glucose concentration and absorbance.

The reducing sugar content is calculated by the formula 1:
Reducing Sugar Content (%) = (X. FP)/BS x 100% (1)

Information:
X = Concentration (ppm)
FP = Dilution factor of sample solution
BS = Sample weight (g)

3. Results and discussion

Measurement of reducing sugar content on the standard curve of reducing sugar. The standard curve is obtained from the ratio of the concentration of reducing sugar to the absorbance value. The results of determining the standard curve of reducing sugar can be seen in Table 1.

Table 1 Comparison of Reducing Sugar Concentration and Absorbance

Reducing Sugar Concentration (ppm)	Absorbance
20	0.318
40	0.347
60	0.367
80	0.387
100	0.405
120	0.432

Based on the data in Table 1, the standard curve of reducing sugar is obtained. So that the linear equation y = 0.0011x + 0.2996 is obtained and has a correlation value of R2 = 0.9946 which shows the diversity between the concentration of reducing sugars and

the absorbance value. The standard curve of reducing sugar and absorbance is show in Figure 1

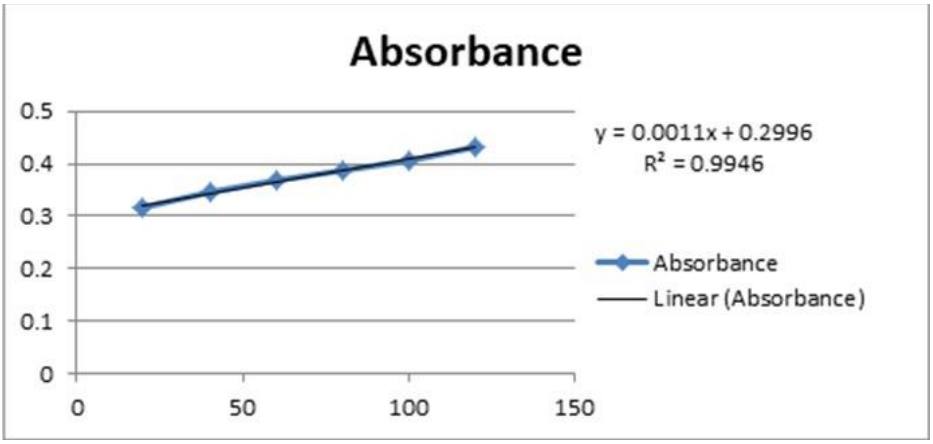

Figure 1 Reducing Sugar Standard Curve

Based on Figure 1, it can be calculated the reducing sugar content of each treatment by substituting the absorbance value from the spectrophotometer results of the plantlet leaf extract of *Cattleya* sp. The absorbance value is entered into the linear equation y= ax – b from the standard curve where y is the absorbance value. The calculation results obtained the value of x as concentration, then substituted in the reducing sugar calculation formula. The results of the calculation of reducing sugars of *Cattleya* sp. orchid plantlets with the addition of fusaric acid at several concentrations are presented in Table 2.

The results of observations based on Table 2 increased reducing sugar occurred from the control 23.476 to 23.506 at a concentration of 10 ppm fusaric acid. Then at a concentration of 20 ppm it became 27.402 followed by 28.405 at a concentration of 30 ppm and 30.142 at a concentration of 40 ppm. These results indicate that there is an effect o n the administration of fusaric acid, where the higher the concentration of fusaric acid given, the higher the content of reducing sugar contained in the plantlets of *Cattleya* sp.

The increased reducing sugar came from starch and sucrose as a result of carbohydrate conversion. Some carbohydrates are also used as respiration materials and form other compounds, this causes reducing sugar levels to increase but carbohydrates to decrease [9].

Table 2 Reducing Sugar Levels of *Cattleya* sp. Orchid Plantlets Induced by Fusaric Acid

Treatment/ 30 Days	**Orchid *Cattleya* sp reducing sugar levels (%)**
0 ppm (Kontrol)	23. 476 ± 1.069
10 ppm	23. 506 ± 2.712
20 ppm	27. 402 ± 2.408
30 ppm	28. 405 ± 2.023
40 ppm	30. 142 ± 2.629

Changes in reducing sugar content are influenced by several factors, one of which is the heating process. Heating during the test for reducing sugar content causes the chemical structure to change. As a result of heating the glycosidic bond breaks causing non-reducing sugars (sucrose) to break down into reducing sugars such as glucose and fructose [5]. In addition, the content of reducing sugar is also influenced by

the administration of fusaric acid. The high content of fusaric acid can reduce reducing sugar levels, as in previous studies conducted on cassava [10].

4. Conclusion

The results showed an increase in reducing sugar levels in plantlets of *Cattleya* sp. This shows that there is an effect on the administration of fusaric acid, where the higher the concentration of fusaric acid given, the higher the reducing sugar content contained in the plantlets of *Cattleya* sp.

Compliance with ethical standards

Acknowledgments

The researcher would like to thank the Botanical Laboratory, especially the In Vitro Culture Room, Department of Biology, Faculty of Mathematics and Natural Sciences, University of Lampung, Bandar Lampung, Lampung, Indonesia, which has provided a place to conduct and process research data.

Disclosure of conflict of interest

All authors have no conflicts of interest

References

[1] WA Qosim, N Istifadah, I Djatnika, Y. Effect of Mutagen Ethyl Methane Sulfonate on Phalaenopsis Hybrid Shoot Regeneration Capacity *In vitro*, *J. Hortik.* 2016; 22(4): 360-365.

[2] CGGK van Steenis. *Flora: For Schools In Indonesia*. Jakarta: Pradnya Paramita; 1981; 495 p.

[3] H Yuswanti. *Cattleya* sp. Orchid Plantlet Growth. with Benzyl Amino Purine Treatment on Modified Leaf Fertilizer Base Media, *Agrotrop J. Agric. Sci.* 2015; 4(2): 158–163.

[4] T Kunz, EJ Lee, V Schiwek, T Seewald, FJ Methner. Glucose - A reducing sugar: Reducing Properties of Sugars in Beverages and Food, *Brewing Science*. 2011; 64(7–8) 61–67.

[5] N Wilberta, NT Sonya, SHR Lydia. Analysis of Reducing Sugar Content in Sugar Ants From Palm Sap Which is Influenced by pH and Water Content, *Bioedukasi (Jurnal Pendidik. Biol.)* 2021; 12(1): 101-108.

[6] AR Razak, NK Sumarni, B Rahmat. Optimization of Sucrose Hydrolysis Using Sulfonate Type Cation Exchange Resin, *J. Nat. Sci. Desember*. 2012; 1(1) 119–131.

[7] YH Pratiwi, O Ratnayani, IN Wirajana. Comparison of Reducing Sugar Test Methods in Determining L- Arabinofuranosidase Activity With Coconut (*Cocos Nucifera*) Leaves Substrate, *J. Kim.* 2018; 134-139.

[8] HK Al-kayyis, H Susanti. Comparison of Somogyi-Nelson and Anthrone-Sulfate Methods for Determination of Reducing Sugar Content in Cilembu (*Ipomea batatas* L. Bulbs). *J. Pharm. Sci. Community*. 2016; 13(2) 81–89.

[9] R Fitriningrum, Sugiyarto, A. Susilowati. Analysis of Carbohydrate Content at Various Maturity Levels of Karika Fruit (*Carica pubescens*) in Kejajar and Sembungan, Dieng Plateau, Central Java, *Bioteknologi*. 2013; 10(1) 6–14.

[10] E Nurcahyani, HI Qudus, F Evlin. Analysis of the reducing sugar of cassava (*Manihot esculenta* Crantz.) mutant plantlets resistant to Fusarium wilt, *AIP Conf. Proc.* April 2021; 2331 (050010); 1-4.